

**A NOVEL FLUIDIZED BED REACTOR FOR
INTEGRATED NO_x ADSORPTION-REDUCTION
WITH HYDROCARBONS**

by

TERRIS TIANXUE YANG

B.A.Sc., Tsinghua University, 1989

M.A.Sc., Tsinghua University, 1991

A THESIS SUBMITTED IN PARTIAL FULFILLMENT OF
THE REQUIREMENTS FOR THE DEGREE OF

DOCTOR OF PHILOSOPHY

in

The Faculty of Graduate Studies

(Chemical and Biological Engineering)

THE UNIVERSITY OF BRITISH COLUMBIA

(Vancouver)

September 2008

© Terris Tianxue Yang, 2008

Abstract

An integrated NO_x adsorption-reduction process has been proposed in this study for the treatment of flue gases under lean-burn conditions by decoupling the adsorption and reduction into two different zones. The hypothesis has then been validated in a novel internal circulating fluidized bed.

The adsorption and reaction performance of Fe/ZSM-5 for the selective catalytic reduction (SCR) of NO_x with propylene was investigated in a fixed bed reactor. The fine Fe/ZSM-5(Albemarle) catalyst showed reasonable NO_x adsorption capacity, and the adsorption performance of the catalyst was closely related to the particle size and other catalyst properties. Fe/ZSM-5 catalyst was sensitive to the reaction temperature and space velocity, and exhibited acceptable activity when O_2 concentration was controlled at a low level. Water in the flue gas was found to slightly enhance the reactivity of Fe/ZSM-5(Albemarle), while the presence of CO_2 showed little effect. SO_2 severely inhibited the reactivity of Fe/ZSM-5(Albemarle), and the deactivated catalyst could be only partially regenerated.

Configurations of the reactor influenced the hydrodynamic performance significantly in a cold model internal circulating fluidized bed (ICFB) reactor. For all configurations investigated, the high gas bypass ratio from the annulus to draft tube (R_{AD}) and low draft tube to annulus gas bypass ratio (R_{DA}) were observed, with the highest R_{DA} associated with the conical distributor which showed the flexible and stable operation over a wide range of gas velocities. Solids circulation rates increased with the increase of gas velocities both in the annulus and the draft tube. Gas bypass was also studied in a hot model ICFB reactor. The

results showed that the orientation of perforated holes on the conical distributor could be adjusted to reduce R_{AD} and/or enhance R_{DA} .

Coarse Fe/ZSM-5(PUC) and fine Fe/ZSM-5(Albemarle) catalysts were used in an ICFB and a conventional bubbling fluidized bed to test the NO_x reduction performance. Coarse Fe/ZSM-5(PUC) catalyst showed poor catalytic activity, while fine Fe/ZSM-5(Albemarle) catalyst exhibited promising NO_x reduction performance and strong inhibiting ability to the negative impact of excessive O_2 in the ICFB reactor, proving that the adsorption-reduction two-zone reactor is effective for the NO_x removal from oxygen-rich combustion flue gases.

Table of Contents

Abstract	ii
Table of Contents	iv
List of Tables	ix
List of Figures	x
Acronyms	xxiii
Nomenclature	xxv
Acknowledgements	xxviii
1 Introduction	1
1.1 Formation of NO _x	1
1.2 Methods for the abatement of NO _x emissions	2
1.3 Selective catalytic reduction of NO _x with NH ₃	4
1.4 Research objectives.....	6
1.5 Thesis layout	7
2 Literature Review	9
2.1 Catalysts	9
2.1.1 Metal-exchanged zeolites	11
2.1.2 Metal-exchanged metal oxides	14
2.2 Hydrocarbon reducing agents	15
2.3 Reaction mechanisms and kinetics of HC-SCR.....	21
2.3.1 Surface redox mechanism	21
2.3.2 Oxidation of NO to NO ₂	22
2.3.3 Partial oxidation of hydrocarbons	22
2.4 Influence of flue gas compositions on HC-SCR.....	23

2.4.1 Influence of SO ₂ and H ₂ O in the flue gas.....	23
2.4.2 Influence of excess oxygen in the flue gas.....	25
2.5 Reactors for SCR of NO _x	28
2.6 NO _x storage-reduction (NSR).....	30
2.7 Summary.....	31
3 Adsorption and Reaction Kinetics.....	33
3.1 Experimental setup.....	33
3.2 Catalyst preparation.....	35
3.2.1 Materials.....	36
3.2.2 Preparation of NH ₄ /ZSM-5 and H/ZSM-5.....	37
3.2.3 Preparation of Fe/ZSM-5 by WIE method.....	38
3.2.4 Preparation of Fe/ZSM-5 by IMPO method.....	38
3.3 Performance of Fe/ZSM-5 (PUC) catalyst prepared by IMPO.....	38
3.3.1 Adsorption performance of Fe/ZSM-5(PUC).....	38
3.3.2 Reaction performance of Fe/ZSM-5(PUC).....	42
3.3.2.1 Effect of reaction temperature on catalytic activity.....	43
3.3.2.2 Catalyst deactivation at low temperatures.....	49
3.3.2.3 Effect of GHSV.....	56
3.3.2.4 Effect of O ₂ and HC concentrations.....	58
3.4 Reaction performance of Fe/ZSM-5 (PUC) catalyst prepared by WIE.....	66
3.5 Performance of Fe/ZSM-5(Albemarle) catalyst.....	69
3.5.1 Adsorption performance of Fe/ZSM-5(Albemarle).....	70
3.5.2 Effect of O ₂ concentration on NO _x adsorption of Fe/ZSM-5(Albemarle).....	73
3.5.3 Effect of H ₂ O and CO ₂ on NO _x adsorption of Fe/ZSM-5(Albemarle).....	74
3.5.4 Adsorption performance of parent H/ZSM-5(Albemarle).....	76
3.5.5 Catalytic activity of parent H/ZSM-5(Albemarle) in HC-SCR.....	77
3.5.6 Reaction performance of Fe/ZSM-5(Albemarle).....	79
3.5.6.1 Effect of reaction temperature.....	79
3.5.6.2 Effect of GHSV.....	84
3.5.6.3 Effect of O ₂ and HC concentrations.....	86
3.5.6.4 Effect of CO ₂ and H ₂ O.....	89

3.5.6.5 Deactivation of Fe/ZSM-5(Albemarle) catalyst by SO ₂	94
3.6 Summary	103
4 Hydrodynamic Study of the ICFB Reactor	105
4.1 Experimental setup.....	106
4.1.1 Estimation of gas bypass ratio	111
4.1.2 Estimation of solids circulation rate	113
4.2 Performance with the flat distributor plate.....	114
4.2.1 Gas bypass	116
4.2.2 Solids circulation rate	120
4.3 Performance with the cylindrical distributor plate.....	122
4.3.1 Gas bypass	123
4.3.2 Solids circulation rate	129
4.4 Performance with the conical distributor plate	131
4.4.1 Gas bypass	132
4.4.2 Solids circulation rate	136
4.5 Gas bypassing in the hot model ICFB reactor	140
4.5.1 Fe/ZSM-5(PUC) catalyst.....	141
4.5.2 Fe/ZSM-5(Albemarle) catalyst.....	144
4.5.3 Prediction of O ₂ concentration in the draft tube and annulus.....	146
4.6 Summary	148
5 Adsorption and Reduction Performance of the ICFB Reactor	151
5.1 Experimental setup.....	151
5.2 Estimation of NO _x and HC conversions and NO _x adsorption ratio	154
5.3 Performance with Fe/ZSM-5(PUC) catalyst.....	158
5.3.1 Selection of adsorption zone in the ICFB reactor	158
5.3.2 Effect of catalyst loading in the ICFB reactor.....	159
5.3.3 Effect of HC:NO molar ratio on NO _x conversion	161
5.3.4 Effect of flue gas O ₂ content on NO _x conversion.....	162
5.3.5 Effect of gas velocities on NO _x conversion and adsorption	163
5.3.6 Performance of fluidized bed reactor with Fe/ZSM-5(PUC).....	165

Table of Contents

5.3.6.1 Effect of inlet NO concentration.....	165
5.3.6.2 Effect of HC:NO ratio on NO _x and HC conversions	167
5.3.6.3 Effect of inlet O ₂ concentration on NO _x and HC conversions.....	172
5.3.7 Comparison of ICFB reactor and fluidized bed reactor	174
5.4 Performance of Fe/ZSM-5(Albemarle) catalyst.....	175
5.4.1 Effect of HC:NO molar ratio on NO _x and HC conversions	175
5.4.2 Effect of flue gas O ₂ concentration on NO _x conversion and adsorption	179
5.4.3 Effect of gas velocities on NO _x conversion and adsorption	182
5.4.4 Performance of the fluidized bed reactor with Fe/ZSM-5(Albemarle)	185
5.4.4.1 Effect of HC:NO ratio on NO _x and HC conversions	185
5.4.4.2 Effect of O ₂ concentration on NO _x and HC conversions.....	188
5.4.5 Comparison of reactor types.....	190
5.5 Summary	191
6 Conclusions and Recommendations for Future Work	194
6.1 Conclusions	194
6.1.1 Adsorption and reaction performance of Fe/ZSM-5 catalyst.....	194
6.1.2 Hydrodynamic study of the ICFB reactor	195
6.1.3 Adsorption and reduction performance of Fe/ZSM-5 in the ICFB reactor	196
6.2 Recommendations for future work	197
References	200
Appendices	
A Summary of Previous Work.....	219
B Calibration	236
B.1 Gas flow meters.....	236
B.2 Peristaltic water pump	239
B.3 Pressure transducers	240
C BET Surface Area	243

D Particle Size Distribution.....	244
E Adsorption and Reaction Kinetics of Fe/ZSM-5 (Crushed PUC) Catalyst..	247
E.1 Adsorption performance of Fe/ZSM-5(crushed PUC)	247
E.2 Reaction performance of Fe/ZSM-5(crushed PUC).....	251
F HC-SCR Performance of FCC and Fe/FCC Catalyst.....	254
G Some Results from the Fixed Bed Experiment.....	255
G.1 Adsorption curves for Fe/ZSM-5(PUC) and Fe/ZSM-5(Albemarle).....	255
G.2 Profiles of NO _x and HC conversions and outlet CO concentration from time-on- stream test	261
G.3 XPS analysis for Fe/ZSM-5(PUC).....	269
H Effects of Gas Velocities on Gas Bypass in Hot Model ICFB Reactor.....	273
H.1 Fe/ZSM-5(PUC).....	273
H.2 Fe/ZSM-5(Albemarle).....	277

List of Tables

Table 1.1 Typical compositions of flue gases from thermal power plant stacks	2
Table 3.1 Properties of the catalyst supports	37
Table 4.1 Dimensions of the cold model ICFB unit	108
Table 5.1 Geometric dimensions of the ICFB reactor	153
Table 5.2 Properties of catalysts used in the hot model experiments	154
Table A.1 HC-SCR catalysts supported by zeolites.....	219
Table A.2 HC-SCR catalysts supported by non-zeolites (Metal oxides).....	220
Table A.3 Specifications of some typical HC-SCR catalysts	221
Table A.4 HC-SCR with methane as reducing agent.....	222
Table A.5 HC-SCR with propane as reducing agent	224
Table A.6 HC-SCR with propylene as reducing agent	226
Table A.7 HC-SCR with iso-C ₄ H ₁₀ (iso-butane) as reducing agent	229
Table A.8 HC-SCR with other hydrocarbons as reducing agent	232
Table A.9 HC-SCR with oxygenated hydrocarbons as reducing agent	234
Table A.10 NSR with reducing agent	235
Table C.1 BET surface areas for catalysts used in this work.....	243

List of Figures

Figure 1.1 NO _x control effectiveness for coal-fired tangential boilers.....	3
Figure 1.2 Schematic of the integrated adsorption-reduction process of NO _x	7
Figure 2.1 NO conversion to N ₂ over Cu/ZSM-5 catalysts as a function of Cu/Al ratio at different temperatures.....	11
Figure 2.2 Dependence of NO conversion on temperature for SCR of NO over various catalysts with alternative reducing agent.....	17
Figure 2.3 Temperature dependence of N ₂ yield over Fe/ZSM-5 with different hydrocarbons	18
Figure 2.4 Effect of the nature of the hydrocarbon on NO reduction selectivity on Co/ZSM-5	19
Figure 2.5 NO conversion to N ₂ on Ag/Al ₂ O ₃ using alternative reducing agent.....	20
Figure 2.6 Effect of H ₂ O on NO conversion to N ₂ over Fe/ZSM-5 or Cu/ZSM-5.....	24
Figure 2.7 Influence of O ₂ concentration on NO conversion to N ₂	27
Figure 3.1 The fixed bed reaction system.....	33
Figure 3.2 Adsorption curves based on NO _x concentrations at the reactor outlet (Catalyst: Fe/ZSM-5(PUC), T=250°C).....	39
Figure 3.3 Fitted adsorption isotherms of NO _x by Freundlich equation (Catalyst: Fe/ZSM- 5(PUC))	41
Figure 3.4 Relationship between α/β and adsorption temperature (Catalyst: Fe/ZSM-5(PUC))	41
Figure 3.5 Profiles of NO _x and HC conversions and outlet CO concentration (Catalyst: Fe/ZSM-5(PUC), T=250°C, [O ₂]=1%).....	44

Figure 3.6 Profiles of NO _x and HC conversions and outlet CO concentration (Catalyst: Fe/ZSM-5(PUC), T=350°C, [O ₂]=1%).....	45
Figure 3.7 Effect of reaction temperature on NO _x conversion (Catalyst: Fe/ZSM-5(PUC)) .	47
Figure 3.8 Effect of reaction temperature on HC conversion (Catalyst: Fe/ZSM-5(PUC))...	47
Figure 3.9 Effect of inlet O ₂ concentration on the catalytic activity (Catalyst: Fe/ZSM-5(PUC))	50
Figure 3.10 Comparison of BET surface areas (Catalyst: Fe/ZSM-5 (PUC)).....	51
Figure 3.11 XPS narrow scan for C 1s (Catalyst: Fe/ZSM-5(PUC))	52
Figure 3.12 TGA result for the catalyst aged at 275°C.....	54
Figure 3.13 TGA result for the catalyst aged at 350°C.....	54
Figure 3.14 Recovery of catalyst activity under different regeneration conditions (Catalyst: Fe/ZSM-5(PUC)).....	55
Figure 3.15 Effect of GHSV on catalytic activity (Catalyst: Fe/ZSM-5(PUC), T=325°C)....	56
Figure 3.16 Effect of GHSV on catalytic activity (Catalyst: Fe/ZSM-5(PUC), T=350°C)....	57
Figure 3.17 Effect of HC:NO ratio and O ₂ level on catalytic activity (Catalyst: Fe/ZSM-5(PUC), T=275°C, 95% confidence level)	59
Figure 3.18 Effect of HC:NO ratio and O ₂ level on catalytic activity (Catalyst: Fe/ZSM-5(PUC), T=300°C).....	61
Figure 3.19 Effect of HC:NO ratio and O ₂ level on catalytic activity (Catalyst: Fe/ZSM-5(PUC), T=325°C).....	62
Figure 3.20 Effect of HC:NO ratio and O ₂ level on catalytic activity (Catalyst: Fe/ZSM-5(PUC), T=350°C).....	63
Figure 3.21 Effect of HC:NO ratio and O ₂ level on catalytic activity (Catalyst: Fe/ZSM-5(PUC), T=375°C).....	64

Figure 3.22 Effect of temperature on catalytic activity for NO _x reduction (Catalyst: Fe/ZSM-5(PUC, WIE)).....	66
Figure 3.23 Effect of temperature on NO _x and HC conversion (Catalyst: Fe/ZSM-5(PUC, WIE)).....	68
Figure 3.24 Adsorption curves based on NO _x concentrations at the reactor outlet (Catalyst: Fe/ZSM-5(Albemarle), T=275°C).....	70
Figure 3.25 Fitting of adsorption isotherms of NO _x by Freundlich equation (Catalyst: Fe/ZSM-5(Albemarle)).....	71
Figure 3.26 Relationship between α/β and adsorption temperature (Catalyst: Fe/ZSM-5(Albemarle))	72
Figure 3.27 Effect of O ₂ concentration in the flue gas on the adsorption capacity of Fe/ZSM-5(Albemarle)) catalyst.....	74
Figure 3.28 Effect of H ₂ O and CO ₂ in the flue gas on adsorption isotherms (Catalyst: Fe/ZSM-5(Albemarle)).....	75
Figure 3.29 Comparison of adsorption isotherm between Fe/ZSM-5(Albemarle) and parent H/ZSM-5(Albemarle) at T=350°C	76
Figure 3.30 Catalytic activity of parent H/ZSM-5(Albemarle)	78
Figure 3.31 Profiles of NO _x and HC conversions and outlet CO concentration (Fe/ZSM-5(Albemarle), T=275°C, [O ₂]=1%).....	80
Figure 3.32 Profiles of NO _x and HC conversions and outlet CO concentration (Fe/ZSM-5(Albemarle), T=350°C, [O ₂]=1%).....	81
Figure 3.33 Effect of temperature on the catalytic activity of Fe/ZSM-5(Albemarle).....	83
Figure 3.34 Effect of GHSV on the catalytic activity of Fe/ZSM-5(Albemarle).....	85
Figure 3.35 Effect of O ₂ and HC concentrations (Fe/ZSM-5(Albemarle), T=350°C).....	87

Figure 3.36 Effect of O ₂ and HC concentrations (Fe/ZSM-5(Albemarle), T=375°C).....	88
Figure 3.37 Effect of CO ₂ on the catalytic activity of Fe/ZSM-5(Albemarle) (T=350°C).....	90
Figure 3.38 Effect of H ₂ O on the catalytic activity of Fe/ZSM-5(Albemarle) (T=350°C).....	91
Figure 3.39 Time-on-stream test on the effect of H ₂ O (Fe/ZSM-5(Albemarle), T=350°C)...	92
Figure 3.40 Combined effect of H ₂ O and CO ₂ on the catalytic activity of Fe/ZSM-5(Albemarle) (T=350°C)	93
Figure 3.41 Effect of the addition of H ₂ O on outlet CO and CO ₂ concentrations (Fe/ZSM-5(Albemarle), T=350°C).....	94
Figure 3.42 Effect of SO ₂ on the catalytic activity of Fe/ZSM-5(Albemarle) (200ppm SO ₂ , Run #1)	96
Figure 3.43 Effect of SO ₂ on the catalytic activity of Fe/ZSM-5(Albemarle) (200ppm SO ₂ , Run #2)	97
Figure 3.44 Effect of SO ₂ on the catalytic activity of Fe/ZSM-5(Albemarle) (200ppm SO ₂ , Run #3)	98
Figure 3.45 Effect of SO ₂ on the catalytic activity of Fe/ZSM-5(Albemarle) (200ppm SO ₂ , Run #4)	98
Figure 3.46 Comparison of the four consecutive runs with 200ppm SO ₂ in the flue gas (Catalyst: Fe/ZSM-5(Albemarle)).....	99
Figure 3.47 Comparison of fresh and regenerated catalysts over four consecutive runs (Catalyst: Fe/ZSM-5(Albemarle)).....	100
Figure 3.48 Effect of SO ₂ on the catalytic activity of Fe/ZSM-5(Albemarle) (30ppm SO ₂)	101
Figure 3.49 Comparison of BET surface areas for fresh and deactivated catalyst (Fe/ZSM-5(Albemarle))	102
Figure 4.1 Schematic of the cold model ICFB reactor	107

Figure 4.2 Schematics of the cold model ICFB system.....	110
Figure 4.3 Schematic of the mass transfer between draft tube and annulus	111
Figure 4.4 Configurations of the flat distributor for the annulus gas flow	115
Figure 4.5 Effect of gas velocities on gas bypass (Flat distributor, $H_G=10$ mm)	118
Figure 4.6 Effect of gas velocities on gas bypass (Flat distributor, $H_G=6$ mm)	119
Figure 4.7 Effect of gas velocities on solids circulation rate (Flat distributor, $H_G=10$ mm) ..	121
Figure 4.8 Effect of gas velocities on solids circulation rate (Flat distributor, $H_G=6$ mm) ..	121
Figure 4.9 Configurations of the cylindrical distributor for the annulus gas flow	123
Figure 4.10 Effect of gas velocities on gas bypass (Cylindrical distributor, $H_{G1}=10$ mm) ..	125
Figure 4.11 Effect of gas velocities on gas bypass (Cylindrical distributor, $H_{G1}=20$ mm) ..	126
Figure 4.12 Effect of gas velocities on gas bypass (Cylindrical distributor, $H_{G1}=60$ mm) ..	128
Figure 4.13 Effect of gas velocities on solids circulation rate (Cylindrical distributor, $H_{G1}=10$ mm)	129
Figure 4.14 Effect of gas velocities on solids circulation rate (Cylindrical distributor, $H_{G1}=20$ mm)	130
Figure 4.15 Effect of gas velocities on solids circulation rate (Cylindrical distributor, $H_{G1}=60$ mm)	131
Figure 4.16 Configuration of the conical distributor for the annulus gas flow.....	132
Figure 4.17 Effect of gas velocities on gas bypass (Conical distributor, $H_G=10$ mm)	133
Figure 4.18 Effect of gas velocities on gas bypass (Conical distributor, $H_G=15$ mm)	135
Figure 4.19 Effect of gas velocities on solids circulation rate (Conical distributor, $H_G=10$ mm).....	136
Figure 4.20 Effect of gas velocities on solids circulation rate (Conical distributor, $H_G=15$ mm).....	137

Figure 4.21 Effect of overall gas velocity on solids circulation rate using conical distributor ($H_G=10$ mm)	139
Figure 4.22 Effect of overall gas velocity on solids circulation rate using conical distributor ($H_G=15$ mm)	139
Figure 4.23 Configuration of the conical distributor in the hot model ICFB reactor	140
Figure 4.24 Effect of gas velocities on gas bypass (Fe/ZSM-5(PUC), $T=350\pm 10^\circ\text{C}$)	143
Figure 4.25 Effect of gas velocities on gas bypass (Fe/ZSM-5(Albemarle), $T=355\pm 15^\circ\text{C}$)	145
Figure 5.1 Schematic of hot model ICFB reaction system	152
Figure 5.2 Effect of gas velocities and HC:NO ratio on NO_x conversion using the draft tube as the adsorption zone (ICFB, Fe/ZSM-5(PUC)).....	159
Figure 5.3 Effect of catalyst loading on NO_x conversion and adsorption (ICFB, Fe/ZSM- 5(PUC))	160
Figure 5.4 Effect of HC:NO ratio on NO_x conversion (ICFB, Fe/ZSM-5(PUC)).....	162
Figure 5.5 Effect of flue gas O_2 concentration on NO_x conversion (ICFB, Fe/ZSM-5(PUC))	163
Figure 5.6 Effect of gas velocities on NO_x conversion and adsorption (ICFB, Fe/ZSM- 5(PUC))	164
Figure 5.7 Effect of inlet NO concentration on NO_x conversion (Fluidized bed, Fe/ZSM- 5(PUC), $[\text{O}_2]=4\%$).....	166
Figure 5.8 Effect of inlet NO concentration on NO_x conversion (Fluidized bed, Fe/ZSM- 5(PUC), $[\text{O}_2]=2.5\%$).....	166
Figure 5.9 Effect of inlet NO concentration on NO_x conversion (Fluidized bed, Fe/ZSM- 5(PUC), $[\text{O}_2]=1\%$).....	167

Figure 5.10 Effect of HC:NO on NO _x and HC conversions (Fluidized bed, Fe/ZSM-5(PUC), [NO]=300ppm)	169
Figure 5.11 Effect of HC:NO on NO _x and HC conversions (Fluidized bed, Fe/ZSM-5(PUC), [NO]=600ppm)	170
Figure 5.12 Effect of HC:NO on NO _x and HC conversions (Fluidized bed, Fe/ZSM-5(PUC), [NO]=900ppm)	171
Figure 5.13 Effect of inlet O ₂ concentration on NO _x and HC conversions (Fluidized bed, Fe/ZSM-5(PUC)).....	173
Figure 5.14 Comparison of NO _x conversion between ICFB and fluidized bed reactors (Fe/ZSM-5(PUC))	174
Figure 5.15 Effect of HC:NO ratio on NO _x and HC conversions (ICFB, Fe/ZSM-5(Albemarle), U _D =0.6 m/s, [O ₂]=4%).....	176
Figure 5.16 Effect of HC:NO ratio on NO _x and HC conversions (ICFB, Fe/ZSM-5(Albemarle), U _D =0.75 m/s, [O ₂]=4%).....	176
Figure 5.17 Effect of HC:NO ratio on NO _x and HC conversions (ICFB, Fe/ZSM-5(Albemarle), U _D =0.9 m/s, [O ₂]=4%).....	177
Figure 5.18 Effect of HC:NO ratio on NO _x and HC conversions (ICFB, Fe/ZSM-5(Albemarle), U _D =0.6 m/s, [O ₂]=8%).....	177
Figure 5.19 Effect of HC:NO ratio on NO _x and HC conversions (ICFB, Fe/ZSM-5(Albemarle), U _D =0.75 m/s, [O ₂]=8%).....	178
Figure 5.20 Effect of HC:NO ratio on NO _x and HC conversions (ICFB, Fe/ZSM-5(Albemarle), U _D =0.9 m/s, [O ₂]=8%).....	178
Figure 5.21 Effect of flue gas O ₂ concentration on NO _x conversion and adsorption (ICFB, Fe/ZSM-5(Albemarle), U _D =0.6 m/s, HC:NO=2)	180

Figure 5.22 Effect of flue gas O ₂ concentration on NO _x conversion and adsorption (ICFB, Fe/ZSM-5(Albemarle), U _D =0.75 m/s, HC:NO=2)	181
Figure 5.23 Effect of flue gas O ₂ concentration on NO _x conversion and adsorption (ICFB, Fe/ZSM-5(Albemarle), U _D =0.9 m/s, HC:NO=2)	181
Figure 5.24 Effect of gas velocities on NO _x conversion and adsorption (ICFB, Fe/ZSM-5(Albemarle), [O ₂]=4%, HC:NO=1)	183
Figure 5.25 Effect of gas velocities on NO _x conversion and adsorption (ICFB, Fe/ZSM-5(Albemarle), [O ₂]=4%, HC:NO=2)	183
Figure 5.26 Effect of gas velocities on NO _x conversion and adsorption (ICFB, Fe/ZSM-5(Albemarle), [O ₂]=8%, HC:NO=2)	184
Figure 5.27 Effect of gas velocities on NO _x conversion and adsorption (ICFB, Fe/ZSM-5(Albemarle), [O ₂]=12%, HC:NO=2)	185
Figure 5.28 Effect of HC:NO ratio on NO _x and HC conversions (Fluidized bed, Fe/ZSM-5(Albemarle), [O ₂]=1%)	186
Figure 5.29 Effect of HC:NO ratio on NO _x and HC conversions (Fluidized bed, Fe/ZSM-5(Albemarle), [O ₂]=4%)	187
Figure 5.30 Effect of HC:NO ratio on NO _x and HC conversions (Fluidized bed, Fe/ZSM-5(Albemarle), [O ₂]=8%)	187
Figure 5.31 Effect of inlet O ₂ concentration on NO _x and HC conversions (Fluidized bed, Fe/ZSM-5(Albemarle), HC:NO=1)	189
Figure 5.32 Effect of inlet O ₂ concentration on NO _x and HC conversions (Fluidized bed, Fe/ZSM-5(Albemarle), HC:NO=2)	189
Figure 5.33 Comparison of NO _x conversion between ICFB and fluidized bed reactors (Fe/ZSM-5(Albemarle))	191

Figure B.1 Calibration curve of FL-1473G rotameter (0.6% NO + N ₂).....	236
Figure B.2 Calibration curve of FL-1473G rotameter (50% O ₂ + N ₂)	237
Figure B.3 Calibration curve of FL-1472S rotameter (1.2% Propylene + N ₂).....	237
Figure B.4 Calibration curve of FL-1473S rotameter (N ₂).....	238
Figure B.5 Calibration curve of FL-1476G rotameter (N ₂)	238
Figure B.6 Calibration curve of peristaltic water pump	239
Figure B.7 Calibration curve of pressure transducer (Channel #1)	240
Figure B.8 Calibration curve of pressure transducer (Channel #2)	241
Figure B.9 Calibration curve of pressure transducer (Channel #3)	241
Figure B.10 Calibration curve of pressure transducer (Channel #4)	242
Figure B.11 Calibration curve of pressure transducer (Channel #6)	242
Figure D.1 Particle size distribution (Fe/ZSM-5(PUC)).....	244
Figure D.2 Particle size distribution (Fe/ZSM-5(crushed PUC)).....	245
Figure D.3 Particle size distribution (Fe/ZSM-5(Albemarle))	245
Figure D.4 Particle size distribution (Fe/FCC(Spent)).....	246
Figure E.1 Adsorption curves based on NO _x concentrations at the reactor outlet (Catalyst: Fe/ZSM-5(crushed PUC), T=325°C).....	248
Figure E.2 Adsorption curves based on NO _x concentrations at the reactor outlet (Catalyst: Fe/ZSM-5(crushed PUC), T=350°C).....	248
Figure E.3 Adsorption curves based on NO _x concentrations at the reactor outlet (Catalyst: Fe/ZSM-5(crushed PUC), T=375°C).....	249
Figure E.4 Fitting of adsorption isotherms of NO _x by Freundlich equation (Catalyst: Fe/ZSM-5(crushed PUC))	250

Figure E.5 Relationship between α/β and adsorption temperature (Catalyst: Fe/ZSM-5 (crushed PUC)).....	251
Figure E.6 Effect of reaction temperature on catalytic activity (Catalyst: Fe/ZSM-5(crushed PUC)).....	252
Figure E.7 Effect of inlet O ₂ concentration on catalytic activity (Catalyst: Fe/ZSM-5(crushed PUC)).....	253
Figure F.1 HC-SCR performance of spent FCC and Fe/FCC	254
Figure G.1 Adsorption curves based on NO _x concentrations at the reactor outlet (Catalyst: Fe/ZSM-5(PUC), T=280°C)	255
Figure G.2 Adsorption curves based on NO _x concentrations at the reactor outlet (Catalyst: Fe/ZSM-5(PUC), T=310°C)	256
Figure G.3 Adsorption curves based on NO _x concentrations at the reactor outlet (Catalyst: Fe/ZSM-5(PUC), T=340°C)	256
Figure G.4 Adsorption curves based on NO _x concentrations at the reactor outlet (Catalyst: Fe/ZSM-5(PUC), T=370°C)	257
Figure G.5 Adsorption curves based on NO _x concentrations at the reactor outlet (Catalyst: Fe/ZSM-5(PUC), T=400°C)	257
Figure G.6 Adsorption curves based on NO _x concentrations at the reactor outlet (Catalyst: Fe/ZSM-5(Albemarle), T=300°C).....	258
Figure G.7 Adsorption curves based on NO _x concentrations at the reactor outlet (Catalyst: Fe/ZSM-5(Albemarle), T=325°C).....	258
Figure G.8 Adsorption curves based on NO _x concentrations at the reactor outlet (Catalyst: Fe/ZSM-5(Albemarle), T=350°C).....	259

Figure G.9 Adsorption curves based on NO _x concentrations at the reactor outlet (Catalyst: Fe/ZSM-5(Albemarle), T=375°C).....	259
Figure G.10 Adsorption curves based on NO _x concentrations at the reactor outlet (Catalyst: Fe/ZSM-5(Albemarle), T=350°C, 10% H ₂ O added).....	260
Figure G.11 Adsorption curves based on NO _x concentrations at the reactor outlet (Catalyst: Fe/ZSM-5(Albemarle), T=350°C, 10% CO ₂ added).....	260
Figure G.12 Adsorption curves based on NO _x concentrations at the reactor outlet (Catalyst: Fe/ZSM-5(Albemarle), T=350°C, 10% H ₂ O + 10% CO ₂ added)	261
Figure G.13 Profiles of NO _x and HC conversions and outlet CO concentration in time-on-stream test (Catalyst: Fe/ZSM-5(PUC), T=275°C, [O ₂]=1%).....	262
Figure G.14 Profiles of NO _x and HC conversions and outlet CO concentration in time-on-stream test (Catalyst: Fe/ZSM-5(PUC), T=275°C, [O ₂]=4%).....	263
Figure G.15 Profiles of NO _x and HC conversions and outlet CO concentration in time-on-stream test (Catalyst: Fe/ZSM-5(PUC), T=300°C, [O ₂]=1%).....	264
Figure G.16 Profiles of NO _x and HC conversions and outlet CO concentration in time-on-stream test (Catalyst: Fe/ZSM-5(PUC), T=325°C, [O ₂]=1%).....	265
Figure G.17 Profiles of NO _x and HC conversions and outlet CO concentration in time-on-stream test (Catalyst: Fe/ZSM-5(Albemarle), T=300°C, [O ₂]=1%).....	266
Figure G.18 Profiles of NO _x and HC conversions and outlet CO concentration in time-on-stream test (Catalyst: Fe/ZSM-5(Albemarle), T=325°C, [O ₂]=1%).....	267
Figure G.19 Profiles of NO _x and HC conversions and outlet CO concentration in time-on-stream test (Catalyst: Fe/ZSM-5(Albemarle), T=375°C, [O ₂]=1%).....	268
Figure G.20 XPS survey scan for fresh Fe/ZSM-5(PUC)	269
Figure G.21 XPS survey scan for spent Fe/ZSM-5(PUC).....	270

Figure G.22 XPS survey scan for regenerated Fe/ZSM-5(PUC)	270
Figure G.23 Comparison of XPS narrow scan of Al 2p	271
Figure G.24 Comparison of XPS narrow scan of Si 2p.....	271
Figure G.25 Comparison of XPS narrow scan of O 1s.....	272
Figure G.26 Comparison of XPS narrow scan of Fe 2p 3/2.....	272
Figure H.1 Effect of U_D on gas bypass (Fe/ZSM-5(PUC), $U_A=0.20$ m/s, $T=350\pm 10^\circ\text{C}$)	273
Figure H.2 Effect of U_D on gas bypass (Fe/ZSM-5(PUC), $U_A=0.30$ m/s, $T=350\pm 10^\circ\text{C}$)	274
Figure H.3 Effect of U_D on gas bypass (Fe/ZSM-5(PUC), $U_A=0.35$ m/s, $T=350\pm 10^\circ\text{C}$)	274
Figure H.4 Effect of U_D on gas bypass (Fe/ZSM-5(PUC), $U_A=0.40$ m/s, $T=350\pm 10^\circ\text{C}$)	275
Figure H.5 Effect of U_D on gas bypass (Fe/ZSM-5(PUC), $U_A=0.45$ m/s, $T=350\pm 10^\circ\text{C}$)	275
Figure H.6 Effect of U_D on gas bypass (Fe/ZSM-5(PUC), $U_A=0.50$ m/s, $T=350\pm 10^\circ\text{C}$)	276
Figure H.7 Effect of U_D on gas bypass (Fe/ZSM-5(PUC), $U_A=0.55$ m/s, $T=350\pm 10^\circ\text{C}$)	276
Figure H.8 Effect of gas velocities on R_{DA} (Fe/ZSM-5(Albemarle), $T=355\pm 15^\circ\text{C}$)	277
Figure H.9 Effect of gas velocities on R_{AD} (Fe/ZSM-5(Albemarle), $T=355\pm 15^\circ\text{C}$)	278
Figure H.10 Effect of U_D on gas bypass (Fe/ZSM-5(Albemarle), $U_A=0.20$ m/s, $T=355\pm 15^\circ\text{C}$).....	278
Figure H.11 Effect of U_D on gas bypass (Fe/ZSM-5(Albemarle), $U_A=0.25$ m/s, $T=355\pm 15^\circ\text{C}$).....	279
Figure H.12 Effect of U_D on gas bypass (Fe/ZSM-5(Albemarle), $U_A=0.30$ m/s, $T=355\pm 15^\circ\text{C}$).....	279
Figure H.13 Effect of U_D on gas bypass (Fe/ZSM-5(Albemarle), $U_A=0.35$ m/s, $T=355\pm 15^\circ\text{C}$).....	280
Figure H.14 Effect of U_D on gas bypass (Fe/ZSM-5(Albemarle), $U_A=0.40$ m/s, $T=355\pm 15^\circ\text{C}$).....	280

Figure H.15 Effect of U_D on gas bypass (Fe/ZSM-5(Albemarle), $U_A=0.45$ m/s, $T=355\pm 15^\circ\text{C}$).....	281
Figure H.16 Effect of U_A on gas bypass (Fe/ZSM-5(Albemarle), $U_D=0.45$ m/s, $T=355\pm 15^\circ\text{C}$).....	281
Figure H.17 Effect of U_A on gas bypass (Fe/ZSM-5(Albemarle), $U_D=0.60$ m/s, $T=355\pm 15^\circ\text{C}$).....	282
Figure H.18 Effect of U_A on gas bypass (Fe/ZSM-5(Albemarle), $U_D=0.75$ m/s, $T=355\pm 15^\circ\text{C}$).....	282
Figure H.19 Effect of U_A on gas bypass (Fe/ZSM-5(Albemarle), $U_D=0.90$ m/s, $T=355\pm 15^\circ\text{C}$).....	283

Acronyms

AOFA	Advanced overfire air
CVD	Chemical vapour deposition
Fe(AA) ₃	Iron(III) acetylacetonate
GHSV	Gas hourly space velocity, h ⁻¹
HC	Hydrocarbon
HC-SCR	Selective catalytic reduction with hydrocarbons
ICFB	Internal circulating fluidized bed
I.D.	Inner diameter
IMP	Impregnation
IMPA	Incipient wetness impregnation in aqueous solution
IMPO	Impregnation in organic solution
LNB	Low NO _x burner
MFI	One type of zeolite
M.W.	Molecular weight
NSCR	Non-selective catalytic reduction
NSR	NO _x storage-reduction
O.D.	Outer diameter
PUC	China University of Petroleum (Beijing, China)
SCR	Selective catalytic reduction
SNCR	Selective non-catalytic reduction
SSIE	Solid state ion exchange
Std. T	Standard temperature, 25°C

SUB	Sublimation
SUZ-4	One kind of zeolite
TGA	Thermogravimetric analysis
TOS	Time on stream
TPD	Temperature programmed desorption
VOC	Volatile organic compound
WIE	Wet ion exchange
XPS	X-ray photoelectron spectroscopy
ZSM-5	One kind of MFI

Nomenclature

C_0	Equilibrium NO_x concentration, ppm
C_{A,O_2}	O_2 concentration in the annulus, %
C_{A0,O_2}	O_2 concentrations at inlet of the annulus, %
$C_{\text{CO},\text{out}}$	CO concentration in gas mixture at reactor outlet, ppm
$C_{\text{CO}_2,0}$	Initial CO_2 concentration in flue gas feed, %
$C_{\text{CO}_2,\text{out}}$	CO_2 concentration in gas mixture at reactor outlet, %
C_{D,O_2}	O_2 concentration in the draft tube, %
C_{D0,O_2}	O_2 concentrations at inlet of the draft tube, %
$C_{\text{HC},\text{in}}$	Inlet concentration of propylene, ppm
$C_{\text{NO}_x,0}$	Initial NO_x concentration in flue gas feed, ppm
$C_{\text{NO}_x,\text{ ads},\text{in}}$	Real initial NO_x concentration for adsorption at adsorption zone inlet, ppm
$C_{\text{NO}_x,\text{ads},\text{ out}}$	NO_x concentration at adsorption zone outlet, ppm
$C_{\text{NO}_x,\text{in}}$	Initial NO_x concentration in total gas flow , ppm
$C_{\text{NO}_x,\text{out}}$	NO_x concentration in gas mixture at reactor outlet, ppm
D_i	Inner diameter of fixed bed reactor, mm
d_p	Mean particle diameter, mm
F	Gas flow rate at ambient temperature, m^3/s
F_A	Volumetric gas flow rate at annulus outlet, m^3/s
$F_{A,0}$	Volumetric gas flow rate at annulus inlet, m^3/s
F_{AD}	Volumetric gas bypass rate from annulus to draft tube, m^3/s
F_D	Volumetric gas flow rate at draft tube outlet, m^3/s
$F_{D,0}$	Volumetric gas flow rate at draft tube inlet, m^3/s
F_{DA}	Volumetric gas bypass rate from draft tube to annulus, m^3/s

Nomenclature

$F_{F,0}$	Flue gas flow rate, m^3/s
F_{FR}	Calculated gas bypass from adsorption zone to reduction zone, m^3/s
$F_{HC,0}$	Flow rate of 40% Propylene + N_2 , m^3/s
$F_{R,0}$	Reductant gas flow rate, m^3/s
F_{RF}	Calculated gas bypass from reduction zone to adsorption zone, m^3/s
h	Catalyst packed height in fixed bed reactor, mm
H_G	Effective gap opening for solids circulation, mm
H_{G1}	Gap between draft tube and annulus gas distributor, mm
H_{G2}	Gap between draft tube and annulus gas distributor, mm
L	Tracer particle downward moving distance along column, m
M_{NO}	Molecular weight of NO, g/mol
P	Operating pressure, atm
q_e	Adsorption equilibrium capacity of NO_x on catalyst, mg/g
R	Universal gas constant, 8.314 J/(mol.K)
R_{AD}	Gas bypass ratio from annulus to draft tube, %
R_{DA}	Gas bypass ratio from draft tube to annulus, %
S	Integrated area from adsorption curve, s
S_A	Cross-sectional area of annulus, m^2
S_D	Cross-sectional area of draft tube, m^2
t	Adsorption time, s
T	Reaction temperature, $^{\circ}C$
T_0	Ambient temperature, $^{\circ}C$
t_m	Time interval for tracer particle moving L , s
U	Overall gas velocity in ICFB reactor, m/s

Nomenclature

U_A	Gas velocity in annulus, m/s
U_D	Gas velocity in draft tube, m/s
U_{mf}	Minimum fluidizing velocity, m/s
U_p	Tracer particle downward velocity in annulus, m/s
W_{cat}	Catalyst loading, g
W_s	Solids circulation rate based on draft tube cross-sectional area, $kg/m^2.s$
x_A	Volume fraction of CO_2 in gas flow at annulus outlet, -
$x_{A,0}$	Volume fraction of CO_2 in gas flow at annulus inlet, -
x_{AD}	Volume fraction of CO_2 in gas bypass flow from annulus to draft tube, -
x_D	Volume fraction of CO_2 in gas flow at draft tube outlet, -
$x_{D,0}$	Volume fraction of CO_2 in gas flow at draft tube inlet, -
x_{DA}	Volume fraction of CO_2 in gas bypass flow from draft tube to annulus, -
X_{HC}	Propylene conversion, %
X_{NO_x}	NO_x conversion, %
$X_{NO_x, ads}$	Adsorption ratio of NO_x in adsorption zone, %
$X_{NO_x, BM}$	Benchmark NO_x conversion caused by bypassing HC from reduction zone, %
α	Coefficient in Freundlich equation, -
β	Coefficient in Freundlich equation, -
ε	Bed voidage in annulus, -
ρ_{air}	Air density, kg/m^3
ρ_{CO_2}	CO_2 density, kg/m^3
ρ_p	Particle bulk density, kg/m^3

Acknowledgements

I would like to take this opportunity to express my sincere gratitude to my supervisor, Dr. Xiaotao Bi, for his immense guidance and financial assistance during my research. I give my utmost appreciation to my research committee members, Dr. Kevin Smith and Dr. Robert Evans, for their valuable suggestions at the start of this work.

Many individuals who contributed to this research would be greatly acknowledged. Mr. Tianzhu Zhang, a former visiting scholar from China, contributed a lot to the setup of the fixed bed reaction system and the design of the cold model unit. Mr. Yuanqing (Larry) Liu, an undergraduate student of class 2008, was of great assistance to the adsorption and reaction kinetics study in the fixed bed reactor during the research on his undergraduate thesis. Mr. Shahin Goodarznia from Dr. Kevin Smith's research group helped with the measurement of the catalyst BET surface area. Ms. Yonika Wiputri from Dr. Peter Englezos's research group helped with the measurement of the particle size distribution. I also appreciate the hard work of the technical and administrative staff in the department stores, workshop and offices.

Na/ZSM-5(PUC) was purchased from the Petroleum University of China with the help of Professors Weisheng Wei and Xiaojun Bao. H/ZSM-5(Albemarle) was a free sample offered by Dr. Maria M. Ludvig from Albemarle Catalysts Co., USA.

This research was financially supported by the Canada Foundation for Innovation (CFI) and the Natural Sciences and Engineering Research Council of Canada (NSERC). I am also grateful to a NSERC postgraduate scholarship (PGS-D).

Last but not least, I am sincerely grateful to my wife Jessica, my daughter Rena, my parents and my parents-in-law, for their endless support and encouragement throughout my whole life.

Chapter 1

Introduction

Nitrogen oxides (NO_x) are emitted primarily from transportation and other industrial sources, and contribute to many problems that threaten the quality of the environment and human health: the formation of acid rain and ground level ozone (smog), and general atmospheric visibility degradation. Man-made nitrogen oxides are mainly classified into two types, depending on their sources: stationary or mobile.

1.1 Formation of NO_x

NO_x form when fuel is burned at high temperatures. N_2 and O_2 present in the fuel and air can combine chemically to form one or more of seven oxides of N: NO , NO_2 , NO_3 , N_2O , N_2O_3 , N_2O_4 and N_2O_5 . For most combustion processes, particularly fossil fuel combustions, both the molecular N in the air and the chemically bound N in the fuel can be oxidized by O_2 to form NO_x , and the only oxides of nitrogen present in significant concentration in flue gases are NO and NO_2 with NO representing 90 to 95% of the total NO_x (Wark et al., 1998). The colorless and odorless NO , in the presence of radicals from VOCs or O_2 in the air, will be gradually oxidized to NO_2 if sufficient time is given. NO_2 is a reddish-brown, toxic gas, which is a precursor for photochemical smog formation in the presence of certain hydrocarbons and sunlight, and along with particles in the air, NO_2 can often be seen as a reddish-brown layer over many urban areas.

NO_x are produced in a variety of processes, mainly in the combustion process of fossil fuels, such as engines of vehicles and aircraft, combustion equipment, gas turbines, incinerators, kilns and power plants. NO_x also are emitted as by-products from many

metallurgical processes where nitric acid is used as an oxidant. Typical NO_x concentrations in flue gases from power plants are shown in Table 1.1.

Table 1.1 Typical compositions of flue gases from thermal power plant stacks

Fuel	Natural gas	Fuel oil	Coal
NO _x (ppm)	25–160	100–600	150–1000
SO _x (ppm)	<0.5–20	200–2000	200–2000
CO ₂ (%)	5–12	12–14	10–15
O ₂ (%)	3–18	2–5	3–5
H ₂ O (%)	8–19	9–12	7–10
N ₂	Balance	Balance	Balance

1.2 Methods for the abatement of NO_x emissions

Due to the increasingly stringent emission regulations on NO_x all over the world, the method for the abatement of NO_x emission has gained extensive attention from academic as well as industrial research groups. In industrial combustion processes, NO_x control can be accomplished by three primary methods, i.e., pre-combustion, combustion modification and post-combustion control techniques, which involve the use of low nitrogen fuels, modification of the combustion design and operating features of the combustion unit, and flue gas treatment, respectively. As an effective pollution prevention practice, the pre-combustion and combustion modification technologies have been widely used in combustion processes (Wark et al, 1998; de Nevers, 2000). Although NO_x abatement at control efficiencies lower than 60% can be achieved by pre-combustion and combustion modification techniques at relatively low cost, expensive downstream treatment (e.g. SCR) is still required to reach control efficiencies higher than 75% in order to meet stringent emission regulations, as shown in Figure 1.1.

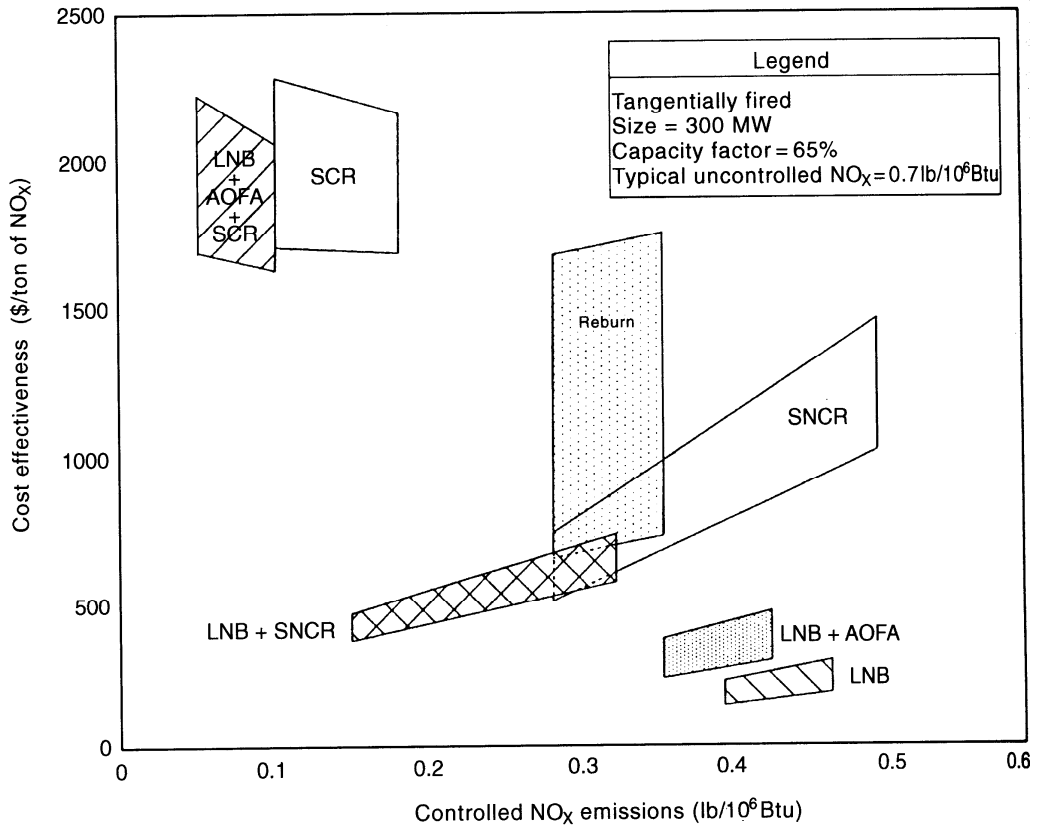


Figure 1.1 NO_x control effectiveness for coal-fired tangential boilers

(Source: Alternative Control Techniques Document – NO_x Emission from Utility Boilers, EPA-453/R-94-023, U.S. EPA OAQPS, 1994).

To date, there are four ways to abate NO_x in flue gases: direct catalytic decomposition, non-selective catalytic reduction (NSCR), selective non-catalytic reduction (SNCR) and selective catalytic reduction (SCR).

Direct catalytic decomposition of NO_x might be the most attractive method for NO_x control, but the NO_x conversion is not high enough for the practical application (Parvulescu et al., 1998; Liu and Woo, 2006; Shi et al., 2008).

The best example of non-selective catalytic reduction (NSCR) of NO_x is the three-way catalytic converter which has been commercialized successfully for reducing NO_x in the

exhaust gases from gasoline engines (Parvulescu et al., 1998). However, it could not be applied to lean-burn engines where excess oxygen is present in the exhaust gases (Goralski and Schneider, 2002).

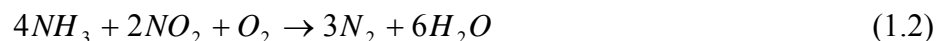
Using gas-phase free-radical reactions instead of a catalyst to promote reactions in the selective non-catalytic reduction (SNCR) process, NH_3 is injected into the flue gas to reduce NO_x via the gas phase homogeneous reaction between NH_3 and NO_x . In order to achieve a high NO_x reduction, the gas mixture must be kept within a relatively narrow and high temperature window of 900~1100°C. If the reaction temperature is lower than 800°C, NO_x conversion will be very low and most NH_3 remains un-reacted in the flue gas. At a temperature higher than 1200°C, NH_3 will be oxidized by O_2 to form NO , rather than being oxidized by NO to form N_2 (Muzio and Quartucy, 1997; Javed et al., 2007).

Selective catalytic reduction, so called SCR, selectively reduces NO_x to N_2 and H_2O by the use of a catalyst and a reducing agent. SCR is the only single method which can achieve more than 75% NO_x control efficiency for the flue gas emitted from stationary combustion sources with a high selectivity toward N_2 . Despite extensive research reported on the selective catalytic reduction (SCR) of NO_x with various catalyst /reductant combinations since 1975, only SCR with NH_3 or urea as the reducing agent offers a practical approach for NO_x abatement, and has been commercialized to date (Forzatti, 2001).

1.3 Selective catalytic reduction of NO_x with NH_3

SCR with NH_3 as the reducing agent has been commercialized in more than 400 industrial and utility plants, mainly in Japan, US and European countries. In this process, liquid ammonia or aqueous ammonia solution is injected into the flue gas to reduce NO_x with $\text{V}_2\text{O}_5/\text{TiO}_2$ catalyst (WO_3 and/or MoO_3 as promoters) following reactions in equations 1.1

and 1.2, with 75%~90% of NO_x conversion being achieved at an NH₃-to-NO_x molar ratio of 1.2~1.5.



Although NH₃-SCR of NO_x has been widely implemented, it has the following disadvantages (Ham and Nam, 2002; Zhou et al., 1996):

- The handling of large quantities of NH₃ is a concern because NH₃ is toxic and corrosive;
- Un-reacted NH₃ may potentially be discharged to the environment (ammonia slippage);
- NH₃ can react with SO₃ and H₂O to form ammonium sulphates, causing the fouling of downstream equipment.

Due to the high installation and operating cost and complexity, the NH₃-SCR system is only used when the highest level of NO_x removal is required, for example, in large power plants located in urban areas where ozone and photochemical smog are serious problems.

Taking the drawbacks of using NH₃ in SCR process into account, a large number of studies on NO_x SCR has been reported in recent years, mainly focusing on the selection and evaluation of NH₃-free alternative reducing agents and catalysts, and the mechanism of SCR.

Hydrocarbons instead of NH₃ are considered the most promising reducing agents for the SCR process. The first study on SCR of NO_x with hydrocarbons was reported by Iwamoto et al. (1988). Thereafter, SCR of NO_x by hydrocarbons (HC-SCR) has attracted considerable attention as an alternative of ammonia or urea process for the treatment of oxygen-rich flue gases, and numerous studies on various types of catalysts and reducing

agents have been widely investigated (Parvulescu et al., 1998; Traa et al., 1999; Wichtelova et al., 2003; Liu and Woo, 2006). However, the NO_x conversion in HC-SCR process is still much lower than that in NH₃-SCR at a given reductant to NO_x stoichiometric ratio because of the existence of excess O₂ and poisoning components (SO_x and H₂O) in the flue gas.

1.4 Research objectives

As a technology under development, most studies have focused on the development of catalysts, the selection of reducing agents, or the understanding of the reaction mechanisms of the process. In order for such a technology to be used in the industrial processes, engineering aspects still need to be considered to address technical challenges in the reactor design and scale-up for the HC-SCR process.

To avoid the negative impact of the poisoning components and excess O₂ in the flue gas, we propose a new concept of an integrated NO_x adsorption-reduction process, as shown schematically in Figure 1.2, where the NO_x adsorption and reduction are carried out in two separate zones of the reactor. The flue gas is passed into the adsorption zone where NO_x is adsorbed by the catalyst. The NO_x-adsorbed catalyst particles then move into the reaction zone where NO_x is reduced by injected hydrocarbons at controlled oxygen concentrations, and at the same time, other adsorbed flue gas contaminants are also stripped from the catalyst. The regenerated catalyst particles are then recirculated back to the adsorption zone to establish a continuous operation.

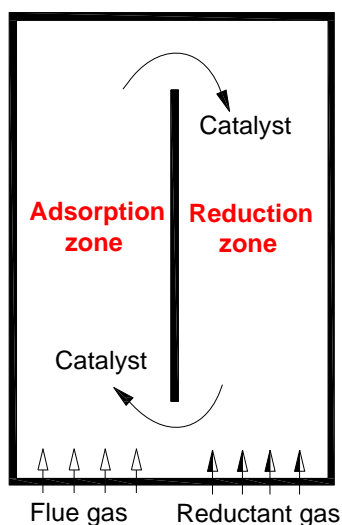


Figure 1.2 Schematic of the integrated adsorption-reduction process of NO_x

The main objective of this work was to evaluate the potential application of the integrated adsorption-reduction process for the selective catalytic reduction of NO_x with hydrocarbons in a dual-zone fluidized bed reactor, i.e. the internal circulating fluidized bed (ICFB) reactor. To achieve this goal, a fixed bed reactor system was set up first to investigate the adsorption performance and reaction kinetics of selected catalysts at various temperatures and flue gas compositions. After the hydrodynamic studies were performed in a cold model ICFB unit, the adsorption and reaction performance of selected catalysts was conducted in the hot model ICFB reactor, with the results compared with a conventional bubbling fluidized bed reactor.

1.5 Thesis layout

A literature review is presented in Chapter 2 to summarize the present status of NO_x SCR with hydrocarbons, including catalysts, effects of the flue gas composition and reducing agents, and mechanisms of HC-SCR. The adsorption performance and reaction kinetics of

HC-SCR over selected catalysts in a fixed bed reaction system are given in Chapter 3. The hydrodynamic study on the ICFB reactor is shown in Chapter 4, including the gas bypass and solids circulation rate. Results of NO_x reduction and adsorption over Fe/ZSM-5 catalysts in a hot model ICFB reactor are discussed in Chapter 5. In addition, the results from a conventional fluidized bed reactor are also reported and compared with those from the ICFB reactor. Finally, Chapter 6 summarizes the conclusions of this study and recommendations for the future work.

Chapter 2

Literature Review

It was first reported by Iwamoto et al. (1988) that the catalytic activity of Cu/ZSM-5 on the reduction of NO_x was remarkably enhanced by the addition of hydrocarbons. Following this discovery, studies on HC-SCR have been expanded to various aspects, including sources of catalyst supports, metal loadings and preparation methods, effects of flue gas compositions and reducing agents, and reaction mechanisms.

2.1 Catalysts

Generally, HC-SCR catalysts can be categorized into two groups according to catalyst supports: zeolite (ZSM-5, Mordenite, Y-zeolite, Ferrierite and Beta zeolite) (Iwamoto et al., 1990; Corma et al., 1997; Amiridis et al., 1997; Traa et al., 1999; Chen et al., 2000b; Wichtelova et al., 2003) and non-zeolite (mainly metal oxides, such as Al₂O₃, SiO₂, and ZrO₂) (Captain et al., 1998; Garcia-Cortes et al., 2000; Lick et al., 2003a; Liu and Woo, 2006). Based on the supports described above, noble metals (Pt, Pd, Rh, Ir, Ag, Au) (Cho et al., 1995; Parvulescu et al., 1998; Kikuchi et al., 2000; Shi et al., 2002; Sato et al., 2003; Ueda et al., 1997), transition metals (Cu, Co, Fe, Cr, Mo, Ni, Mn, Al, Ti, V, Zn, Zr) (Iwamoto et al., 1990; Witzel et al., 1994; Hall et al., 1998; Wang et al., 2000; Mosqueda-Jimenez et al., 2003; Lucas et al., 2004), alkali and alkaline metals (Na, K, Li, Ba, Ca, Mg, Sr) (Sato et al., 1992), rare earth metals (La, Nd, Ru, Sm) (Bosch and Janssen, 1988) and others (Ga, In) (Tabata et al., 1995) were loaded as active elements in the prepared HC-SCR catalysts.

Metals are often loaded onto the supports in four ways:

1. **Wet Ion-Exchange (WIE):** The support is added to the chemical solution with expected active metal element. The mixture is stirred for a given time period, at a given temperature, with or without inert gas blanket. At the end of this process, the mixture is filtered and washed thoroughly with deionized water, dried and calcined under different conditions. This process may be repeated several times to gain various ion-exchange rates (Wang et al., 2000).
2. **Impregnation (IMP):** The support is added to the chemical solution (aqueous or organic) with expected metal ion, volume and concentration. The solution is stirred for a given time period, at a given temperature. After that, the mixture is filtered or evaporated, with or without washed thoroughly with deionized water, dried and calcined under different conditions (Chen et al., 1998a; Delahay et al., 2005).
3. **Sublimation (SUB) or Chemical Vapour Deposition (CVD):** The metal compound is sublimated under given conditions while the support is put into this atmosphere. After a given time period, the sample is removed and washed with deionized water thoroughly, then dried and calcined (Chen et al., 1998b).
4. **Solid State Ion Exchange (SSIE):** The support and metal compound are physically mixed and grounded. After a given time period, the mixture is washed thoroughly by deionized water, dried and calcined (Berndt et al., 2003).

Different loading methods will give different metal loading ratios. Nevertheless, higher metal loading doesn't always mean higher reactivity (such as Cu/ZSM-5, as shown in Figure 2.1). The catalyst reactivity is closely related to the preparation process and the reaction

conditions. In general, catalysts with various metal loadings described above have all shown catalytic activity for HC-SCR of NO_x .

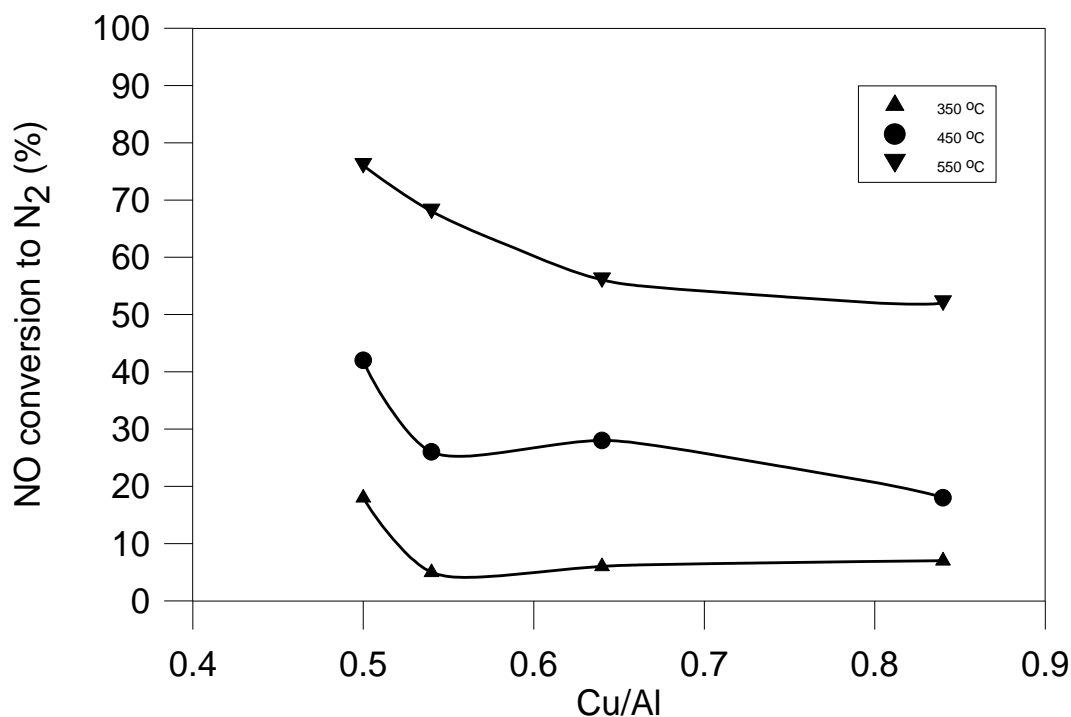


Figure 2.1 NO conversion to N_2 over Cu/ZSM-5 catalysts as a function of Cu/Al ratio at different temperatures

Reaction conditions: 2000 ppm NO, 2000 ppm C_3H_6 , 2% O_2 , balanced by He; 1.0 g catalyst and 150 ml/min^{-1} total flow rate (Seyedeyn-Azad et al., 2001).

2.1.1 Metal-exchanged zeolites

Much effort has been devoted to the group of metal-exchanged zeolite. So far, Cu, Fe, Pt, Co, Pd supported by zeolite, mainly as ZSM-5, gained extensive attention. Cu/ZSM-5 might be the most studied catalyst for its higher NO conversion (NO conversion to N_2 could reach up to 85% in the absence of H_2O and SO_2 (Seyedeyn-Azad et al., 2001)) over a wide temperature window (300~550°C) by using various reducing agents. However, deactivation of Cu/zeolite catalyst by H_2O and SO_2 in the flue gas is still the obstacle in the practical applications (Gilot et al., 1997; Chen et al., 1998a; Li et al., 2004). Many papers also reported

that Cu exchanged with other types of zeolite as HC-SCR catalysts could achieve similar results as Cu/ZSM-5, although differences existed in the maximum reactivity and operating temperature windows of these catalysts (Shelf, 1995; Walker, 1995; Corma et al., 1997; Ohtsuka et al., 1997; Park et al., 2000; Cho et al., 2003). As indicated in Figure 2.1, with the increase of Cu/Al ratio, NO conversion to N₂ decreased, suggesting that increasing the quantity of implanted Cu²⁺ did not improve the activity of Cu/ZSM-5.

Most recently, Subbiah et al. (2003) reported that a new catalyst Cu/SUZ-4, which was supported by SUZ-4 zeolite, gave a high reactivity (NO conversion of 44~68%, based on 2.3%Cu/SUZ-4) and a wide operating temperature window (350~600°C) even in the presence of H₂O and SO₂. The reactivity of this catalyst increased as the Cu-exchanged level increased.

Fe/ZSM-5 was widely reported in recent years to possess high effectiveness without the production of N₂O and good resistance to H₂O (Feng and Hall, 1997; Yamada et al., 1998; Kogel et al., 1999; Chen et al., 2000b; Battiston et al., 2003; Sobalik et al., 2002). However, large amount of CO was detected when Fe/ZSM-5 was used as the HC-SCR catalyst (Chen et al., 2000b). According to the literature, Fe loading level on zeolite also played an important role. Although catalysts with low Fe loadings gave some activity for NO reduction (NO conversion to N₂ of ~20%), only catalysts with higher Fe loadings prepared by chemical vapour deposition showed satisfactory NO conversion (>60%) (Chen and Sachtler, 1998a; Saaid et al., 2002). Nevertheless, it is very difficult to prepare large amount of catalyst by chemical vapour deposition method from the practical application point of view. More recently, Fe/ZSM-5 catalyst prepared by an impregnation method using a solution of Fe(AA)₃ (Iron(III) Acetylacetonate) in toluene was reported to show similar activities for

NH₃-SCR of NO_x as catalyst prepared by chemical vapour deposition method (Delahay et al., 2005).

Pt/ZSM-5 is more active at lower temperatures and is less affected by SO₂ and water vapour, but its active temperature window is very narrow (200~250°C) and most of NO is reduced to N₂O in the presence of oxygen (Le et al., 1994; Xin et al., 1999; Woo et al., 2003).

Cobalt-containing zeolite showed good activity when methane was used as the reducing agent (Witzel et al., 1994). Moreover, neither N₂O nor CO was detected in the HC-SCR using Co-containing catalyst. However, the effective operating temperature of Co/zeolite is too high (450~550°C) and the catalytic activity is also inhibited by H₂O and SO₂ (Ohtsuka et al., 1997; Park et al., 2000; Wang et al., 2000).

Like Co/ZSM-5, Palladium-containing zeolite can reduce NO with methane. Nishizaka et al. (1994) reported a NO conversion to N₂ of ~70% at a temperature around 475°C by using Pd/ZSM-5 in CH₄-SCR without water in the model flue gas. Many researchers studied the reduction on Pd-containing zeolites using reducing agents other than methane, e.g. C₂H₄, C₃H₆, (CH₃)₂O and CH₃OH (Shin, et al., 1995; Keiski et al., 1996; Adelman and Sachtler, 1997; Kato et al., 1997; Masuda et al., 1998). However, very low NO conversions (< 20%) were obtained.

Much effort has been devoted to the investigation of HC-SCR on metal-containing zeolite promoted by other metals, such as Co promoted Pd/ZSM-5, Pt promoted Co/ZSM-5, etc (Kagawa et al., 1998; Gutierrez et al., 1998; Bustamante et al., 2002). Ogura et al. (2002) tried the use of Co as the promoter of Pd/ZSM-5, and observed a significant improvement on the durability of catalyst in the presence of water (NO conversion to N₂ kept 60% in CH₄-SCR, 500°C, 50 hours time-on-stream period).

Other metal loadings on zeolite have also received much attention, but no evidence showed that the catalytic performance was good enough even for model flue gases.

2.1.2 Metal-exchanged metal oxides

Numerous metal oxides (such as Al_2O_3 , TiO_2 , ZrO_2 , V_2O_5 , Fe_2O_3 , CoO , NiO and MnO_2 etc.) have been investigated as supports of HC-SCR catalysts, but most of them showed low or no activity to NO reduction (Parvulescu et al., 1998; Liu and Woo, 2006). Among them, only Pt, Cu, Co, Fe, Ag, Pd supported by Al_2O_3 , $\text{SO}_4^{2-}/\text{TiO}_2$ and $\text{SO}_4^{2-}/\text{ZrO}_2$ exhibited some catalytic activity (Burch et al., 1998; Captain et al., 1998; Lick et al., 2003a). Some researchers found that when promoters were added to metal-exchanged Al_2O_3 , the catalytic activity could have a significant increase (Naito and Tanimoto, 1993; Obuchi et al., 1993).

Chin et al. (1999) reported that Pd-Sulphated Zirconia catalyst could tolerate the effect of SO_2 , and that the inhibition of water in the flue gas was weak (NO conversion dropped from 48% to 38%) and reversible.

Efthimiadis et al. (2001) used a fluidized bed reactor loaded with $\gamma\text{-Al}_2\text{O}_3$, $\text{Rh}/\text{Al}_2\text{O}_3$ or 5% $\text{Rh}/\text{Al}_2\text{O}_3$ -95% FCC for the control of NO_x emitted from the regenerator of a FCC pilot-plant unit. They found that $\gamma\text{-Al}_2\text{O}_3$ with CH_3OH exhibited significant reactivity (maximum NO conversion of 97% at 400°C), $\text{Rh}/\text{Al}_2\text{O}_3$ also reduced more than 70% of NO to N_2 (C_3H_6 as reducing agent, 300°C). Furthermore, although 5% $\text{Rh}/\text{Al}_2\text{O}_3$ -95% FCC showed lower NO conversion (40%, 350°C), its catalytic activity was enhanced by the presence of SO_2 in the flue gas. This result is notable, although the NO content was low (80 ppm) and no H_2O was present in the treated flue gas.

Shimizu et al. (2000) reported a high reactivity of $\text{Ag}/\text{Al}_2\text{O}_3$ in the SCR with higher hydrocarbons. They also compared the performance of several metal-containing Al_2O_3 catalysts, and found that higher NO conversion to N_2 could be obtained by using n-octane as

the reducing agent. Satokawa et al. (2001) further showed the impressive tolerance of Ag/Al₂O₃ to SO₂ in a 50 hours time-on-stream test.

Although significant research has been made, the development of catalysts with both very stable supports and highly active catalytic metal ingredients for practical applications is still a challenge to researchers.

2.2 Hydrocarbon reducing agents

Hydrocarbons, which have been proven effective as reducing agents in SCR of NO_x, include methane, propane, propylene, iso-butane and oxygenated hydrocarbons, such as methanol and acetic acid etc.

Among them, taking into account that methane is the main component of natural gas, it is not surprising that methane was the mostly studied reducing agent in the past years (Witzel et al., 1994; Tabata et al., 1995; Mitome et al., 1998; Kameoka et al., 2000; Bustamante et al., 2002; Berndt et al., 2003). Nevertheless, due to its preference to combustion, methane has been shown to be only effective in the SCR of NO_x over Co/zeolite, Ga/ZSM-5, In/ZSM-5, Pd/Al₂O₃ and Pd/TiO₂. The catalytic activity of these catalysts decreased significantly when water was added into the model flue gas. For example, the NO conversion to N₂ decreased from 75% to 5% over Ga/ZSM-5 and 60% to 10% over In/ZSM-5 (Tabata et al., 1995) when H₂O was added. Ogura et al. (2002) reported that Pd promoted Co/ZSM-5 in the CH₄-SCR showed good NO conversion to N₂ (60% at 500°C) in the presence of water, similar to the result of Bustamante et al. (2002) (Pd-Co/Mordenite, 60% at 550°C). Berndt et al. (2003) obtained high catalytic activity over Ce-In/ZSM-5. NO conversion to N₂ dropped from 100% to 88% when 5% water was added.

Due to the non-selective performance of methane, many researchers focused on other hydrocarbons, i.e., propane and propylene.

Fe, Cu or Co exchanged zeolite and Co supported by alumina showed acceptable catalytic activity using propane as the reducing agent (Kogel et al., 1999; Park et al., 2000; Lick et al., 2003b; Martinez-Hernandez and Fuentes, 2004). Moreover, Co/Beta-zeolite (Tabata et al., 1996; Ohtsuka et al., 1997), Fe/Beta-zeolite (Chen et al., 2000b) and Ce-In/ZSM-5 (Berndt et al., 2003) exhibited high activity with propane even in the presence of water. This suggests that, by using these catalysts, the SCR of NO_x with propane may be a good choice in the practical applications without the presence of SO₂.

When propylene was used as the reducing agent, Fe or Cu exchanged zeolite gave high NO conversion in the absence of H₂O and SO₂. At the same reaction conditions, the temperature with the maximum NO conversion over Cu/ZSM-5 was reported to be 100°C higher for propylene (500°C) than for propane (400°C) (Park et al., 2000). The temperature window of Fe/zeolite was found to be relatively low (300~400°C) for both propane and propylene. Figure 2.2 compared the NO conversion to N₂ over Cu/ZSM-5 and Co/ZSM-5 using CH₄ or C₃H₆ as the reducing agent under the same reaction condition. Obviously, Cu/ZSM-5 showed significantly different activity for tests with CH₄ or C₃H₆ as the reducing agent, while Co/ZSM-5 kept almost the same activity for both reducing agents.

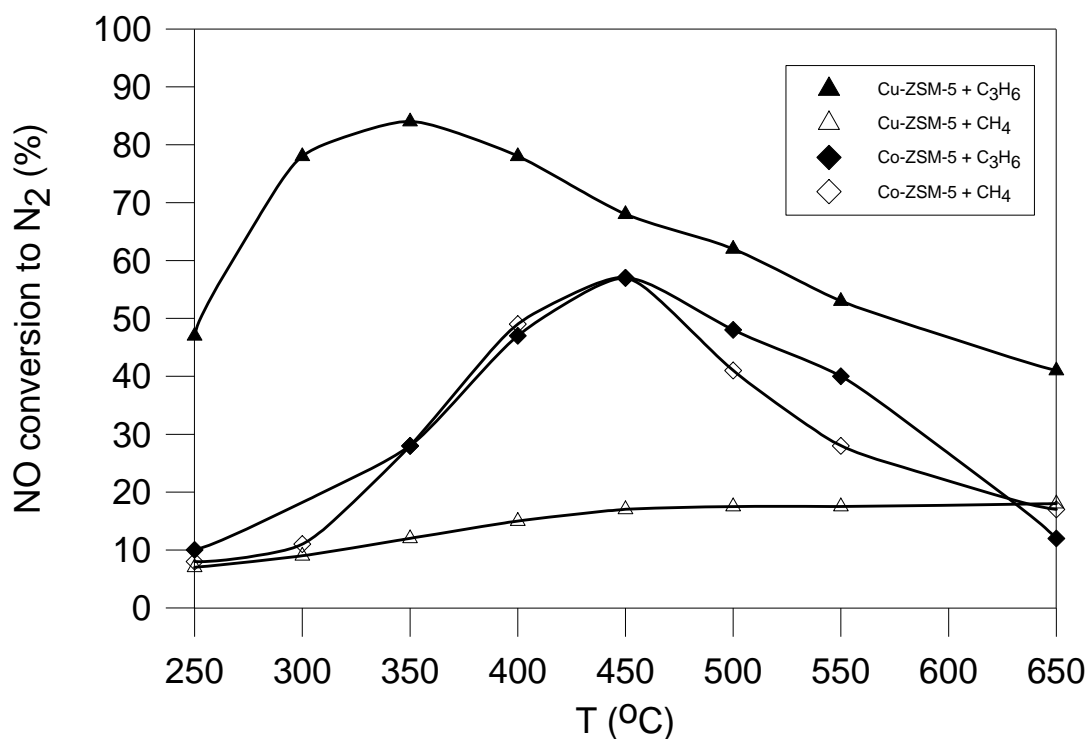


Figure 2.2 Dependence of NO conversion on temperature for SCR of NO over various catalysts with alternative reducing agent

Reaction conditions: 2000 ppm NO, 2000 ppm CH₄ or C₃H₆, 2% O₂, balanced by He; 1.0 g catalyst; total flow rate: 100 ml/min⁻¹. (Seyedeyn-Azad et al., 2001)

Co, Fe, Ni, Mn, Ga and Cu exchanged ZSM-5 gave high NO conversion when iso-butane was used as the reducing agent (Witzel et al., 1994; Chen et al, 2000b; Saaid et al., 2002). Specifically, Co/ZSM-5 was resistant to water in the flue gas and gave very high N₂ yield (>94%) (Wang et al., 2000).

In the SCR of NO_x over Fe/ZSM-5, various types of hydrocarbons were tested as reducing agents by Chen et al. (1998b), and the performance followed the order of i-butane > propane > propylene > methane, as shown in Figure 2.3.

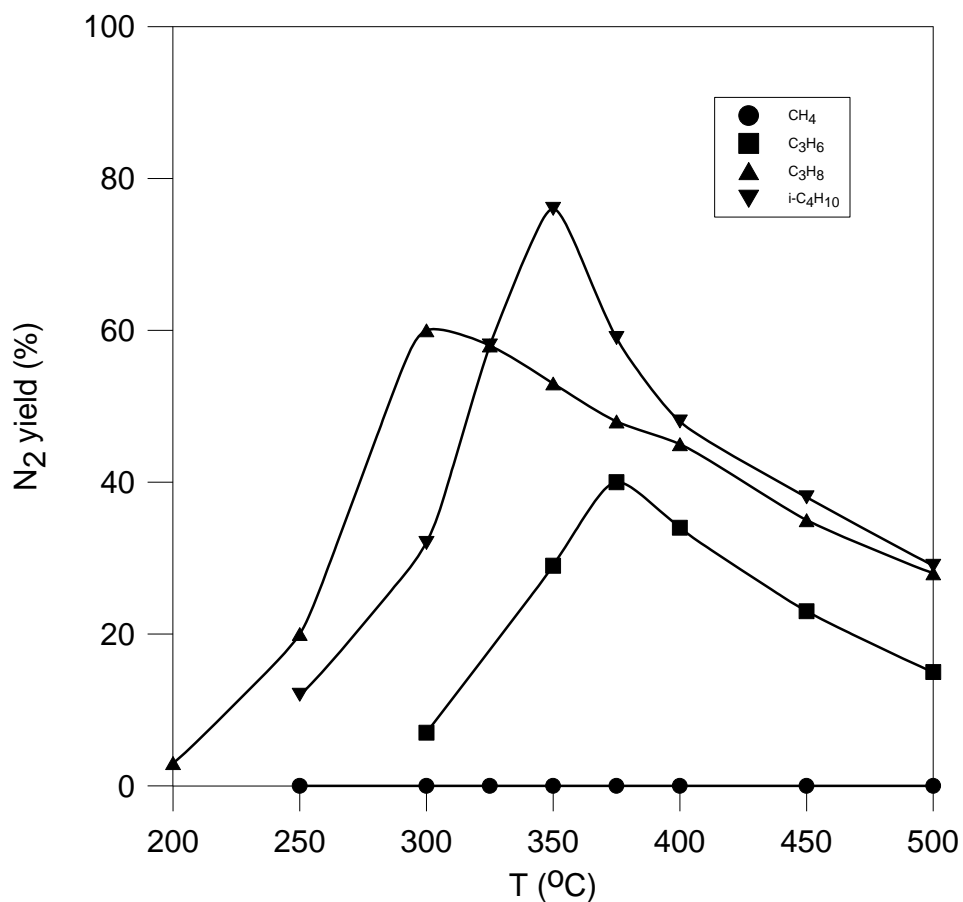


Figure 2.3 Temperature dependence of N₂ yield over Fe/ZSM-5 with different hydrocarbons. Reaction conditions: 0.2 g Fe/ZSM-5, 0.2% NO, 3% O₂, 0.2% i-C₄H₁₀ (0.8% CH₄, 0.27% C₃H₈ or C₃H₆), flow rate: 280 ml/min (Chen et al., 1998b)

Witzel and coworkers (1994) examined the NO_x reduction performance of methane, propane, iso-butane, n-pentane, 2, 2-dimethylpropane (neopentane), 3, 3-dimethylpentane, 2, 2, 4-trimethylpentane and 3, 3-diethylpentane (neononane) on Co/ZSM-5 catalyst. The maximum NO conversion as a function of the reducing agent followed the order of iso-butane > methane > neopentane > n-pentane > 2, 2, 4-trimethylpentane > propane > 3, 3-dimethylpentane > neononane (see Figure 2.4).

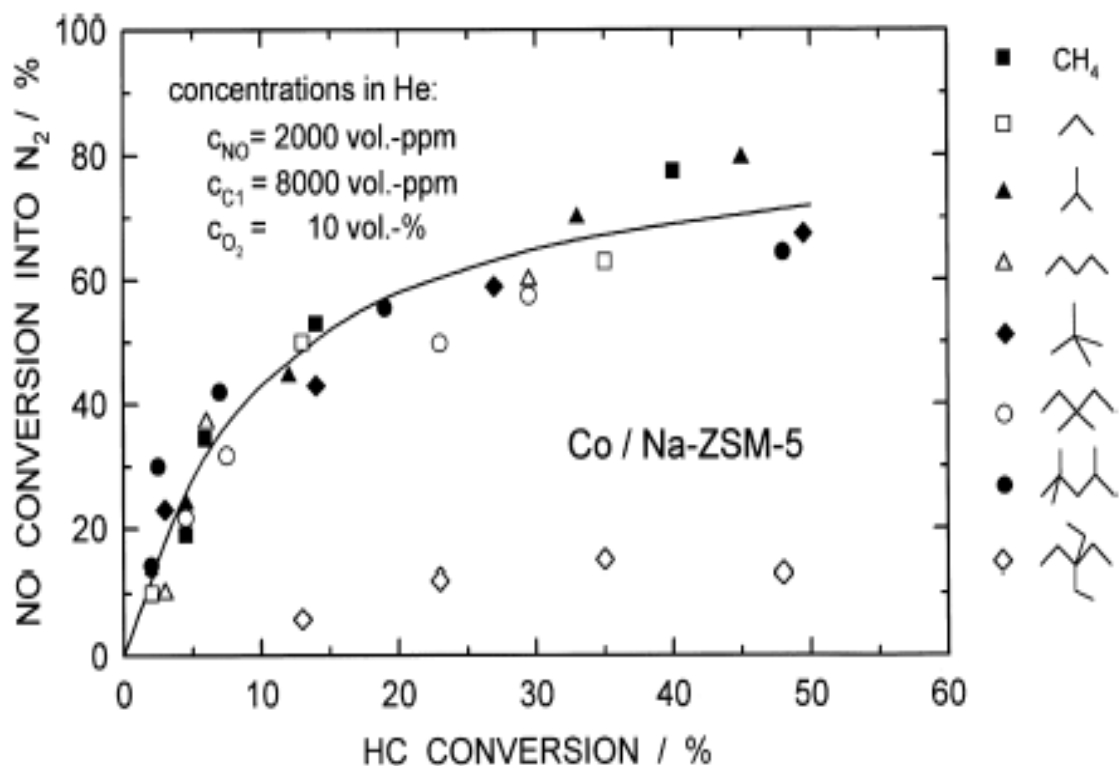


Figure 2.4 Effect of the nature of the hydrocarbon on NO reduction selectivity on Co/ZSM-5 (Witzel et al., 1994)

Some other hydrocarbons, such as C_2H_6 , $n\text{-C}_6\text{H}_{14}$, $n\text{-C}_4\text{H}_{10}$, $n\text{-C}_8\text{H}_{18}$ and $n\text{-C}_{10}\text{H}_{22}$, were also examined and found to give similar performance (Shimizu et al., 2000b; Shibata et al., 2002; Sato et al., 2003; Subbiah et al., 2003). Shimizu et al (2000) reported that the SCR activity of 2% Ag/ Al_2O_3 notably increased as the carbon number in the reducing agent increased in the presence of water (Figure 2.5).

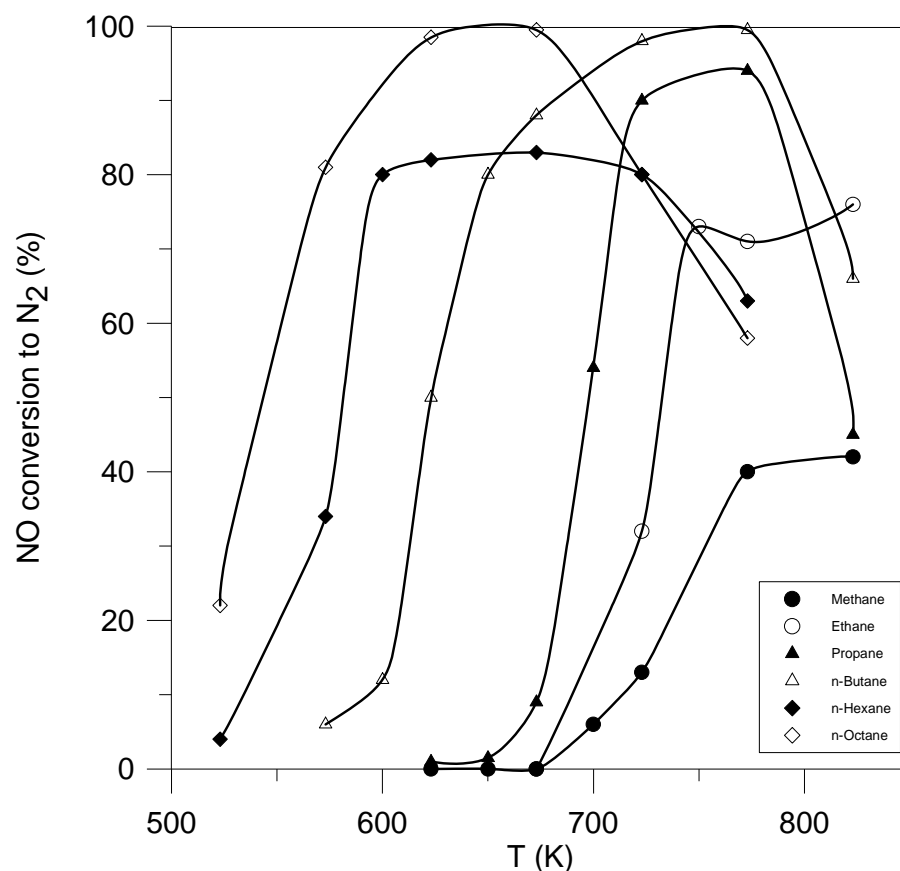


Figure 2.5 NO conversion to N_2 on Ag/Al_2O_3 using alternative reducing agent
 Reaction conditions: $NO/n\text{-alkane}/O_2 = 1000 \text{ ppm}/6000 \text{ ppm C}/10\%$; $2\% H_2O$, $W/F = 0.12 \text{ g-s/ml}$ except for $CH_4\text{-SCR}$ ($W/F = 0.9 \text{ g-s/ml}$) (Shimizu et al., 2000)

Oxygenated hydrocarbons were investigated as reducing agents in the SCR (Masters et al., 1999b; Elkaim et al., 2000). The case over Al_2O_3 or Sulphated- Al_2O_3 catalyst with methanol as the reducing agent reached a high NO conversion (Efthimiadis et al, 2001; Burch et al., 1998). This implies that Al_2O_3 may have good tolerance to SO_2 under given conditions, but the influence of water needs to be investigated further.

Acetic acid was also reported in the SCR of NO over Pd/Mordenite. In the presence of water, the NO conversion reached 94% with a high acetic acid to NO ratio of 22 (Uchida et al., 1995).

Although hydrocarbons gained extensive attention in the area of SCR of NO_x, the substantial difference between hydrocarbons and ammonia in NO_x conversion and H₂O and SO₂ inhibition shows that there is still a long way to go for the practical application of HC-SCR process.

2.3 Reaction mechanisms and kinetics of HC-SCR

The mechanism of HC-SCR has been investigated extensively. Due to the complexity of the HC-SCR process, different mechanisms were proposed for different catalysts, reducing agents and/or reaction conditions. Generally, according to the reaction pathways and rate-limiting steps, reaction mechanisms can be categorized into three groups (Parvulescu et al., 1998; Traa et al., 1999; Sadykov et al., 2003): surface redox, oxidation of NO to NO₂, and partial oxidation of hydrocarbons.

2.3.1 Surface redox mechanism

Based on microscopic reaction results, Inui et al.(1994) proposed that NO first decomposed to molecular nitrogen and chemisorbed oxygen on reduced surface sites of the catalyst, and the adsorbed oxygen oxidized the catalyst surface. The hydrocarbon then reacted with adsorbed oxygen and reduced the active site (Burch et al., 1996b; Cho et al., 1995).



Reaction (2.1) is considered to be the rate-limiting step.

2.3.2 Oxidation of NO to NO₂

NO is first oxidized to NO₂ and/or surface nitrite-nitrate complexes by oxygen. Then the oxidized compounds are reduced by hydrocarbons to molecular nitrogen, possibly via intermediate organic nitro compounds (Yokoyama et al., 1994; Adelman et al., 1996; Yan et al., 1998; Kikuchi et al., 1996).



As indicated in the literature, the oxidation of NO to NO_x (reaction 2.3) is the rate-controlling reaction.

2.3.3 Partial oxidation of hydrocarbons

In this mechanism, hydrocarbons are partially oxidized to oxygen- and/or nitrogen-containing organic intermediates (e.g. cyanide or nitro species) by oxygen or NO_x. The oxidized hydrocarbon intermediates subsequently react with NO to produce N₂, CO and/or CO₂, and H₂O (Li et al., 1994c; Lobree et al., 1997; Shelf, 1995; Lukyanov et al., 1996; Hayes et al., 1996).



The rate-limiting step is reaction (2.5).

It should be noted that the mechanism of HC-SCR is still not clearly understood due to the complexity of HC-SCR under different reaction conditions. Therefore, mechanisms suggested above are not universal. For some specific processes, a combination of those

mechanisms may work better than any one of them (Meunier et al., 2000). For the same reason, the kinetic expression of the HC-SCR process is still not readily available.

2.4 Influence of flue gas compositions on HC-SCR

So far, compositions of the model flue gas in most investigations are far from the real ones. Most researchers reported their results without considering the influence of both water and sulphur dioxide, or either one of them. Hence, although some researchers claimed that they achieved very high NO conversion in the HC-SCR process, the results still need to be verified under practical operating conditions or using real combustion flue gases.

2.4.1 Influence of SO₂ and H₂O in the flue gas

For a HC-SCR system, one of the most important issues for the practical application is the durability of catalyst to the poisoning components, i.e., H₂O and SO₂.

Tabaka et al (1996) reported that Co/Beta-zeolite exhibited stable activity (NO conversion to N₂ kept at about 70%) in the SCR with propane for the treatment of model flue gas with 9% H₂O and 0.3ppm SO₂ in a long term run (4000 hours) at 400°C, while under the same reaction conditions, Co/ZSM-5 was deactivated rapidly. Co/Al₂O₃ showed stable activity (NO conversion ~45%) in the HC-SCR with propylene when 10% H₂O was presented in the model flue gas during 125 hours operation at 550°C (Yan et al., 1997). Berndt et al (2003) revealed that the SCR of NO_x with propane over Ce-In/ZSM-5 was enhanced when 5% water was introduced into the system. The NO conversion to N₂ increased slightly from 67% to 70%, yet the optimum temperature shifted from 550°C to 600°C. Chen et al. (1998a) reported the performance of Fe/ZSM-5 and Cu/ZSM-5 as a function of time on stream (see Figure 2.6). Although Cu/ZSM-5 showed 60% NO

conversion in the absence of water, its activity decreased quickly to 0 when water was injected into the stream, and the deactivation was partially irreversible. On the other hand, Fe/ZSM-5 showed stable activity no matter whether water was present or not.

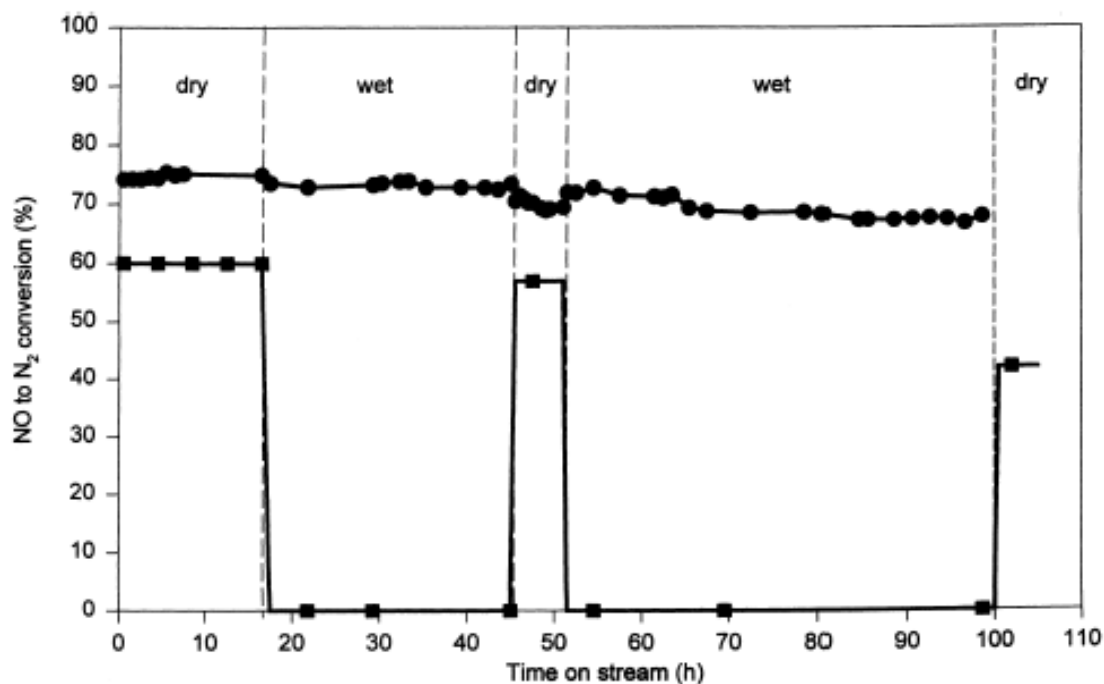


Figure 2.6 Effect of H₂O on NO conversion to N₂ over Fe/ZSM-5 or Cu/ZSM-5 (●) Fe/ZSM-5 (temperature=375°C, GHSV=42,000 h⁻¹, iso-C₄H₁₀=0.2%, NO=0.2%, O₂=3%, H₂O=0% for dry; 10% for wet); (■) Cu/ZSM-5 (temperature=400°C, GHSV=120,000 h⁻¹, C₃H₈= 0.1%, NO=0.1%, O₂=2%, H₂O: 0% for dry; 10% for wet). (Chen et al., 1998a)

Ag/Al₂O₃ exhibited some long-term stable reactivity under real lean-burn gas engine conditions (Shimizu et al., 2000b). In a time-on-stream test, in the presence of 4ppm SO₂, Ag/Al₂O₃ deactivated very quickly at temperatures lower than 500°C, but exhibited stable activity at 550°C even after 50 hours (Satokawa et al., 2001).

Yan et al. (1997) reported that Co/Al₂O₃ was durable to the flue gas of 950ppm NO + 1000ppm propylene + 5% O₂ + 1.5% H₂O + 30ppm SO₂ with NO conversion remaining at ~63% over a time-on-stream test of 6.5 hours (T=450°C), except for that the propylene

conversion decreased from 78% to 67% over time. The activities of Ag/Al₂O₃, Ni/Al₂O₃, Co/Al₂O₃ and In/Al₂O₃ were seriously inhibited by 100ppm SO₂ in the flue gas (Meunier et al., 2001), worsened with prolonged exposure time. With the removal of SO₂ from the flue gas, the catalytic activities were partially recovered except for Ag/Al₂O₃. Similarly, Cu/SUZ-4 (Cho et al., 2003) exhibited some tolerance and stable activity to both H₂O and SO₂.

Decyk et al. (2001) investigated the effect of SO₂ on the reactivity of Fe/ZSM-5. Using i-butane as the reducing agent, in the absence of SO₂, NO conversion to N₂ reached 59.1%. With the feed of 150ppm SO₂, NO conversion decreased to 36%, and partially recovered to 43.8% after SO₂ was removed from the flue gas. They also found that increasing the concentration of SO₂ to 300ppm could further deactivate the catalyst. According to their analysis, the presence of SO₂ suppressed the formation of Fe-NO_y complexes on the catalyst surface and increased the formation of carbonaceous deposits, thus further deactivated the catalyst.

In summary, Fe/ZSM-5, Pt/ZSM-5, Co/Beta-zeolite, Ag/Al₂O₃ and Ce-In/ZSM-5 exhibited a good hydrothermal resistance. On the other hand, only Co/Al₂O₃, Ag/Al₂O₃ and Cu/SUZ-4 showed some tolerance to sulfur dioxide at low concentrations.

2.4.2 Influence of excess oxygen in the flue gas

As a key component of the flue gas under lean-burn conditions, the influence of excess oxygen has been widely investigated. One of the main NO reduction mechanisms states that NO is first oxidized to NO₂, followed by the reduction by the reducing agent. The presence of O₂ is thus essential for the HC-SCR process. This mechanism appears to agree with many experimental findings that the presence of small amount O₂ (e.g., <2%) is essential for HC-SCR (Captain et al., 1998; Shi et al., 2002; Lee, et al., 1997).

Li et al. (2004) reported that, using Sn/Al₂O₃ as the catalyst in a TPD experiment, after the adsorption process for the flue gas containing NO and O₂, the amount of desorbed species was much higher than that for the gas containing NO only (without O₂), which indicates the fact that O₂ in the flue gas could enhance the adsorption of NO.

As shown in Figure 2.7, Corma et al. (1997) reported that NO conversion to N₂ increased from 10% to 70% on Cu/ZSM-5 and 27% to 76% on Cu/Beta as O₂ concentration increased from 0% to 2%. Thereafter, NO conversion to N₂ decreased significantly to 43% on Cu/ZSM-5 and 42% on Cu/Beta in the presence of 6% O₂. For Fe/ZSM-5 catalyst (Chen et al., 1998b), when O₂ concentration was 0%, no N₂ was produced. As O₂ concentration increased, N₂ yield increased and reached a maximum of 73% at 2% O₂. Further increase of O₂ concentration from 2% to 10% made N₂ yield drop slightly to 69%. Li and Armor (1994a) studied NO reduction rate with low O₂ concentration over Co/Ferrierite with CH₄, and found that NO reduction rate increased from 0.12 to 0.58 mmol/h-g catalyst when O₂ concentration rose from 0 to 5000ppm (0.5%v/v). Lee (2000) investigated the influence of oxygen on NO reduction using oxygenated hydrocarbons (acetic acid) as the reducing agent. The result revealed that with the increase of oxygen concentration from 2.25% to 9.36% in the model flue gas, NO conversion dropped from 52.2% to 21.8%. Elkaim and Bai (2000) reported high tolerance of V₂O₅/γ-Al₂O₃ catalyst to H₂O with acetic acid as the reductant, and the catalyst kept high activity in the O₂-free flue gas even in the presence of up to 15% H₂O. However, it is sensitive to the concentration of O₂ in the flue gas, with the NO_x conversion dropped from 100% to 38% when the O₂ concentration increased from 0% to 10%.

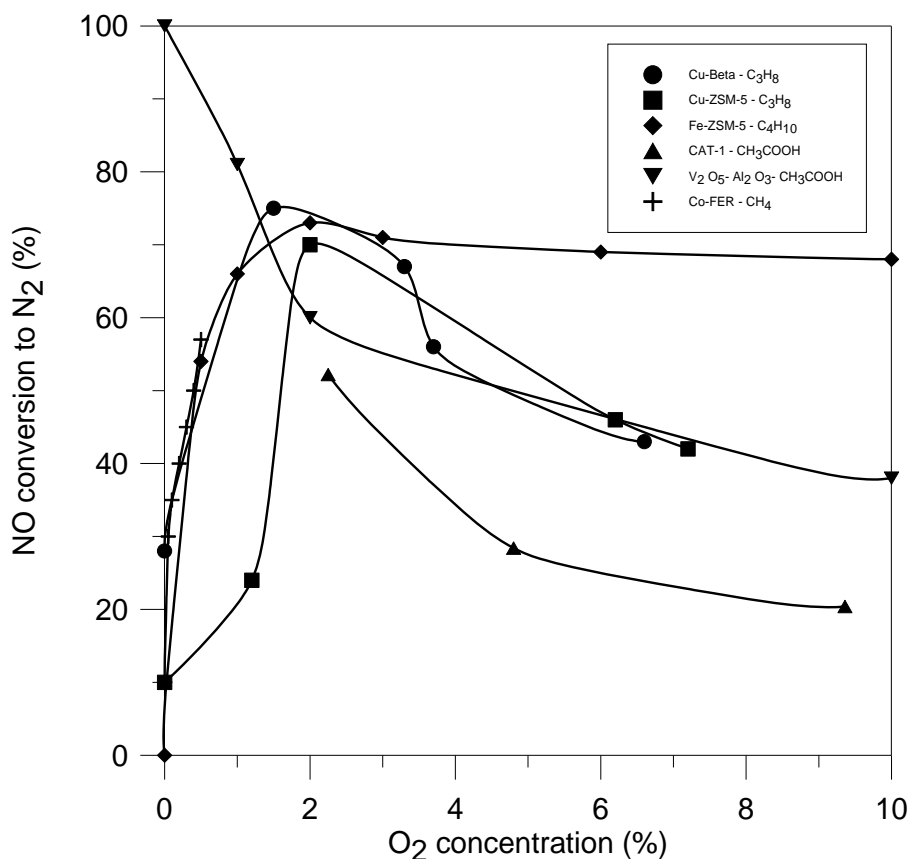


Figure 2.7 Influence of O₂ concentration on NO conversion to N₂

Reaction conditions:

1. Cu/Beta (●) and Cu/ZSM-5 (■) : T=350°C, 850ppm NO, 450ppm C₃H₈ (Corma et al., 1997);
2. Fe/ZSM-5 (◆) : T=350°C, 0.2% NO, 0.2% i-C₄H₁₀, 280 ml/min (Chen et al., 1998a);
3. Cat-1 (▲) : T=320°C, 377ppm NO, 1663ppm acetic acid, GHSV: 8.87s⁻¹ (Lee, 2000);
4. V₂O₅/γ-Al₂O₃ (▼) : T=300°C; 500ppm NO, 500-2250ppm acetic acid, GHSV: 5,000h⁻¹ (Elkaim and Bai, 2000);
5. Co/FER (⊕) : T=450°C, 1600ppm NO, 1000ppm CH₄, GHSV: 30,000h⁻¹ (Li et al., 1994a).

To summarize, O₂ influences the selectivity of HC-SCR catalyst. In most cases, NO conversion increased when the oxygen concentration was kept at low levels (0~2%). With the increase of oxygen concentration to beyond 2%, NO conversion decreased significantly. For most combustion processes, O₂ concentration in the flue gas is higher than 2% (as listed in Table 1.1). Therefore, O₂ will inhibit the activity/selectivity of most HC-SCR catalysts because excess oxygen reacts with hydrocarbons, leading to increased hydrocarbon consumption. In fact, many researchers considered O₂ as one of the major factors negatively

impacting the performance of HC-SCR under lean-burn conditions. On the other hand, the presence of O₂ is essential for the HC-SCR process because the presence of small amount O₂ (e.g., <2%) is necessary for NO to be oxidized to NO₂, and then adsorbed by the catalyst before it is reduced to N₂ in the HC-SCR process.

2.5 Reactors for SCR of NO_x

The most commonly used reactors in the NH₃-SCR process are packed bed reactors with honeycomb monolith, metal plate-type monolith, or coated metal monolith catalyst with parallel channels (Beretta et al., 1998; Forzatti, 2001). Compared to other packed bed reactors, the monolithic reactor has the advantages of low-pressure drop, superior attrition resistance and low tendency to fly ash plugging, and high specific surface area. However, because of the relatively lower gas/solid contacting efficiency, large amounts of catalysts need to be loaded into the reactor. The flux range of the flue gas is also restricted by the volume of catalysts. From the operating point of view, the replacement of catalysts is difficult.

For NH₃-SCR of NO_x, fluidized bed reactors have been used for NO_x or simultaneous SO_x/NO_x removal by various SO₂ sorbents and NH₃- or urea-SCR catalysts (Snip et al., 1996; Gao et al., 1996; Roh et al., 2003). Compared to conventional monolithic reactors, the catalyst loading is decreased, fly ash can easily pass through and the gas/solid contact efficiency is enhanced in the fluidized bed reactor. Furthermore, the replacement of catalysts does not require the SCR system to be shut down. On the other hand, the high pressure drop in the reactor and attrition of catalyst particles and adsorbent particles may limit the application of fluidized beds in NH₃-SCR processes.

For the HC-SCR process, since the development of the catalyst and the screening of reducing agents are still the primary impediments for practical applications, most of studies were carried out in fixed bed reactors. Few researchers focused on the selection and application of reactor types for the HC-SCR process.

Iwamoto et al. (1998) introduced a new method, intermediate addition of reductant (IAR), for the HC-SCR process. An oxidation catalyst (e.g. Pt/MFI), which oxidized NO to NO₂, and a reduction catalyst (e.g. Zn/MFI), which reduced NO_x to N₂, was combined for the removal of NO_x in the presence of excess oxygen. The conversion of NO to N₂ at 300°C increased to 54% on combined Pt/MFI and Zn/MFI catalysts from 5% on Zn/MFI or 6% on Pt-MFI using ethane as the reducing agent.

Perez-Ramirez et al. (2000) reported a dual-bed catalytic system for the combined deNO_x-deN₂O process. In this system, NO was removed in the first stage over Pt/AC catalyst with propane. To further reduce the large amounts of N₂O produced in the first stage to N₂, a second deN₂O reactor bed was employed using ex-Co-Rh/Al-HTlc or Fe/ZSM-5 with propane.

Efthimiadis et al (2001) reported a fluidized bed HC-SCR process (dimensions not mentioned) using 30g Al₂O₃, Rh/Al₂O₃ or 5:95Rh/Al₂O₃-FCC as the SCR catalyst, and CH₃OH (1500ppm) or C₃H₆ (500ppm) as the reducing agent. The flue gas was the exhaust gas emitted from the regenerator of a FCCU, having following compositions: 80ppm NO_x, 4% O₂, 7% CO₂, 225ppm CO and 235ppm SO₂, with a total flow rate of 1000 ml/min treated in the SCR reactor.

2.6 NO_x storage-reduction (NSR)

Recently, a new NO_x removal process, NO_x storage-reduction (NSR), gained much attention for the application under O₂-rich lean-burn conditions, especially to truck exhaust gas. Although the mechanism of NSR is still not well understood, the common view is that, in the NSR process, NO is first oxidized to NO₂ and then trapped during lean operations over a NO_x adsorbent. The adsorbent is then regenerated with NO_x released with the released NO_x being reduced by carbon monoxide, hydrogen or hydrocarbons over the catalyst bed when the engine is run under stoichiometric or rich burn conditions for a short period of time.

Similar to HC-SCR catalyst, some catalysts, such as Pt/Al₂O₃, had been proposed but showed insufficient activity for the NSR process (Olsson et al., 2001; Shinjoh et al., 1998). A new type of catalyst, which combines NO_x adsorption and reduction materials, was extensively investigated. Typically, alkali or alkaline earth metals, such as barium and potassium, were chosen as NO_x storage components, and noble metals, such as platinum and rhodium, as NO_x oxidation and reduction components with the support of some metal oxides (Al₂O₃, etc.) (Fridell et al., 1999; Epling et al., 2003; Abdulhamid et al., 2004). Among them, Pt-Ba/Al₂O₃ was the mostly investigated NSR catalyst with CO, H₂ or C₃H₆ as the reducing agent, which can provide high NO_x removal efficiency (>90%) in successive sequences of lean and rich modes (Bogner et al., 1995). However, the inhibition of SO₂ is still a problem (Hodjati et al., 1998a; Schreier et al., 2005; Hammache et al. 2008).

Although NSR gained extensive attention as a potential solution to automobile exhaust gas NO_x control because the engine can be relatively easily controlled to be run over the lean and rich cycles, it is difficult to apply NSR for the flue gas emitted from stationary sources because the oxygen concentration cannot be easily adjusted without upsetting the upstream process.

Similar to NSR, Elkaim and Bai (2000) proposed a method for removing O₂ from the flue gas by adsorption/desorption in order to create an oxygen-free stream for the effective reduction of NO_x. According to their patent, NO was first temporarily adsorbed by an adsorbent (activated carbon), then NO in the NO-rich adsorbent was desorbed by heating the adsorbent or by contacting an inert carrier gas (N₂) to create an oxygen-free gas stream. NO in the oxygen-free gas stream was subsequently passed to a catalyst bed to have NO reduced by a reducing agent (hydrocarbons). This patent first reported the concept of separating HC-SCR process into two steps: adsorption and reduction.

2.7 Summary

HC-SCR has been widely studied in recent years, with focus mainly on the preparation and evaluation of catalysts, effects of flue gas compositions and reducing agents, and reaction mechanisms.

ZSM-5 and Al₂O₃ are commonly used catalyst supports in HC-SCR process, and many metals have been loaded onto catalyst supports as active elements, such as Pt, Ag, Cu, Co and Fe. Among reported catalysts in the literature, Fe/ZSM-5 gained extensive attention due to its stable reactivity and high hydrothermal durability. Although Pt/ZSM-5 and Ag/Al₂O₃ also exhibited good performance in HC-SCR, they are not economical for the treatment of the flue gas from stationary combustion processes due to the high cost in the preparation of these catalysts using Pt or Ag as active elements.

Many hydrocarbons have been proven effective in HC-SCR, such as methane, propane, propylene, and iso-butane. Although methane has been widely investigated as the reducing agent in HC-SCR, it has been found to be effective only in SCR of NO_x over Co/zeolites and some other catalysts at temperatures higher than 450°C. Propane, propylene

and iso-butane showed different performance in HC-SCR, depending on the type of catalyst and reaction conditions used in the experiment. If Fe/ZSM-5 is chosen as the HC-SCR catalyst, then propylene will be a good candidate as the reducing agent because of its relatively high reaction temperature window which can avoid the catalyst deactivation caused by the formation of a carbonaceous deposit on the catalyst surface at low temperatures (Chen et al., 1999).

The poisoning components (SO_2 and H_2O) and excess O_2 in the flue gas showed significant negative impacts on HC-SCR. Fe/ZSM-5, Pt/ZSM-5, Co/Beta-zeolite, Ag/ Al_2O_3 and Ce-In/ZSM-5 exhibited a good hydrothermal resistance. However, only Co/ Al_2O_3 , Ag/ Al_2O_3 and Cu/SUZ-4 showed some tolerance to SO_2 at low concentrations. As a key component of the flue gas under lean burn conditions, the excess O_2 inhibited the activity/selectivity of most catalysts in HC-SCR process. On the other hand, according to one of the reaction mechanisms, a small amount of O_2 is necessary for NO_x reduction.

Chapter 3

Adsorption and Reaction Kinetics

3.1 Experimental setup

To investigate the reaction kinetics and adsorption performance of selected catalysts under various temperatures and flue gas compositions, a fixed bed reaction system was constructed as shown schematically in Figure 3.1. The system consists of a tubular reactor, a gas supply and flow rate control unit, a gas preheating unit, a gas heating unit (furnace), a gas analysis unit and a data acquisition unit. A stainless steel tubular reactor with an inner diameter of 13.5mm was used in this experiment, and the catalyst packing height was maintained at 50.8 mm throughout all the tests.

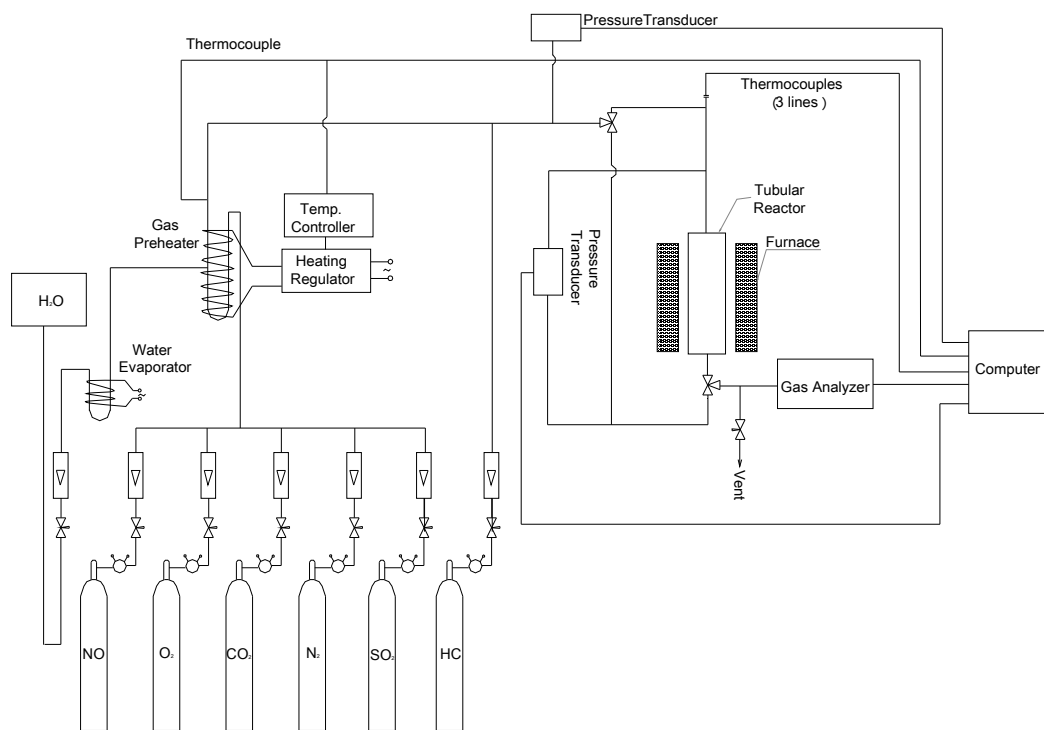


Figure 3.1 The fixed bed reaction system

The model flue gas used in the experiment was a mixture prepared from several gas cylinders: 50% O₂ balanced with N₂, 0.6% NO balanced with N₂, 10% SO₂ balanced with N₂, pure CO₂ and pure N₂ gas cylinders from Praxair Products Inc. The reducing agent used in the experiment was propylene. The gas cylinder containing 1.2% propylene balanced with N₂ was also supplied by Praxair. Deionized water was pumped into the system using a LKB Microperpex peristaltic pump, heated and evaporated through a water evaporator, and then pre-mixed with other gases if necessary. The compositions of the effluent gases (NO_x, CO, CO₂, and SO₂) were analyzed by a Horiba PG-250 flue gas analyzer. In the presence of oxygen, NO in the model flue gas will be partially oxidized to NO₂. Since the gas analyzer measures NO and NO₂ together, all calculations related to NO adsorption and conversion throughout this work were based on NO_x (NO + NO₂) although only NO was fed into the reaction system.

Before the start up of the experiment, the reactor was first heated to the desired temperature with pure N₂ gas passing through the catalyst bed. After the reactor temperature was stabilized, the flow of a gas mixture at a preset composition was turned on to start the experiment, with the gas mixture composition determined by the gas analyzer via bypassing the gas from the reactor.

In the adsorption experiment, the model flue gas was pre-mixed with pure N₂ as the balancing gas according to the preset flow rate and concentrations of NO and O₂. The mixed flue gas was then preheated to 150°C by the preheating system, and the composition was measured by the gas analyzer. After stable readings of the analyzer were reached, which corresponded to the inlet model flue gas concentrations, the three way valves were switched to the reactor and the time was recorded as the starting point of the adsorption. During the adsorption process, the gas composition at the reactor's outlet was continuously monitored

until the NO_x concentration became stable, with the final NO_x concentration defined as the equilibrium NO_x concentration. Thereafter, the NO flow from the gas cylinder was turned off and, at the same time, HC (i.e. propylene) at the same flow rate of NO was added into the $\text{O}_2 + \text{N}_2$ flow to start the catalytic reduction process by reacting propylene with the adsorbed NO_x on the catalyst. After 45 minutes, the HC flow was turned off and the gas composition passing through the catalyst bed was adjusted to 10% $\text{O}_2 +$ balanced N_2 at a flow rate of 500 ml/min to further remove the adsorbed HC or other intermediate species produced in the reduction process. This stripping process took 30~45 minutes or even longer to lower the outlet CO concentration to below 5 ppm. Afterward, pure N_2 was used to purge the catalyst bed for another 45 minutes to remove all adsorbed CO_x and O_2 from the catalyst.

In the reaction kinetics experiment, the flue gas was prepared in the same way as in the adsorption experiment, and the HC flow at the desired HC:NO ratio was injected right after the pre-heater to have it mix with other model flue gases and to minimize the oxidation of the HC outside the reactor. The composition of the gas mixture was first measured via bypassing the gas mixture to the gas analyzer before the gas flow was switched to the reactor for the reaction experiment. After the reaction was finished, the gas flow was switched back to the bypass route to have the inlet gas concentration checked.

3.2 Catalyst preparation

In most HC-SCR processes using ZSM-5 as the catalyst support, $\text{NH}_4/\text{ZSM-5}$ or $\text{H}/\text{ZSM-5}$ was first prepared from $\text{Na}/\text{ZSM-5}$ via wet ion-exchange method using aqueous NH_4NO_3 solution, followed by calcination in air at 500°C for 4 hours.

As the active element in the SCR process, Fe is often loaded onto the catalyst support in four ways: conventional wet ion-exchange (WIE), incipient wetness impregnation in

aqueous solution (IMPA), impregnation in organic solution (IMPO) and sublimation or chemical vapour deposition (CVD). FeCl_2 , FeCl_3 , $\text{Fe}(\text{NO}_3)_3$, $\text{Fe}_2(\text{SO}_4)_3$ and iron (III) acetylacetonate ($\text{Fe}(\text{AA})_3$) are most common used iron sources.

It was reported that catalysts prepared by both WIE and IMPA methods had similar activity for NH_3 -SCR of NO_x , except that the IMPA method was simpler and less costly than WIE method (Long and Yang, 1999; Qi and Yang, 2005). Although Fe/ZSM-5 prepared by CVD method showed high catalytic activity and stability in HC-SCR of NO_x (Chen et al, 1998), it is difficult to implement this process for the production of large quantities of catalysts considering the complexity of the preparation process. Fe/ZSM-5 prepared by IMPO method was first used in the study of NH_3 -SCR process by Delahay et al. (2005). A recent study from Lima et al. (2008) showed that Fe/ZSM-5 prepared by IMPO demonstrated high activity in NH_3 -SCR and acceptable NO conversion in HC-SCR using n-decane as the reducing agent. Based on all the above aspects, WIE and IMPO were selected for the preparation of the catalysts in this study.

3.2.1 Materials

Two types of ZSM-5 were selected as the support of the catalyst in this experiment, i.e., Na/ZSM-5 (PUC) purchased from The China University of Petroleum (Beijing, China) and a free sample of H/ZSM-5 (Albemarle) kindly supplied by Albemarle Corporation (USA). It should be noted that both particles are not pure ZSM-5 but a mixture of pure ZSM-5 and additives which were added in the prilling process. To examine the influence of particle size, the coarse Na/ZSM-5(PUC) was crushed and sieved to obtain a fine Na/ZSM-5 (crushed PUC). A spent FCC catalyst was also selected as the catalyst support. The properties of the catalyst supports are listed in Table 3.1.

Table 3.1 Properties of the catalyst supports

Catalyst support	Average particle size	Apparent bulk density	S _{BET}	Provider
Na/ZSM-5 (PUC)	1042 μm	903 kg/m ³	118 m ² /g	China University of Petroleum
H/ZSM-5 (Albemarle)	155 μm	968 kg/m ³	171 m ² /g	Albemarle Corp.(USA)
Na/ZSM-5 (Crushed PUC)	234 μm	764 kg/m ³	192 m ² /g	Crushed from original Na/ZSM-5 (PUC)
Spent FCC	116 μm	922 kg/m ³	N/A	Chevron Refinery

The following chemicals were used in the preparation of the catalysts:

- Ammonium nitrate : NH₄NO₃, 99.0%, M.W.=80.04 g/mol, Sigma-Aldrich
- Iron (III) acetylacetonate (Fe(AA)₃): [CH₃COCH=C(O-)CH₃]₃Fe, 97%, M.W.=353.18 g/mol, Sigma-Aldrich
- Ferrous chloride: FeCl₂ · 4H₂O, 102.0% (as FeCl₂ · 4H₂O), M.W.=198.81 g/mol, Fisher
- Toluene: C₇H₈, >=99.5%, M.W.=92.14 g/mol, Sigma-Aldrich
- Deionized water

3.2.2 Preparation of NH₄/ZSM-5 and H/ZSM-5

NH₄/ZSM-5 was prepared from Na/ZSM-5 by exchanging with NH₄NO₃ solution. 100g of Na/ZSM-5 was mixed with 100ml of 0.5M NH₄NO₃ solution at the room temperature, and the slurry was stirred periodically. After 3 hours, the catalyst in the slurry was separated from the NH₄NO₃ solution, mixed with another batch of fresh 0.5M NH₄NO₃ solution (100ml). After 3 times of the aqueous ion-exchange process, the catalyst was washed thoroughly with 250ml of deionized water for 5 times, dried in air at 120°C for 12 hours to form NH₄/ZSM-5, and then calcined in air at 500°C for 4 hours to form H/ZSM-5.

3.2.3 Preparation of Fe/ZSM-5 by WIE method

20g NH₄/ZSM-5 was added to 500ml of 0.5M FeCl₂ solution with constant stirring. After 24 hours, the mixture was filtered and then washed five times with deionized water, dried at 120°C for 12 hours and then calcined in air at 500°C for 6 hours.

3.2.4 Preparation of Fe/ZSM-5 by IMPO method

56g H/ZSM-5 was added to a solution containing 20g Fe(AA)₃ + 200 ml toluene. The slurry was stirred periodically for 24 hours. Toluene was then evaporated from the slurry and recycled, and the residue after the evaporation was dried in air at 120°C for 12 hours and calcined in air at 500°C for 6 hours.

3.3 Performance of Fe/ZSM-5 (PUC) catalyst prepared by IMPO

3.3.1 Adsorption performance of Fe/ZSM-5(PUC)

The adsorption isotherm behaviour of the Fe/ZSM-5(PUC) catalyst prepared by IMPO method was investigated under various temperatures and inlet NO concentrations using a model flue gas with 5% (v/v) O₂ balanced with N₂ at GHSV=5000 h⁻¹. The catalyst loading in the reactor was 6.58g. The NO concentration of the model flue gas varied from 200 to 1000 ppm with an increment of 200 ppm and the temperature from 250 to 400°C with an increment of 30°C. For each given temperature and gas composition, the adsorption curve was determined experimentally, with the result at T=250°C shown in Figures 3.2. Adsorption curves at other temperatures are shown in Appendix G (Figures G.1 to G.5)

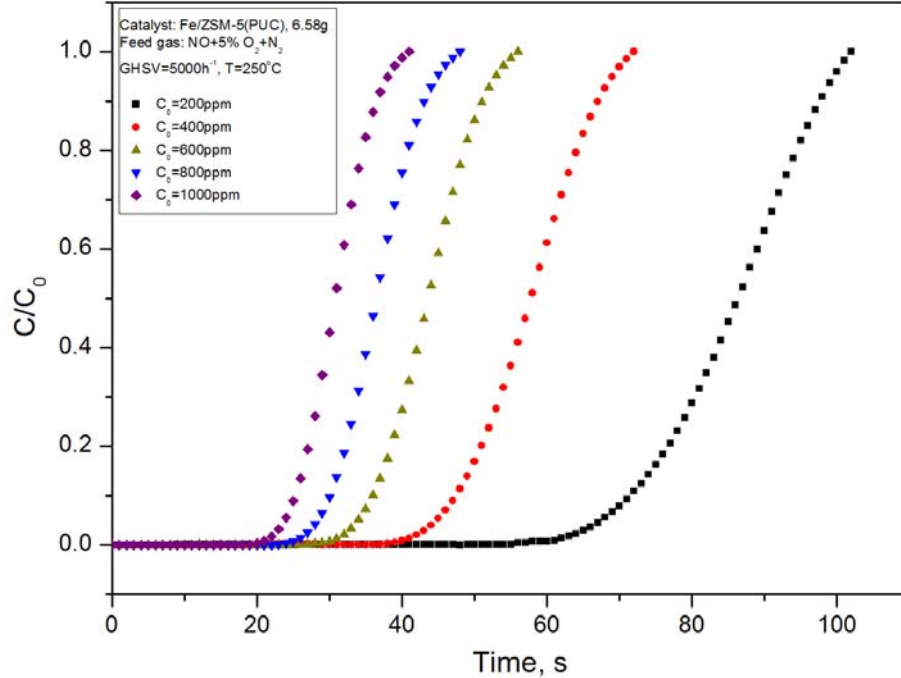


Figure 3.2 Adsorption curves based on NO_x concentrations at the reactor outlet (Catalyst: Fe/ZSM-5(PUC), $T=250^\circ\text{C}$)

Since there exists a delay in system response time for the gas analyzer, the delay time needs to be subtracted from the recorded adsorption time. Because the response time varied with the operating temperature, the delay time was determined separately for each operating temperature. It is clear from Figure 3.2 that, at a given temperature, with the increase of equilibrium NO_x concentration (C_0), the adsorption curve moved towards the left, indicating that the catalyst bed was saturated more quickly by NO_x at higher C_0 .

The equilibrium adsorption capacity of NO_x on the catalyst was calculated by

$$q_e = \frac{P \times C_0 \times 10^{-3} \times F \times M_{\text{NO}}}{R \times (T_0 + 273)} \times \frac{S}{W_{\text{cat}}} \quad (3.1)$$

where

q_e , adsorption equilibrium capacity of NO_x on the catalyst, mg/g

P , operating pressure, Pa

C_0 , equilibrium NO_x concentration, ppm

F , model flue gas flow rate at room temperature, m^3/s

M_{NO} , molecular weight of NO, 30 g/mol

R , universal gas constant, 8.314 J/(mol.K)

T_0 , ambient temperature, $^\circ\text{C}$

S , integrated area of the adsorption curve, s

$W_{\text{cat.}}$, catalyst loading, g

The integrated area, S , of the adsorption curve was calculated by

$$S = \int_0^t \left(1 - \frac{C_{\text{NO}_x, \text{out}}}{C_0}\right) dt \quad (3.2)$$

where

$C_{\text{NO}_x, \text{out}}$, the outlet concentration of NO_x , ppm

t , adsorption time, s

The Freundlich equation

$$q_e = \alpha C_0^\beta \quad (3.3)$$

was applied to fit q_e as a function of C_0 . The calculated q_e and the curve fitting results using Freundlich equation were shown in Figure 3.3. For a given temperature, the adsorption capacity of the catalyst increased significantly with the increase of the equilibrium NO_x concentration. At a given equilibrium NO_x concentration, the adsorption capacity of the catalyst decreased with the increase of the adsorption temperature.

Using α and β fitted in Figure 3.3, correlations of α and β as a function of temperature were derived (Figure 3.4) by least-square curve fitting with a second-order polynomial function:

$$\alpha = 0.46179 - 0.00123T + 8.7123 \times 10^{-7} T^2 \quad (3.4)$$

$$\beta = -7.13236 + 0.024T - 1.81409 \times 10^{-5} T^2 \quad (3.5)$$

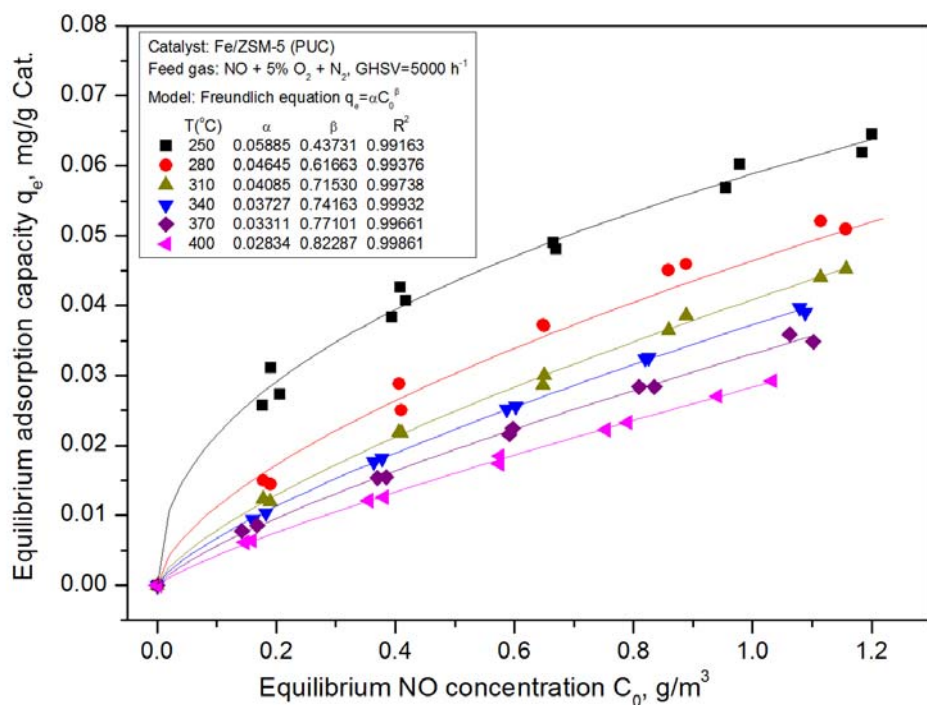


Figure 3.3 Fitted adsorption isotherms of NO_x by Freundlich equation (Catalyst: Fe/ZSM-5(PUC))

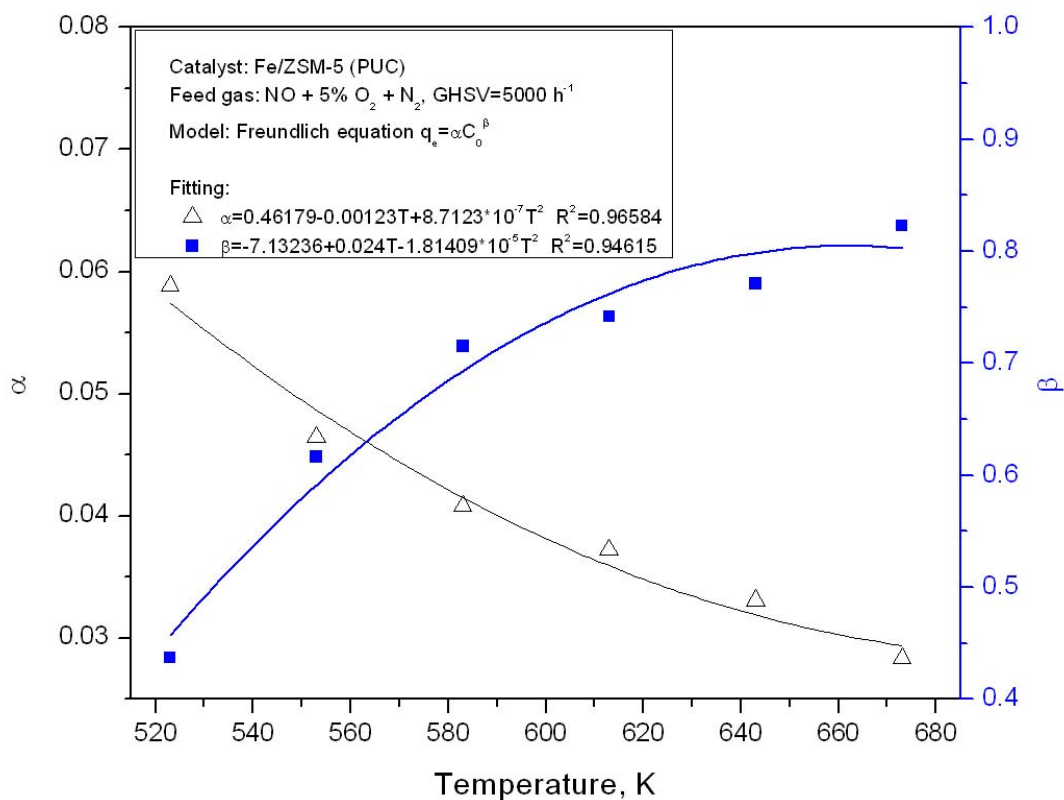


Figure 3.4 Relationship between α/β and adsorption temperature (Catalyst: Fe/ZSM-5(PUC))

3.3.2 Reaction performance of Fe/ZSM-5(PUC)

To investigate the influence of temperature, gas hourly space velocity (GHSV), HC and O₂ concentrations on the SCR performance of the catalyst, the HC-SCR of NO_x was conducted in the tubular reactor. The model flue gas consisted of 600ppm NO, 0.5% to 8% (v/v) O₂, balanced with N₂. The HC:NO molar ratio in the model flue gas ranged from 0.5:1 to 4:1. The time-on-stream test was also performed to evaluate the durability and stability of the catalyst.

As a promising catalyst, Fe/ZSM-5 has shown effectiveness in the SCR of N₂O by propylene (Yamada et al., 1998). Since N₂O can be converted completely to N₂ over Fe/ZSM-5 catalyst under experimental conditions similar to this study, and only NO was used in the model flue gas in this study, the concentration of N₂O in the flue gas exiting the reactor was expected to exist only at very low level in comparison with NO_x. Therefore, N₂O in the stream exiting the reactor was not monitored in this study.

The NO_x conversion was calculated based on measured inlet and outlet NO_x concentrations by

$$X_{NO_x} = \frac{C_{NO_x,in} - C_{NO_x,out}}{C_{NO_x,in}} \times 100\% \quad (3.6)$$

Because the gas analyzer used in the experiment can only measure the concentrations of CO and CO₂, the conversion of propylene was calculated by carbon balance based on the measured concentrations of CO and CO₂ at the reactor's outlet,

$$X_{HC} = \frac{C_{CO,out} (ppm) + C_{CO_2,out} (\%) \times 10^4}{3 \times C_{HC,in} (ppm)} \times 100\% \quad (3.7)$$

The inlet concentration of propylene ($C_{\text{HC,in}}$) in equation 3.7 was estimated based on the measured flow rate from the certified (1.2% propylene + N₂) gas cylinder and the total feed gas flow rate. For example, if the total flow rate of gas feed is 600 ml/min and 60 ml/min is from the (1.2% HC + N₂) cylinder, the HC concentration in the feed gas should be $60 \times 1.2\% / 600 = 0.12\%$ or 1200ppm. A coefficient of 3 is included in equation 3.7 because one mole of propylene could produce 3 moles of carbon. It should be noted that other intermediate species (or incompletely oxidized products) might be generated from propylene, which had not been monitored and considered in the calculation for HC conversion. Thus, equation 3.7 may underestimate the HC conversion.

3.3.2.1 Effect of reaction temperature on catalytic activity

Using 600 ppm NO + 1200 ppm HC + 1% O₂ + balanced N₂ as the reacting gas mixture, the time-on-stream test at a gas space velocity of 5000 h⁻¹ was conducted on the Fe/ZSM-5 (PUC) catalyst. Typical profiles of NO_x and HC conversions and the outlet concentration of CO at 250°C and 350°C are shown in Figures 3.5 and 3.6, respectively. Results at other temperatures are shown in Figures G.13 to G.16 in Appendix G.

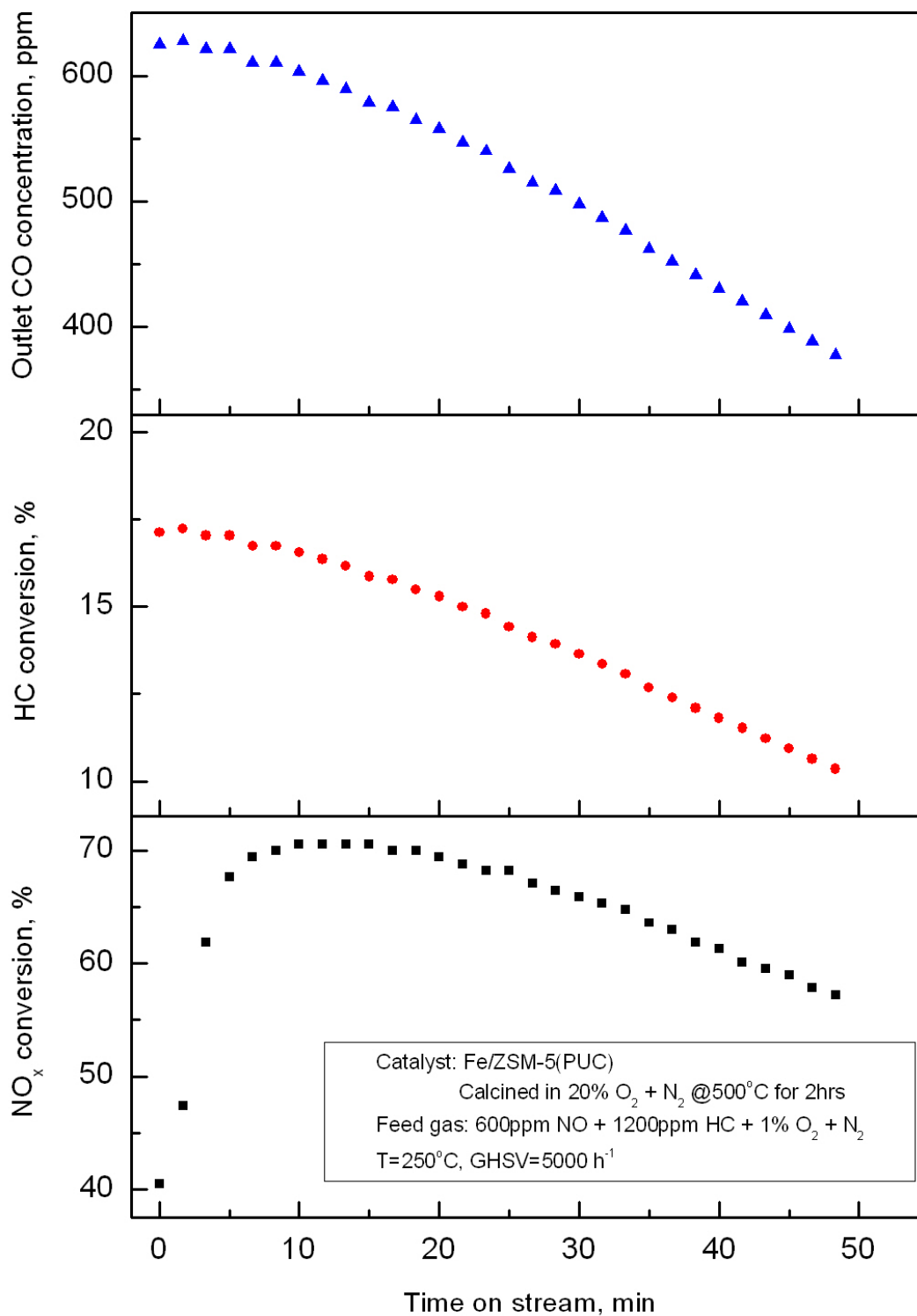


Figure 3.5 Profiles of NO_x and HC conversions and outlet CO concentration (Catalyst: Fe/ZSM-5(PUC), T=250°C, [O₂]=1%)

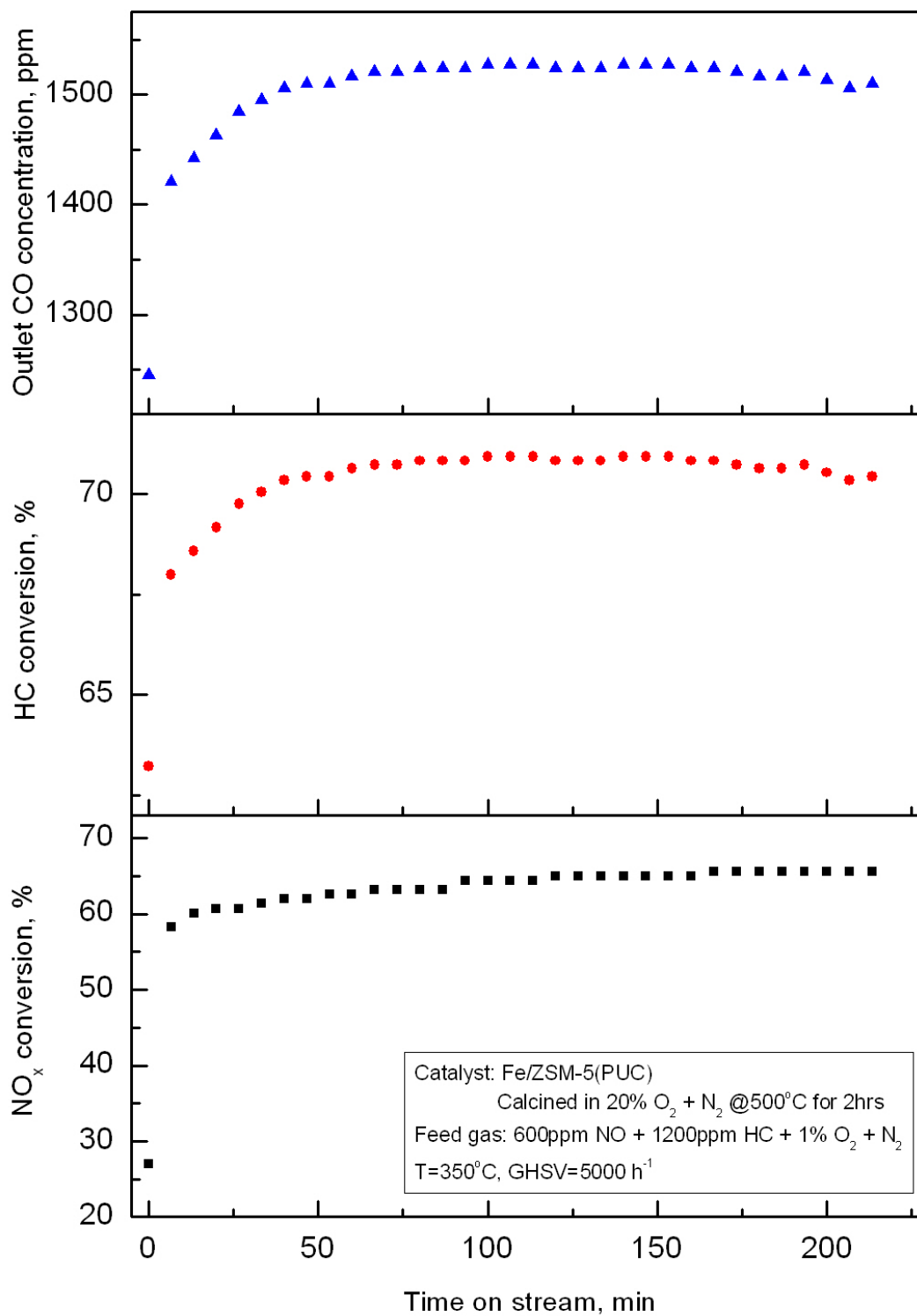


Figure 3.6 Profiles of NO_x and HC conversions and outlet CO concentration (Catalyst: Fe/ZSM-5(PUC), T=350°C, [O₂]=1%)

It should be noted that the catalyst was calcined in 20% O₂ + N₂ at 500°C for 2 hours to fully regenerate the catalyst prior to each test at a given temperature.

As shown in Figure 3.5, the NO_x conversion increased quickly to a maximum and then decreased steadily with time, indicating a decaying catalytic activity at T=250°C. Meanwhile, HC conversion was low and decreased with time, which is also reflected by the low and decreasing outlet CO concentration. It was found that CO was the main product from HC oxidation and almost no CO₂ was detected at this temperature.

When the reaction temperature was increased to 350°C, as shown in Figure 3.6, both NO_x and HC conversions and outlet CO concentration kept relatively stable within the tested period. Furthermore, the outlet CO concentration and HC conversion increased very quickly with the increase in temperature. At this temperature, the CO to CO₂ ratio in the flue gas exiting the reactor was 58%:42%. Although CO₂ increased significantly, it was still lower than CO in the exhaust gas stream. This result agreed with those reported in the literature using Fe/ZSM-5 as the deNO_x catalyst (Chen et al, 1998).

To investigate the effect of the reaction temperature on the catalytic performance of Fe/ZSM-5(PUC), the time-on-stream test was conducted with the temperature ranging from 250 to 350°C with an increment of 25°C, with the results shown in Figures 3.7 and 3.8 for NO_x and HC conversions, respectively.

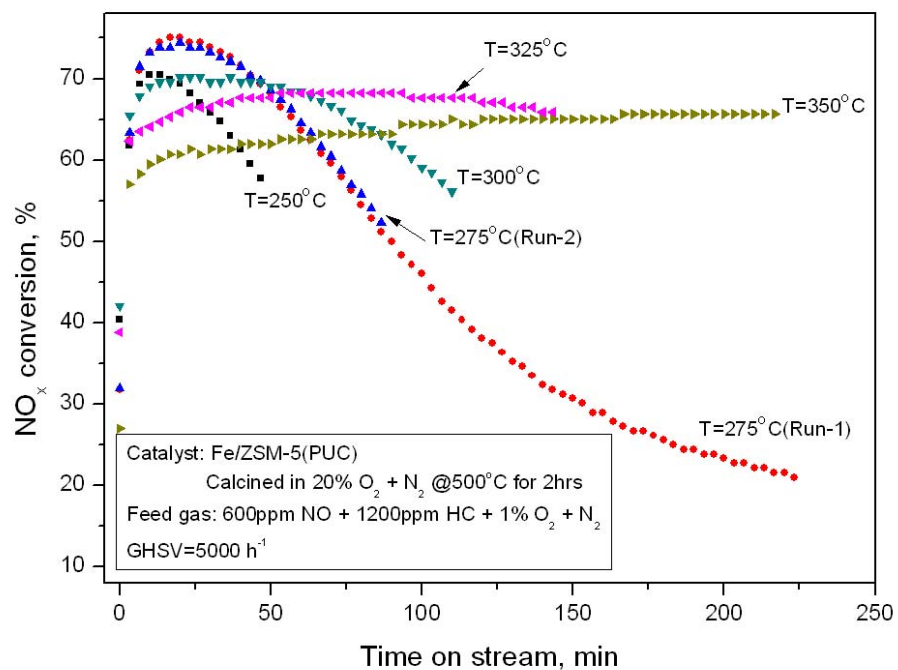


Figure 3.7 Effect of reaction temperature on NO_x conversion (Catalyst: Fe/ZSM-5(PUC))

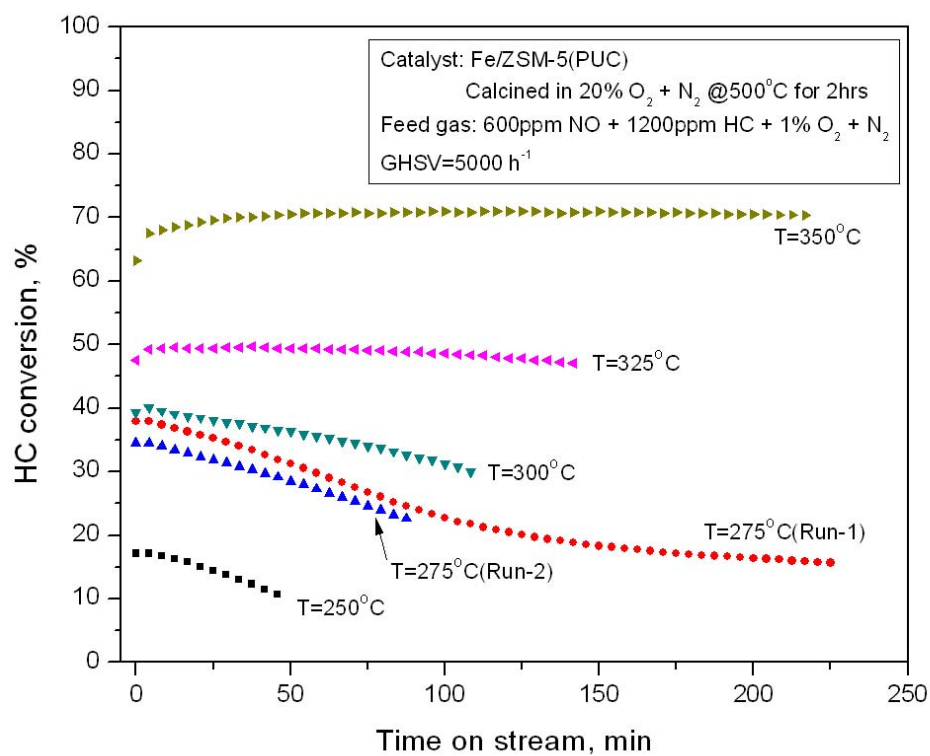


Figure 3.8 Effect of reaction temperature on HC conversion (Catalyst: Fe/ZSM-5(PUC))

Peak NO_x conversions at different reactor temperatures were around 70.5% (250°C), 75% (74.4% for repeated run) (275°C), 70.2% (300°C), 68.2% (325°C) and 65.6% (350°C), respectively, for the current Fe/ZSM-5 (PUC) catalyst, with the highest NO_x conversion achieved at 275°C. With the further increase of the temperature beyond 275°C, the peak NO_x conversion decreased. However, at lower temperatures (<325°C), the catalyst activity was quite unstable and the conversion decreased very quickly with time. This result is consistent with findings from Chen et al. (1999, 2000b) using iso-butane or n-butane as the reducing agent. According to their study, the deactivation of Fe/ZSM-5 was caused by the formation of a carbonaceous deposit which was not swiftly volatilized at a low temperature (300°C).

The durability or stability of the catalyst improved with the increase of reaction temperature. At T=350°C, the catalyst showed stable, yet lowest NO_x conversion. This means that to achieve a high NO_x conversion, a low temperature is preferred. On the other hand, the stable catalytic activity could be achieved only at high temperatures. Considering the requirement of catalyst durability in practical applications, coupling with the desired high reaction activity of NO_x reduction, the optimal reaction temperature should be around 350°C for the Fe/ZSM-5(PUC) catalyst prepared by the IMPO method.

Compared to NO_x conversion in Figure 3.7, HC conversion always increased with increasing reaction temperature (Figure 3.8). Peak HC conversions were 17.2% (250°C), 38.2% (34.8% for repeated run) (275°C), 40.2% (300°C), 49.6% (325°C) and 71.0% (350°C), respectively. This is because the oxidation reaction generally increased with increasing reactor temperature. It is noted that when the reactor was operated in the right temperature window, the catalytic activity kept stable and the consumption of hydrocarbon by the SCR process also remained at a relatively stable level. On the contrary, when the catalyst lost its activity gradually with time at low temperatures, the amount of hydrocarbon consumed in the

SCR process also decreased, leading to a decrease of HC conversion with time. The peak HC conversion did not always correspond to the peak NO_x conversion at each temperature, because HC was catalytically oxidized by both NO_x and O₂.

3.3.2.2 Catalyst deactivation at low temperatures

Further investigation revealed that the catalyst deactivation at temperatures lower than 325°C might be induced by intermediates generated from the incomplete oxidation of hydrocarbons. As shown in Figure 3.9, when O₂ concentration in the flue gas increased from 1% to 4%, the peak NO_x conversion decreased from 75% to 67.9%, but the catalyst activity remained stable for a much longer time at higher O₂ level. One may infer that the intermediate species of the hydrocarbon and carbon deposit produced in the NO_x reduction process gradually covered the active sites of the catalyst in the reaction process, and resulted in the catalyst deactivation at low O₂ concentrations. At high O₂ concentrations, the intermediate species were oxidized by excessive O₂ and thus left the catalyst sites active for the adsorption of NO_x. Similarly, high temperatures can promote the complete combustion of the HC intermediate species and thus reduce the amount of hydrocarbon intermediates and carbon deposit on active sites.

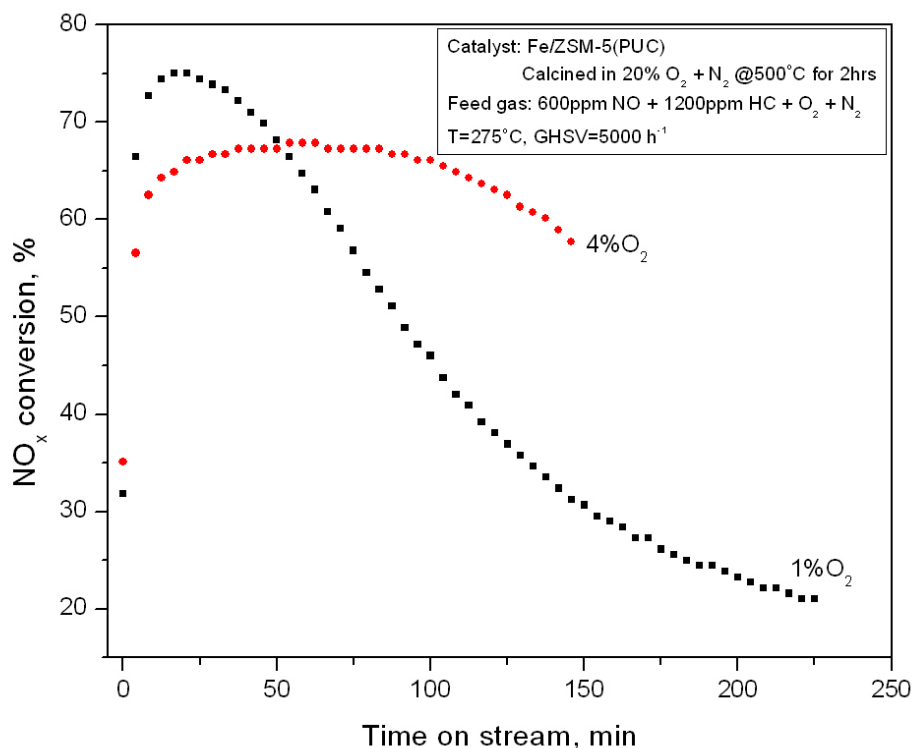


Figure 3.9 Effect of inlet O₂ concentration on the catalytic activity (Catalyst: Fe/ZSM-5(PUC))

To elucidate the catalyst deactivation, the single point BET surface area of fresh, deactivated and regenerated catalysts under T=275°C was measured and shown in Figure 3.10. The deactivated catalyst was regenerated in the flow of 20% O₂ + N₂ at T=500°C for 2 hours, followed by N₂ flush for 20 minutes. The instrument used for measuring the catalyst surface area was a Micromeritics Flowsorb II 2300 with a gas flow of 30%V N₂ + 70%V He.

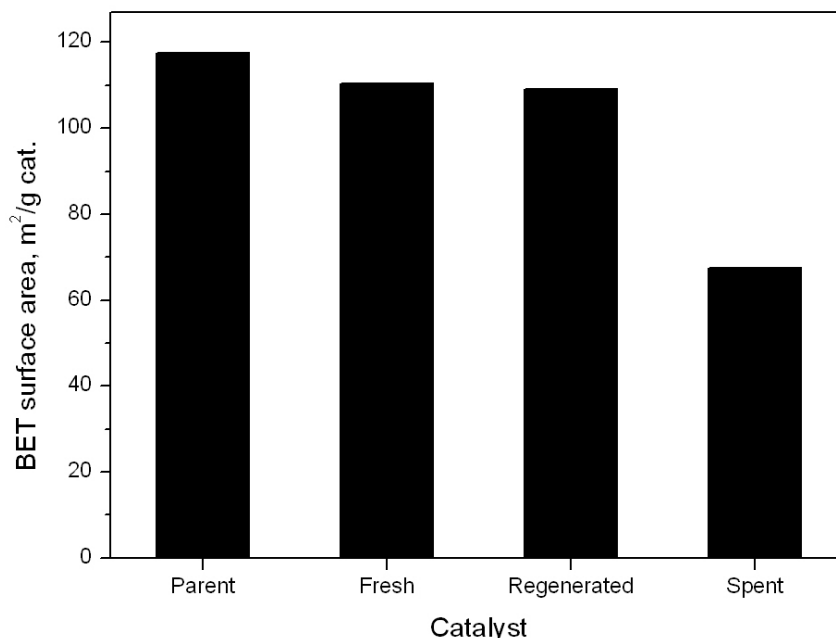


Figure 3.10 Comparison of BET surface areas (Catalyst: Fe/ZSM-5 (PUC))

The impregnation of Fe led to a slight decrease in the surface area from 118 m²/g (parent Na/ZSM-5) to 110 m²/g (fresh Fe/ZSM-5). The surface area of the deactivated catalyst decreased significantly to 68 m²/g, and was almost completely recovered to 109 m²/g after regeneration. Since only NO, propylene, O₂ and N₂ were introduced into the reactor, the only explanation for the decrease of the BET surface area of the deactivated catalyst was the deposit of the partially oxidized hydrocarbon intermediates or graphitic carbon.

Further evaluation was carried out based on X-ray photoelectron spectroscopy (XPS) on the surface element of fresh, deactivated and regenerated catalysts, with differences identified in the C 1s region as shown in Figure 3.11 (see also Figures G.20 to G.26 in Appendix G for other XPS results).

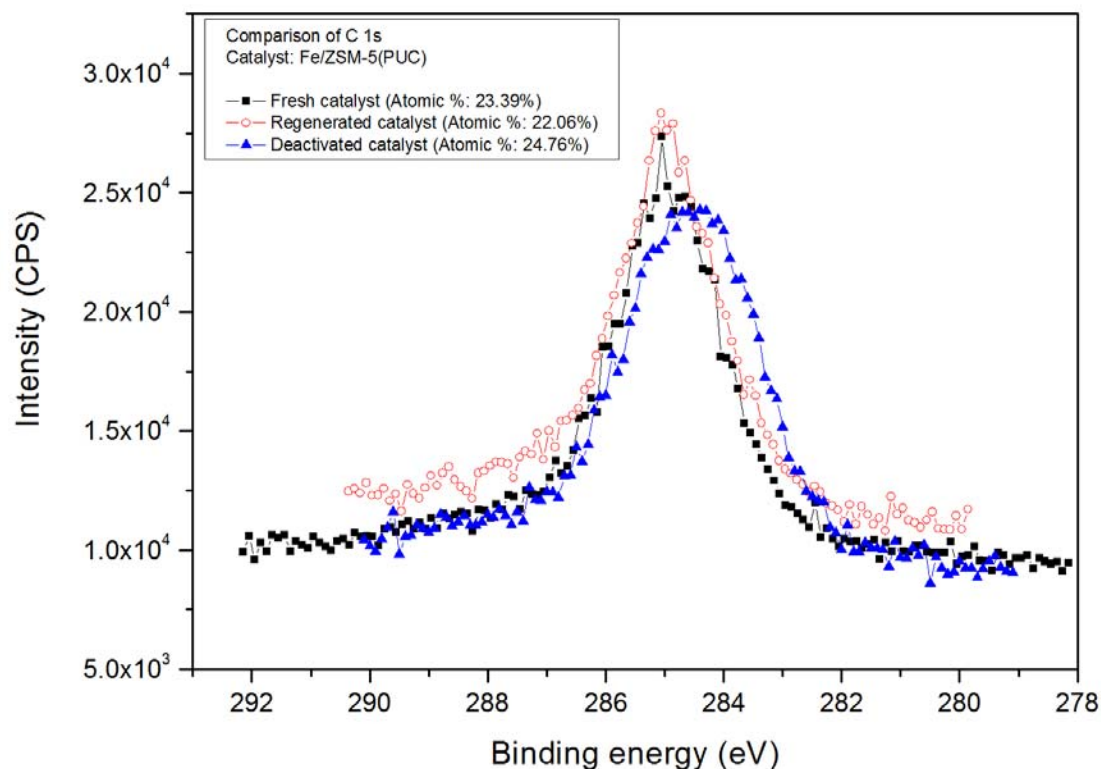


Figure 3.11 XPS narrow scan for C 1s (Catalyst: Fe/ZSM-5(PUC))

The binding energy corresponding to the peak intensity in the narrow spectra scan for C 1s region of the fresh, deactivated and regenerated catalyst were 285.05, 284.40 and 285.06, respectively. The atomic percentages of the C 1s on the surface of the catalysts were 23.39%, 24.76%, and 22.06%, respectively, for fresh, deactivated and regenerated catalyst. Because of the existence of the adsorbed gaseous carbon, i.e., CO_2 , the difference among the atomic percentages of the C 1s on the surface of the catalysts could not prove the existence of the graphitic carbon. However, the peak position shift from the higher binding energy for the fresh and regenerated catalysts to the lower binding energy for the deactivated catalyst may be attributed to the deposit of the graphitic carbon on the catalyst surface which covered the active sites of the catalyst, and was considered as the possible reason for the deactivation of the catalyst.

To further investigate the possible reason for the deactivation of the catalyst at low temperatures, a thermogravimetric analysis (TGA) was performed using a Shimadzu TGA-50 thermogravimetric analyzer. In the experiment, catalyst samples were aged in the tubular reactor for 6 hours by contacting the flue gas consisting of 600ppm NO + 1200 ppm HC +1% O₂ + N₂ at 275 and 350°C, respectively. The sample was then placed into the TGA under a N₂ atmosphere and heated up from room temperature to 250°C with a ramp of 20°C/min. The temperature was maintained at 250°C for 10 minutes to volatilize adsorbed gas components. Thereafter, the temperature was increased to 500°C with a ramp of 5°C/min and maintained at 500°C for 30 minutes. Weight changes during above period were recorded and are shown in Figure 3.12 for the sample aged at 275°C and Figure 3.13 for the sample aged at 350°C.

Both samples showed some weight loss (-2.03% in Figure 3.12 and -1.53% in Figure 3.13) when heated up from room temperature to 250°C, which indicates that both samples contained some adsorbed gas components. Over the period of the temperature rise from 250 to 500°C and stabilized at 500°C, the catalyst aged at 275°C lost 1.38% of its total weight while the catalyst aged at 350°C lost only 0.23% of its weight, which suggests that more carbonaceous compounds were deposited onto the catalyst at 275°C than at 350°C, and led to catalyst deactivation. Also, most of deposited carbonaceous compounds on the catalyst aged at 350°C could be removed at relatively lower temperatures than those deposited on the catalyst aged at 275°C, implying that catalyst aged at 350°C could be regenerated at lower temperatures or over a shorter period of time than catalyst aged at 275°C.

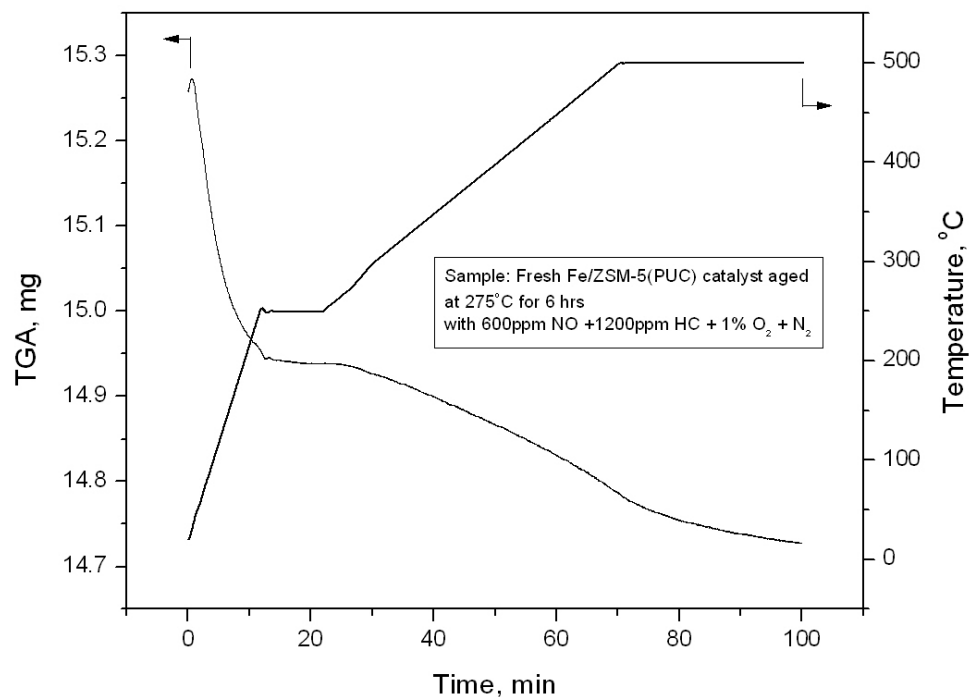


Figure 3.12 TGA result for the catalyst aged at 275°C

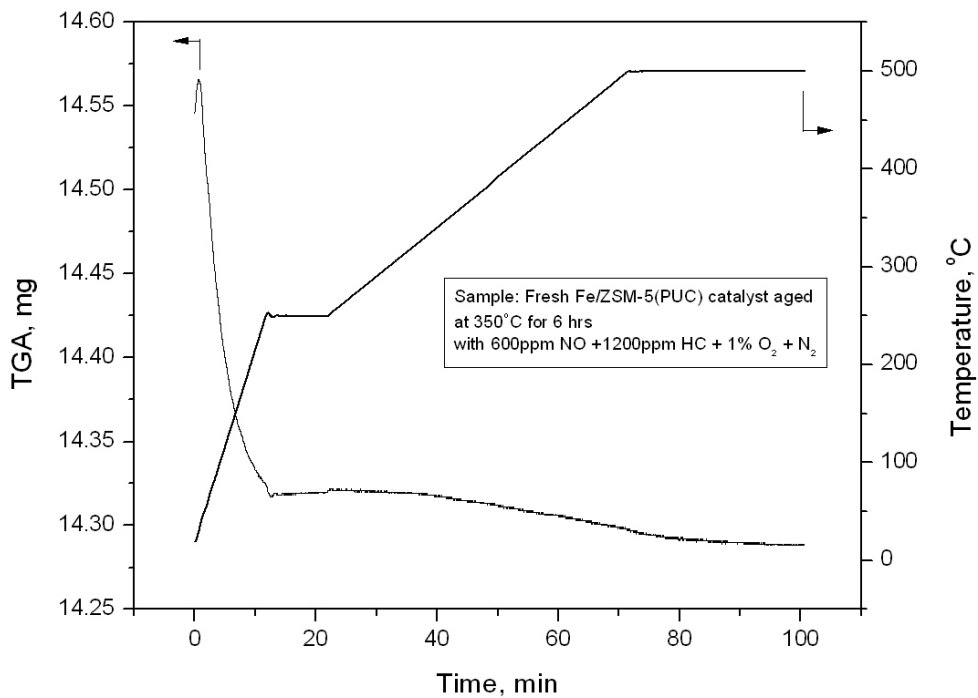


Figure 3.13 TGA result for the catalyst aged at 350°C

To improve the recovery of the catalytic activity of the catalyst deactivated at low reaction temperatures, several regeneration methods were tested at 275°C with the results shown in Figure 3.14.

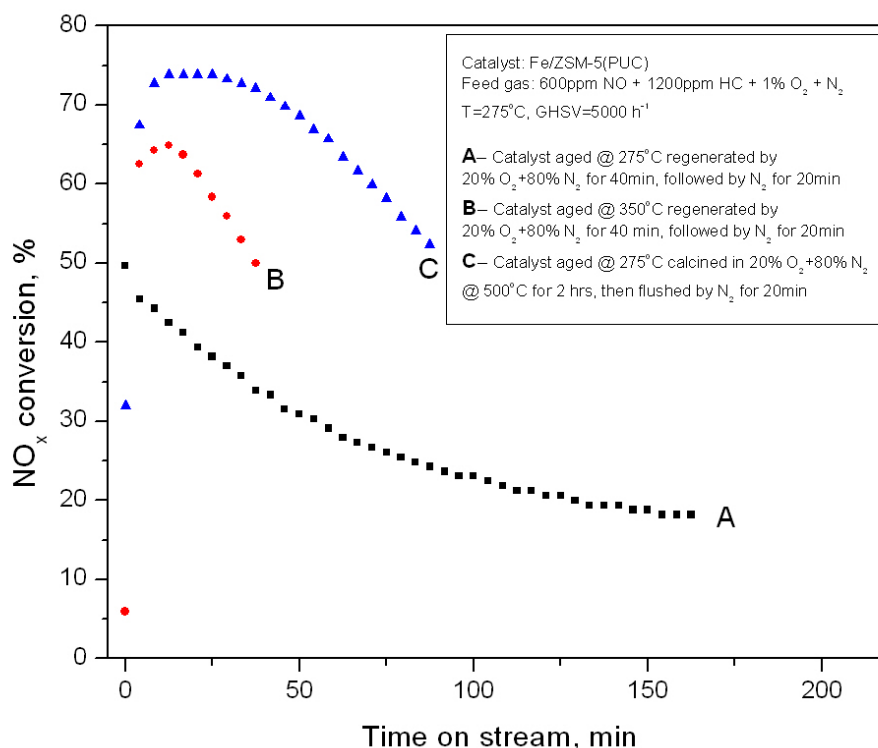


Figure 3.14 Recovery of catalyst activity under different regeneration conditions (Catalyst: Fe/ZSM-5(PUC))

At 275°C, the reacting gas mixture was switched off after the catalyst was aged and deactivated, then the catalyst was regenerated by passing 20% O₂ + N₂ for 40 minutes at the same temperature (i.e. 275°C). It is seen in Figure 3.14 (line A) that the catalytic activity could not be fully recovered after regeneration, with a highest NO_x conversion of only 49.7% for the regenerated catalyst. When the same regeneration method was used for the catalyst aged at 350°C (line B in Figure 3.14), the peak NO_x conversion increased to 64.9%, which was still much lower than the fresh catalyst (75%). The catalyst activity could be fully recovered only if the catalyst was calcined in air or 20% O₂ + N₂ at 500°C or higher

temperatures to have the deposited graphitic carbons and other adsorbed intermediate species of HC removed from the catalyst surface completely.

3.3.2.3 Effect of GHSV

Effects of gas space velocities on NO_x conversion at 325°C and 350°C are shown in Figures 3.15 and 3.16.

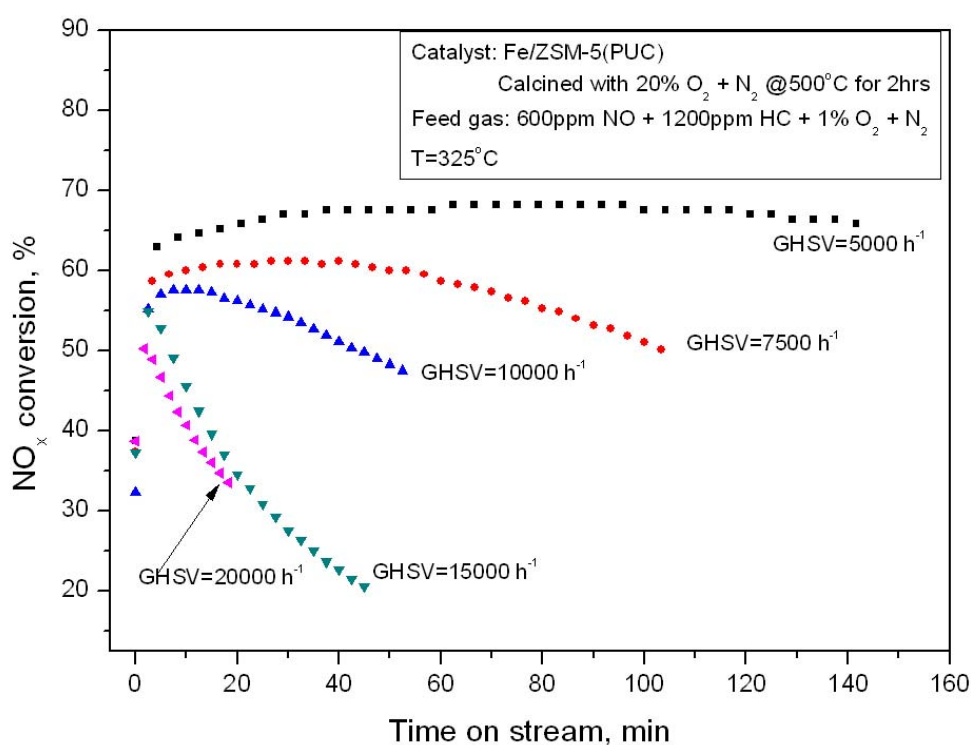


Figure 3.15 Effect of GHSV on catalytic activity (Catalyst: Fe/ZSM-5(PUC), T=325°C)

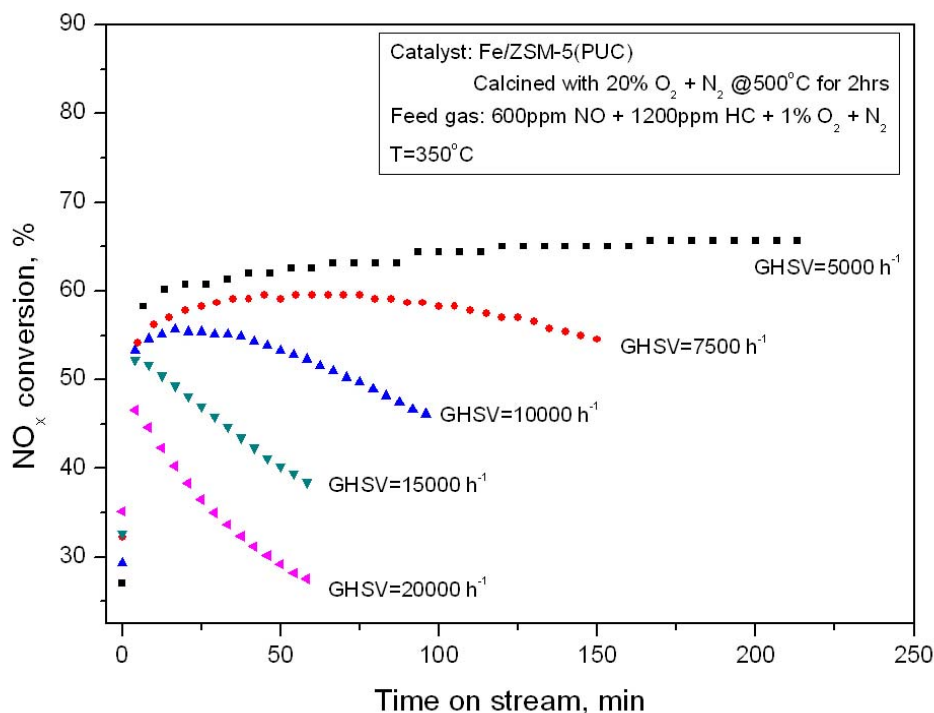


Figure 3.16 Effect of GHSV on catalytic activity (Catalyst: Fe/ZSM-5(PUC), T=350°C)

It is worth noting that the gas hourly space velocity (GHSV) was calculated based on the gas flow rate at room temperature:

$$GHSV = \frac{60 \times F}{\frac{\pi}{4} \times D_i^2 \times h} \quad (3.8)$$

where

GHSV, gas hourly space velocity, h⁻¹

F, gas flow rate at room temperature, ml/min

D_i, inner diameter of the reactor, 13.5 mm

h, catalyst packed height in the reactor, 50.8 mm

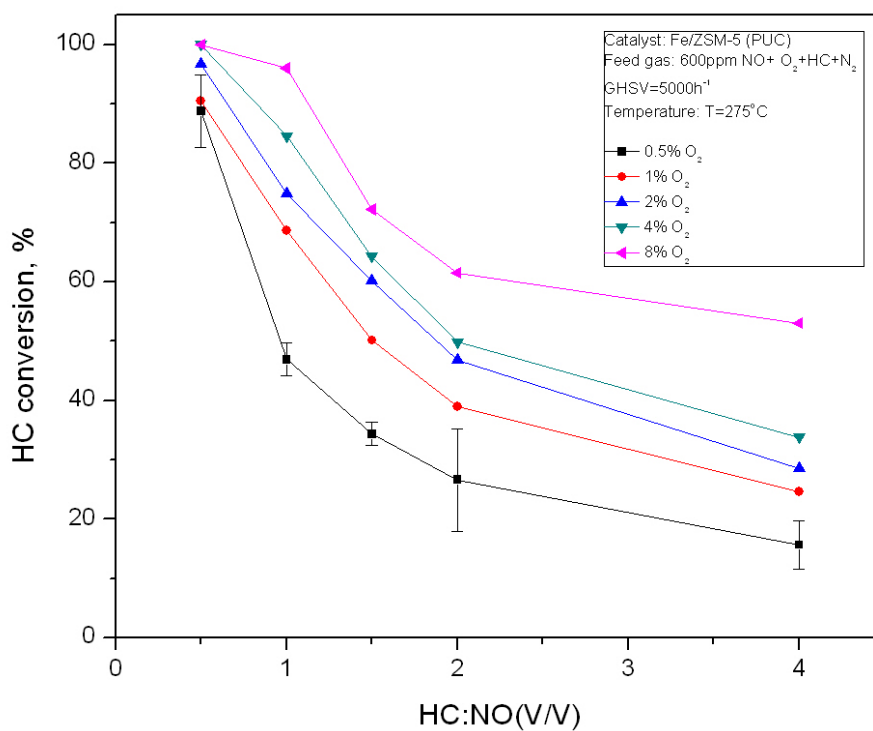
At T=325°C (Figure 3.15), the peak NO_x conversions were 68.2% (GHSV=5000 h⁻¹), 61.3% (GHSV=7500 h⁻¹), 57.6% (GHSV=10000 h⁻¹), 55.0% (GHSV=15000 h⁻¹) and 50.3% (GHSV=20000 h⁻¹). At GHSV=5000 h⁻¹, the catalyst showed relatively stable activity.

At $T=350^{\circ}\text{C}$ (Figure 3.16), the peak NO_x conversions were 65.6% (GHSV=5000 h^{-1}), 59.5% (GHSV=7500 h^{-1}), 55.7% (GHSV=10000 h^{-1}), 52.2% (GHSV=15000 h^{-1}) and 47.1% (GHSV=20000 h^{-1}). The highest NO_x conversion was achieved at GHSV=5000 h^{-1} , and the conversion remained stable over the tested time period. For a given GHSV, NO_x conversion at $T=325^{\circ}\text{C}$ was always 2~3% higher than at $T=350^{\circ}\text{C}$. However, at both temperatures, with the increase of GHSV, the peak NO_x conversion decreased. At the same time, at a higher GHSV, NO_x conversion decreased more quickly with time. This indicates that the space velocity has a significant influence on the catalyst activity, and must be considered as a key operating parameter in the design and operation of the dual-zone reactor.

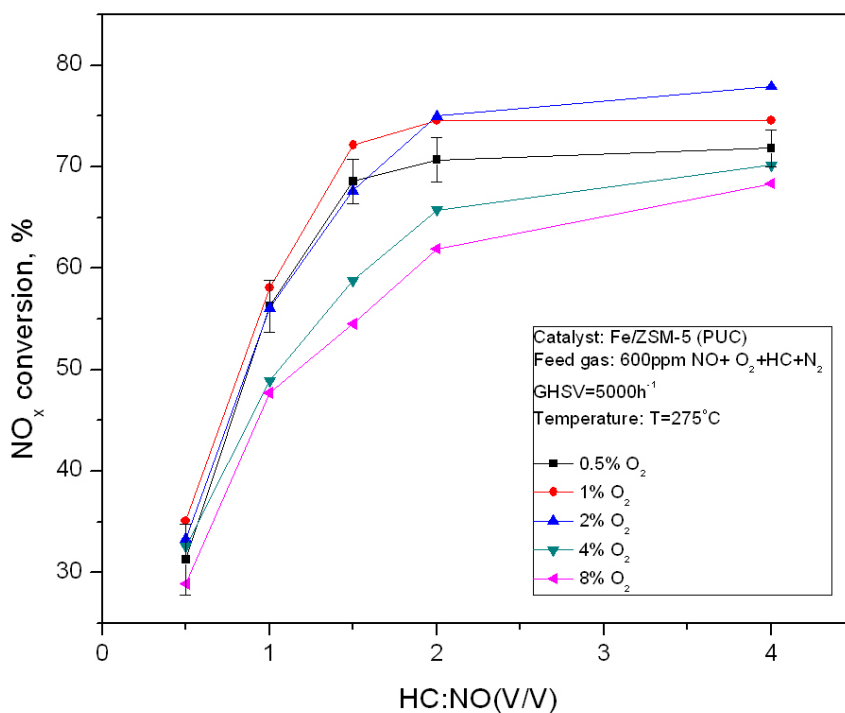
3.3.2.4 Effect of O_2 and HC concentrations

Effects of O_2 and HC concentrations on the catalytic activity at temperatures from 275°C to 375°C are shown in Figures 3.17 to 3.21. As discussed previously, the catalytic activity was unstable for the reaction temperatures lower than 325°C . Therefore, NO_x conversions shown in Figures 3.17 to 3.21 were the peak conversions obtained at each temperature.

Error bars shown in Figure 3.17 are calculated based on the standard deviation method. Four to eight repeated runs were used for the calculation of NO_x and HC conversions to obtain the standard deviation, with two times of standard deviations corresponding to 95% of confidence level plotted in this figure. The possible sources of errors include the measurement of gas concentrations by the gas analyzer, rotameter readings of gas flow rates and the reproducibility of the experiment. Throughout all fixed bed experiments, the errors for calculated NO_x conversions ranged from 0.37% to 2.86%, with an average around 1.42%. Due to the large number of figures in this work, error bars were added only in a few selected figures.



(a) HC conversion

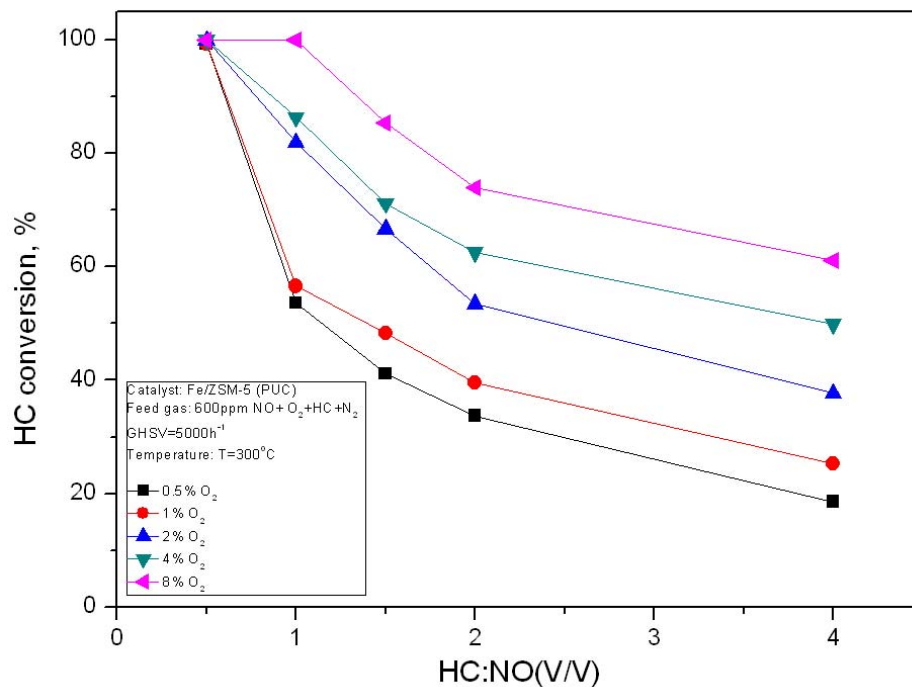


(b) NO_x conversion

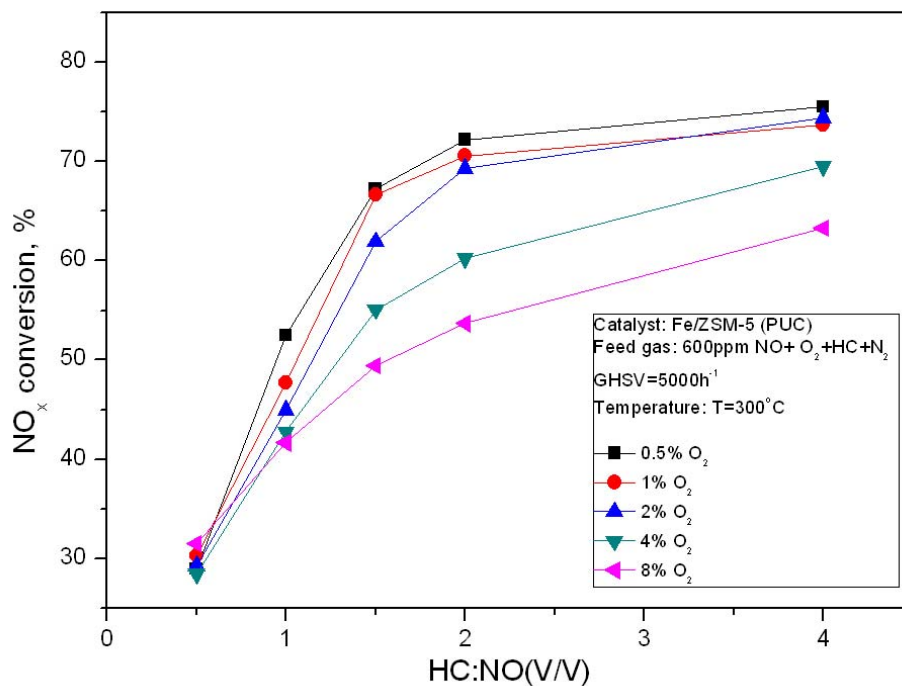
Figure 3.17 Effect of HC:NO ratio and O₂ level on catalytic activity (Catalyst: Fe/ZSM-5(PUC), T=275°C, 95% confidence level)

For $T=275^{\circ}\text{C}$ shown in Figure 3.17, the NO_x conversion was very low at $\text{HC:NO}=0.5$, ranging from 28.9% (8% O_2) to 35.1% (1% O_2) while the HC conversion was high from 88.8% (0.5% O_2) to 100% ($\geq 4\%$ O_2). The increase of O_2 concentration had no remarkable impact on both NO_x and HC conversions. When the HC:NO ratio was increased to 1, NO_x reduction was greatly enhanced. For low O_2 concentrations ($\leq 2\%$), NO_x conversion increased to 56.1% (2% O_2) and 58.1% (1% O_2). On the contrary, the HC conversion dropped significantly to 46.9% (0.5% O_2) and 74.9% (2% O_2). At high O_2 concentrations ($\geq 4\%$), the increase of HC:NO led to an increase of NO_x conversion to 48.9% (4% O_2) and 47.8% (8% O_2), but the influence of the change of HC:NO was not as significant as that for $\text{O}_2 \leq 2\%$. Although the HC conversion also decreased to 84.6% (4% O_2) and 96% (8% O_2), it was still much higher than that at 0.5% O_2 . Further increase of HC:NO to 1.5, 2 and 4 showed similar influence on NO_x and HC conversions as in the case with $\text{HC:NO}=1$, except for that at $\text{HC:NO} \geq 2$, the highest NO_x conversion occurred at 2% O_2 (75% for $\text{HC:NO}=2$ and 77.9% for $\text{HC:NO}=4$).

In general, for a given O_2 concentration, HC conversion decreased very quickly with the increase of HC:NO ratio. The increase of HC:NO ratio from 0.5 to 1.5 could greatly improve the catalytic activity for the flue gases containing 0.5% to 8% O_2 at $T=275^{\circ}\text{C}$. For $\text{O}_2 \leq 1\%$, the increase of HC:NO from 1.5 to 4 had little influence on NO_x conversion. For $\text{O}_2 \geq 2\%$, the NO_x conversion improved significantly with the increase of HC:NO from 1.5 to 4. The same trend was observed for $T=300, 325, 350$ and 375°C , as shown in Figures 3.18 to 3.21, except that the highest NO_x conversion was always obtained at 0.5% O_2 for $\text{HC:NO}=1$ to 4.

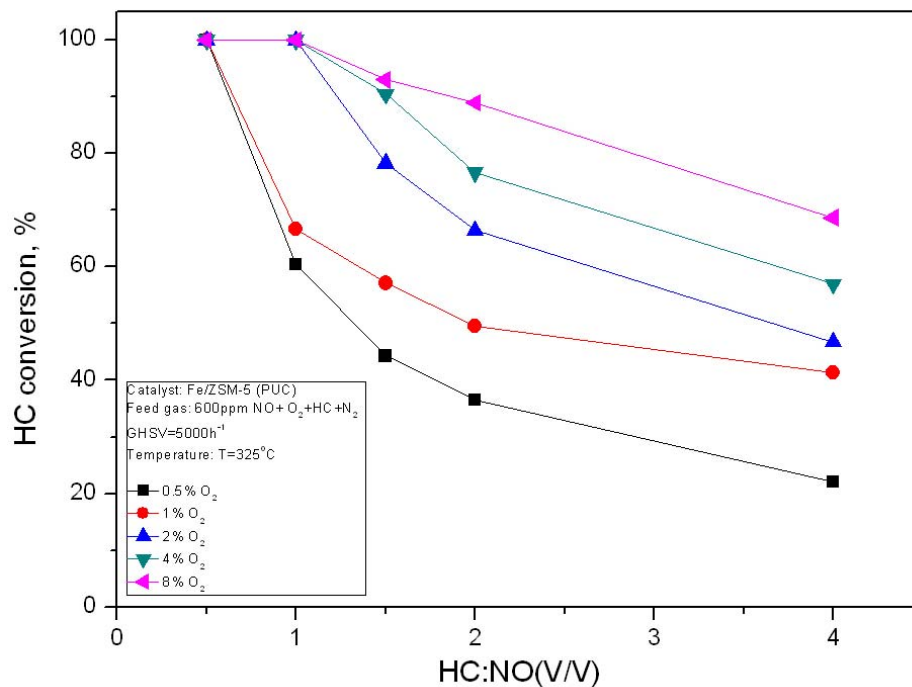


(a) HC conversion

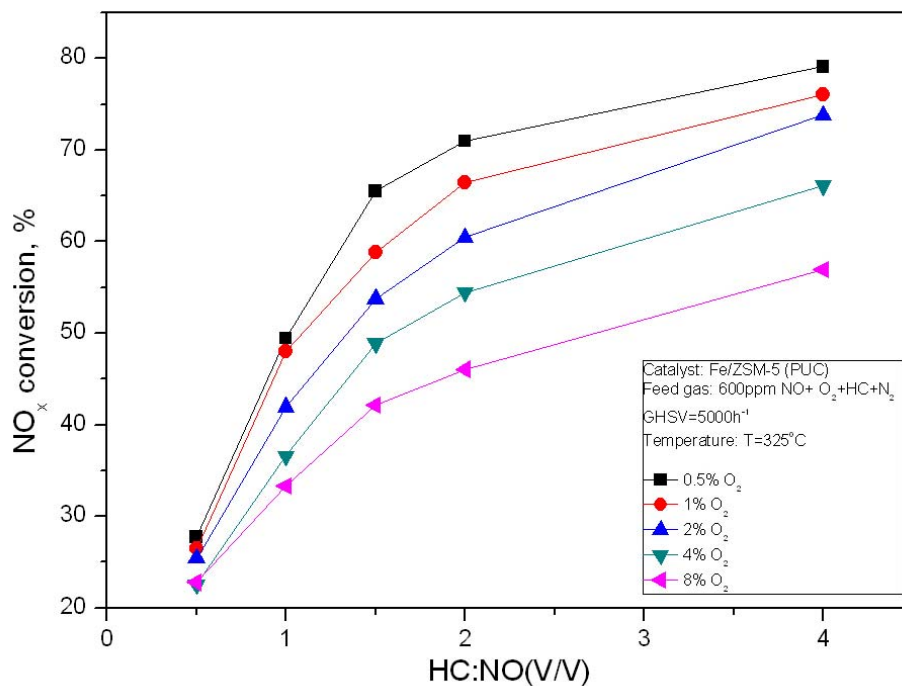


(b) NO_x conversion

Figure 3.18 Effect of HC:NO ratio and O₂ level on catalytic activity (Catalyst: Fe/ZSM-5(PUC), T=300°C)

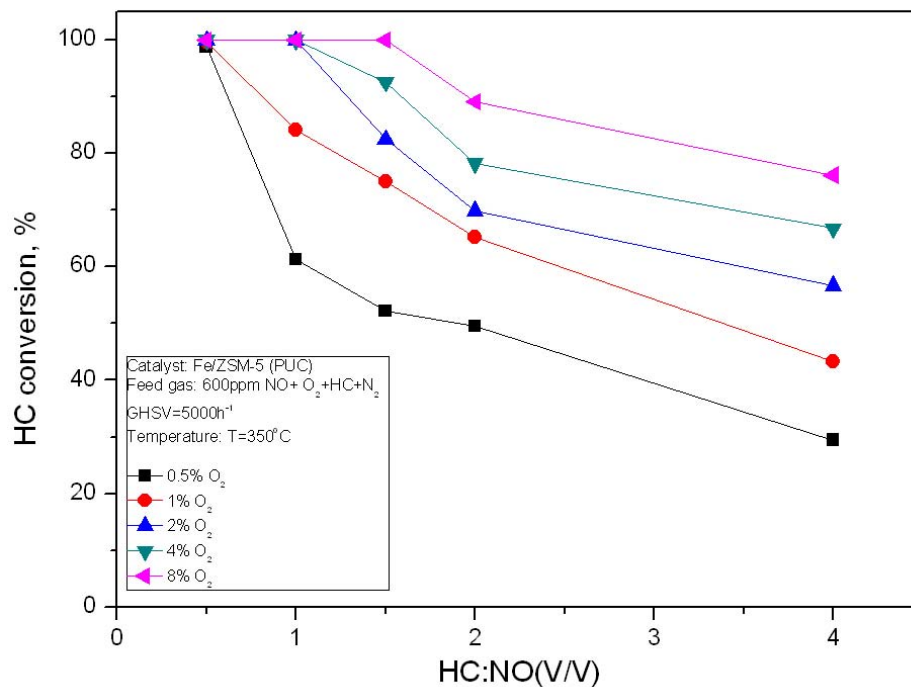


(a) HC conversion

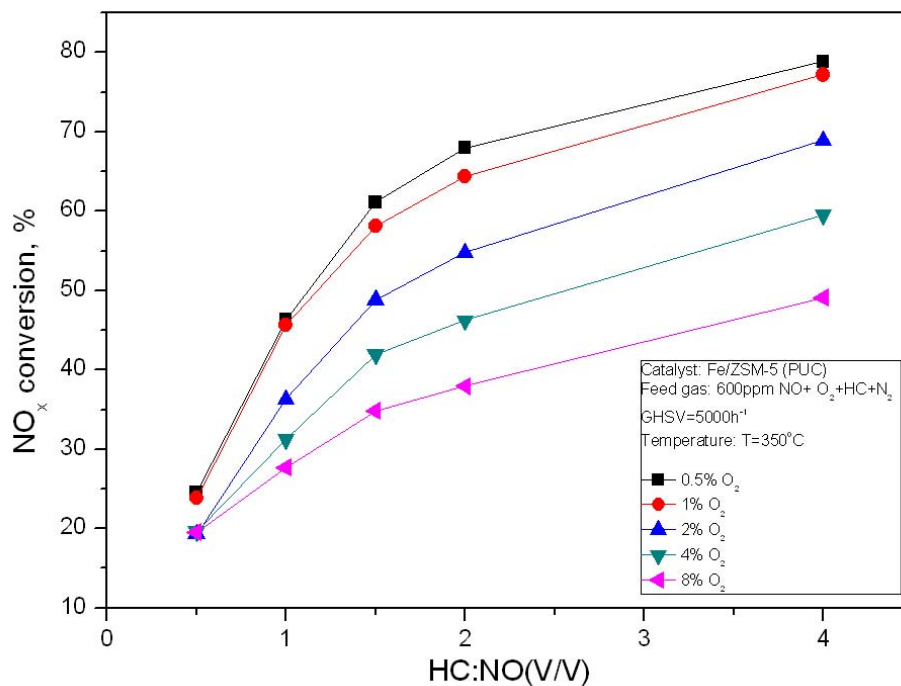


(b) NO_x conversion

Figure 3.19 Effect of HC:NO ratio and O₂ level on catalytic activity (Catalyst: Fe/ZSM-5(PUC), T=325°C)

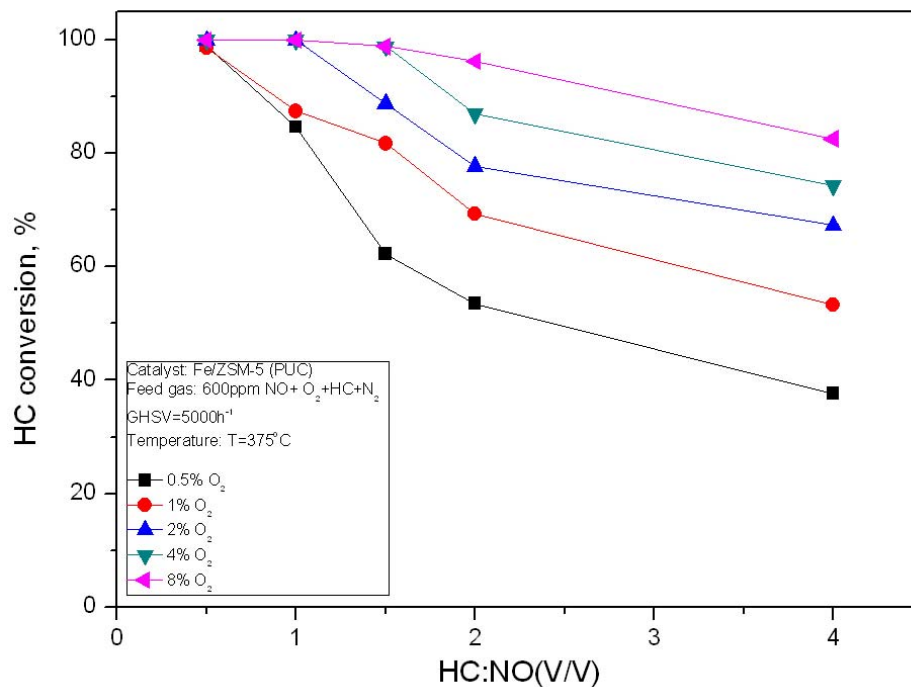


(a) HC conversion

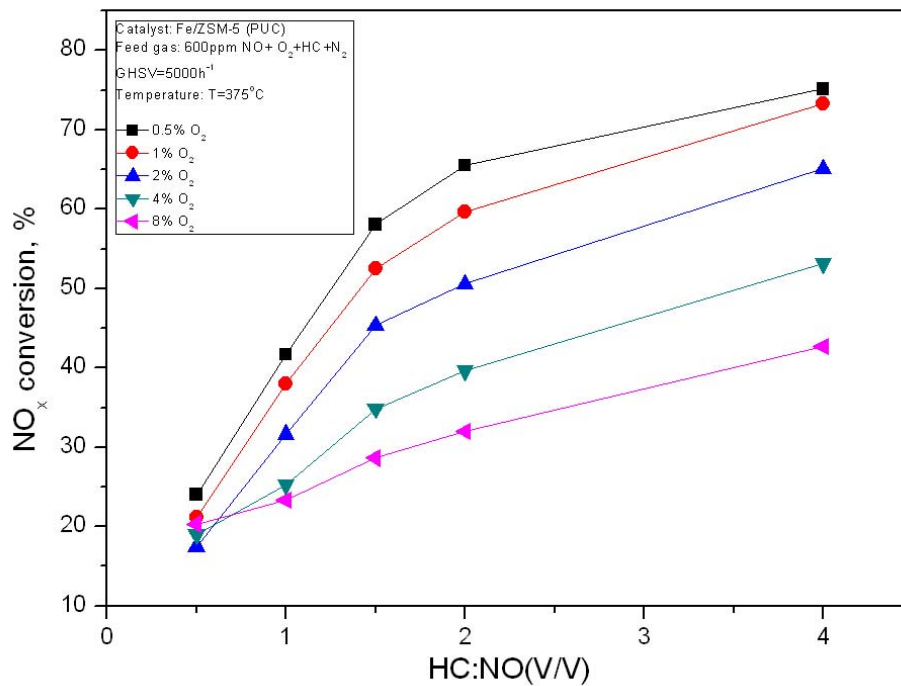


(b) NO_x conversion

Figure 3.20 Effect of HC:NO ratio and O₂ level on catalytic activity (Catalyst: Fe/ZSM-5(PUC), T=350°C)



(a) HC conversion



(b) NO_x conversion

Figure 3.21 Effect of HC:NO ratio and O₂ level on catalytic activity (Catalyst: Fe/ZSM-5(PUC), T=375°C)

For all cases tested, the increase of HC concentration enhanced NO_x conversion significantly. NO_x conversion remained at a very low level (between 15% to 35%) when HC:NO molar ratio was 0.5 at all temperatures and O_2 concentrations. With the increase of HC:NO to 2, NO_x conversion increased very quickly, especially for those at low O_2 concentrations ($\leq 2\%$). However, further increase of HC:NO from 2:1 to 4:1 had little influence on NO_x conversion at low temperatures ($\leq 300^\circ\text{C}$) compared to at high temperatures ($\geq 325^\circ\text{C}$).

For HC:NO=0.5, the increase of O_2 concentration had less impact over the investigated temperature range. At a given HC:NO ratio, the increase of O_2 concentration showed more negative impact on NO_x conversion when HC:NO ≥ 1 , especially at high temperatures ($\geq 325^\circ\text{C}$). However, at low temperatures ($\leq 300^\circ\text{C}$), NO_x conversion remained almost independent of HC:NO ratio at O_2 concentrations $\leq 2\%$.

For a given O_2 concentration, the increase of HC:NO ratio led to a significant decrease of HC conversion at all temperatures. In contrast, for a given HC:NO, the HC conversion increased with the increase of O_2 concentration in the model flue gas. It is generally anticipated that high HC to NO ratio can lead to a high NO_x conversion, at a cost of high hydrocarbon consumption which is not economical for the practical application. From this point of view, a HC to NO molar ratio of 2:1 appears to be a good choice. Oxygen played an important role in the HC-SCR under lean-burn conditions, which agrees well with the results from other researchers (Chen et al, 1998; Lee, 2000; Elkaim and Bai, 2000).

3.4 Reaction performance of Fe/ZSM-5 (PUC) catalyst prepared by WIE

Fe/ZSM-5(PUC) was prepared by the WIE method to evaluate the catalyst performance prepared by different methods. The time-on-stream test was performed at 275°C and 350°C with the result shown in Figure 3.22.

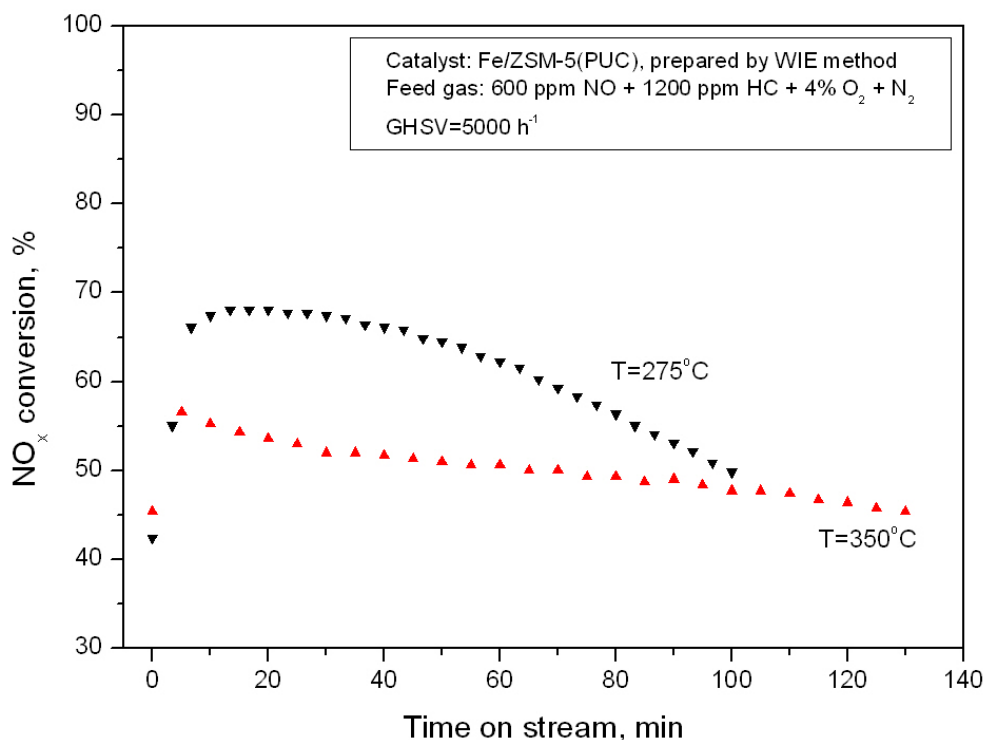


Figure 3.22 Effect of temperature on catalytic activity for NO_x reduction (Catalyst: Fe/ZSM-5(PUC, WIE))

In the experiment, the inlet NO_x concentration was first measured by bypassing the model flue gas to the gas analyzer. When switching the model flue gas to the reactor, there was a time delay ranging from 5 to 10 minutes before the real concentration of NO_x exiting from the reactor was obtained from the analyzer, which caused the initial increase of NO_x conversion in the time-on-stream experiment as shown in Figure 3.22. This part of time-on-stream data was not considered in the analysis of experimental data.

At $T=275^{\circ}\text{C}$ and with a feed gas composition of 600ppm NO + 1200ppm HC + 4%O₂ + N₂ and GHSV=5000 h⁻¹, the peak NO_x conversion for the catalyst prepared by WIE (Fe/ZSM-5(PUC, WIE)) was 68.1%, which was almost the same as the catalyst prepared by IMPO method (Fe/ZSM-5(PUC, IMPO)). However, the NO_x conversion decreased quickly to 49.2% in 100 minutes, in comparison to 66.1% for Fe/ZSM-5(PUC, IMPO) within the same time period as shown in Figure 3.9.

Previous results showed that Fe/ZSM-5(PUC) prepared by IMPO method exhibited stable activity at 350°C, even for the flue gas containing only 1% O₂. Although the peak NO_x conversion for Fe/ZSM-5 (PUC, WIE) at 350°C in Figure 3.22 was 57.6%, 11% higher than Fe/ZSM-5(PUC, IMPO), the activity of Fe/ZSM-5(PUC, WIE) was not stable even for the feed gas containing as high as 4% O₂.

The effect of the reaction temperature on NO_x and HC conversions for Fe/ZSM-5(PUC, WIE) with the feed gas composition of 600ppm NO + 1200ppm HC + 4% O₂ + N₂ and GHSV=5000 h⁻¹ is shown in Figure 3.23. Again, only the peak NO_x conversion and corresponding HC conversion were plotted. The catalyst was calcined in 20% O₂ + N₂ at 500°C for 2 hours prior to each run in order to recover the catalytic activity.

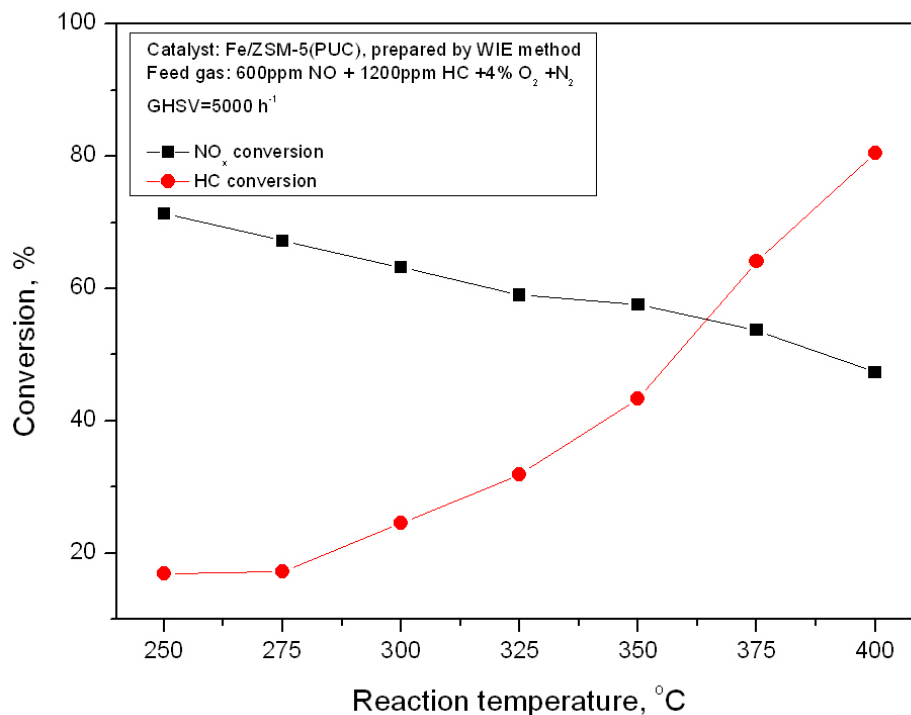


Figure 3.23 Effect of temperature on NO_x and HC conversion (Catalyst: Fe/ZSM-5(PUC, WIE))

The highest peak NO_x conversion was 71.3% (T=250°C) within the tested temperature window, and the peak NO_x conversion decreased to 47.3% when the reaction temperature was increased to 400°C. The HC conversion increased with the increase in the reaction temperature, but only reached 43% at T=350°C, which was much lower than Fe/ZSM-5(PUC, IMPO).

The catalyst was observed to be unstable, even at 400°C. Although the peak NO_x conversion was higher than Fe/ZSM-5(PUC, IMPO) at the same reaction condition, the poor stability prevents it from the practical application in the HC-SCR. It was thus concluded that IMPO is a better method than WIE for the preparation of Fe/ZSM-5 catalyst using current Na/ZSM-5(PUC) particles.

3.5 Performance of Fe/ZSM-5(Albemarle) catalyst

Although the Fe/ZSM-5(PUC) catalyst prepared via IMPO method exhibited good performance for the catalytic reduction of NO_x, the adsorption performance of Fe/ZSM-5(PUC) was not satisfactory because the equilibrium adsorption capacity was lower than 0.07 mg/g cat. with a very short breakthrough time of the catalyst bed ranging from 15 to 60 seconds. To increase the adsorption capacity of the catalyst, the parent Na/ZSM-5(PUC) particles were crushed and sieved to obtain fine particles with an average particle size of 234 μm and BET surface area of 192 m²/g, which were then used to prepare the fine Fe/ZSM-5(crushed PUC) catalyst by the IMPO method. As discussed in Appendix E, the fine Fe/ZSM-5(crushed PUC) catalyst showed several times the NO_x adsorption capacity than the coarse Fe/ZSM-5(PUC) (See Figure E.4). Therefore, it would be desirable to use fine catalyst particles in order to have both a high adsorption capacity for NO_x capture in the adsorption zone and an acceptable catalytic activity for NO_x reduction in the reduction zone for the proposed dual zone deNO_x reactor. Another type of fine particles, a spent Fluid Catalytic Cracking (FCC) catalyst, was also evaluated as a potential catalyst support. Unfortunately, as shown in Appendix F, both spent FCC and Fe/FCC showed very poor catalytic activity in HC-SCR.

A newly developed FCC catalyst support with ZSM-5 structure was obtained as a free sample from Albemarle Corporation. Fe/ZSM-5(Albemarle) catalyst was then prepared via the standard IMPO method, and its adsorption and reaction performances were investigated in the tubular reactor.

3.5.1 Adsorption performance of Fe/ZSM-5(Albemarle)

Experiments on the adsorption performance of the Fe/ZSM-5(Albemarle) catalyst were conducted at temperatures from 275°C to 375°C and GHSV=5000h⁻¹ using model flue gases with NO concentrations ranging from 200ppm to 1000ppm and 4% O₂. The typical adsorption curves are shown in Figure 3.24, with the remaining curves at other temperatures shown in Figures G.6 to G.9 in Appendix G.

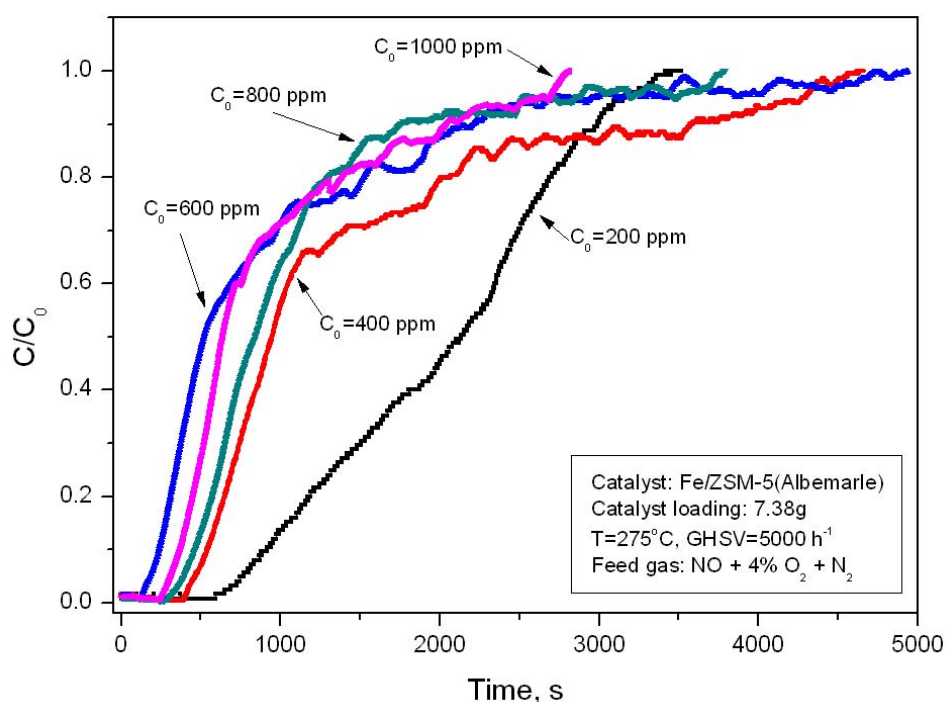


Figure 3.24 Adsorption curves based on NO_x concentrations at the reactor outlet (Catalyst: Fe/ZSM-5(Albemarle), T=275°C)

Compared with previously used coarse Fe/ZSM-5(PUC) and fine Fe/ZSM-5(crushed PUC) catalyst, the breakthrough time for the fine Fe/ZSM-5(Albemarle) catalyst was much longer for all tested conditions, indicating a much higher adsorption capacity of the Fe/ZSM-5 (Albemarle) catalyst. Furthermore, the equilibrium NO_x concentration was not reached at a

time of thousand seconds, which was tens of times of fine Fe/ZSM-5(crushed PUC)) although irregular shapes appeared on the adsorption curves.

Based on the adsorption profiles, the equilibrium adsorption capacity of the catalyst was calculated and plotted as a function of the equilibrium NO_x concentration in Figure 3.25. Again, the Freundlich equation was used to fit the relationship between q_e and C_0 , and the parameters α and β were fitted with the 2nd order polynomial function with the results shown in Figure 3.26. Equations 3.9 and 3.10 are obtained for α and β as a function of the adsorption temperature (T, K).

$$\alpha = -2.88632 + 0.01696T - 1.69966 \times 10^{-5} T^2 \quad (3.9)$$

$$\beta = 8.11218 - 0.02732T + 2.43429 \times 10^{-5} T^2 \quad (3.10)$$

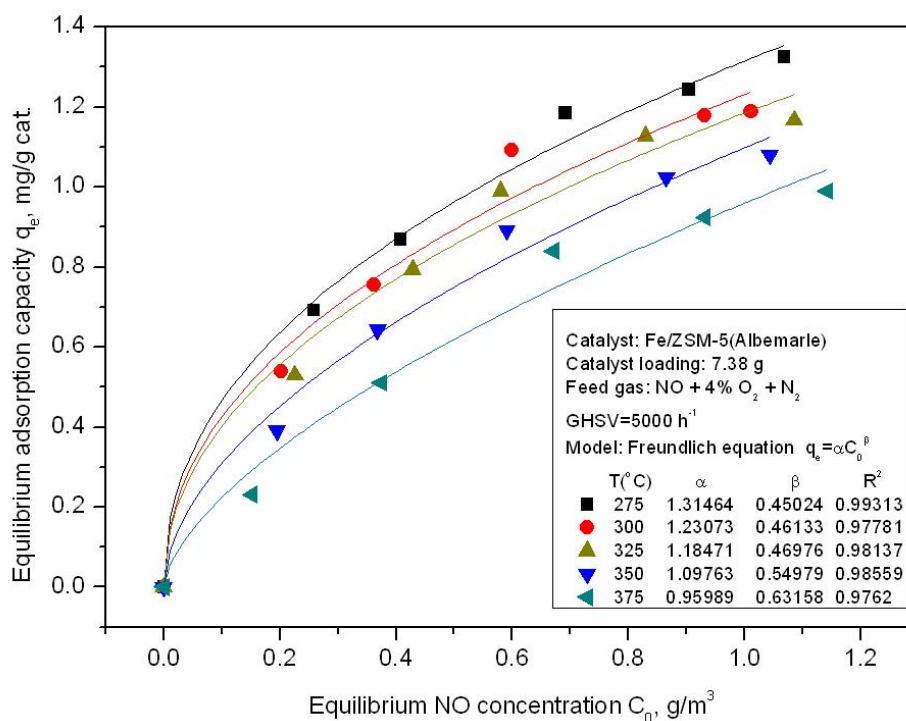


Figure 3.25 Fitting of adsorption isotherms of NO_x by Freundlich equation (Catalyst: Fe/ZSM-5(Albemarle))

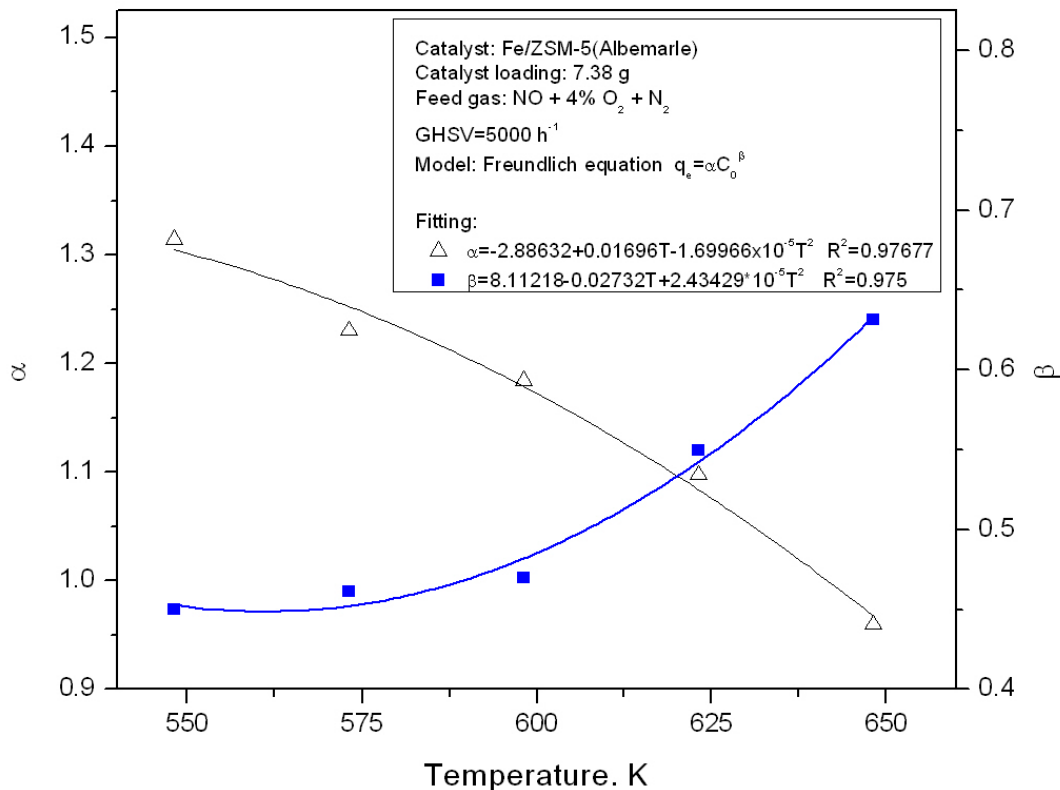


Figure 3.26 Relationship between α/β and adsorption temperature (Catalyst: Fe/ZSM-5(Albemarle))

Generally, the coefficient β in the Freundlich equation reflects the intensity of adsorption. $\beta=1$ indicates one active site adsorbs one molecule of NO. In Figure 3.26, the value of β is around 0.5, meaning that one molecule of NO occupies about 2 active sites indicating a weak adsorption of NO on the Fe active site.

Fe/ZSM-5(Albemarle) exhibited excellent adsorption performance as shown in Figure 3.25. As discussed earlier, at $T=350^\circ\text{C}$ and $C_0=0.4 \text{ g/m}^3$, the fine Fe/ZSM-5(crushed PUC) showed better adsorption capacity ($q_e=0.058 \text{ mg/g cat.}$) than the coarse Fe/ZSM-5(PUC) ($q_e=0.016 \text{ mg/g cat.}$). This difference demonstrates that a small particle size is beneficial to the adsorption of NO_x. At the same operating condition, q_e for the fine Fe/ZSM-5(Albemarle) catalyst is 0.66 mg/g cat. , which is 11.4 and 41.3 times of the capacity of the fine Fe/ZSM-

5(crushed PUC) and the coarse Fe/ZSM-5(PUC), respectively. This result clearly shows that the structure or the manufacturing procedure of the catalyst support could also have a significant effect on the adsorption performance of the catalyst.

3.5.2 Effect of O₂ concentration on NO_x adsorption of Fe/ZSM-5(Albemarle)

According to one of the mechanisms of HC-SCR suggested in the literature (Traa et al., 1999), NO is first oxidized to NO₂ by O₂ in the flue gas and then reduced by HC at the surface of the catalyst. This mechanism implies that NO_x adsorption onto the catalyst surface may be affected by the oxygen concentration. To verify this mechanism, the effect of O₂ concentration on NO_x adsorption of Fe/ZSM-5(Albemarle) was investigated, with the result shown in Figure 3.27. Without the presence of O₂ in the flue gas, the catalyst showed very low equilibrium NO_x adsorption capacity (q_e). With the increase of O₂ concentration from 0 to 4%, q_e increased significantly from lower than 0.1 to around 0.7 mg/g cat. Further increase of O₂ concentration from 4 to 8% enhanced the adsorption performance, but not as significant as that at low O₂ concentrations.

This result clearly demonstrates that the presence of O₂ in the flue gas is essential for achieving high NO adsorption ratio using Fe/ZSM-5(Albemarle) catalyst. Based on the experimental result, for Fe/ZSM-5(Albemarle) catalyst, one can postulate that, in the adsorption process, NO is first oxidized to NO₂ by the adsorbed O₂ on the active site of the catalyst, and NO₂ is then captured to the active site. According to the Langmuir-Hinshelwood theory, the following surface reactions can be assumed:



The increase of O_2 concentration in the flue gas increases the surface concentration of O^* in reaction (3.11), and therefore more NO can be adsorbed to active sites of the catalyst when the adsorption equilibrium in reaction (3.12) is reached.

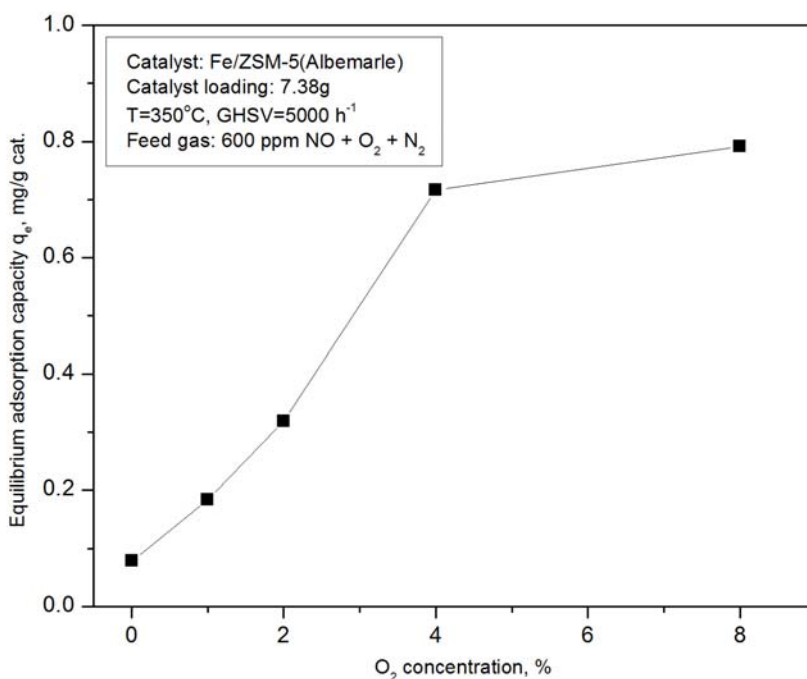


Figure 3.27 Effect of O_2 concentration in the flue gas on the adsorption capacity of Fe/ZSM-5(Albemarle) catalyst

3.5.3 Effect of H_2O and CO_2 on NO_x adsorption of Fe/ZSM-5(Albemarle)

Since Fe/ZSM-5(Albemarle) appears to be the most promising potential candidate for the dual zone ICFB reactor, the effect of other major components of the flue gas, such as H_2O and CO_2 , on the adsorption performance of the catalyst was further investigated. The model flue gas containing 4% O_2 was supplemented with 10% H_2O and/or 10% CO_2 and then used in the experiment at $T=350^\circ C$ and $GHSV=5000\text{ h}^{-1}$, with the adsorption curves shown in Figures G.10 to G.12 in Appendix G.

Based on the adsorption curve, the equilibrium adsorption capacity q_e for the model flue gas with the addition of 10% H_2O , 10% CO_2 and 10% CO_2 + 10% H_2O was calculated,

with the result shown in Figure 3.28. For comparison, data from the model flue gas without the addition of H₂O and CO₂ are also plotted in the same figure.

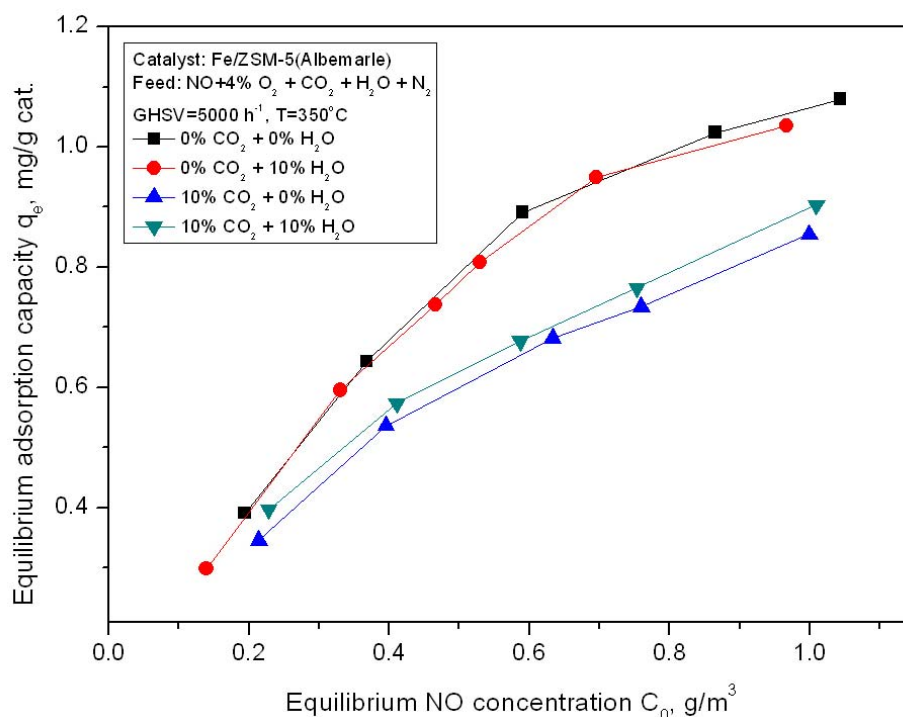


Figure 3.28 Effect of H₂O and CO₂ in the flue gas on adsorption isotherms (Catalyst: Fe/ZSM-5(Albemarle))

The addition of 10% H₂O to the model flue gas showed no effect on the adsorption capacity of Fe/ZSM-5(Albemarle). However, when compared with the case without H₂O and CO₂, q_e dropped by about 20% when 10% CO₂ was added into the flue gas. When 10% H₂O was introduced to the flue gas containing 10% CO₂, q_e increased by about 5% but was still lower than that without the presence of CO₂. Clearly, CO₂ exhibited a negative impact on the adsorption of NO, which might be caused by the competitive adsorption between CO₂ and NO. Although H₂O had no effect on the adsorption of NO_x in the flue gas without CO₂, the addition of H₂O to the CO₂-containing flue gas could slightly improve the adsorption of NO on Fe/ZSM-5(Albemarle) catalyst.

3.5.4 Adsorption performance of parent H/ZSM-5(Albemarle)

The adsorption capacity of H/ZSM-5(Albemarle) was measured and is shown in Figure 3.29. For comparison, the adsorption capacity of Fe/ZSM-5(Albemarle) is also plotted in Figure 3.29.

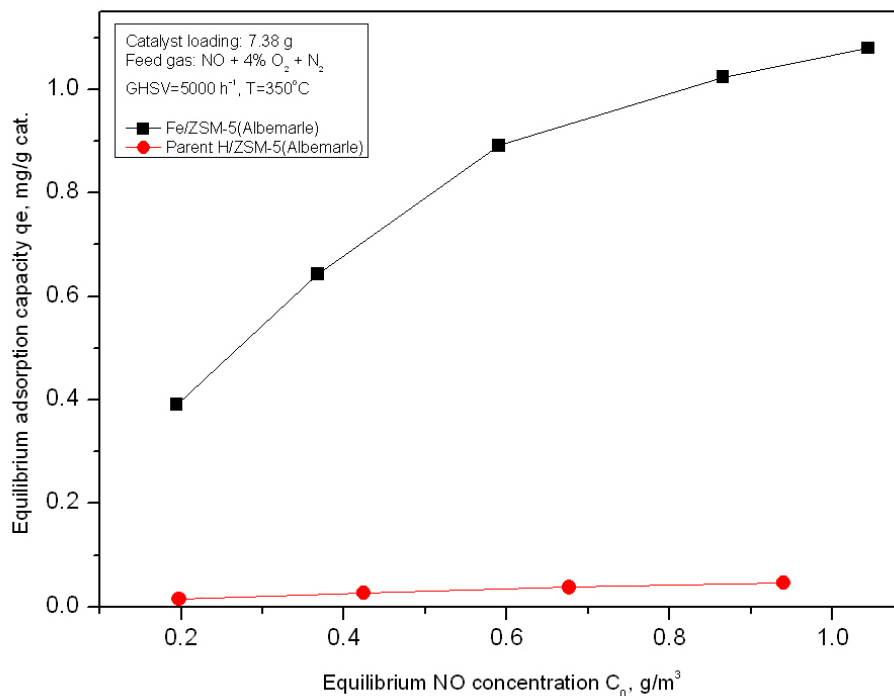


Figure 3.29 Comparison of adsorption isotherm between Fe/ZSM-5(Albemarle) and parent H/ZSM-5(Albemarle) at T=350°C

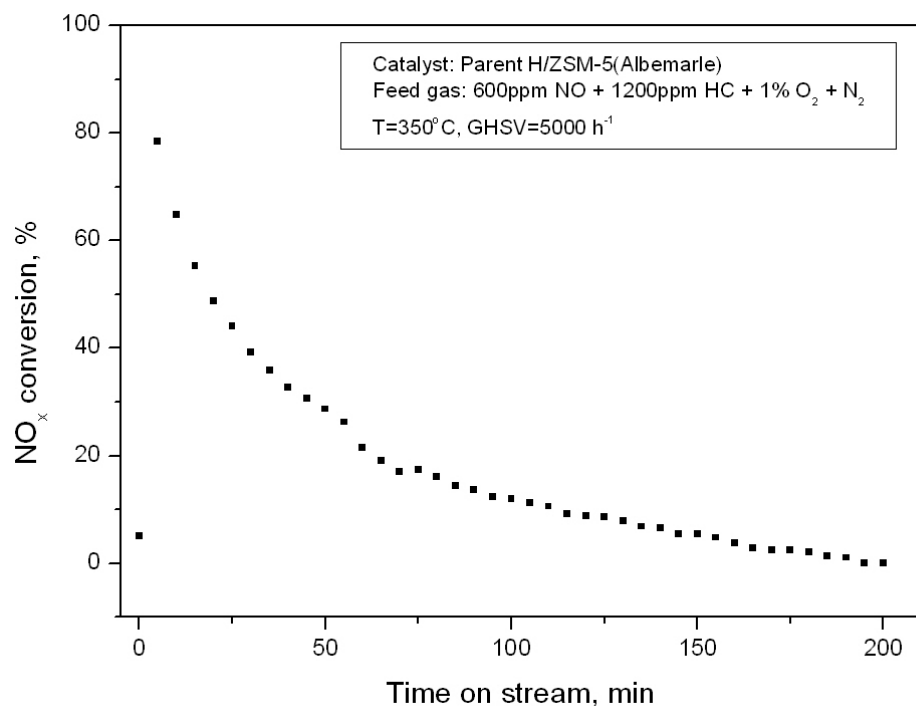
The adsorption capacity of the parent H/ZSM-5(Albemarle) was very low compared to Fe/ZSM-5(Albemarle). This means that the high adsorption capacity of Fe/ZSM-5(Albemarle) was contributed not by the catalyst support, but by the impregnated active Fe site or the combined effect of Fe and the ZSM-5 support. For catalyst prepared by the IMPO method, it is estimated that about 5% (wt.) of Fe was impregnated into Fe/ZSM-5(Albemarle), which means that there was around 1.0 mmol of Fe per gram of catalyst. The

adsorption capacity of NO on the Fe/ZSM-5 (Albemarle) was measured to be around 1 mg/g cat. or 0.033 mmol/g cat., which is much lower than the loaded Fe content on the catalyst. This may suggest that, in the adsorption process, most of the active sites are occupied by the adsorbed N₂ or O₂ because of the high N₂ and O₂ concentrations in the flue gas, while only a small fraction of active sites are taken by the adsorbed NO₂.

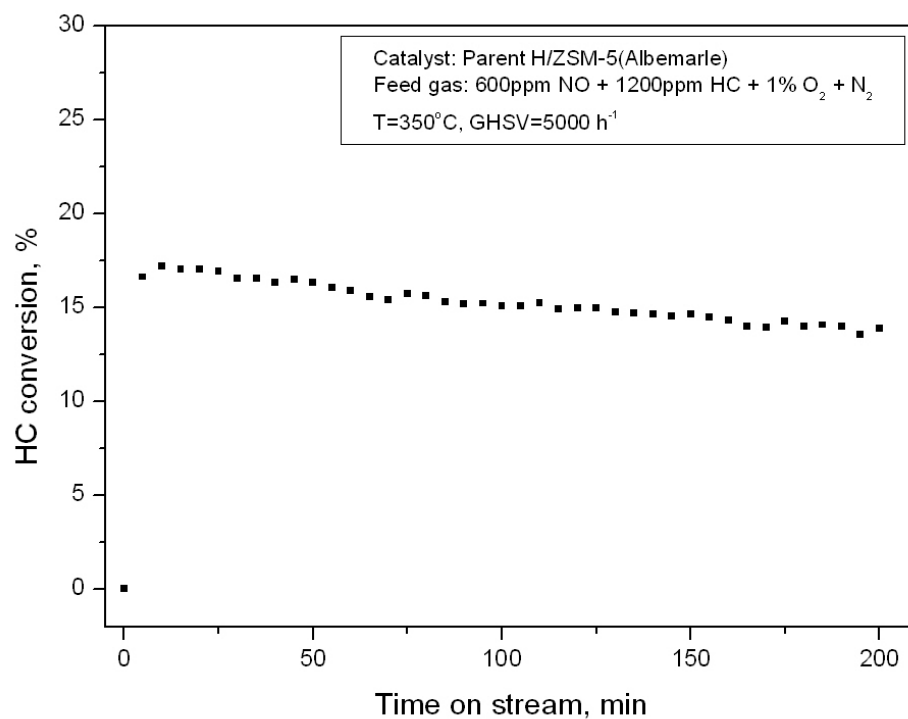
3.5.5 Catalytic activity of parent H/ZSM-5(Albemarle) in HC-SCR

To investigate the HC-SCR capability of H/ZSM-5(Albemarle), the time-on-stream test was conducted with the feed gas consisting of 600ppm NO + 1200ppm HC + 1% O₂ + N₂ at T=350°C and GHSV=5000 h⁻¹, with the result shown in Figure 3.30.

It can be seen that NO_x conversion quickly decreased to near zero in 200 minutes. The low HC conversion in Figure 3.30(b), on the other hand, indicates that H/ZSM-5 (Albemarle) does not catalyze the oxidation of hydrocarbons appreciably.



(a) NO_x conversion



(b) HC conversion

Figure 3.30 Catalytic activity of parent H/ZSM-5(Albemarle)

3.5.6 Reaction performance of Fe/ZSM-5(Albemarle)

A series of time-on-stream tests were carried out to investigate the reduction performance of Fe/ZSM-5(Albemarle) catalyst at various temperatures and GHSV. Further study on the effect of O₂ and HC concentrations in the model flue gas was also conducted. Moreover, the influence of H₂O, CO₂ and SO₂ on the catalytic activity was investigated preliminarily.

3.5.6.1 Effect of reaction temperature

Since the reaction temperature plays an important role in HC-SCR of NO_x, it is necessary to seek for the optimum temperature window for the future study. As before, the feed gas mixture of 600 ppm NO + 1200 ppm HC + 1% O₂ + N₂ was used in the time-on-stream test at GHSV=5000 h⁻¹ while the reaction temperature varied from 275 to 375°C with an increment of 25°C. Typical profiles of NO_x and HC conversions and outlet CO concentration are shown in Figure 3.31 (T=275°C) and Figure 3.32 (T=350°C) (see Figures G.17 to G.19 in Appendix G for profiles at other temperatures).

At T=275°C, the catalyst showed unstable activity which is similar to Fe/ZSM-5(PUC). The peak NO_x conversion was found to correspond to the time when HC conversion and outlet CO concentration reached their maximum values. The discontinuity in the HC conversion curve in Figure 3.32 is caused by the resolution of the gas analyzer at low CO₂ concentrations (<100ppm or 0.01%) while the CO concentration is recorded at the 1ppm level.

At all temperatures, large amount of CO was observed in the outlet gas flow, indicating that the production of CO is inevitable if Fe/ZSM-5 is used as the HC-SCR catalyst. Similar trends were observed for the NO_x and HC conversions and the outlet CO concentration at all temperatures covered by this study. To avoid the potential release of

unconverted hydrocarbons and produced CO into the environment, a reactor filled with oxidation catalyst can be added to the downstream of the HC-SCR reactor to convert CO and unconverted hydrocarbons to CO₂.

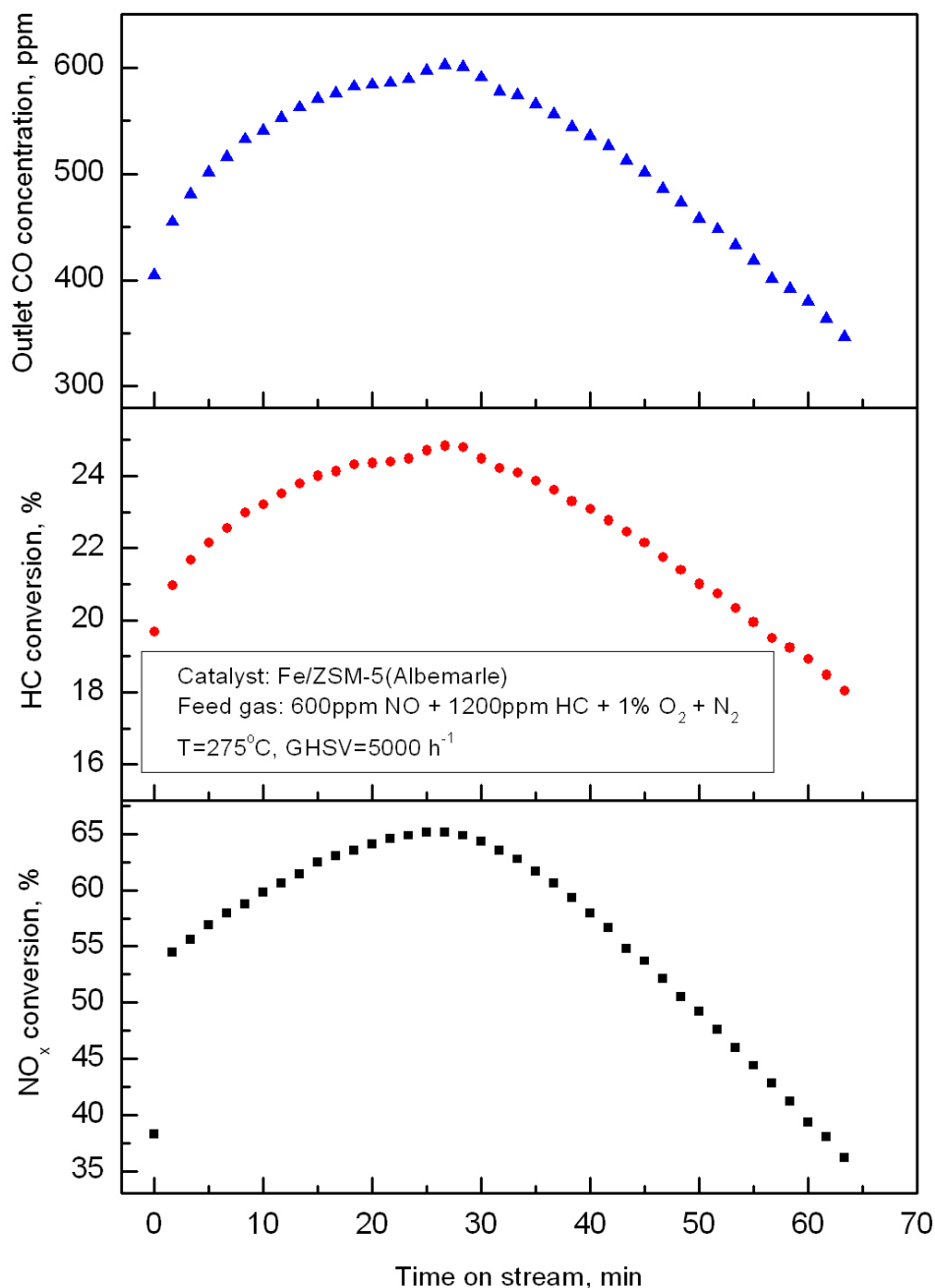


Figure 3.31 Profiles of NO_x and HC conversions and outlet CO concentration (Fe/ZSM-5(Albemarle), T=275°C, [O₂]=1%)

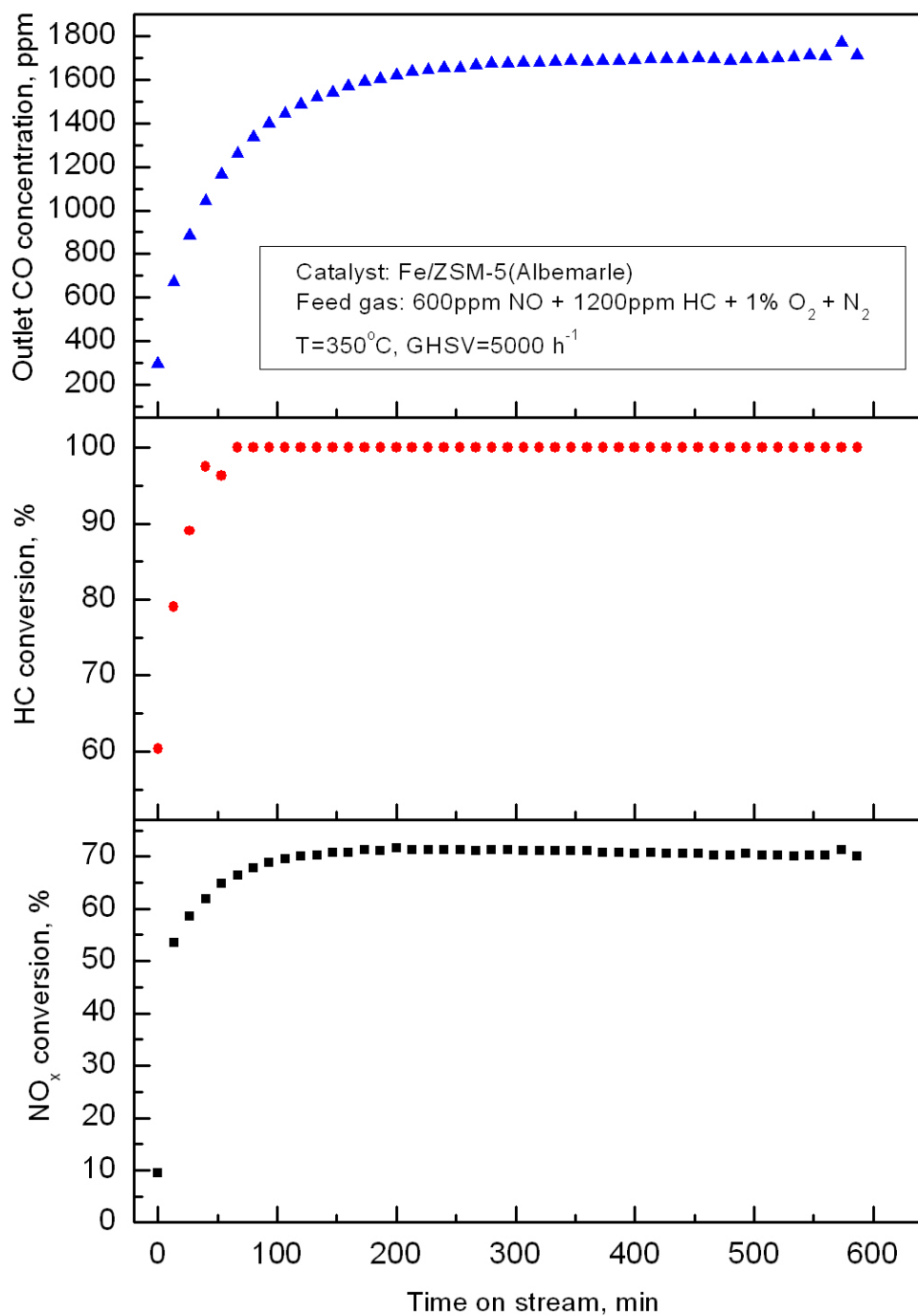
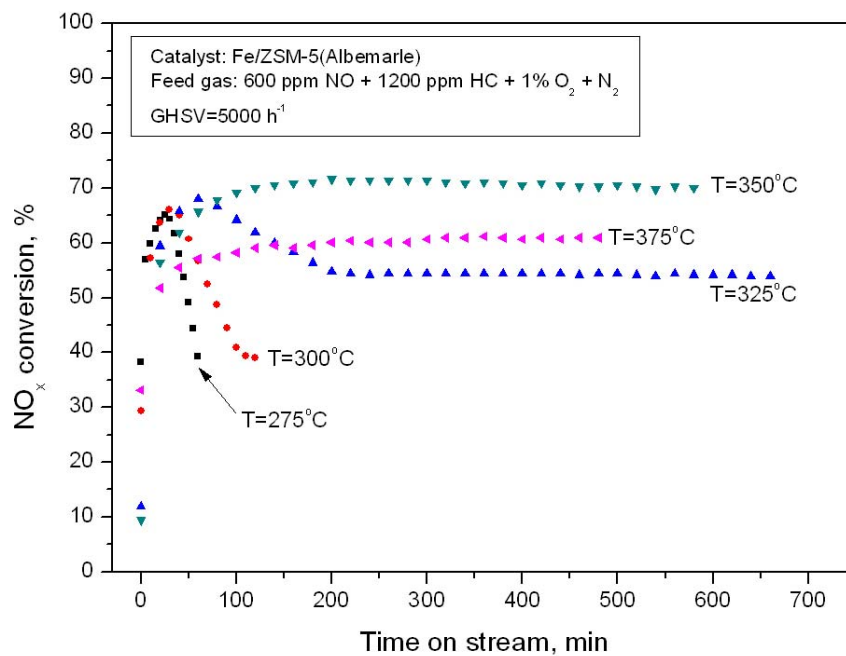
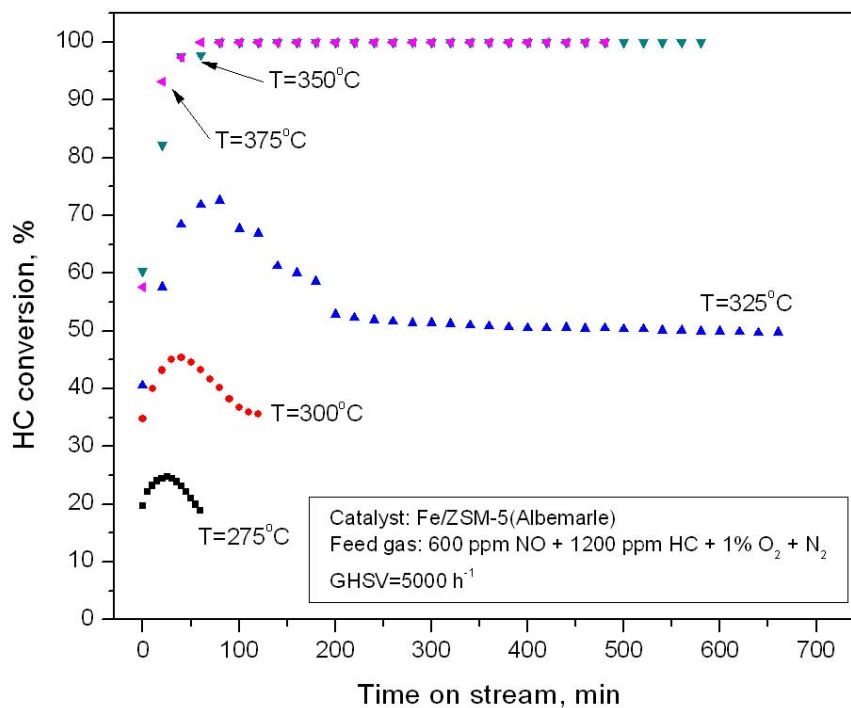


Figure 3.32 Profiles of NO_x and HC conversions and outlet CO concentration (Fe/ZSM-5(Albemarle), T=350°C, [O₂]=1%)

The NO_x and HC conversions at all investigated temperatures are shown in Figure 3.33. Peak NO_x conversions were observed to be 65.2% (275°C), 66.3% (300°C), 68.3% (325°C), 71% (350°C) and 61.2% (375°C) with corresponding HC conversions of 24.8% (275°C), 45.3% (300°C), 72.3% (325°C), 100% (350°C) and 100% (375°C). Again, the discontinuous profiles of HC conversion in Figure 3.33(b) were caused by the low resolution of the gas analyzer at low CO₂ concentrations. At T ≤ 325°C, NO_x and HC conversions increased with time. After the peak was reached, both NO_x and HC conversions at T = 275°C decreased quickly. At T = 300°C and 325°C, the NO_x conversion decreased from the peak values to 38.8% and 54.2%, respectively, and then remained stable afterward. The maximum stable NO_x conversion was observed at T = 350°C (71%). The catalytic activity remained stable with further increase in temperature up to 375°C although the NO_x conversion was lower (61.2%) at this temperature.



(a) NO_x conversion

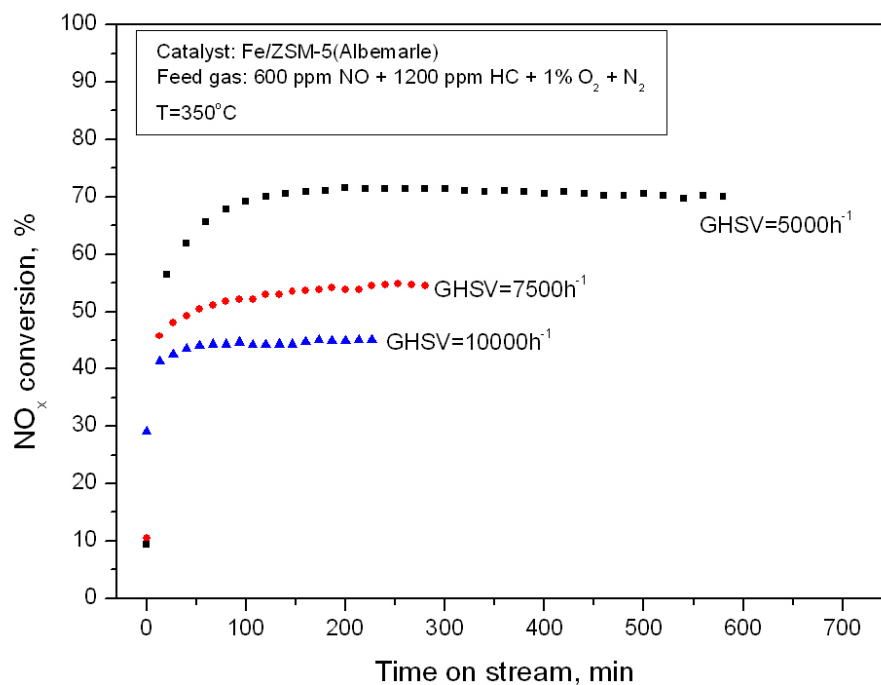


(b) HC conversion

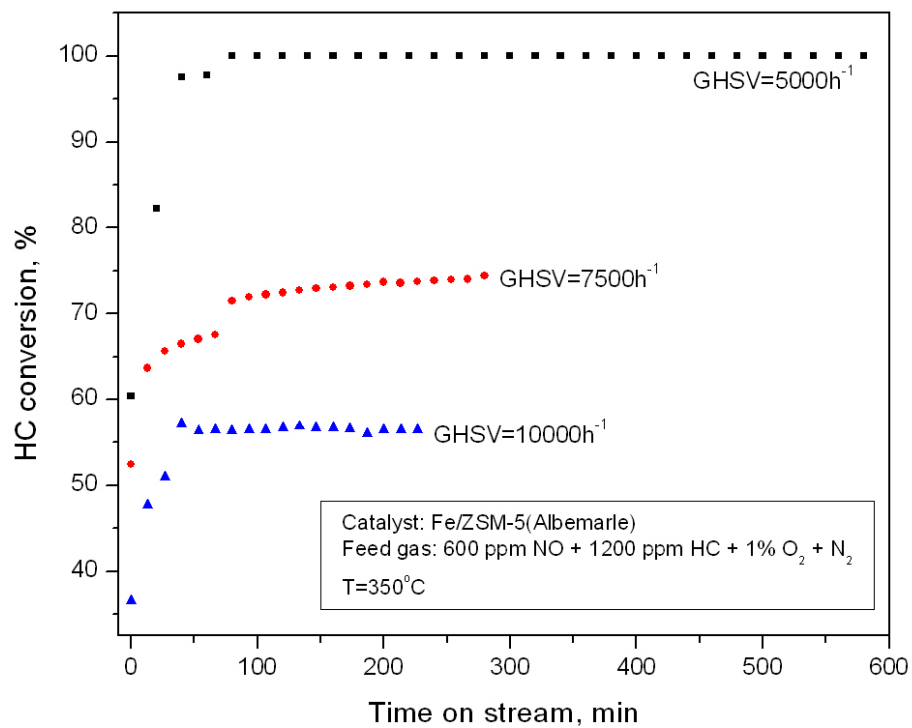
Figure 3.33 Effect of temperature on the catalytic activity of Fe/ZSM-5(Albemarle)

3.5.6.2 Effect of GHSV

Fe/ZSM-5(PUC) showed high sensitivity to the variation in GHSV where the catalyst maintained its stable activity with time only at $\text{GHSV} \leq 5000 \text{ h}^{-1}$ at 350°C (see Figure 3.16). In contrast, Fe/ZSM-5(Albemarle) exhibited good durability to the change of GHSV. As shown in Figure 3.34, the catalytic activity remained stable with the change in GHSV. However, with the increase of GHSV from 5000 h^{-1} to 10000 h^{-1} , the NO_x conversion decreased from 71% (GHSV= 5000 h^{-1}) to 55% (GHSV= 7500 h^{-1}) and 45% (GHSV= 10000 h^{-1}), respectively. Moreover, the corresponding HC conversion dropped from 100% (GHSV= 5000 h^{-1}) to 74% (GHSV= 7500 h^{-1}) and 57% (GHSV= 10000 h^{-1}). The drop in NO_x conversion as well as HC conversion could be induced by the decrease of the resident time in the catalyst bed as the GHSV increased.



(a) NO_x conversion



(b) HC conversion

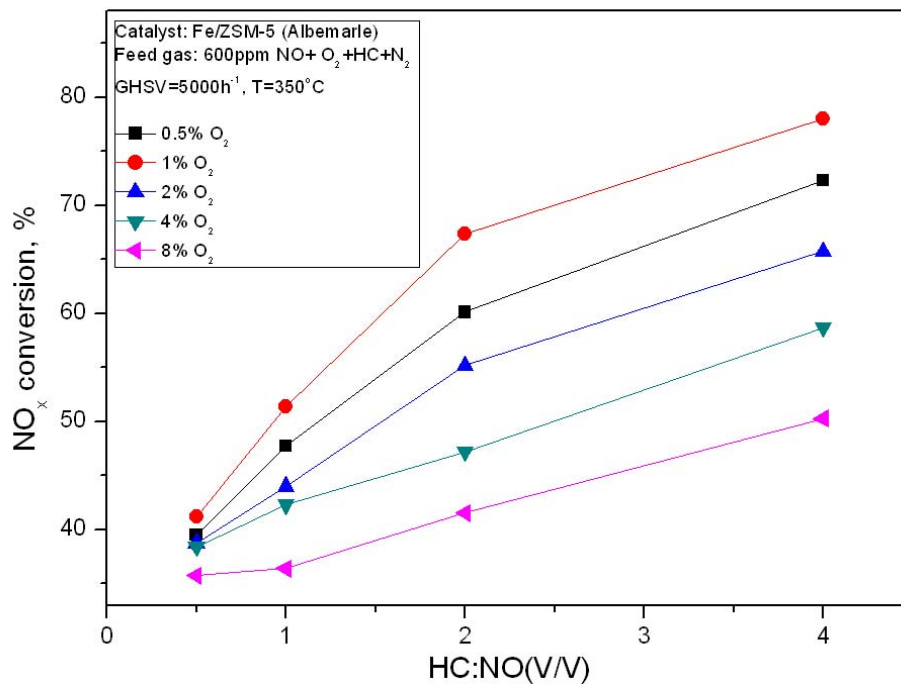
Figure 3.34 Effect of GHSV on the catalytic activity of Fe/ZSM-5(Albemarle)

3.5.6.3 Effect of O₂ and HC concentrations

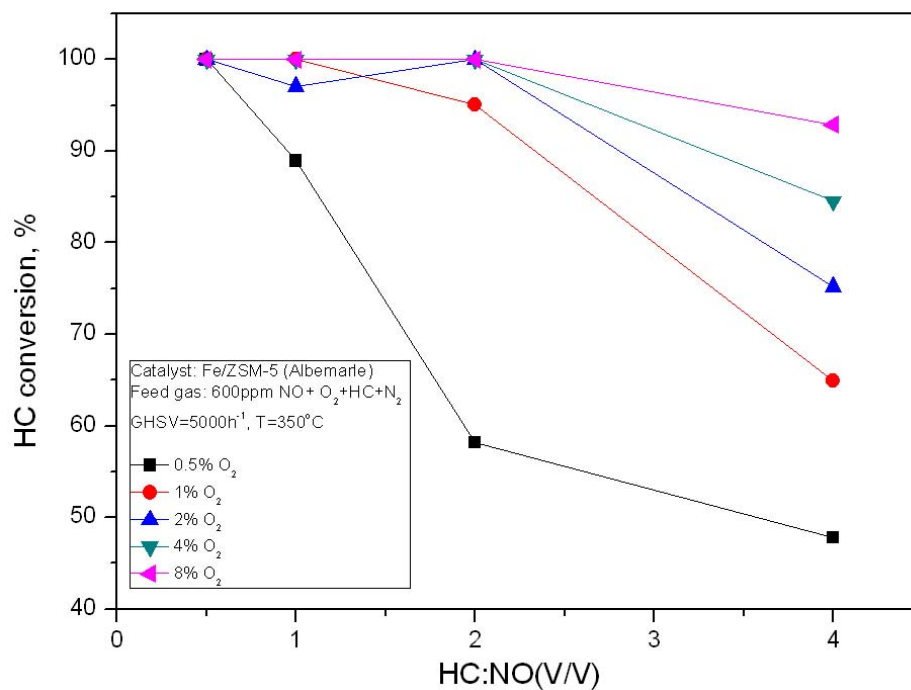
The effect of O₂ and HC concentrations in the model flue gas on the catalytic activity of Fe/ZSM-5(Albemarle) was investigated at reactor temperatures of 350°C and 375°C and GHSV=5000 h⁻¹. The inlet NO concentration was kept at 600ppm throughout the experiment. O₂ concentration in the feed gas was set as 0.5, 1, 2, 4 or 8% with a HC:NO(V/V) ratio of 0.5, 1, 2 or 4.

As shown in Figure 3.35 for T=350°C, at a given O₂ concentration, NO_x conversion generally increased with increasing HC:NO. At HC:NO=0.5, NO_x conversion was in a range of 35%~40% without distinct variation with the change in O₂ concentration. HC conversion reached 100% at all O₂ concentrations at such a low HC:NO ratio. When HC:NO ratio increased to 1, NO_x conversion increased at a given O₂ concentration, and HC conversion kept at around 100%, except for 0.5% O₂ where HC conversion dropped to 89%. Further increase of HC:NO to 2 greatly enhanced the catalytic activity. However, HC conversion at 0.5% O₂ steeply decreased to 58% because of the lack of O₂ for the combustion of HC. Over 95% of HC conversion was obtained at HC:NO=2 for cases with 1% or more O₂. Although the increase of HC:NO to 4 could improve the catalytic activity further, the HC conversion decreased quickly, especially for cases with O₂ concentrations lower than 2%.

In all cases, at a given ratio of HC:NO, the maximum NO_x conversion was always observed when O₂ concentration was around 1%. For 2% or more of O₂ concentration, NO_x conversion decreased with the increase of O₂ concentration. For instance, at HC:NO=2, NO_x conversion was in the order of 1% O₂ (67.4%) > 0.5% O₂ (60.1%) > 2% O₂ (55.2%) > 4% O₂ (47.2%) > 8% O₂ (41.5%).

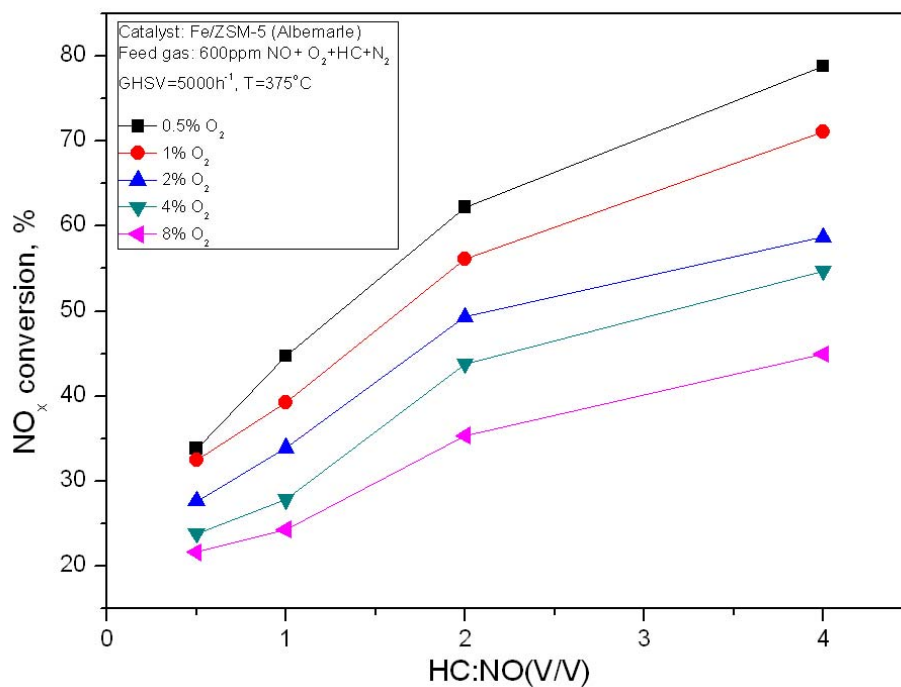


(a) NO_x conversion

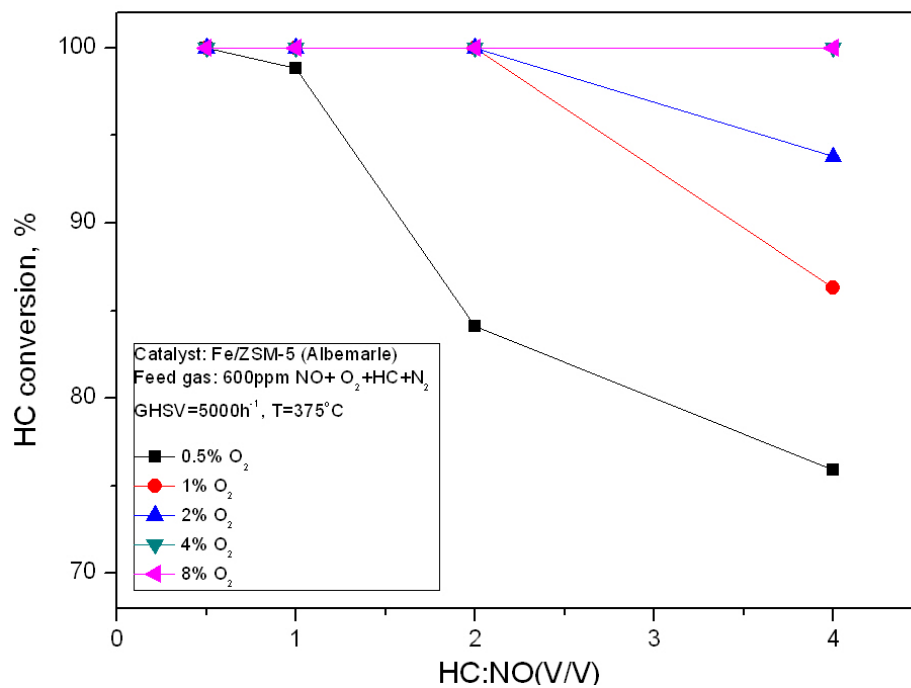


(b) HC conversion

Figure 3.35 Effect of O₂ and HC concentrations (Fe/ZSM-5(Albemarle), T=350°C)



(a) NO_x conversion



(b) HC conversion

Figure 3.36 Effect of O₂ and HC concentrations (Fe/ZSM-5(Albemarle), T=375°C)

Figure 3.36 showed similar trend as in Figure 3.35 on the influence of the HC:NO ratio for $T=375^{\circ}\text{C}$. The exception is that, at a given HC:NO, NO_x conversion always decreased with the increase of O_2 concentration. In the range of studied O_2 concentrations at HC:NO=2, NO_x conversion was in the order of 0.5% O_2 (62.2%) > 1% O_2 (56.1%) > 2% O_2 (49.3%) > 4% O_2 (43.8%) > 8% O_2 (35.3%). For a given HC:NO ratio and O_2 concentration, NO_x conversion at $T=375^{\circ}\text{C}$ was always lower while the HC conversion was equal to or higher than at $T=350^{\circ}\text{C}$.

3.5.6.4 Effect of CO_2 and H_2O

The real flue gas from the combustion process contains not only NO_x and O_2 , but also large amount of CO_2 and water vapour (see Table 1.1). To investigate the influence of CO_2 on the catalytic activity of Fe/ZSM-5(Albemarle), 5, 10 and 15% CO_2 was added into the feed gas of 600ppm NO + 1200ppm HC + O_2 + N_2 with various O_2 concentration of 1, 4 and 8% at $T=350^{\circ}\text{C}$ and GHSV=5000 h^{-1} with the result shown in Figure 3.37.

Compared with the case without the addition of CO_2 , for feed gas containing 1% O_2 , CO_2 showed minor negative influence with NO_x conversion slightly decreased from 69.7% (0% CO_2) to 68.1% (5% CO_2), 66.9% (10% CO_2) and 66.8% (15% CO_2). For the feed gas containing 4% and 8% O_2 , NO_x conversion fluctuated at values between 52% (4% O_2) and 44% (8% O_2) with a difference of around 1% after the addition of 5%, 10% or even 15% CO_2 . In general, it could be concluded that the presence of CO_2 in the feed gas had an insignificant influence on the catalytic activity of Fe/ZSM-5(Albemarle), and the effect could be well neglected.

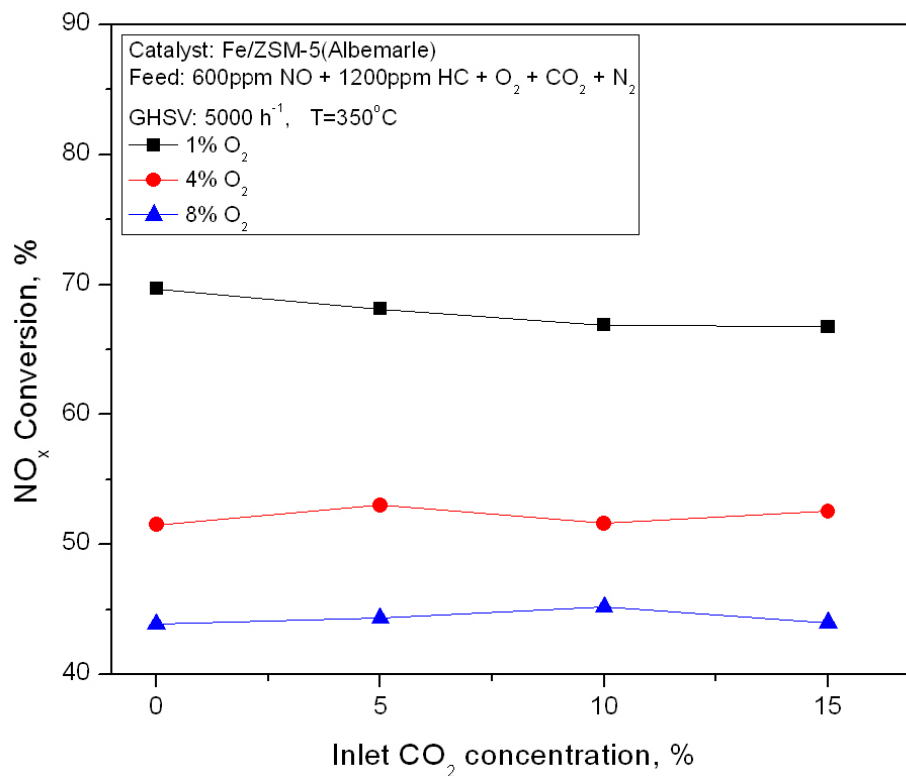


Figure 3.37 Effect of CO₂ on the catalytic activity of Fe/ZSM-5(Albemarle) (T=350°C)

When 5% H₂O was added into the feed gas of 600ppm NO + 1200ppm HC + 1% O₂ + N₂, as shown in Figure 3.38, the NO_x conversion increased from 68.5% (0% H₂O) to 71.7% (5% H₂O). Further increase in NO_x conversion was not observed for the addition of 10% and 15% H₂O. For the flue gas containing 4% O₂, the NO_x conversion without H₂O was 47%, and the addition of 5%, 10% and 15% H₂O led to the increase of NO_x conversion to 51%, 53.3% and 54.2%, respectively. For the flue gas containing 8% O₂, NO_x conversion increased from 39.1% (0% H₂O) to 45.4% (5% H₂O), 47% (10% H₂O) and 49.1% (15% H₂O).

It is clear that the presence of H₂O in the model flue gas somewhat enhanced the SCR activity of Fe/ZSM-5(Albemarle) catalyst, especially at high O₂ concentrations in the flue gas.

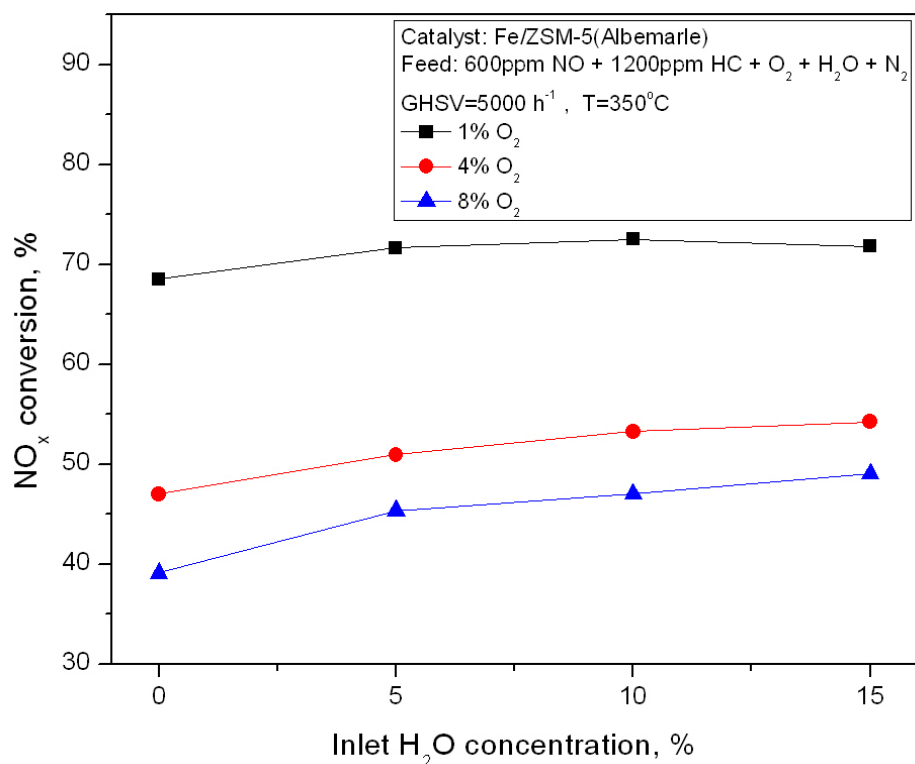


Figure 3.38 Effect of H₂O on the catalytic activity of Fe/ZSM-5(Albemarle) (T=350°C)

The time-on-stream test was carried out to further investigate the long-term influence of H₂O on the SCR activity of Fe/ZSM-5(Albemarle), with the result shown in Figure 3.39. Test A was carried out using the catalyst aged at T=350°C for several runs without regeneration. After test A, the catalyst was regenerated in 10% O₂ + N₂ at 500°C for 2 hours before test B was performed under the same operating condition. It can be seen that the aged Fe/ZSM-5(Albemarle) still kept a stable activity over a time period of 450 minutes for the feed gas of 600ppm NO + 1200ppm HC + 4% O₂ + 10% H₂O + N₂ at T=350°C and GHSV=5000 h⁻¹. After regeneration, the catalytic activity remained almost the same.

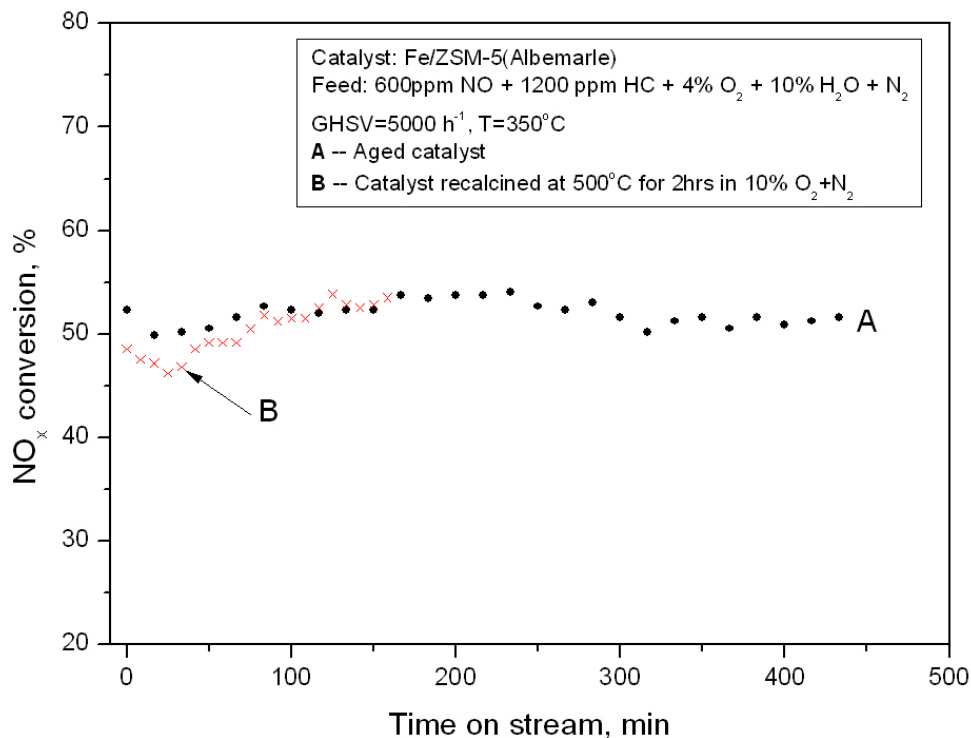


Figure 3.39 Time-on-stream test on the effect of H₂O (Fe/ZSM-5(Albemarle), T=350°C)

The combined effect of CO₂ and H₂O was also investigated for the model flue gas with 10% CO₂ and 10% H₂O, with the results plotted in Figure 3.40. Clearly, the addition of 10% CO₂ had almost no effect on the SCR activity of the catalyst. The presence of 10% H₂O showed some improvement on NO_x conversion for the flue gas containing various O₂ concentrations. Compared with the case with only 10% H₂O, further addition of 10% CO₂ seemed to have no effect on the catalytic activity when O₂ concentration was low (1%). However, a combined positive impact was obtained at 4% O₂, with the impact being more significant at 8% O₂.

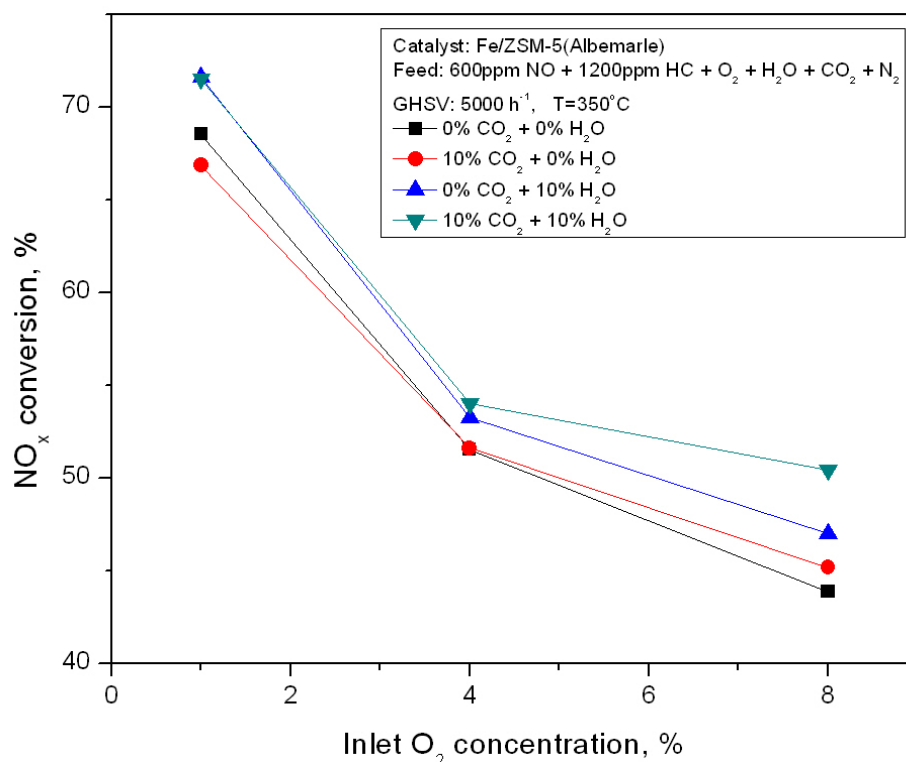


Figure 3.40 Combined effect of H₂O and CO₂ on the catalytic activity of Fe/ZSM-5(Albemarle) (T=350°C)

One of the possible mechanisms for the enhanced deNO_x performance by the addition of H₂O is the contribution of H₂ and CO, produced from the water gas shift reaction (equation 3.13) or steam reforming of propylene (equation 3.14) which can take place at low temperatures.



As shown in Figure 3.41, for the flue gas containing 4% O₂, without the presence of H₂O, CO and CO₂ concentrations at the outlet of the reactor were around 1000ppm and 0.30%, respectively. The addition of 5% H₂O led to the decrease of CO concentration to 500ppm, but the increase of CO₂ concentration to 0.34%. Further increase of H₂O had no significant influence on both CO and CO₂ concentrations. The significant drop of the CO

concentration and the increase of the CO_2 concentration caused by the addition of H_2O reflect the fact that water gas shift reaction (equation 3.13) or the combination of equations 3.13 and 3.14 played a role in the SCR process. It is well known that both CO and H_2 are strong reducing agents, which are commonly used for NO_x reduction in the three-way catalytic converters. Further controlled experiments, in which both CO and H_2 concentrations will be monitored, are needed in the future to elucidate the reaction mechanism on the enhancement of NO_x reduction by water.

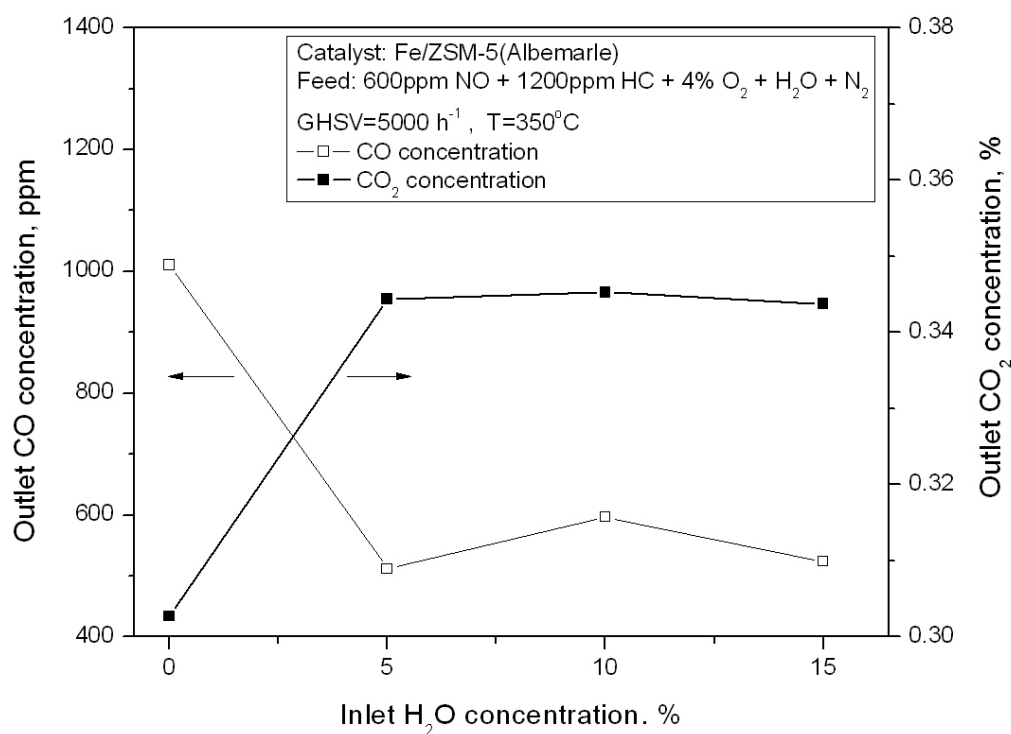


Figure 3.41 Effect of the addition of H_2O on outlet CO and CO_2 concentrations (Fe/ZSM-5(Albemarle), $T=350^\circ\text{C}$)

3.5.6.5 Deactivation of Fe/ZSM-5(Albemarle) catalyst by SO_2

Sulphur oxides (SO_2 and SO_3) are considered as the most poisonous components in the combustion flue gas on SCR process. Although the content of SO_2 in the flue gas could be reduced to a relatively low level (10 to 30ppm) after the wet scrubbing process, this small

amount of SO₂ can still seriously inhibit the catalytic activity of most of the catalysts used in the SCR process, damaging the application of HC-SCR. Since Fe/ZSM-5(Albemarle) showed an acceptable activity in the HC-SCR process, the effect of SO_x on the catalyst performance is further investigated to examine the durability of the catalyst in the presence of SO₂.

To monitor the gradual decay of the catalyst activity with time, the time-on-stream test was performed with the result of total four runs shown in Figures 3.42 to 3.45. In each run, four time-on-stream (TOS) tests were conducted as described below:

- A. The fresh catalyst was first treated with the model flue gas of 600ppm NO +1200ppm HC + 1% O₂ + N₂ at 350°C and GHSV=5000 h⁻¹ until the stable NO_x conversion was reached to establish the baseline.
- B. Then, SO₂ was introduced into the feed gas stream and the outlet NO_x and SO₂ concentrations were continuously monitored.
- C. After several hours, SO₂ was switched off from the feed gas flow and the SO₂ deactivated catalyst was used in another TOS test. When the outlet NO_x concentration reached a relatively stable value, the test was terminated.
- D. The catalyst was then calcined *in-situ* with 20% O₂ + N₂ at 500°C for 2 hours in order to regenerate the catalyst. Thereafter, the regenerated catalyst was used in the final TOS test to finish the first cycle or Run #1.
- E. The TOS result in step D from the regenerated catalyst was then used as the new baseline for the next cycle, and steps B to D were repeated for the 2nd to 4th test cycles, or Runs #2-4.

It could be seen from those figures that, in Run #1 for the baseline without the presence of SO₂, the NO_x conversion was stable with time. When 200ppm SO₂ was introduced into the feed gas flow, the measured SO₂ concentration at the outlet of the reactor

showed that SO_2 was adsorbed onto the catalyst. As time passed by, the outlet SO_2 concentration increased gradually when more catalyst surface was occupied by SO_2 . Finally, the outlet SO_2 reached the inlet concentration, or even higher because some of the adsorbed SO_2 might also be washed out by the model flue gas flow. With the addition of 200ppm SO_2 , the NO_x conversion quickly reached a maximum value and then gradually headed down due to the deactivation of the catalyst by SO_2 adsorption. Because of the malfunction of the data logging system, the TOS test result of step C in Run #1 was not recorded and thus not plotted in Figure 3.42. The TOS result from the regenerated catalyst without the presence of 200ppm SO_2 showed that, the catalytic activity was partially recovered, and the NO_x conversion was stable with time but couldn't reach the level with the original catalyst, which means that the catalyst was permanently poisoned by SO_2 .

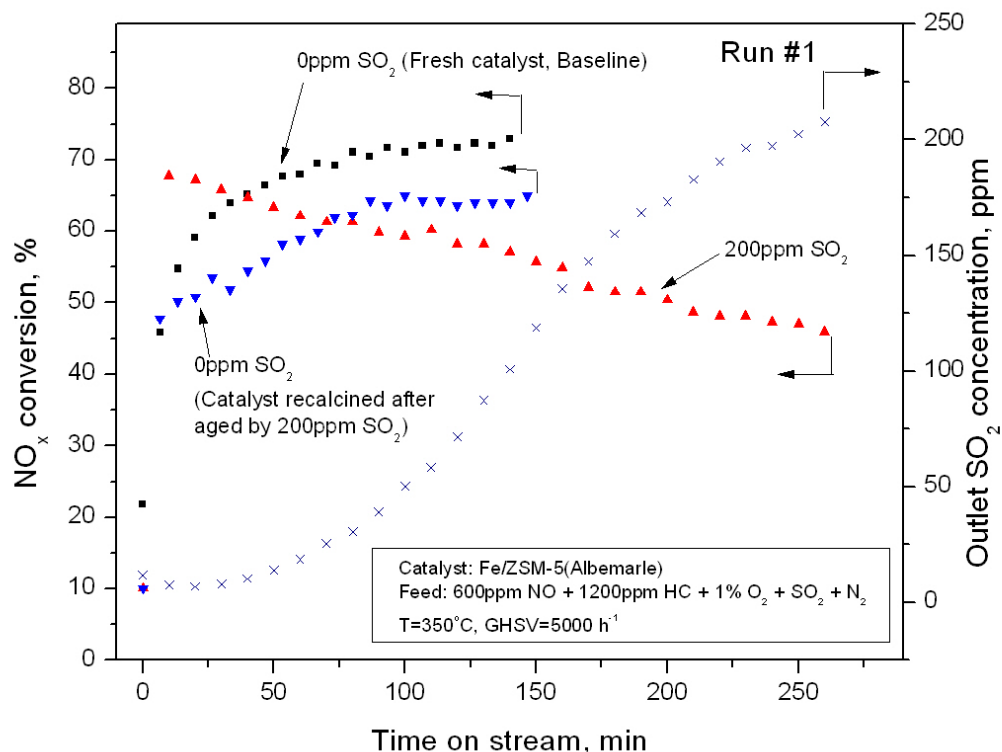


Figure 3.42 Effect of SO_2 on the catalytic activity of Fe/ZSM-5(Albemarle) (200ppm SO_2 , Run #1)

The result of Run #2 in Figure 3.43 showed the similar trend as in Run #1 for the presence of 200ppm SO₂ in the flue gas. When SO₂ feed was switched off, the catalytic activity was partially recovered and remained stable with time because the adsorbed SO₂ on the catalyst was partially stripped by the SO₂-free flue gas flow, which led to part of the active sites being recovered. Immediate calcination of the catalyst could further recover part of the catalytic activity, but the NO_x conversion was still much lower than the baseline value. Run #3 (Figure 3.44) and Run #4 (Figure 3.45) revealed the same trend except for that the catalytic activity became lower and lower.

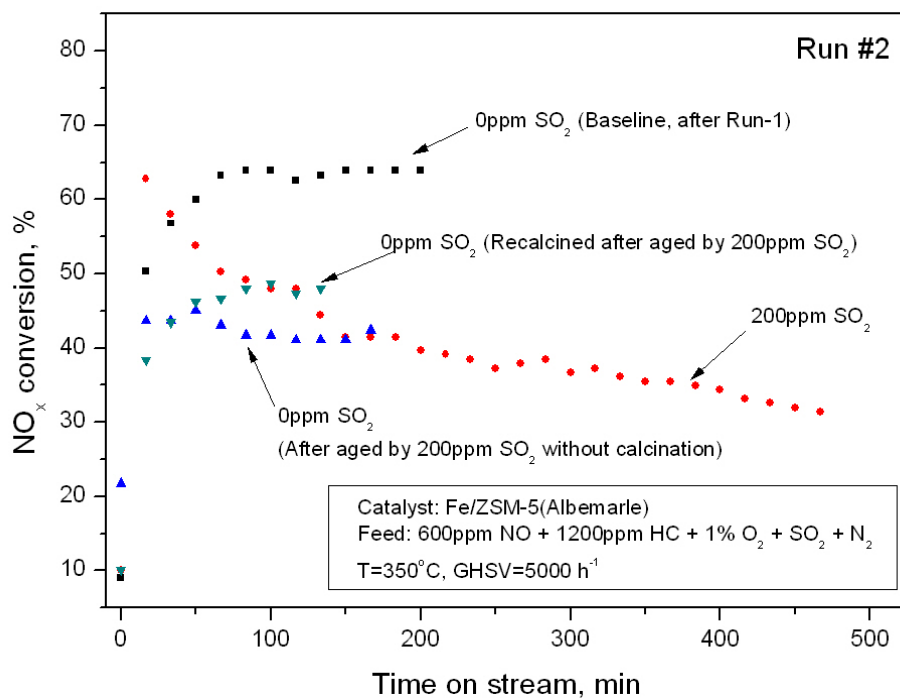


Figure 3.43 Effect of SO₂ on the catalytic activity of Fe/ZSM-5(Albemarle) (200ppm SO₂, Run #2)

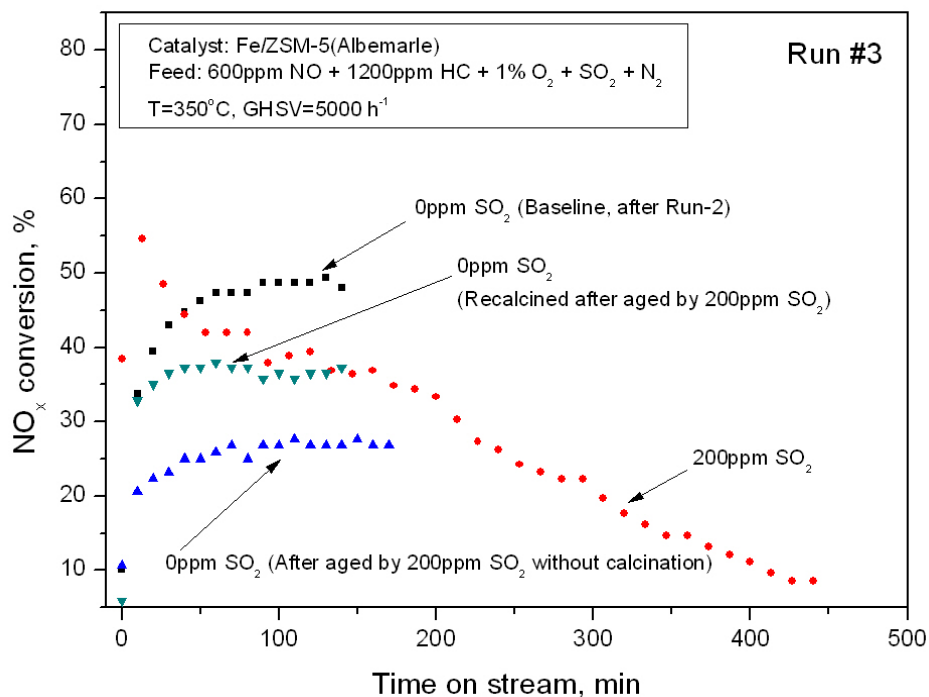


Figure 3.44 Effect of SO₂ on the catalytic activity of Fe/ZSM-5(Albemarle) (200ppm SO₂, Run #3)

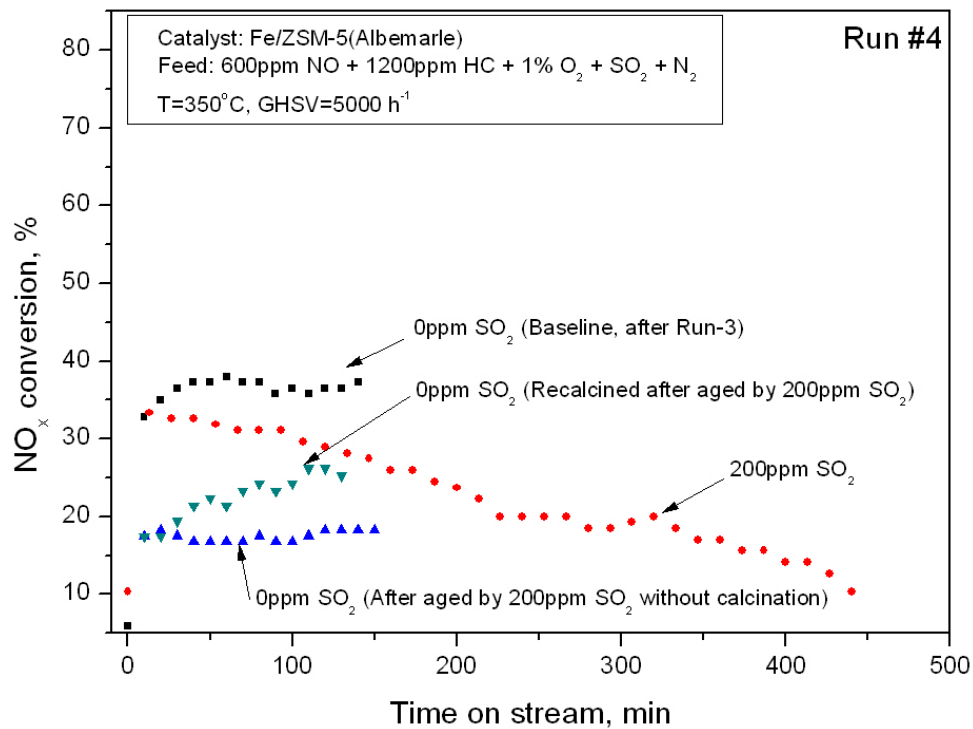


Figure 3.45 Effect of SO₂ on the catalytic activity of Fe/ZSM-5(Albemarle) (200ppm SO₂, Run #4)

To further analyze the results from all four runs, TOS tests with 200ppm SO₂ present in the flue gas are compared in Figure 3.46. The highest NO_x conversion was obtained in Run #1. After 250 minutes, the NO_x conversion dropped from the peak value of 68% to 47%. Over the same period of time, the NO_x conversion decreased from 64% to 37%, 56% to 25%, and 36% to 19% for Run #2, #3 and #4, respectively, using regenerated catalyst. The difference of the peak NO_x conversion between runs increased, indicating the permanent loss of reactivity after each deactivation and regeneration cycle because more and more active sites on the catalyst were blocked by SO₂ or S-containing compounds.

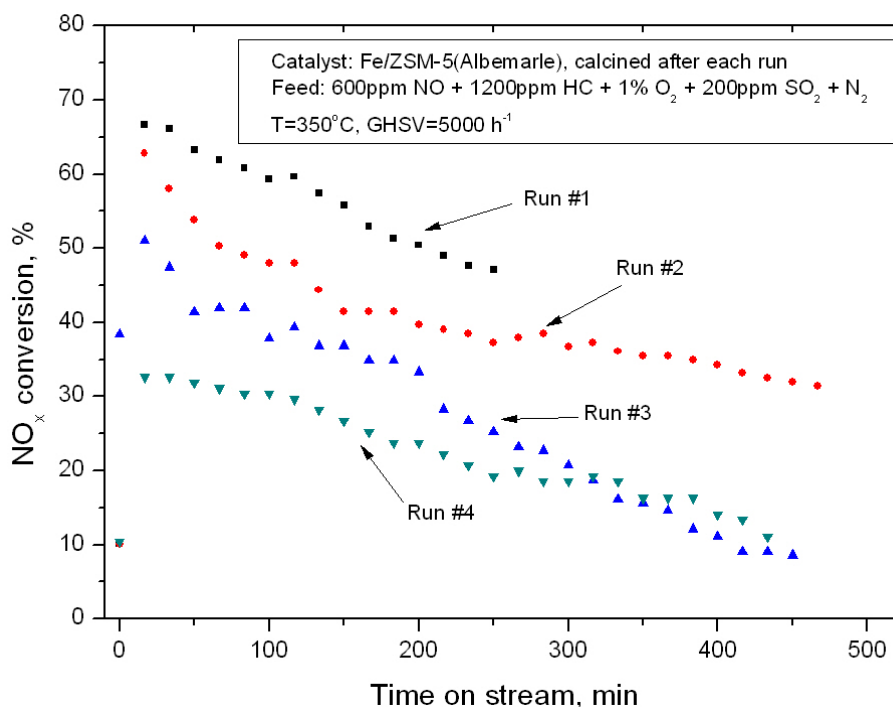


Figure 3.46 Comparison of the four consecutive runs with 200ppm SO₂ in the flue gas (Catalyst: Fe/ZSM-5(Albemarle))

Figure 3.47 compares the performance of the fresh and regenerated catalyst on NO_x reduction over the four consecutive runs, after repeated exposure to the flue gas containing 200ppm SO₂. It can be seen that the permanent damage of SO₂ on the catalyst gradually built

up with time by contacting the SO₂-containing flue gas with the catalyst. After Run #1, only 7% of permanent loss of the NO_x conversion was observed (72% to 65%). Run #2 caused another 17% of loss (65% to 48%). The catalyst lost 11% (48% to 37%) and 12% (37% to 25%) of the reactivity in Run #3 and Run #4, respectively. In other words, the catalytic activity dropped from 72% to 25% in about 27 hours with regeneration between runs because of the addition of 200ppm SO₂ into the flue gas.

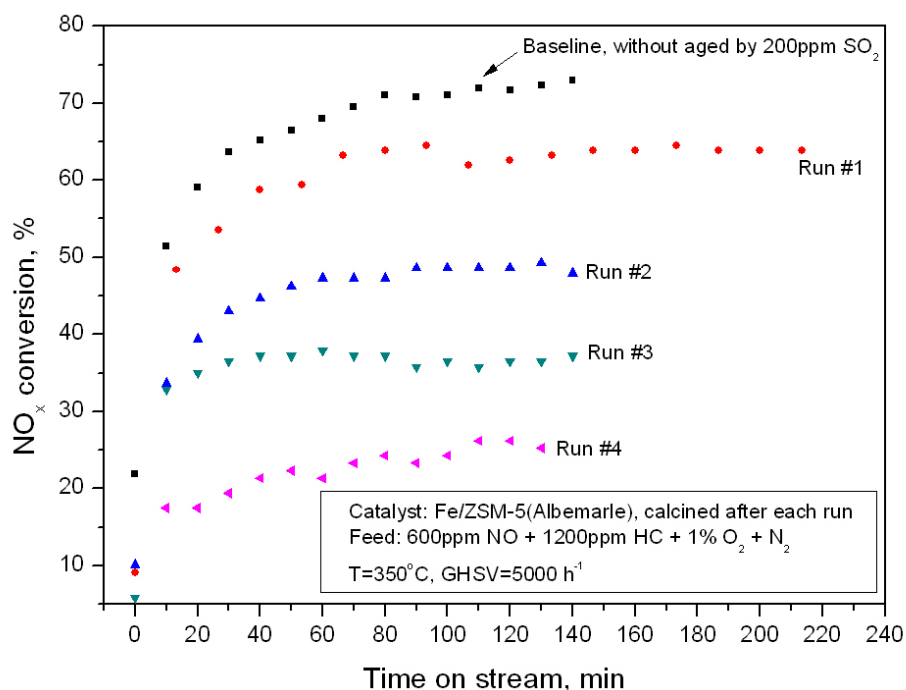


Figure 3.47 Comparison of fresh and regenerated catalysts over four consecutive runs (Catalyst: Fe/ZSM-5(Albemarle))

Another set of tests was conducted at lower SO₂ concentration (30ppm) to simulate flue gases after SO₂ removal in the combustion process. Fresh catalyst was used in this test, with the results shown in Figure 3.48. The NO_x conversion decreased with time when 30ppm SO₂ was added into the flue gas, but at a much slower pace than the one with 200ppm SO₂. Over about 11 hours, the NO_x conversion dropped from 69% to 50%, in comparison to a drop from 68% to 47% in 4 hours at 200ppm SO₂. However, if the catalyst was aged by the 30ppm

SO₂ and placed overnight without immediately flushed by SO₂-free gas flow or calcined at 500°C, the catalyst was almost totally deactivated, giving only 6.5% of NO_x conversion when the reactor was restarted with SO₂-free model flue gas. Further calcination of the catalyst could only bring the NO_x conversion back to 32%. This permanent activity loss might be caused by the aging of adsorbed SO₂ over a long time on the active sites. As time passed, the adsorbed SO₂ also reacted with the active Fe, leading to the formation of Fe-S bond and/or FeSO_x compounds, which caused the irreversible poisoning to the catalyst.

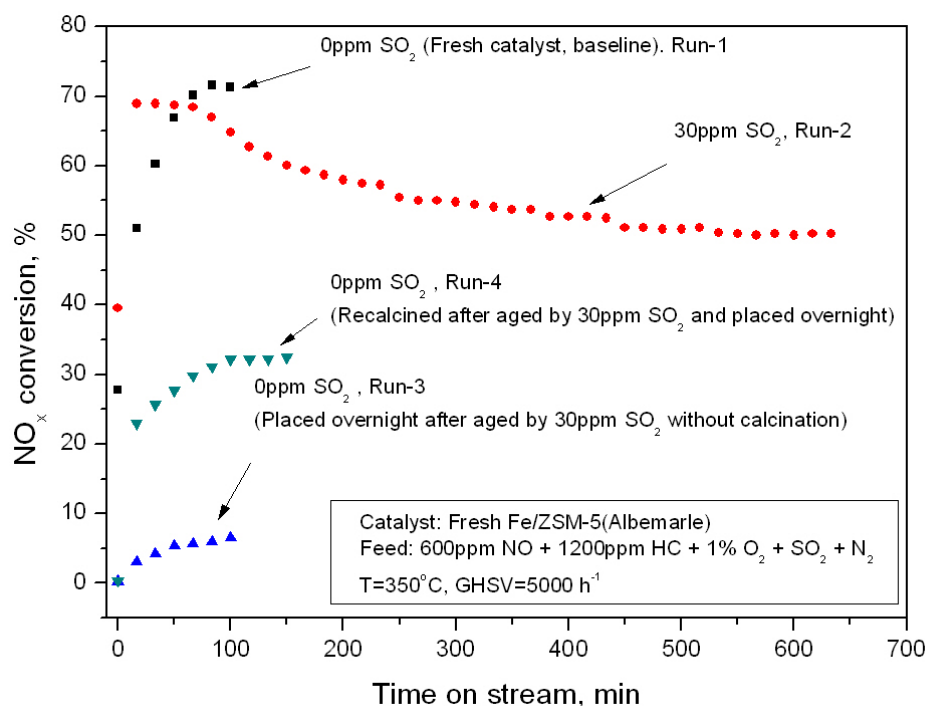


Figure 3.48 Effect of SO₂ on the catalytic activity of Fe/ZSM-5(Albemarle) (30ppm SO₂)

Measured BET surface area of the fresh Fe/ZSM-5(Albemarle) catalyst (Figure 3.49) showed that the impregnation of Fe to the parent ZSM-5(Albemarle) led to a slight loss (around 5%) of BET surface area (171 m²/g (parent) to 162 m²/g (Fe/ZSM-5(Albemarle))). After the catalyst was aged in the flue gas containing 200ppm SO₂ for 27 hours and then regenerated, the BET surface area dropped to 129 m²/g, a 20% loss compared to the fresh

Fe/ZSM-5(Albemarle). For the catalyst aged by 30ppm SO₂ for 11 hours and calcined after being placed over night, the BET surface area decreased remarkably by 36% to 103 m²/g. These data proved that SO₂ could have serious negative impact on the catalytic activity of Fe/ZSM-5(Albemarle) especially when the catalyst had a long-term exposure to SO₂-containing flue gases. The poisoning is irreversible although part of the deactivated sites caused by the adsorbed SO₂ could be recovered by immediate calcination.

In the proposed dual-zone deNO_x reactor, when the SO₂-containing flue gas is injected into the adsorption zone and contacts with the catalyst, both SO₂ and NO_x will be adsorbed onto the catalyst. After the SO₂/NO_x-adsorbed catalyst moves into the reduction zone, due to the lack of SO₂ in the reductant gas, the adsorbed SO₂ will be stripped off from the catalyst by the reductant gas flow. Since the contact time between the catalyst and SO₂ is very short in the adsorption zone, the negative effect of SO₂ to the catalyst could be reduced in the dual-zone deNO_x reactor, although such a speculation still needs to be confirmed experimentally in the future.

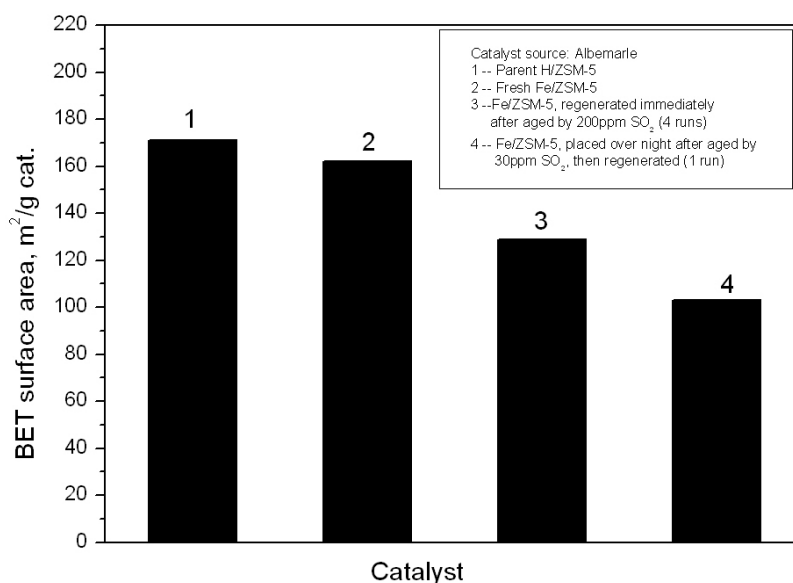


Figure 3.49 Comparison of BET surface areas for fresh and deactivated catalyst (Fe/ZSM-5(Albemarle))

3.6 Summary

Fe/ZSM-5 prepared from Na/ZSM-5 (PUC) with an average particle size of 1042 μm showed very low NO_x adsorption capacity. The adsorption performance was greatly improved when the catalyst was prepared using crushed Na/ZSM-5(PUC) with smaller particle size (234 μm). The most promising adsorption performance was offered by Fe/ZSM-5(Albemarle) with the finest particle size (155 μm) among tested catalysts. This result proves that the adsorption performance of the catalyst is closely related to the particle size and the structure of the catalyst support. The addition of water vapour to the model flue gas had little effect on the adsorption capacity of Fe/ZSM-5(Albemarle). However, negative impact was observed when CO_2 was added into the flue gas, and the further addition of H_2O to the CO_2 -containing flue gas slightly improved the adsorption performance of Fe/ZSM-5(Albemarle).

Although Fe/ZSM-5(PUC, WIE) showed the same or higher peak NO_x conversion compared with Fe/ZSM-5(PUC, IMPO) at the same reaction condition, its reactivity was not stable with time, even at higher temperatures and excessive O_2 concentration. However, Fe/ZSM-5(PUC, IMPO) showed stable HC-SCR performance at $T \geq 350^\circ\text{C}$ even with very low O_2 concentration. From this point of view, IMPO is a preferred method for the preparation of Fe/ZSM-5.

The catalytic activity of Fe/ZSM-5 catalyst was sensitive to the reaction temperature and space velocity. The catalyst deactivated very quickly at temperatures lower than 325°C because of the deposit of graphitic carbon on the catalyst surface. Fe/ZSM-5 catalysts using Na/ZSM-5(PUC), Na/ZSM-5(crushed PUC) and H/ZSM-5(Albemarle) as supports exhibited stable reactivity at $T \geq 350^\circ\text{C}$ and $\text{GHSV} = 5000 \text{ h}^{-1}$. Among them, Fe/ZSM-5(PUC) showed the highest reactivity, but lowest adsorption capacity, at the same reaction condition, which

implies that the reaction activity of the catalyst is not directly proportional to the adsorption capacity in the conventional HC-SCR process.

To reach a high NO_x conversion, a high HC:NO ratio is needed. Considering both the economic aspect and the reduction efficiency of NO_x, HC:NO=2:1 is a reasonable choice. O₂ concentration played an important role in the SCR of NO_x with propylene as the reducing agent. Fe/ZSM-5(PUC), Fe/ZSM-5(crushed PUC) and Fe/ZSM-5(Albemarle) catalysts exhibited acceptable activity when O₂ concentration was controlled at relatively low levels (e.g. ≤1%).

Water vapour could slightly enhance the reactivity of Fe/ZSM-5(Albemarle) in HC-SCR, while CO₂ showed little effect. SO₂ in the flue gas could seriously poison Fe/ZSM-5(Albemarle) catalyst, especially for the long time contact between SO₂-containing flue gas and the catalyst. The damage caused by SO₂ was permanent, and only partial catalytic activity could be recovered via calcination at high temperatures.

Chapter 4

Hydrodynamic Study of the ICFB Reactor

Based on the literature review, the catalytic activity of most HC-SCR catalysts is severely inhibited by the presence of excess O₂ in the flue gas. On the other hand, one of the main NO reduction mechanisms states that NO is first oxidized to NO₂, followed by the reduction of NO₂ by the reducing agent. That means the presence of O₂ is essential for the HC-SCR process. Therefore, in the proposed dual-zone reactor, the presence of oxygen in the reduction zone is essential but must be controlled within an appropriate range in order to keep the O₂ concentration at a relatively low level (lower than 2%, according to the results from the fixed bed experiment). On the other hand, gas bypassing from the reduction zone to the adsorption zone will cause an increase in the consumption of the reducing agent in the dual-zone reactor, which should be minimized.

In addition, the solids circulation rate will be directly linked to the transfer of the adsorbed NO_x from the adsorption zone to the reduction zone and the NO_x reduction in the reaction zone of the reactor.

Based on the above requirements, the fluidized bed reactor with a draft tube, or so-called internal circulating fluidized bed (ICFB) reactor, could meet the requirement of the dual-zone reactor. The ICFB with different configurations has been studied extensively on its hydrodynamics (Fusey, et al., 1986; Milne et al., 1992; Kim et al., 1997; Ishikura et al., 2003), heat and mass transfer (Freitas and Freire, 2001; Stocker et al., 1990; Kim, et al., 2000), and its applications for particle drying (Ando et al., 2002), coating of tablets (Shelukar et al., 2000), coal combustion and gasification (Yang and Keairns, 1978a, b), and other industrial processes (Yang, 1998).

In order to provide design and operating criteria for the hot model ICFB unit, it is essential to investigate the hydrodynamic performance of the ICFB reactor.

4.1 Experimental setup

A cold model ICFB reactor was constructed with the configuration shown in Figure 4.1. Gas bypass both from the annulus to the draft tube and the draft tube to the annulus and the solids circulation rate were investigated in this cold model unit, which was made of Plexiglass with dimensions listed in Table 4.1.

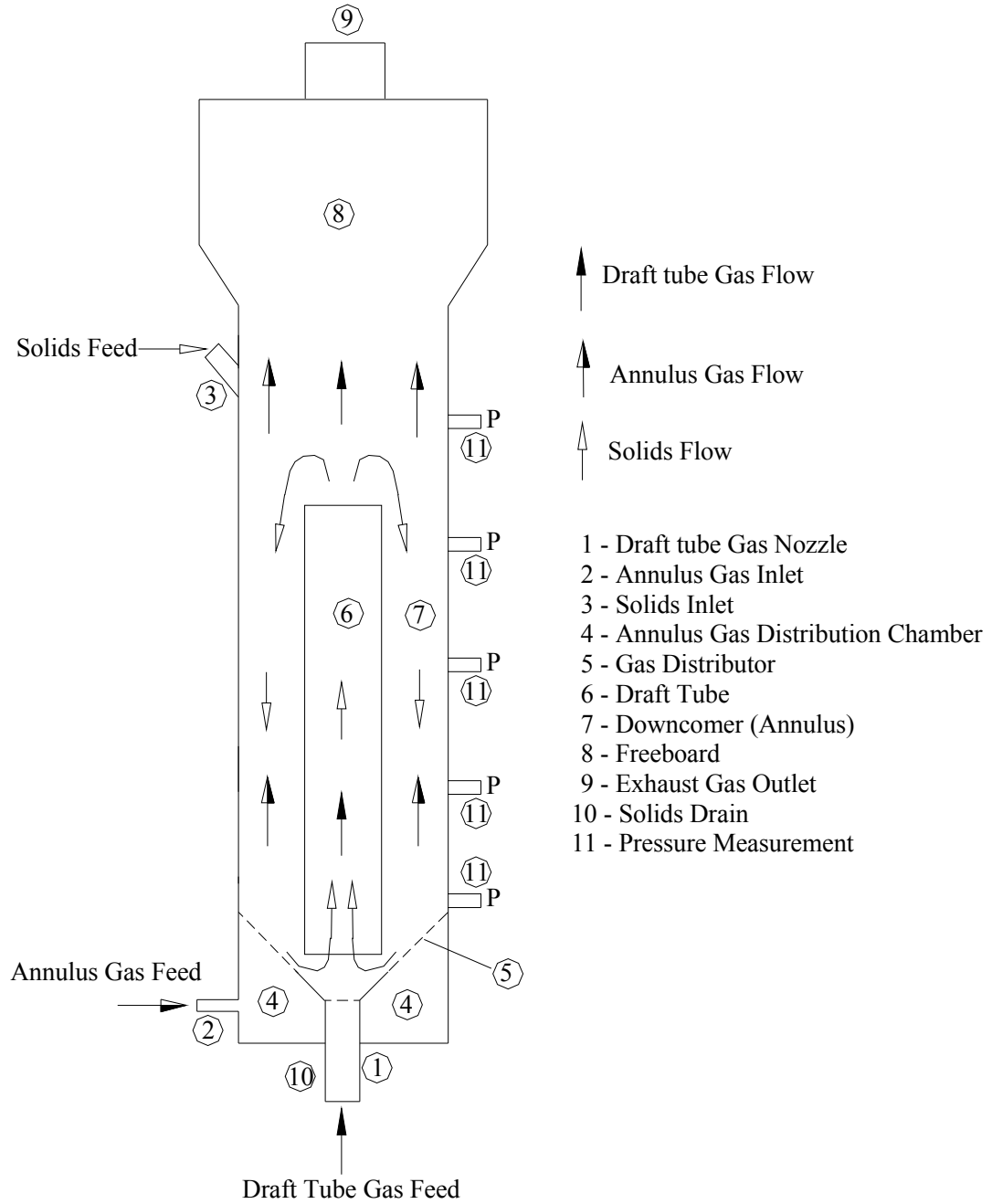


Figure 4.1 Schematic of the cold model ICFB reactor

Table 4.1 Dimensions of the cold model ICFB unit

Item	Dimension
Draft tube diameter, mm	50.8 (I.D.), 63.5 (O.D.)
Draft tube diameter, mm (for cylindrical gas distributor only)	38.1 (I.D.), 44.5 (O.D.)
Draft tube length, mm	1016.0
Column diameter, mm	101.6 (I.D.), 114.3 (O.D.)
Column height, mm	1092.2
Freeboard diameter, mm	254.0 (I.D.), 266.7 (O.D.)
Freeboard height, mm	508.0
Annulus gas distributor opening ratio	2.1%
Holes on the distributor	52 holes of 1.6mm diameter
Gas nozzle diameter, mm	34.9 (I.D.), 38.1 (O.D.)

The geometry of the cold model ICFB unit was developed based on the design criteria described by Yang (1998) in order to achieve high solids circulation rate and retain certain degree of gas bypassing between the core and the annulus regions. The desired solids circulation rate was calculated based on the adsorption performance of the catalyst from the fixed bed experiments, and the reactor diameter was selected with the consideration of the available flow rate of the building air.

The bed material used in the experiment was millet with a particle density ($\rho_p=837$ kg/m³) and average particle size ($d_p=1.1$ mm) similar to the Fe/ZSM-5(PUC) catalyst used in the fixed bed experiment. The building air was used as the fluidizing gas. Pure CO₂ from Praxair was used as the tracer gas to study the gas bypass.

The cold model ICFB system is shown schematically in Figure 4.2. In the experiment, the building air was injected into the draft tube via the gas nozzle and the gas flow rate was

adjusted to have the draft tube region operated at a pneumatic transport condition to carry particles upward to create a continuous circulation of the particles between the annulus and the draft tube. At the same time, the mixture of the building air and the tracer gas was introduced into the annulus or downcomer region through the gas chamber and the annulus gas distributor. The flow rate was controlled to keep the annulus region being operated at the moving bed or minimum fluidization condition. Flow rates in both the draft tube and the annulus were adjusted to investigate the gas bypass between the two regions and the solids circulation from the annulus to the draft tube. Gas compositions at the inlet of the annulus gas chamber, the inlet of the gas nozzle, the outlet of the draft tube, the outlet of the annulus, and the gas mixture in the freeboard region were measured by a Horiba PG-250 flue gas analyzer.

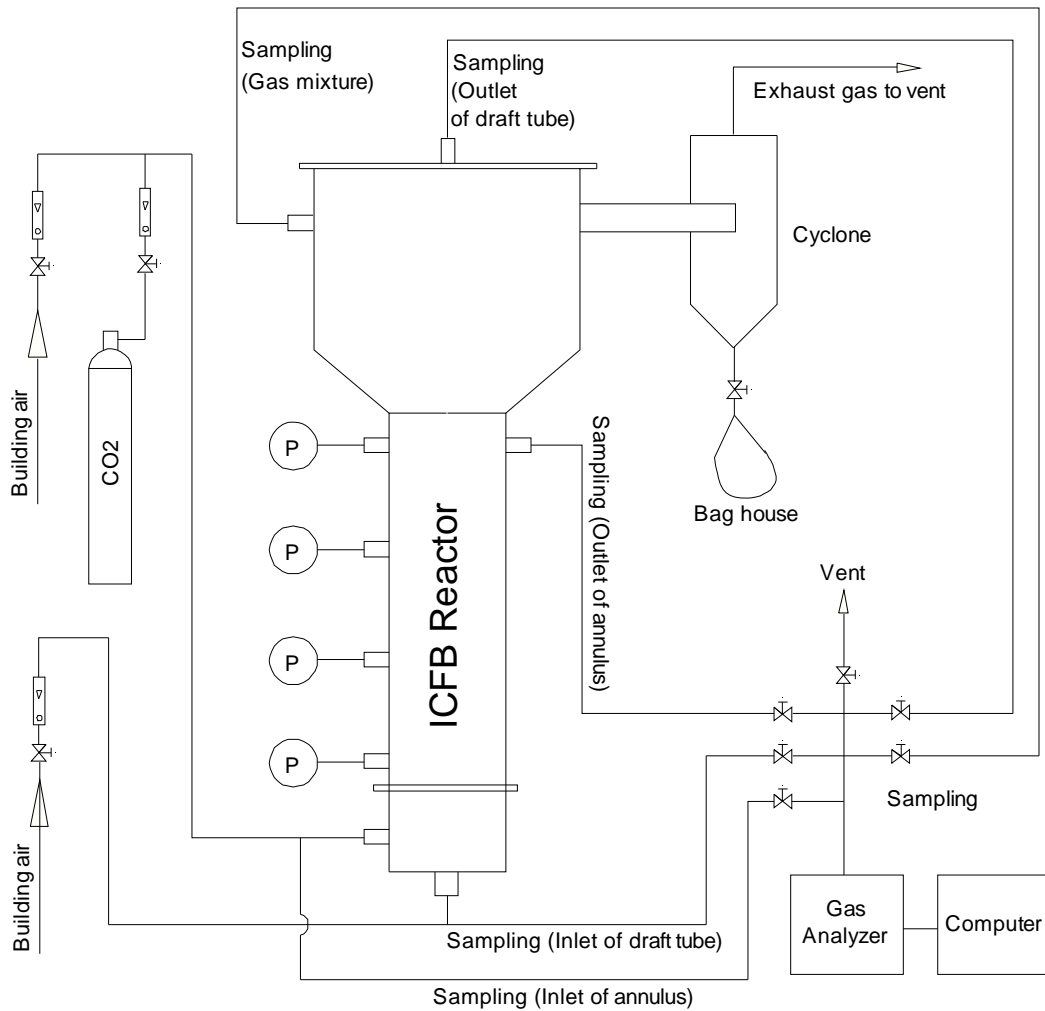


Figure 4.2 Schematics of the cold model ICFB system

As reported by Yang and Keairns (1983), for a given ICFB reactor, the gas bypass and solids circulation rates are significantly affected by the gap opening between the inlet of the draft tube and the distributor plate. Three types of annulus gas distributors, a flat plate, a cylindrical plate and a conical plate, were tested, together with the effective gap opening between the draft tube and the distributor plate being adjusted to investigate the hydrodynamic performance of the ICFB reactor. All three perforated distributors had the same opening ratio of 2.1% for easy comparison of the experimental results.

4.1.1 Estimation of gas bypass ratio

The gas bypass between the draft tube and the annulus was evaluated by CO₂ tracer method. At given operating conditions, continuous CO₂ tracer was injected into the inlet gas flow of the annulus, with CO₂ concentrations at the outlet of the draft tube and the annulus, and the inlet of the draft tube and the annulus being analyzed and recorded.

Gas bypass ratios are calculated by the mass balance method as illustrated in Figure 4.3.

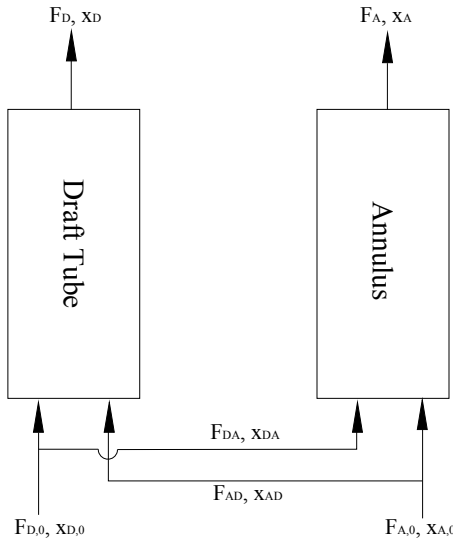


Figure 4.3 Schematic of the mass transfer between draft tube and annulus

The total mass balance over the draft tube and the annulus in Figure 4.3 is given by,

$$\begin{aligned} & [\rho_{air}(1-x_{D,0}) + \rho_{CO_2}x_{D,0}]F_{D,0} + [\rho_{air}(1-x_{A,0}) + \rho_{CO_2}x_{A,0}]F_{A,0} \\ & = [\rho_{air}(1-x_D) + \rho_{CO_2}x_D]F_D + [\rho_{air}(1-x_A) + \rho_{CO_2}x_A]F_A \end{aligned} \quad (4.1)$$

where

ρ_{air} , air density, kg/m³

ρ_{CO_2} , CO₂ density, kg/m³

$F_{D,0}$, volumetric gas flow rate at the inlet of the draft tube, m³/s

$x_{D,0}$, volume fraction of CO₂ in the gas flow at the inlet of the draft tube

$F_{A,0}$, volumetric gas flow rate at the inlet of the annulus, m³/s

$x_{A,0}$, volume fraction of CO₂ in the gas flow at the inlet of the annulus

F_D , volumetric gas flow rate at the outlet of the draft tube, m³/s

x_D , volume fraction of CO₂ in the gas flow at the outlet of the draft tube

F_A , volumetric gas flow rate at the outlet of the annulus, m³/s

x_A , volume fraction of CO₂ in the gas flow at the outlet of the annulus

Since the bed material used in the cold model ICFB unit was millet, which had a very low CO₂ adsorption capacity, the change of CO₂ concentration contributed from particle adsorption was thus neglected in the mass balance equation.

The total mass balance on CO₂ over the draft tube and the annulus is given by,

$$\rho_{CO_2} x_{D,0} F_{D,0} + \rho_{CO_2} x_{A,0} F_{A,0} = \rho_{CO_2} x_D F_D + \rho_{CO_2} x_A F_A \quad (4.2)$$

With $x_{A,0}$, $x_{D,0}$, x_D , and x_A being measured, flow rates at the outlet of the annulus (F_A) and the outlet of the draft tube (F_D) can be calculated by combining equations 4.1 and 4.2:

$$F_A = \frac{(x_{D,0} - x_D) F_{D,0} + (x_{A,0} - x_D) F_{A,0}}{x_A - x_D} \quad (4.3)$$

$$F_D = \frac{(x_{A,0} - x_A) F_{A,0} + (x_{D,0} - x_A) F_{D,0}}{x_D - x_A} \quad (4.4)$$

The total mass balance and the CO₂ mass balance over the draft tube are given by equations 4.5 and 4.6 below,

$$\begin{aligned} & [\rho_{air} (1 - x_{D,0}) + \rho_{CO_2} x_{D,0}] F_{D,0} + [\rho_{air} (1 - x_{AD}) + \rho_{CO_2} x_{AD}] F_{AD} \\ & = [\rho_{air} (1 - x_D) + \rho_{CO_2} x_D] F_D + [\rho_{air} (1 - x_{DA}) + \rho_{CO_2} x_{DA}] F_{DA} \end{aligned} \quad (4.5)$$

$$\rho_{CO_2} x_{D,0} F_{D,0} + \rho_{CO_2} x_{AD} F_{AD} = \rho_{CO_2} x_D F_D + \rho_{CO_2} x_{DA} F_{DA} \quad (4.6)$$

where

F_{DA} , volumetric gas bypass rate from draft tube to annulus, m^3/s

x_{DA} , volume fraction of CO_2 in the gas bypass flow from draft tube to annulus

F_{AD} , volumetric gas bypass rate from annulus to draft tube, m^3/s

x_{AD} , volume fraction of CO_2 in the gas bypass flow from annulus to draft tube

The volumetric gas bypass rates from the annulus to the draft tube (F_{AD}) and from the draft tube to the annulus (F_{DA}) are derived from equations 4.3 to 4.6 with $x_{DA}=x_{D,0}$ and $x_{AD}=x_{A,0}$,

$$F_{DA} = F_{D,0} - \frac{x_{A,0} - x_D}{x_{A,0} - x_{D,0}} F_D \quad (4.7)$$

$$F_{AD} = \frac{x_D - x_{D,0}}{x_{A,0} - x_{D,0}} F_D \quad (4.8)$$

The percentage gas bypass ratios from the draft tube to the annulus (R_{DA}) and the annulus to the draft tube (R_{AD}) are defined as:

$$R_{DA} = \frac{F_{DA}}{F_{D,0}} \times 100\% \quad (4.9)$$

$$R_{AD} = \frac{F_{AD}}{F_{A,0}} \times 100\% \quad (4.10)$$

4.1.2 Estimation of solids circulation rate

The solids circulation rate was measured by the visual observation method. Coloured millet particles were added into the bed material as tracer particles. For given gas flow rates in the draft tube and the annulus, the motion of a specific tracer particle on the column wall was tracked by marking its moving distance L in a given time interval t_m . The tracer particle downward velocity in the annulus was then calculated by

$$U_p = \frac{L}{t_m} \quad (4.11)$$

The solids circulation rate W_s ($\text{kg/m}^2 \cdot \text{s}$) through the unit cross-sectional area of the draft tube was calculated by

$$W_s = \frac{S_A}{S_D} U_p \rho_p (1 - \varepsilon) \quad (4.12)$$

where S_A and S_D are cross-sectional areas of the annulus and the draft tube respectively, ρ_p is the particle density, and ε is the bed voidage in the annulus which is assumed to be equal to the packed voidage.

4.2 Performance with the flat distributor plate

The flat gas distributor with two configurations used in the experiment is shown schematically in Figure 4.4. For the first configuration (Figure 4.4(a)), the top of the gas nozzle was flush with the surface of the flat distributor, and the gap, called the effective gas opening, between the bottom of the draft tube and the surface of the distributor was fixed at $H_{G1}=10$ mm. The top of the gas nozzle was flush with the bottom of the draft tube for the second configuration (Figure 4.4(b)) with H_{G1} remaining at 10 mm, but the effective gap opening for the solids circulation in the second configuration was reduced to $H_{G2}=6$ mm, which corresponds to the distance between the inner surface of the draft tube and the outer surface of the gas nozzle.

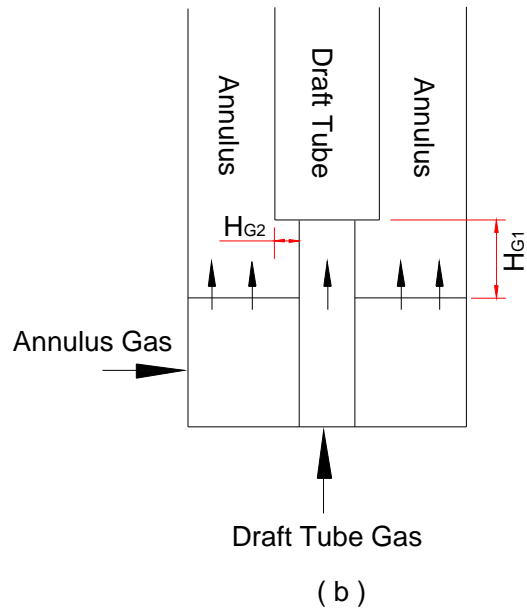
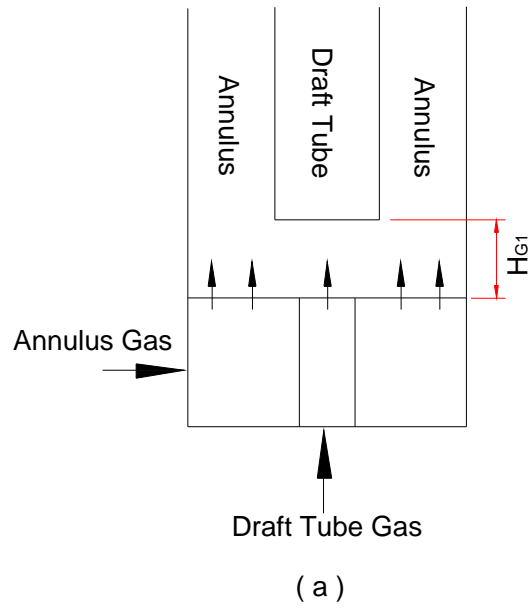


Figure 4.4 Configurations of the flat distributor for the annulus gas flow

4.2.1 Gas bypass

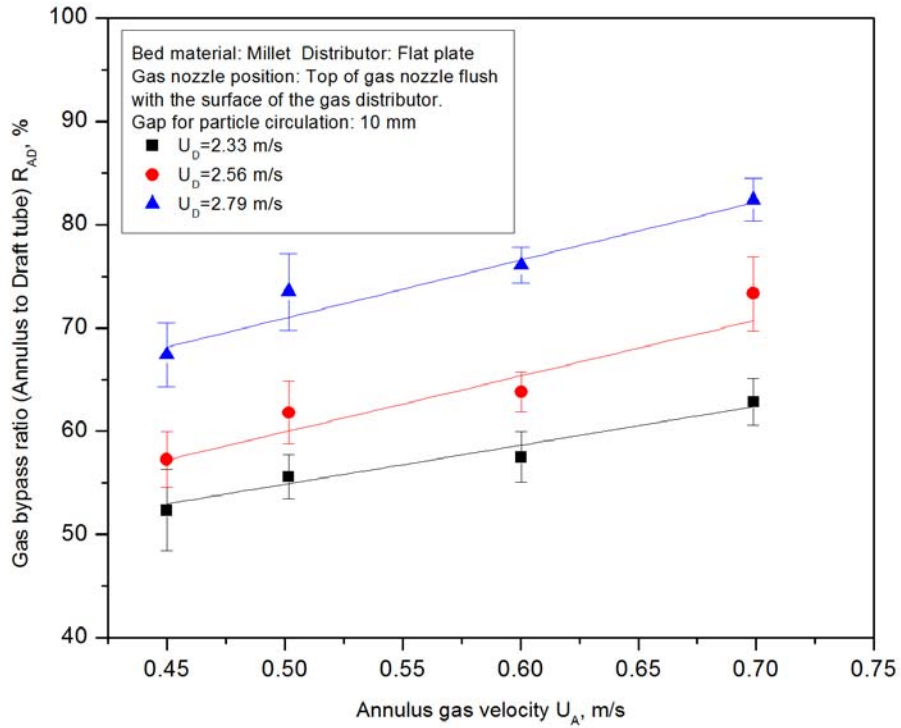
For the configuration one with an effective gap opening of $H_G=10$ mm, the effect of gas velocities in the annulus (U_A) and the draft tube (U_D) on the gas bypass from both the annulus to the draft tube and the draft tube to the annulus is shown in Figure 4.5.

Within the range of tested gas velocities, the ICFB with a flat distributor plate showed more than 50% of gas bypass from the annulus to the draft tube (R_{AD}) (Figure 4.5(a)), but less than 1.5% from the draft tube to the annulus (R_{DA}) (Figure 4.5(b)). R_{AD} increased with the increase of both U_A and U_D . Although R_{DA} decreased with the increase of U_A at a given U_D , there was no clear trend with respect to the effect of U_D on the gas bypass at a given U_A (see Figure 4.5(b)). One should note that R_{DA} values were very small and could be associated with significant measurement errors.

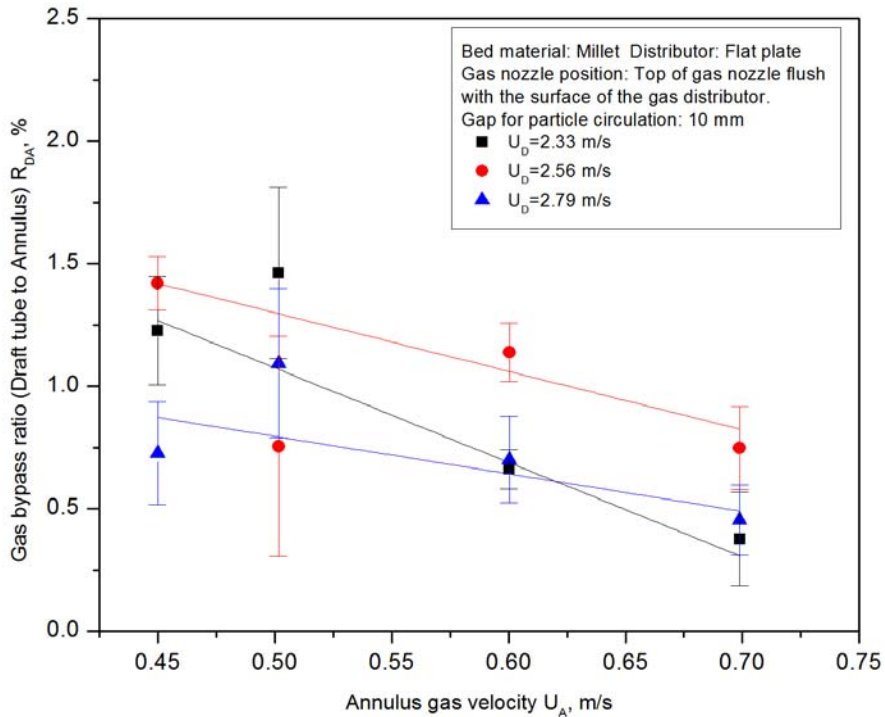
For the second distributor configuration with the top of the gas nozzle flushed with the bottom of the draft tube while keeping $H_{G1}=10$ mm (see Figure 4.4(b)), it is seen from Figure 4.6(a) that the gas bypass ratio from the annulus to the draft tube was 10% more than that in Figure 4.5(a) at given U_A and U_D . On the other hand, R_{DA} was further reduced to lower than 0.3%. This can be explained by the fact that the configuration of the distributor used in Figure 4.6 allows gas from the nozzle to directly flow into the draft tube with less chance to escape into the annulus region. Furthermore, this configuration increased the pressure drop around the inlet of the draft tube, and thus more annulus gas was sucked into the draft tube from the annulus region.

It was observed that, because of the high gas bypass from the annulus to the draft tube in both cases, insufficient gas was supplied to the annulus. As a result, particles could not be stably circulated if the annulus gas velocity was lower than 0.45 m/s.

Error bars plotted in Figure 4.5 were obtained from 6 repeated runs based on a 95% confidence interval. The possible source of errors came from the readings of the rotameters and the measured CO₂ concentrations, as well as the reproducibility of the operating conditions. Errors ranged from 1.61% to 4.52%, with an average around 3.35% for calculated gas bypass ratios from the annulus to the draft tube, and from 0.08% to 0.69%, with an average around 0.49% for calculated gas bypass ratios from the draft tube to the annulus.

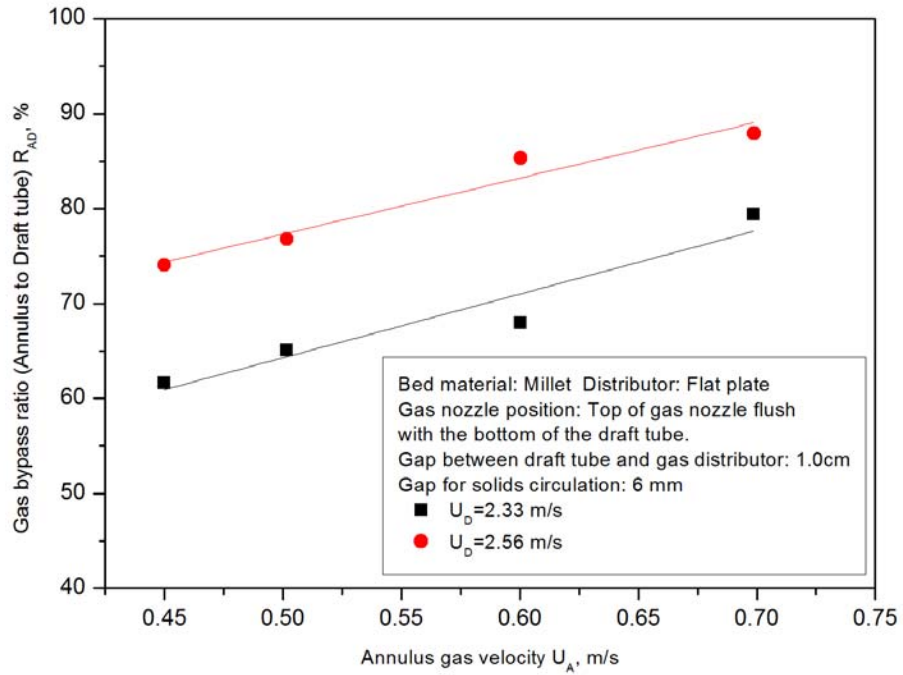


(a) Annulus to draft tube

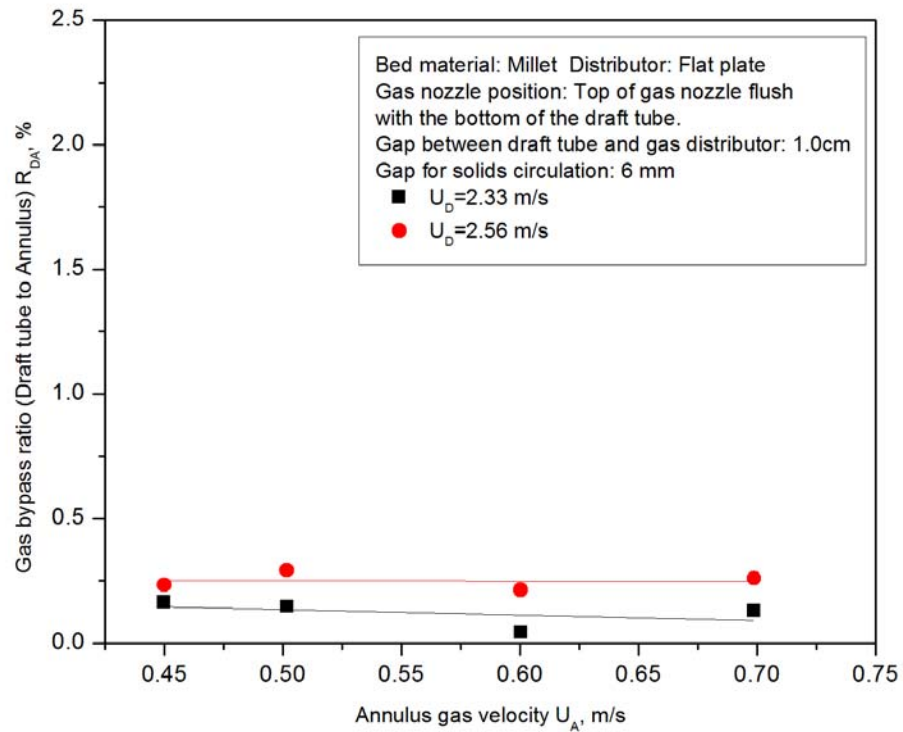


(b) Draft tube to annulus

Figure 4.5 Effect of gas velocities on gas bypass (Flat distributor, $H_G=10$ mm)



(a) Annulus to draft tube



(b) Draft tube to annulus

Figure 4.6 Effect of gas velocities on gas bypass (Flat distributor, $H_G = 6$ mm)

4.2.2 Solids circulation rate

The influence of gas velocities on the solids circulation rate (W_s) is shown in Figures 4.7 and 4.8 for distributor configurations with $H_G=10$ mm and 6 mm, respectively. In both cases, W_s increased with increasing annulus gas velocity (U_A) at a given U_D . Meanwhile, the same tendency was observed for the influence of U_D at a given U_A . However, U_A clearly showed more influence on W_s than U_D . At given U_A and U_D , although the gas bypass from the annulus to the draft tube (R_{AD}) was higher at $H_G=6$ mm than $H_G=10$ mm, W_s at $H_G=10$ mm (Figure 4.7) was always higher than at $H_G=6$ mm in Figure 4.8. In addition, the influence of U_A and U_D on W_s in Figure 4.7 where $H_G=10$ mm was more significant than $H_G=6$ mm shown in Figure 4.8. This is because the small effective gap opening (H_G) obstructed the solids circulation, while the increase in gas bypassing was counteracted by the smaller H_G in the second configuration.

Error bars plotted in Figure 4.7 were based on 4 repeated runs for each point with 90% confidence interval. The possible source of errors came from the readings and the timing of the traveling distance of the coloured particles, the change of bed voidage and the reproducibility of the experimental conditions. Errors for calculated solids circulation rates ranged from 0.79 to 8.05 kg/m².s, with an average around 4.55 kg/m².s.

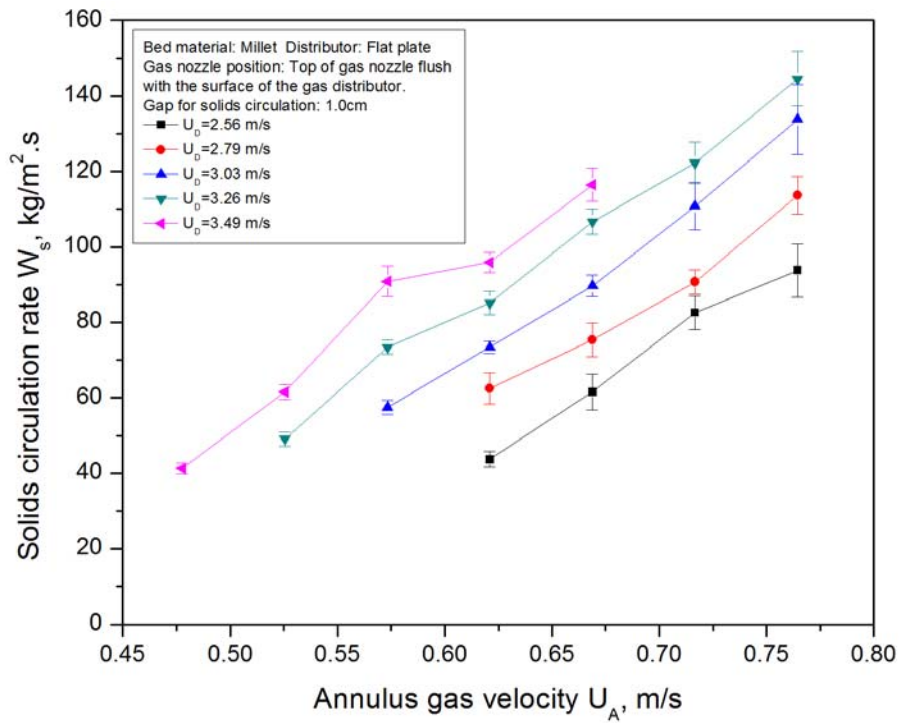


Figure 4.7 Effect of gas velocities on solids circulation rate (Flat distributor, $H_G=10$ mm)

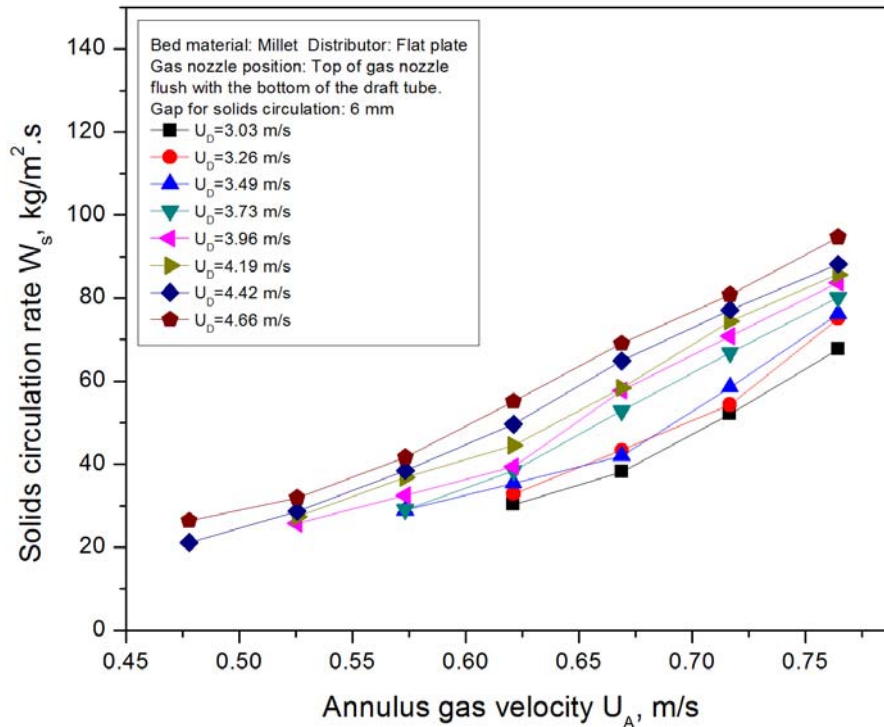


Figure 4.8 Effect of gas velocities on solids circulation rate (Flat distributor, $H_G=6$ mm)

4.3 Performance with the cylindrical distributor plate

The flat distributor plate showed very high gas bypassing from the annulus to the draft tube which is undesirable for the dual zone reactor if the annulus is operated as the adsorption zone for the HC-SCR of NO_x . To decrease gas bypassing from the annulus to the draft tube, another type of gas distributor for the annulus, namely cylindrical distributor plate, was designed and built, as shown in Figure 4.9. The draft tube was also changed to a size of 38.1 mm I.D. with the wall thickness of 3.2 mm in order to keep the same opening ratio of the distributor (2.1%). In the experiment, the top of the gas nozzle was always flush with the bottom of the cylindrical distributor, and three configurations were tested in the experiment, with the distance (H_{G1}) between the bottom of the draft tube and the top of the gas nozzle set at 10, 20 and 60 mm, respectively. Note that, for $H_{G1}=10$ mm and 20 mm, as shown in Figure 4.9(a), the effective gap openings were the same, i.e., the gap between the outer surface of the draft tube and the inner surface of the cylinder ($H_{G2}=9.5$ mm). For $H_{G1}=60$ mm, since the bottom of the draft tube was 9 mm higher than the surface of the annulus gas distributor, the effective gap opening was thus changed to $H_{G2}=13$ mm (see Figure 4.9(b)).

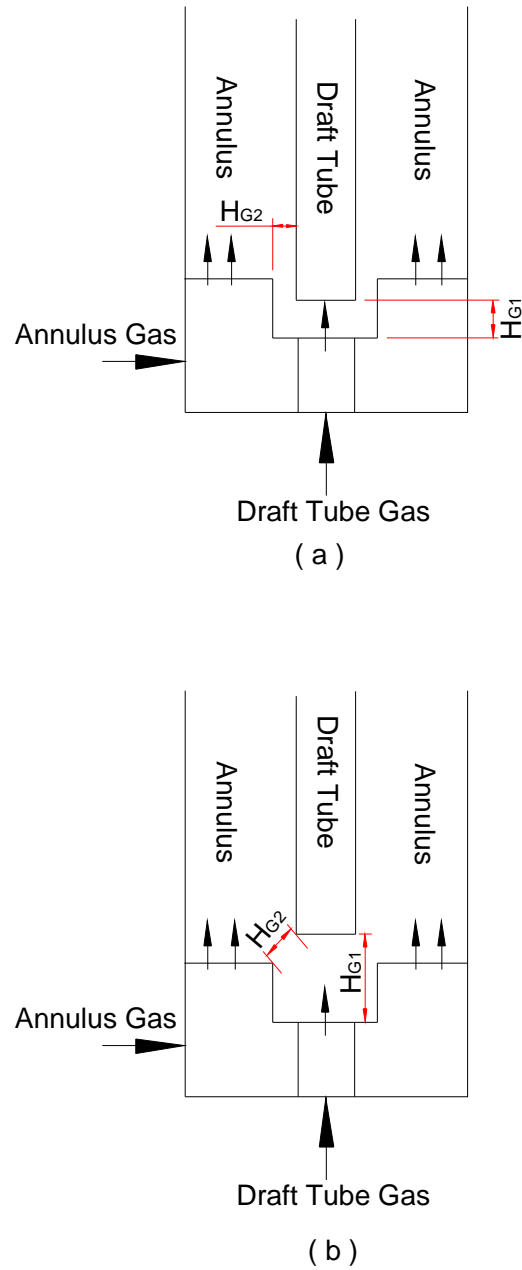


Figure 4.9 Configurations of the cylindrical distributor for the annulus gas flow

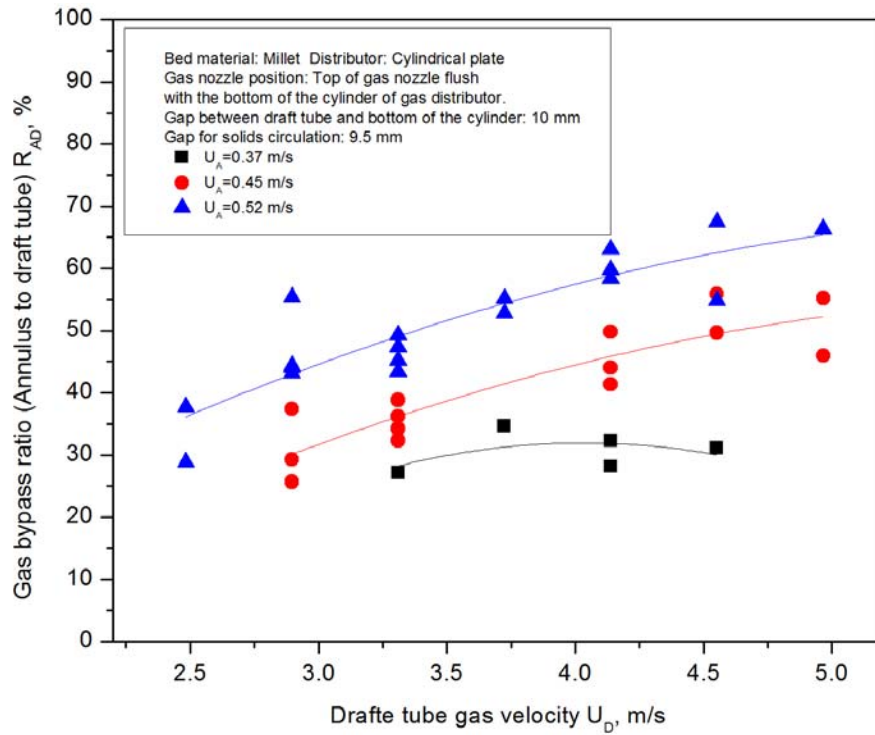
4.3.1 Gas bypass

Gas bypass ratios at $H_{G1}=10$ mm are shown in Figure 4.10. When the annulus gas velocity was low ($U_A=0.37$ m/s), the draft tube gas velocity (U_D) showed less influence on the gas bypass ratio from the annulus to the draft tube (R_{AD}) (Figure 4.10(a)). However, the increase

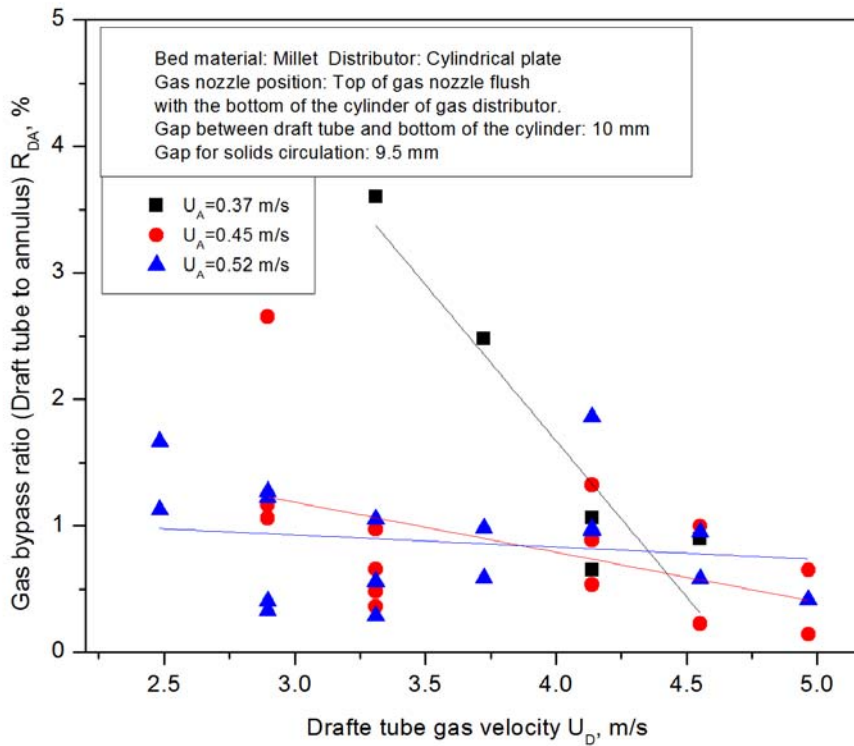
of U_D decreased the gas bypass from the draft tube to the annulus (R_{DA}) effectively at $U_A=0.37$ m/s (Figure 4.10(b)). Further increase of U_A to 0.45 m/s resulted in an increase of R_{AD} by 5%~15%, while R_{DA} dropped to lower than 1.5% in most cases for the U_D range of 3.31 to 4.55 m/s. R_{AD} increased by another 15% with R_{DA} remaining at around 1% when U_A increased from 0.45 to 0.52 m/s.

Although R_{AD} increased with the increase of both U_A (>0.37 m/s) and U_D , when compared with the flat distributor (Figure 4.5(a)), R_{AD} for the flat distributor was always 20~30% higher than for the cylindrical distributor at given U_A and U_D . The change of the annulus distributor showed no significant influence on R_{DA} , which always remained at a very low level in both cases. It is not surprising to see the significant decrease of R_{AD} in Figure 4.10(a) in comparison to Figure 4.5(a) in view of the fact that the use of a smaller size draft tube for the cylindrical distributor led to an increase of the annulus cross-sectional area from 4940 to 6556 mm², and a corresponding decrease of the draft tube cross-sectional area from 2027 to 1140 mm².

When H_{G1} was set to 20 mm, the influence of gas velocities on gas bypass is shown in Figure 4.11. R_{AD} was also observed to increase with the increase in both U_A and U_D , although the influence of U_D was not as significant as U_A . It appears that the increase of H_{G1} from 10 to 20 mm had no effect on the gas bypass from both directions, which could be attributed to the fact that the effective gap opening remained the same for both cases. R_{DA} remained lower than 2.5% within the range of gas velocities tested.

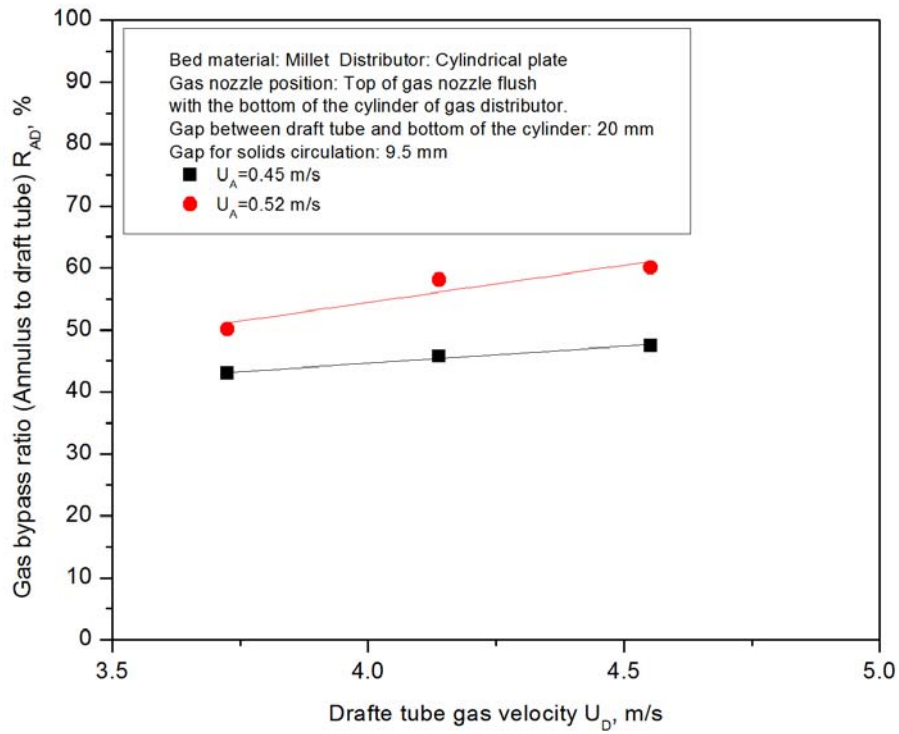


(a) Annulus to draft tube

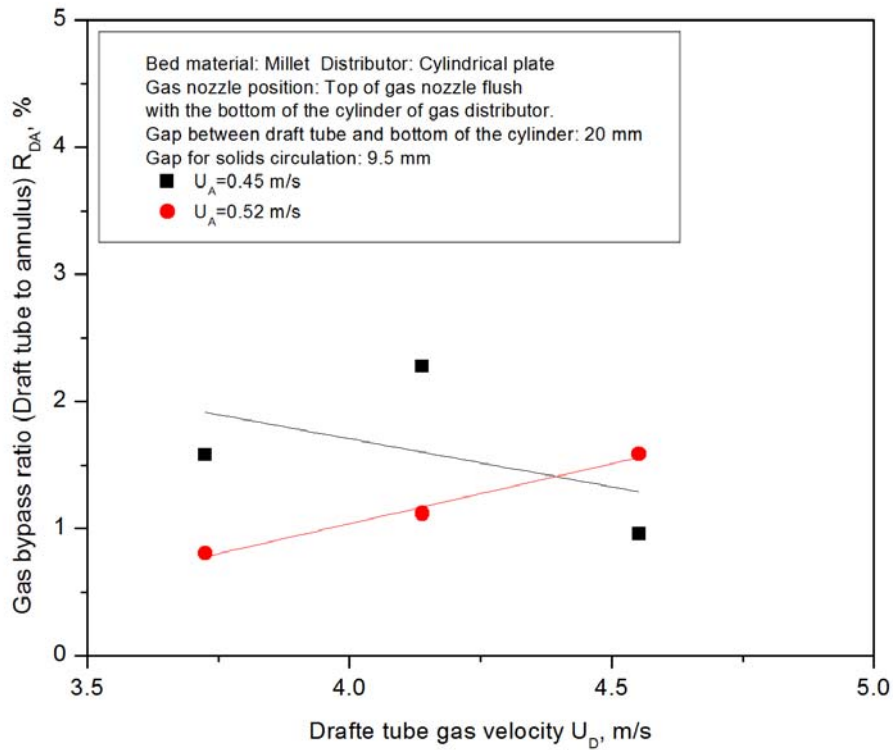


(b) Draft tube to annulus

Figure 4.10 Effect of gas velocities on gas bypass (Cylindrical distributor, $H_{G1}=10$ mm)



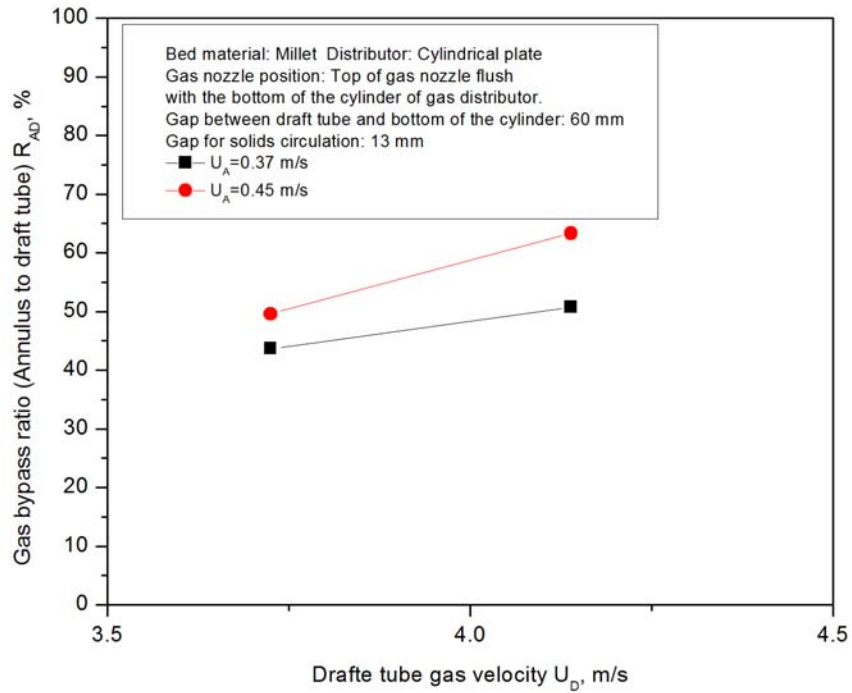
(a) Annulus to draft tube



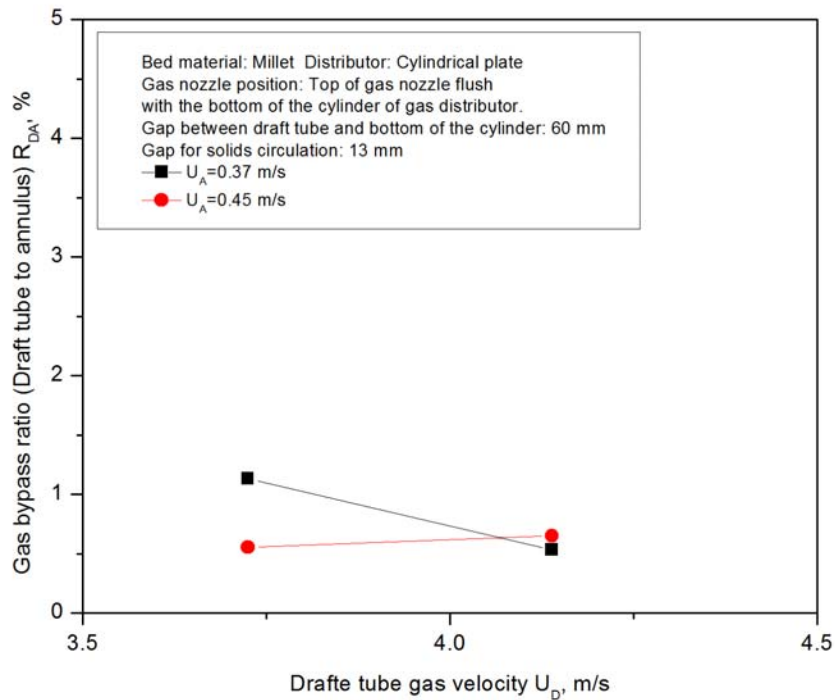
(b) Draft tube to annulus

Figure 4.11 Effect of gas velocities on gas bypass (Cylindrical distributor, $H_{G1} = 20$ mm)

The increase in both U_D and U_A increased R_{AD} when the draft tube was lifted further to $H_{G1} = 60$ mm, as shown in Figure 4.12. At $U_A = 0.45$ m/s, R_{AD} was even higher than that at $U_A = 0.52$ m/s in Figure 4.11, but still much lower than that in Figure 4.5 where the flat distributor was used. This indicates that the increase of the effective gap opening enhanced gas bypassing from the annulus to the draft tube, but had no significant effect on gas bypassing from the draft tube to the annulus for this type of distributor.



(a) Annulus to draft tube



(b) Draft tube to annulus

Figure 4.12 Effect of gas velocities on gas bypass (Cylindrical distributor, $H_{G1}=60$ mm)

4.3.2 Solids circulation rate

Solids circulation rates (W_s) for the cylindrical distributor with $H_{G1}=10$ mm are shown in Figure 4.13. For a given U_A , W_s increased with the increase of U_D . For a given U_D , lower W_s was observed at $U_A=0.37$ m/s. Further increase of U_A beyond 0.45 m/s showed less influence on W_s indicating that W_s was mainly affected by U_D . This trend is different from the flat distributor with $H_G=10$ mm where W_s was more sensitive to U_A than to U_D (see Figure 4.7).

Moreover, the cylindrical distributor exhibited much higher W_s than the flat one. For example, at $U_A=0.52$ m/s and $U_D=3.26$ m/s, W_s was 105 kg/m².s and 49 kg/m².s for the cylindrical and the flat distributor, respectively.

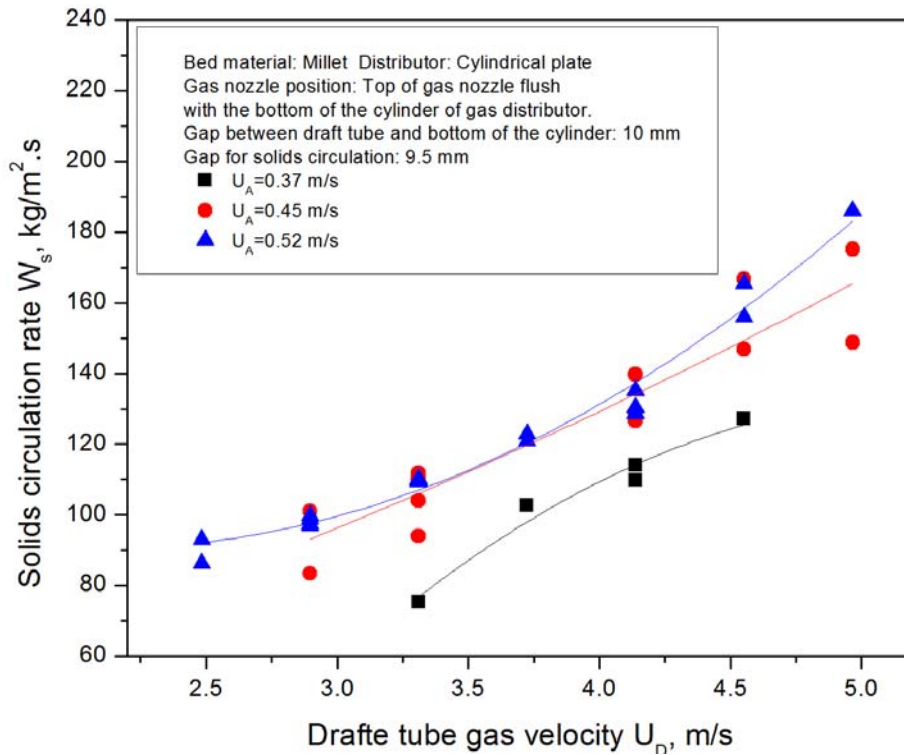


Figure 4.13 Effect of gas velocities on solids circulation rate (Cylindrical distributor, $H_{G1}=10$ mm)

With the gap between the bottom of the draft tube and the top of the gas nozzle increased from 10 to 20 mm, both U_A and U_D showed minor effect on W_s at $U_A \geq 0.45$ m/s and

$U_D \geq 3.72$ m/s, although the trend that W_s increased with the increase of both U_A and U_D was still observed. The change of H_{G1} from 10 to 20 mm showed no influence on W_s , which could be explained by the fact that the effective gap opening remained the same for both cases.

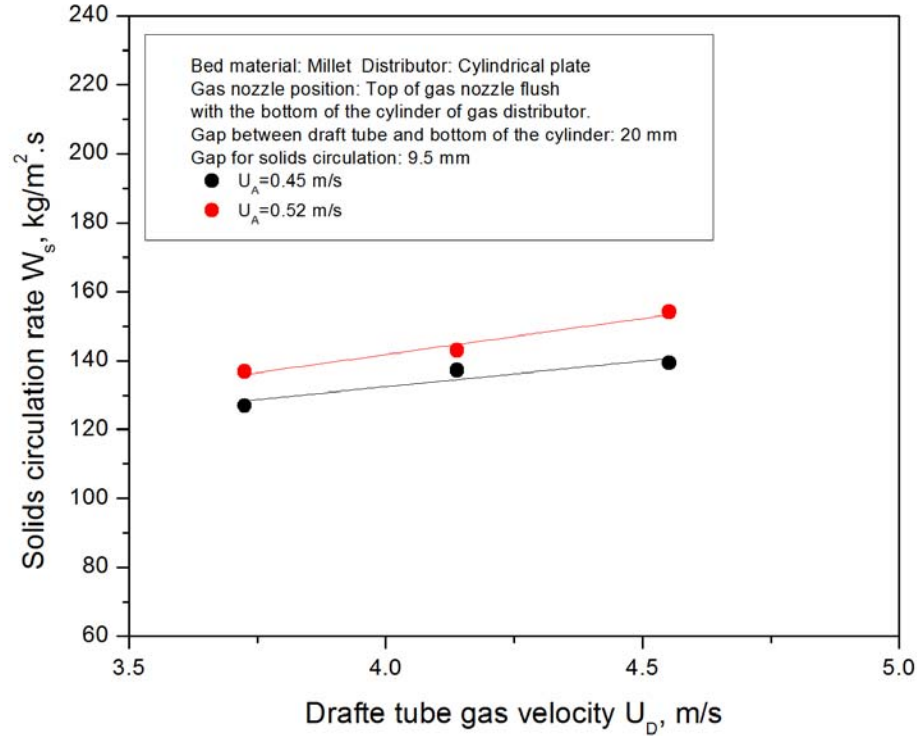


Figure 4.14 Effect of gas velocities on solids circulation rate (Cylindrical distributor, $H_{G1}=20$ mm)

As shown in Figure 4.15, U_A dominated the change of W_s while U_D showed less effect when the draft tube was lifted to $H_{G1}=60$ mm, which is different from $H_{G1}=10$ and 20 mm but consistent with the trend from the flat distributor experiment. Considering that the bottom of the draft tube was 9 mm higher than the surface of the annulus gas distributor, which was almost identical to that for the flat distributor (Figure 4.5), it is not surprising that the same trend was observed. The higher W_s for the cylindrical distributor is associated with its bigger gap opening ($H_{G2}=13$ mm).

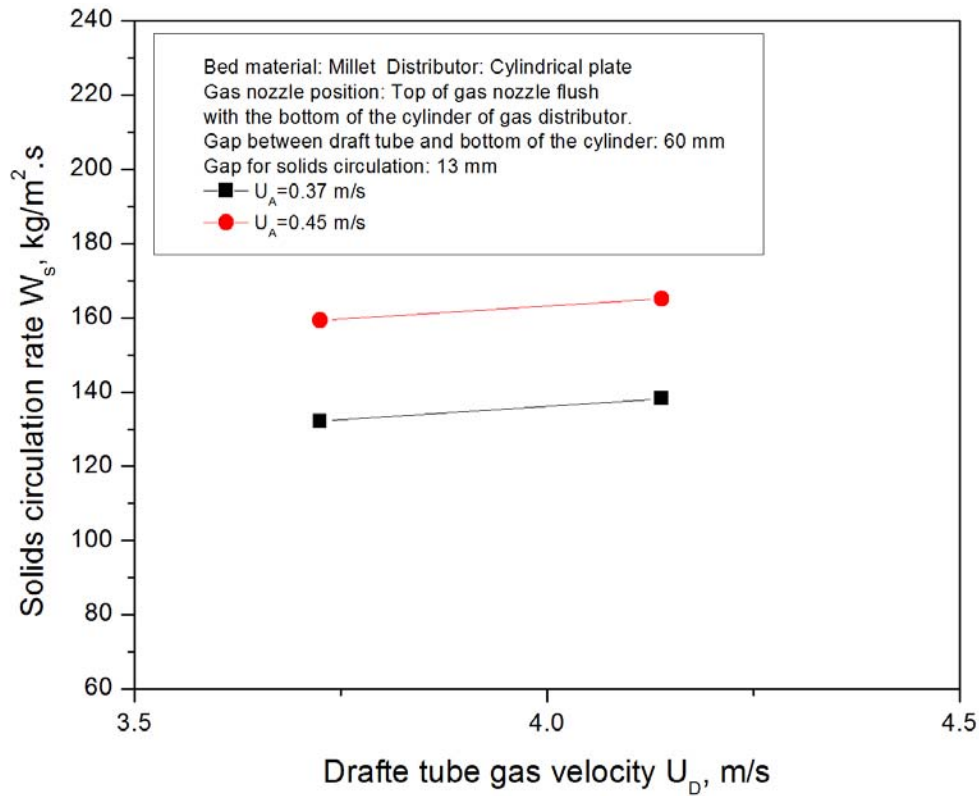


Figure 4.15 Effect of gas velocities on solids circulation rate (Cylindrical distributor, $H_{G1}=60\text{mm}$)

The cylindrical distributor exhibited lower gas bypassing from the annulus to the draft tube and relatively higher solids circulation rate than the flat distributor, at given U_A and U_D . However, as observed in the experiment, constrained by the shape of the distributor, the particles could not be circulated at low draft tube gas velocities, which limited the possible operation window of the gas flow rate.

4.4 Performance with the conical distributor plate

As one of the most commonly used gas distributors for ICFB reactors, the conical distributor was also tested in this study. The perforated holes on the distributor were aligned in perpendicular to the surface of the distributor and the effective gap opening for the solids

circulation was defined as H_G , as shown in Figure 4.16. In the experiment, two configurations with $H_G=10$ and 15 mm were investigated, separately, with the top of the gas nozzle always flush with the bottom of the conical plate.

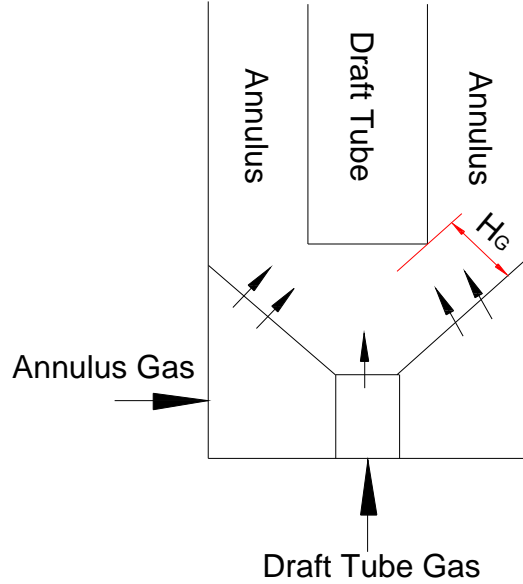
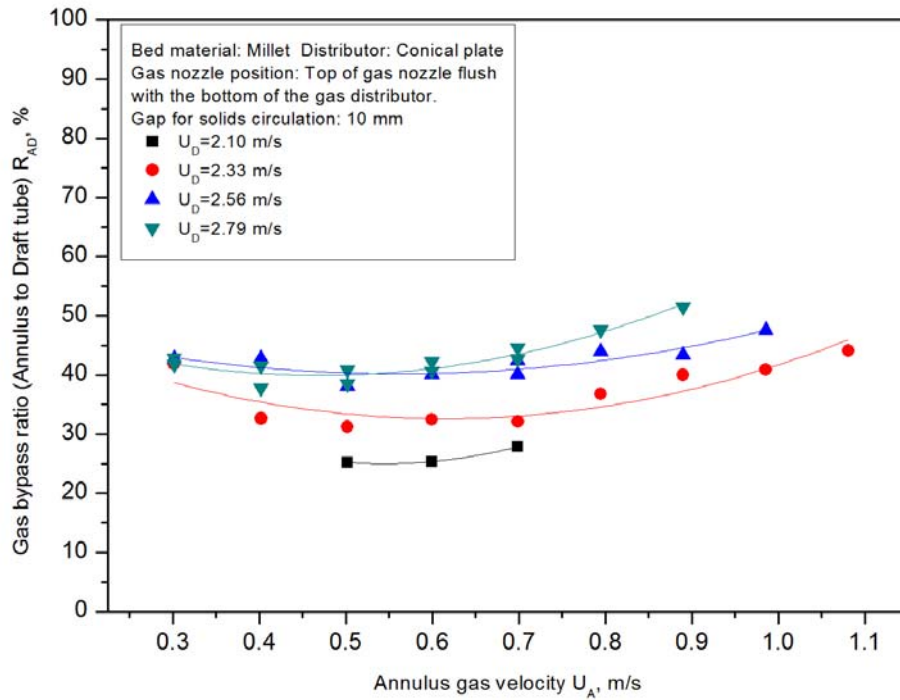


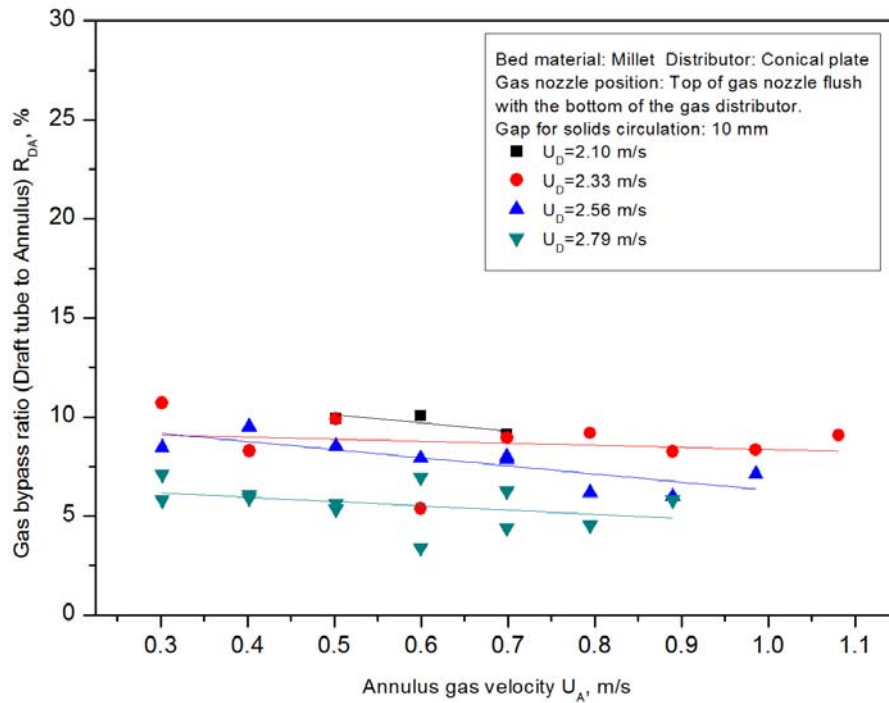
Figure 4.16 Configuration of the conical distributor for the annulus gas flow

4.4.1 Gas bypass

As seen in Figure 4.17(a), the increase of U_D increased the gas bypass ratio from the annulus to the draft tube, but not as significantly as the flat and cylindrical distributors. For a given U_D , U_A showed less influence on R_{AD} , with R_{AD} ranging from 20 to 50% over the tested range of gas velocities. Relatively high values of R_{DA} were observed using the conical distributor, ranging from 5~10%, as shown in Figure 4.17(b). R_{DA} remained almost constant with the variation of U_A at a given U_D , but decreased with increasing U_D at a given U_A .



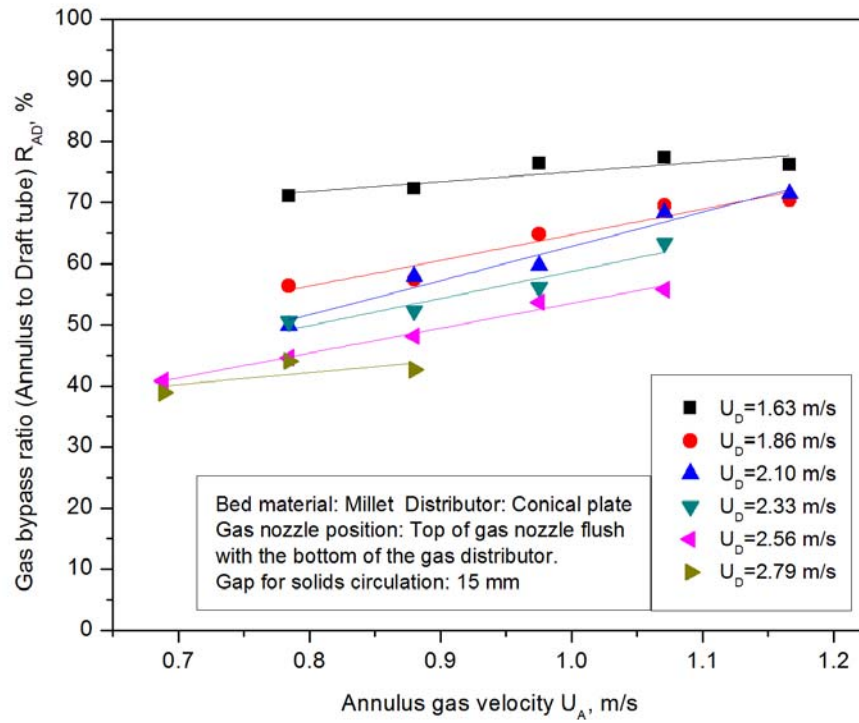
(a) Annulus to draft tube



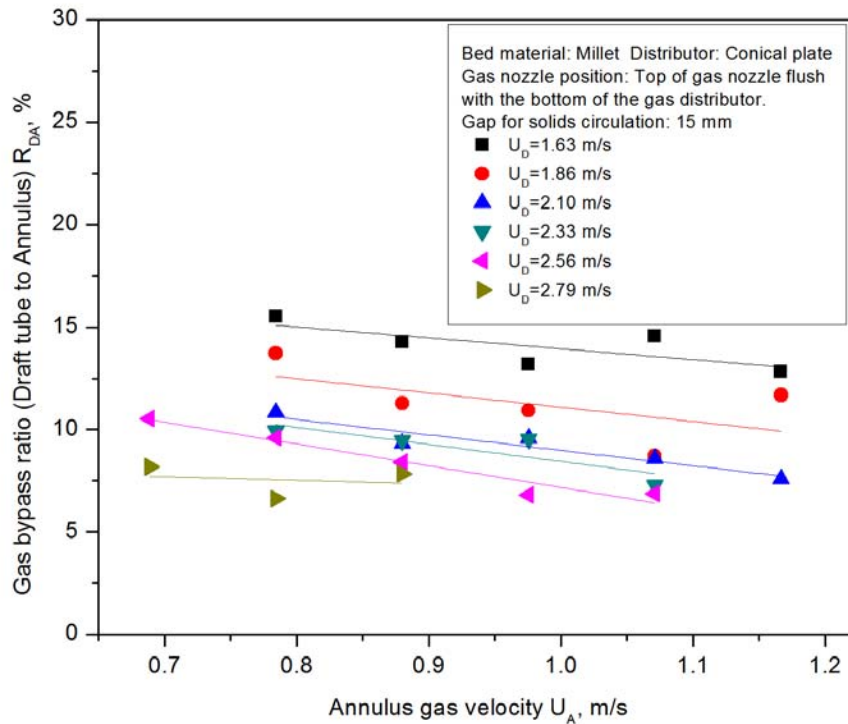
(b) Draft tube to annulus

Figure 4.17 Effect of gas velocities on gas bypass (Conical distributor, $H_G=10$ mm)

When the effective gap opening for the solids circulation was set to 15 mm, rather than 10 mm, the increase in U_A enhanced gas bypass from the annulus to the draft tube, as shown in Figure 4.18(a). The influence of U_D on the gas bypass showed a trend opposite to $H_G=1.0$ cm. At $U_D=1.63$ m/s, R_{AD} was very high at 70%~75%. As U_D increased to 2.79 m/s, R_{AD} dropped to around 40%. This indicates that the gas bypass from the annulus to the draft tube was reduced with the increase in U_D . According to the configuration of the conical plate, at $H_G=10$ mm, all perforated holes were blocked by the outer surface of the draft tube and the annulus gas could not flow directly into the draft tube but was forced into the annulus region, and the gas could only be dragged from the annulus to the draft tube by the circulating particles. As a result, U_D dominated R_{AD} . At $H_G=15$ mm, over 50% of the perforated holes on the conical plate were directly exposed to the inlet of the draft tube. Therefore, the gas flow through these annulus distributor holes could partially flow upward into the draft tube, and thus enhanced gas bypassing from the annulus to the draft tube. With the increase of U_D , the increased gas flow to the draft tube pushed part of the annulus gas back to the annulus area and thus decreased R_{AD} . As a result of the coupling impact from both U_A and U_D , R_{DA} increased by around 5% compared to that at $H_G=10$ mm, as shown in Figure 4.18(b).



(a) Annulus to draft tube



(b) Draft tube to annulus

Figure 4.18 Effect of gas velocities on gas bypass (Conical distributor, $H_G=15$ mm)

4.4.2 Solids circulation rate

For $H_G=10$ mm, W_s increased with increasing the annulus gas velocity (U_A) at a given draft tube gas velocity (U_D), as shown in Figure 4.19. When U_A reached a certain level, i.e. >0.90 m/s, further increase in U_A had only little influence on W_s . Meanwhile, the same tendency was observed for the influence of U_D at a given U_A . However, the increase of U_A clearly showed more influence on W_s than that of U_D .

For $H_G=15$ mm, as shown in Figure 4.20, a similar trend was observed except with a relatively higher W_s than that in Figure 4.19 at given U_A and U_D . Moreover, both U_A and U_D exhibited significant influence on W_s .

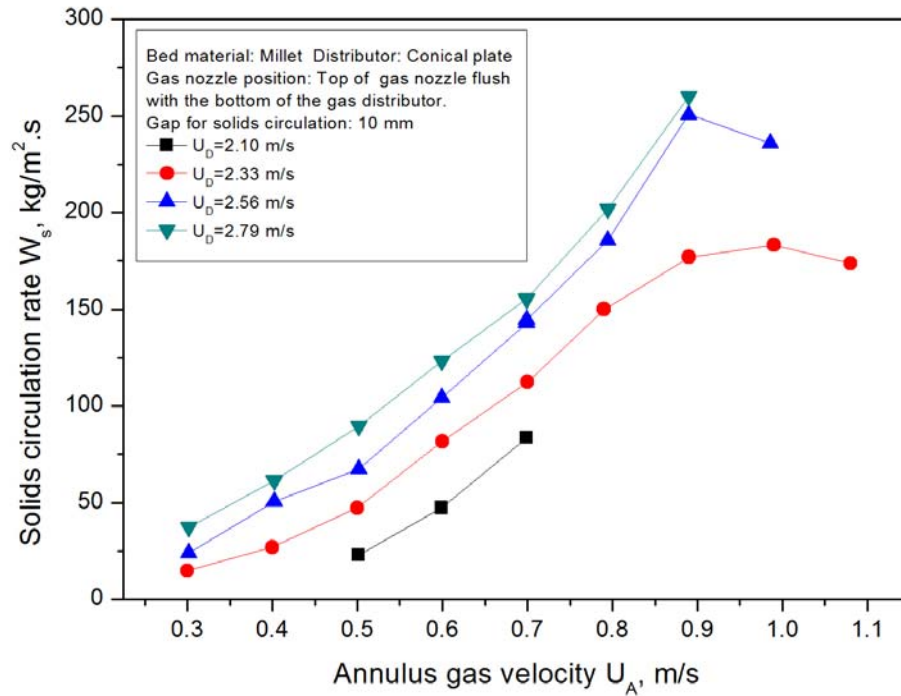


Figure 4.19 Effect of gas velocities on solids circulation rate (Conical distributor, $H_G=10$ mm)

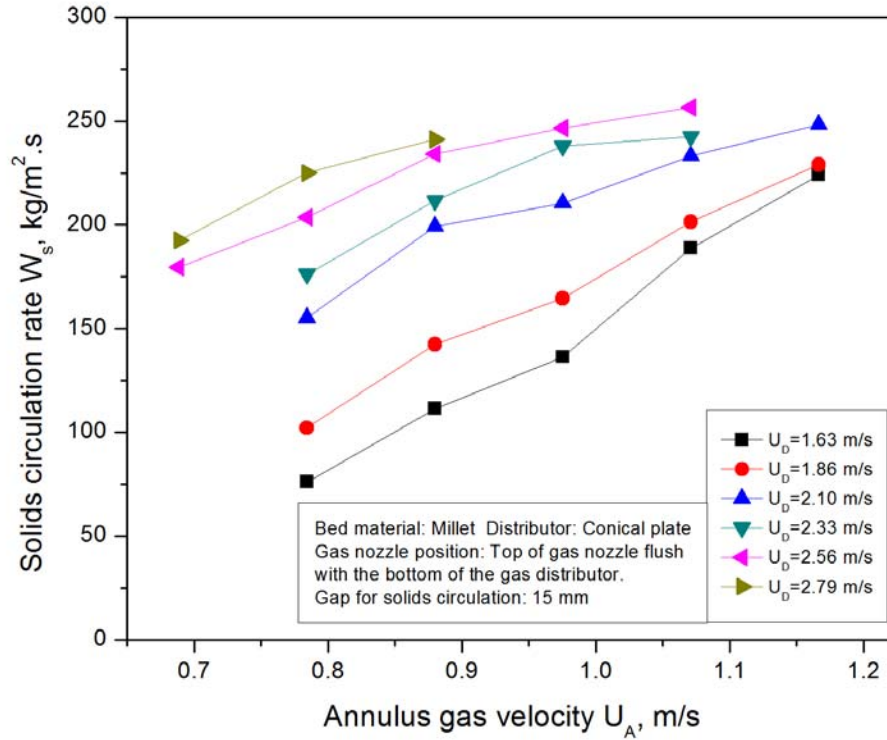


Figure 4.20 Effect of gas velocities on solids circulation rate (Conical distributor, $H_G=15$ mm)

Since the solids circulation rate was mainly influenced by both U_A and U_D for a given configuration of the conical plate, and there existed uncertainties on the actual gas velocities inside the draft tube and the annulus because of the gas bypass between the annulus and the draft tube, an overall gas velocity is introduced here to evaluate its impact on W_s .

The overall gas velocity U is defined as the total gas flow rate divided by the total cross-sectional area of the draft tube and the annulus

$$U = \frac{F_{A,0} + F_{D,0}}{S_A + S_D} \quad (4.13)$$

where $F_{A,0}$ and $F_{D,0}$ are gas flow rates at the inlet of the annulus and the draft tube, and S_A and S_D are the cross-sectional areas of the annulus and the draft tube, respectively.

As shown in Figure 4.21, for $H_G=10$ mm, W_s increased with the increase of U , and could be well fitted by a 2nd order polynomial equation with most of the data points falling into an error range of $\pm 20\%$.

According to the fixed bed experimental data for Fe/ZSM-5(PUC) catalyst, to keep a stable NO_x conversion for a long term operation in the hot model ICFB reactor, the reaction temperature must be remained at 350°C or higher and the gas space velocity in the reduction zone should be lower than 5000h^{-1} (Std. T, i.e., 25°C). Based on the results from the cold model unit which has the same configuration as the hot model ICFB reactor, the gas velocity in the draft tube (U_D) must be lower than 1.41 m/s (Std. T) if the draft tube is to be used as the reduction zone.

If U_D is set to 1.0 m/s and $U_A=0.4$ m/s (Std. T) which are equivalent to $U_D=2.09$ m/s and $U_A=0.84$ m/s at $T=350^\circ\text{C}$ in the hot model ICFB reactor, the particle circulation rate will be around 50 $\text{kg/m}^2\cdot\text{s}$ based on the annulus cross-sectional area, according to the cold model experimental result shown in Figure 4.21.

For a model flue gas containing 600 ppm (0.75 g/m^3) NO at a gas velocity of $U_A=0.4$ m/s (Std. T), the amount of NO input to the annulus will be 0.3 $\text{g/m}^2\cdot\text{s}$, while the adsorption capacity (i.e., the amount of NO at the equilibrium adsorption) of the catalyst at 350°C will be 1.34 $\text{g/m}^2\cdot\text{s}$ according to the adsorption performance data for Fe/ZSM-5(PUC) catalyst in the fixed bed reactor, which is higher than the amount of input NO . This means that the input NO in the annulus region of the ICFB reactor could be completely adsorbed by the catalyst.

For $H_G=15$ mm, in Figure 4.22, although the shape of the fitted curve switched from minor concave to convex style in comparison with Figure 4.21, the data can also be well correlated by the overall gas velocity, with an error range of $\pm 10\%$.

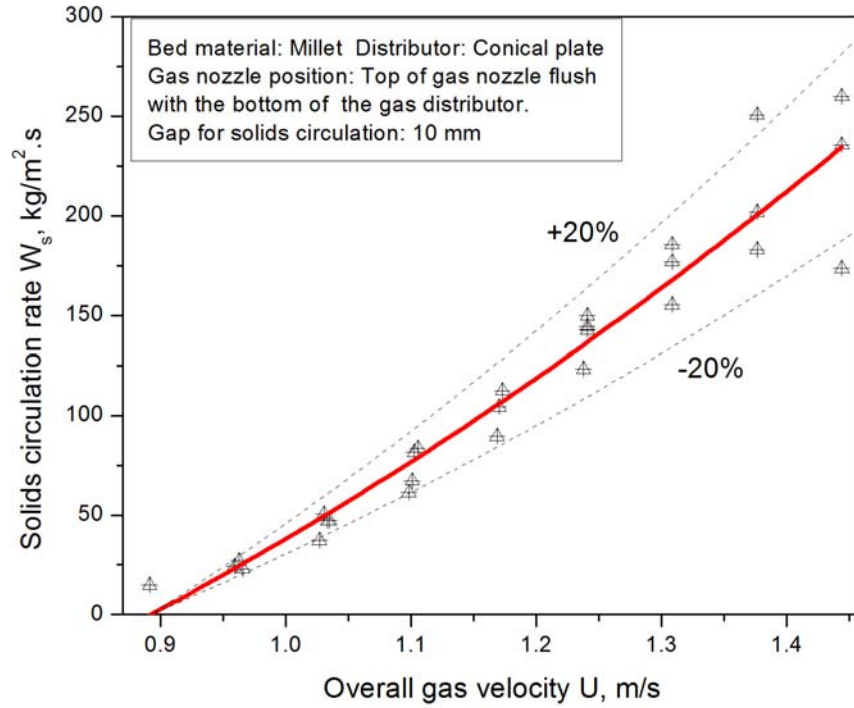


Figure 4.21 Effect of overall gas velocity on solids circulation rate using conical distributor ($H_G=10$ mm)

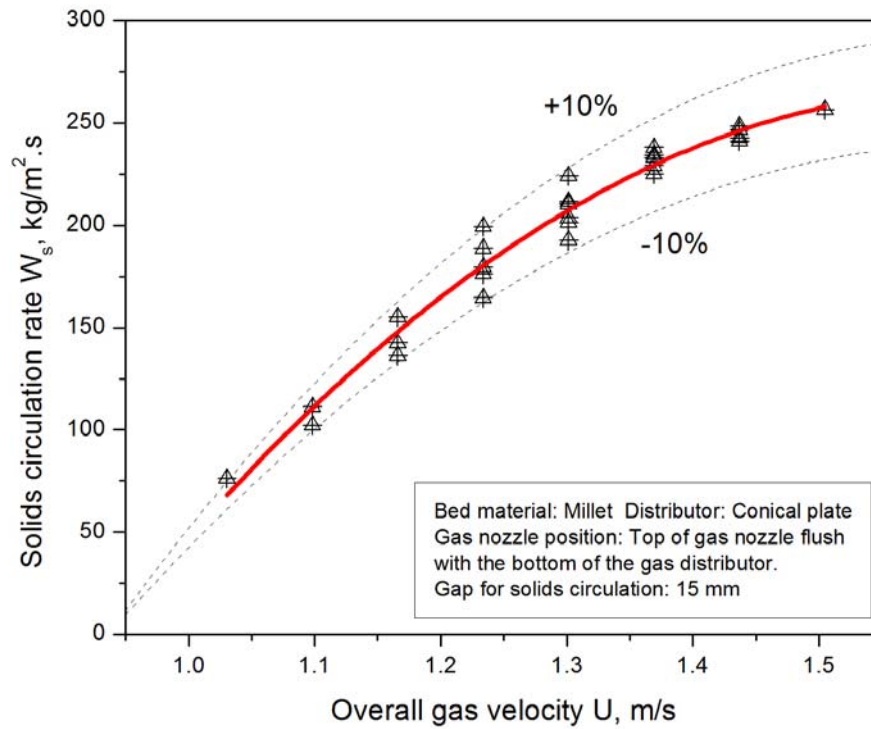


Figure 4.22 Effect of overall gas velocity on solids circulation rate using conical distributor ($H_G=15$ mm)

The same effect of the overall gas velocity on the solids circulation rate was also observed for the ICFB with a cylindrical distributor plate which is not shown here. However, for the flat distributor, the data showed a great scattering with poor correlation between U and W_s .

4.5 Gas bypassing in the hot model ICFB reactor

In the cold model experiment, the conical distributor plate exhibited high solids circulation rate, high gas bypass from the draft tube to the annulus and relatively low gas bypassing from the annulus to the draft tube compared to the flat and cylindrical distributor plates. Moreover, the conical distributor plate showed flexible and stable operation within wide ranges of gas velocities for both U_A and U_D . As a result, the conical distributor plate was selected as the annulus gas distributor for the hot model ICFB reactor. To further reduce gas bypassing from the annulus to the draft tube, the perforated holes were aligned in parallel to the draft tube or the column wall in the hot model unit, as shown in Figure 4.23.

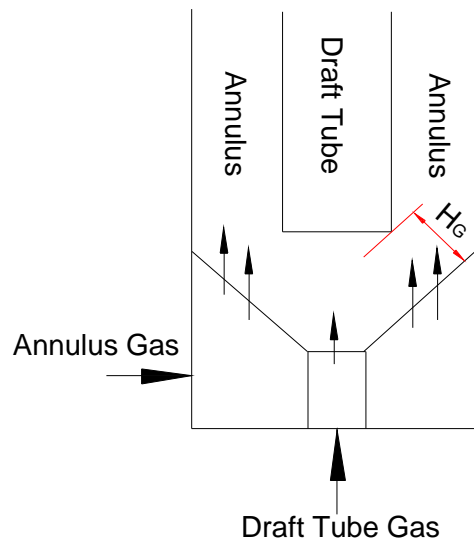


Figure 4.23 Configuration of the conical distributor in the hot model ICFB reactor

In the hot model experiments, gas bypassing was studied using O₂ as the tracer gas. Using the same method shown in Figure 4.3 and equations 4.1 to 4.10, R_{AD} and R_{DA} could be evaluated based on O₂ balance instead of CO₂ balance for the hot model test.

Two kinds of catalysts were investigated in the hot model experiment, Fe/ZSM-5(PUC) with an average particle diameter of 1042 μm and Fe/ZSM-5(Albemarle) with an average particle diameter of 155 μm. The effective gap opening (H_G) for the solids circulation was set to be 10 mm for all experiments.

4.5.1 Fe/ZSM-5(PUC) catalyst

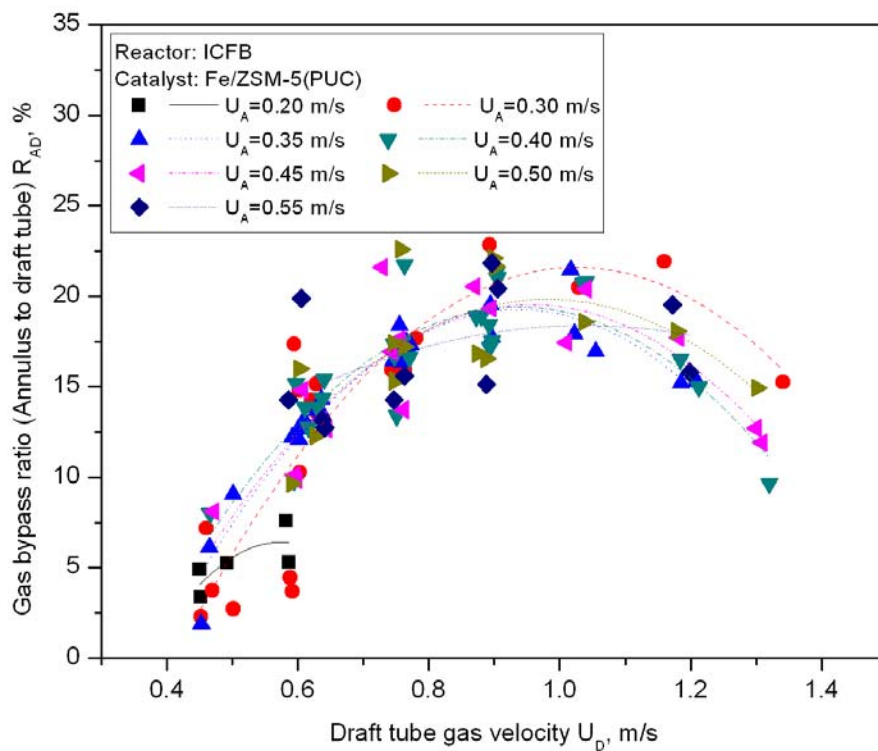
Effects of gas velocities on gas bypass for Fe/ZSM-5(PUC) in the hot model ICFB reactor are shown in Figure 4.24.

In the range of velocities investigated, the gas bypass from the draft tube to the annulus (R_{DA}) was always higher than that from the annulus to the draft tube (R_{AD}) for Fe/ZSM-5(PUC) catalyst at given U_A and U_D (see Figures H.1 to H.7 in Appendix H). For cases with U_A ≥ 0.3 m/s, with the increase of U_D from 0.45 to 1.30 m/s, R_{AD} increased from 3~7% to a peak value of 17~18% at U_D = 0.9~1.1 m/s, then decreased to 10~13% (Figure 4.24(a)) with further increase in U_D, while R_{DA} increased monotonically from 18% to 40% (Figure 4.24(b)) with the increase in U_D. For U_A = 0.20 m/s, as U_D increased from 0.45 to 0.59 m/s, R_{DA} increased from 11% to 14%, while R_{AD} increased from 4% to 6%. Compared to the effect of U_D, it seemed that U_A had less influence on both R_{AD} and R_{DA}. Furthermore, for a given U_D, there was no clear relationship between U_A and R_{AD} because of the scattering of data.

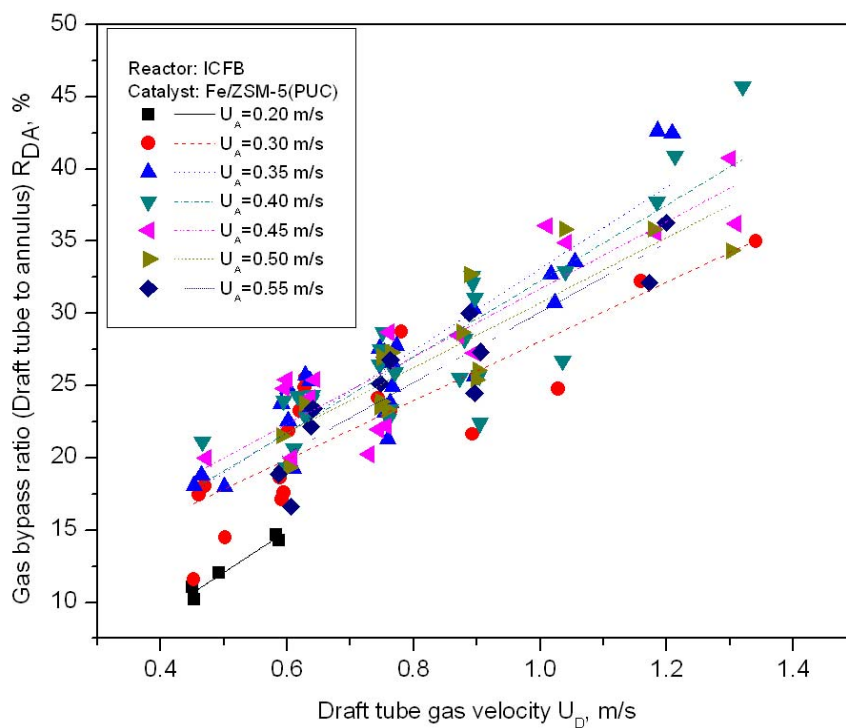
Based on those results, if the annulus is selected as the adsorption zone and the draft tube as the reduction zone, the gas bypass from the annulus to the draft tube could supply

sufficient O_2 to keep the O_2 concentration in the draft tube at a desired level. To minimize R_{DA} but also achieve a reasonably high solids circulation rate, U_D should be controlled to be in the range of 0.45~0.6m/s.

In conclusion, the change of the opening direction of perforated holes on the annulus gas distributor has been demonstrated to be successful in reducing the gas bypass from the annulus to the draft tube. At the same time, R_{DA} was enhanced, which is beneficial for the SCR of NO_x in the adsorption zone.



(a) Annulus to draft tube



(b) Draft tube to annulus

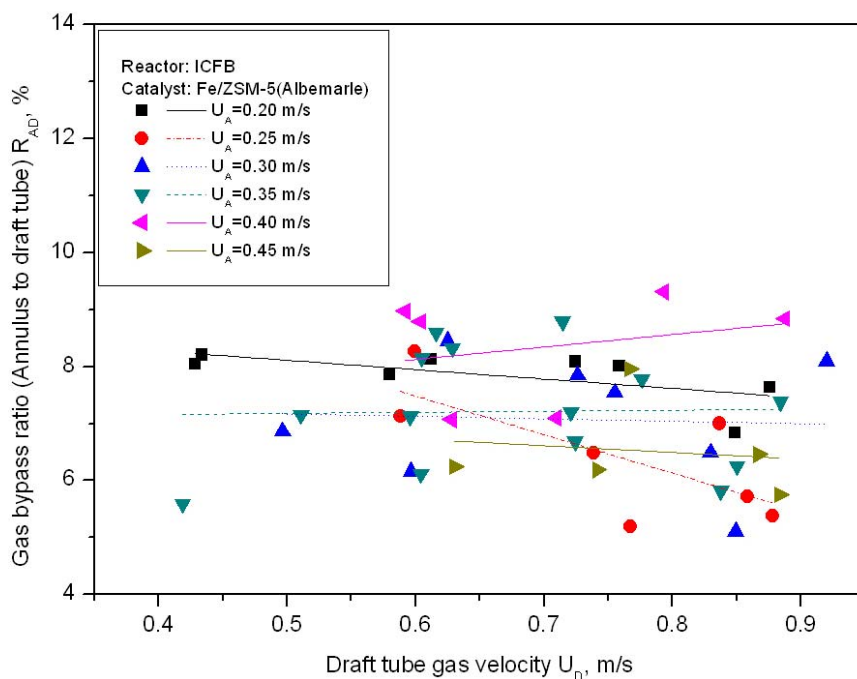
Figure 4.24 Effect of gas velocities on gas bypass (Fe/ZSM-5(PUC), $T=350\pm 10^\circ\text{C}$)

4.5.2 Fe/ZSM-5(Albemarle) catalyst

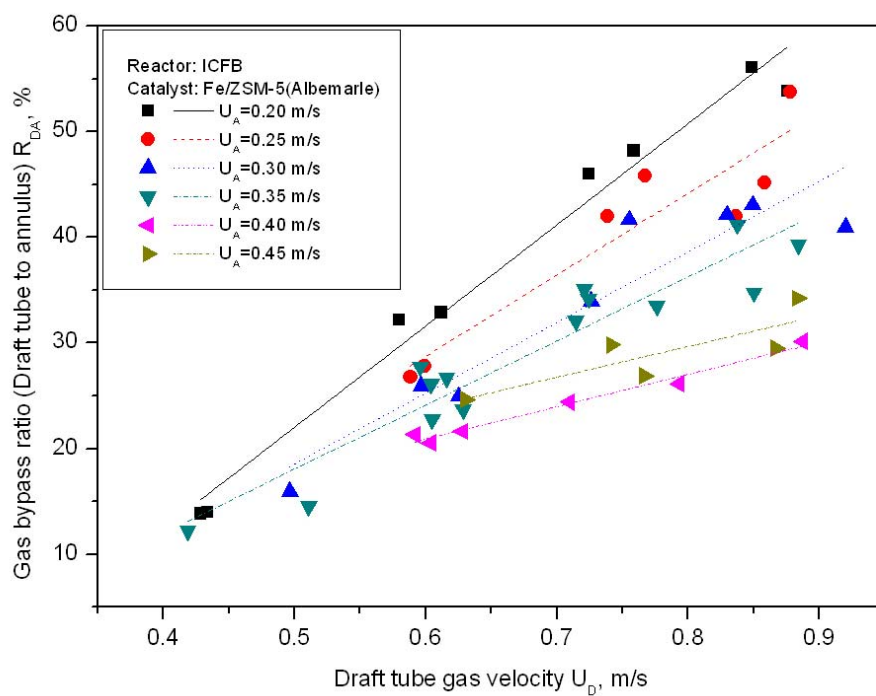
Effects of gas velocities on gas bypass using Fe/ZSM-5(Albemarle) catalyst are shown in Figure 4.25.

Unlike Fe/ZSM-5(PUC), the change of both U_A and U_D had almost no effect on the gas bypass from the annulus to the draft tube (R_{AD}), which fluctuated in the range of 5~9% as shown in Figure 4.25(a) (see also Figures H.9 to H.19 in Appendix H). This feature could be useful for controlling the O_2 concentration to a desired constant level when the draft tube region is used as the reduction zone.

For all cases in Figure 4.25(b), with the increase of U_D at a given U_A , the gas bypass ratio from the draft tube to the annulus (R_{DA}) was higher than using Fe/ZSM-5(PUC), but following a similar trend. As U_A increased, R_{DA} decreased (Figure H.8 in Appendix H). At $U_D=0.45$ m/s, the decrease of R_{DA} was not significant, remaining at a level around 14% (see Figure H.16 in Appendix H). With U_D increased from 0.60 to 0.90 m/s, R_{DA} decreased quickly with the increase in U_A (see Figures H.17 to H.19 in Appendix H). In the gas velocity range of the current experiment, a higher U_A and a lower U_D are preferred in order to control R_{DA} to a relatively low level. The reactor would not work properly if $U_D < 0.40$ m/s and $U_A > 0.45$ m/s.



(a) Annulus to draft tube



(b) Draft tube to annulus

Figure 4.25 Effect of gas velocities on gas bypass (Fe/ZSM-5(Albemarle), $T=355\pm 15^\circ\text{C}$)

4.5.3 Prediction of O₂ concentration in the draft tube and annulus

For a given U_A and U_D , gas bypass ratios from the annulus to the draft tube (R_{AD}) and from the draft tube to the annulus (R_{DA}) can be obtained from Figures 4.24 and 4.25, and the volumetric gas bypass rates can then be calculated by

$$F_{AD} = U_D \times S_D \times R_{AD} \quad (4.13)$$

$$F_{DA} = U_A \times S_A \times R_{DA} \quad (4.14)$$

where

F_{AD} , volumetric gas bypass rate from annulus to draft tube, m³/s

F_{DA} , volumetric gas bypass rate from draft tube to annulus, m³/s

S_A , cross-sectional area of the annulus, m²

S_D , cross-sectional area of the draft tube, m²

If O₂ concentrations at inlets of both the annulus (C_{A0, O_2}) and the draft tube (C_{D0, O_2}) are measured, O₂ concentrations in the annulus and the draft tube can be predicted by:

$$C_{A, O_2} = \frac{(U_A \times S_A - F_{AD}) \times C_{A0, O_2} + F_{DA} \times C_{D0, O_2}}{U_A \times S_A - F_{AD} + F_{DA}} \quad (4.15)$$

$$C_{D, O_2} = \frac{(U_D \times S_D - F_{DA}) \times C_{D0, O_2} + F_{AD} \times C_{A0, O_2}}{U_D \times S_D - F_{DA} + F_{AD}} \quad (4.16)$$

where

C_{A, O_2} , O₂ concentration in the annulus, %

C_{D, O_2} , O₂ concentration in the draft tube, %

It should be noted that certain amount of O₂ in the flue gas could be adsorbed onto the catalyst surface and carried into the draft tube region. However, this part of O₂ was negligibly

small compared to the amount of O_2 bypassing in the bulk gas phase from the annulus to the draft tube, and thus was not considered in deriving eqs. (4.15) and (4.16).

For Fe/ZSM-5(PUC) catalyst, if the draft tube is used as the adsorption zone, i.e., $C_{A0,O_2}=0$, at $U_A=0.4$ m/s and $U_D=0.6$ m/s, with C_{D0,O_2} increasing from 4 to 8 and 12%, O_2 concentration in the annulus or reduction zone increases from 0.8 to 1.5 and 2.3%, respectively. However, if U_D increases to 1.2 m/s while U_A remaining at 0.4 m/s, the increase of C_{D0,O_2} from 4 to 8 and 12% leads to an increase of O_2 concentration in the annulus from 1.2 to 2.5 and 3.7%. On the other hand, if the annulus is selected as the adsorption zone, at $U_A=0.4$ m/s, with U_D in the range of 0.6 to 1.2 m/s and the flue gas O_2 concentration from 4 to 12%, O_2 concentration in the draft tube will vary from 0.7 to 2.2%, which is much lower than that with the draft tube serving as the adsorption zone. This result shows that, to treat flue gases with high O_2 concentrations in the ICFB with Fe/ZSM-5 (PUC) catalyst, the annulus should be selected as the adsorption zone in order to control O_2 to a relatively low level in the reduction zone.

For Fe/ZSM-5(Albemarle) catalyst, at a low U_D , both the annulus and the draft tube can be used as the adsorption zone. For example, at $U_A=0.3$ m/s and $U_D=0.5$ m/s, the increase of O_2 concentration from 4 to 12% in the flue gas in the adsorption zone increases O_2 concentrations in the reduction zone from 0.4 to 1.2% when the draft tube is used as the reduction zone, and from 0.6 to 1.7% when the annulus is used as the reduction zone. However, at $U_A=0.3$ m/s and $U_D=0.9$ m/s, O_2 concentration increases from 0.5 to 1.4% in the reduction zone if the draft tube is used as the reduction zone due to the relatively constant R_{AD} , and from 1.3 to 4% if the annulus serves as the reduction zone because of the increased gas bypass from the draft tube to the annulus at high draft tube gas velocities. This implies that

only the annulus can be used as the adsorption zone if the ICFB reactor is to be operated at a high U_D for the treatment of flue gases with high O_2 concentrations.

Considering the operation feature of the ICFB reactor where the annulus is operated at a moving bed or at the minimum fluidization while the draft tube is at pneumatic transport, the annulus should be used as the adsorption zone to provide a relatively long contact or adsorption time between the flue gas and the catalyst to achieve high adsorption ratio.

4.6 Summary

The hydrodynamic performance of an ICFB cold model unit was investigated using three types of annulus gas distributors, i.e., flat, cylindrical and conical distributor plates. For each distributor, the influence of the effective gap opening on the gas bypass and the solids circulation was studied at various gas velocities in the annulus and the draft tube.

For the flat distributor, the gas bypass ratio from the annulus to the draft tube (R_{AD}) was over 50% and the gas bypass ratio from the draft tube to the annulus (R_{DA}) was very low (0~1.5%) in the tested range of gas velocities. The increase of both U_A and U_D could enhance the gas bypass from the annulus to the draft tube. The solids circulation rate (W_s) increased with the increase of both U_A and U_D , although U_A showed more influence on W_s than U_D . Because of the high gas bypass from the annulus to the draft tube, particles could not be stably circulated if the annulus gas velocity was lower than 0.45 m/s.

For the cylindrical distributor, the same trend as the flat distributor was observed with respect to the influence of U_A and U_D on R_{AD} , R_{DA} and W_s , except that the use of cylindrical distributor could greatly decrease R_{AD} and enhance the solids circulation when compared with the flat distributor.

As observed in the experiment, both distributors showed a relatively narrow operating window of gas velocities.

The conical distributor showed a flexible and stable operation in a wide range of velocities for both U_A and U_D . The increase of U_D could enhance R_{AD} while U_A showed less effect on R_{AD} . R_{DA} ranged from 5% to 15% in the test, which is much higher than that using the other two distributors. R_{AD} and R_{DA} were sensitive to the change of the effective gap opening. The increase of both U_A and U_D could increase W_s , but U_A showed more influence on W_s than U_D . The solids circulation rate was found to be well correlated with the overall gas velocity for the ICFB with conical and cylindrical gas distributors.

In the hot model ICFB reactor, the gas bypass ratio of Fe/ZSM-5(PUC) from the annulus to the draft tube (R_{AD}) reached a maximum value when the draft tube gas velocity (U_D) was equal to 0.9~1.0 m/s in this study. Meanwhile, R_{DA} continuously increased with increasing U_D . In the range of velocities investigated, the gas bypass ratio from the draft tube to the annulus (R_{DA}) was always higher than that from the annulus to the draft tube (R_{AD}) for Fe/ZSM-5(PUC) catalyst. U_A had less influence on both R_{AD} and R_{DA} than U_D .

For Fe/ZSM-5(Albemarle) in the hot model ICFB reactor, at a given U_A , the gas bypass ratio from the draft tube to the annulus (R_{DA}) increased with increasing U_D . At given U_A and U_D , the ICFB using Fe/ZSM-5(Albemarle) possessed higher R_{DA} but lower R_{AD} than that using Fe/ZSM-5(PUC). The increase of U_A could decrease R_{DA} , and the increase of U_D or U_A had almost no effect on the gas bypass ratio from the annulus to the draft tube (R_{AD}).

It was found in the cold model experiment that all three types of distributors showed very low gas bypassing from the draft tube to the annulus, but high gas bypassing in the reverse direction. The data from the hot model experiment showed that the change in the direction of perforated holes on the conical distributor reduced the gas bypass from the

annulus to the draft tube, but enhanced the gas bypass from the draft tube to the annulus. Thus, the change of the reactor configurations could have a significant impact on the operating characteristics of the ICFB reactor. Further detailed investigation is needed in order to fully understand the hydrodynamics of the ICFB reactor.

Chapter 5

Adsorption and Reduction Performance of the ICFB Reactor

According to the reaction kinetic test results, Fe/ZSM-5 catalyst exhibited promising performance on the selective catalytic reduction of NO_x with propylene as the reductant. O₂ exhibited a significant negative impact on NO_x reduction when O₂-rich flue gas was used in the experiment. To achieve a high NO_x conversion, O₂ concentration in the flue gas must be controlled to be lower than 2%, which is not commonly encountered for most combustion flue gases. To overcome the negative impact of excessive O₂ in the flue gas, the integrated adsorption-reduction process has been proposed in this study. Based on the result obtained from the hydrodynamic experiment, a hot model internal circulating fluidized bed (ICFB) reactor with a similar configuration as the cold model unit presented in Chapter 4 (Figure 4.1) was built and tested.

5.1 Experimental setup

In the proposed configuration, the flue gas is passed into the adsorption zone (annulus) where NO_x is adsorbed by the catalyst particles. The NO_x-rich catalyst particles then move downward and into the reduction zone (draft tube) where NO_x is reduced by injected hydrocarbons. Meanwhile, the catalyst particles are depleted of the adsorbed NO_x in the draft tube. The NO_x-depleted catalyst particles are then recirculated back to the adsorption zone to keep a continuous operation. By adjusting the gas flow rates in the annulus and the draft tube, the bypassing of the flue gas from the adsorption zone to the reduction zone can be controlled

to have the O_2 concentration in the reduction zone maintained at desired levels. The hot model ICFB reaction system is shown schematically in Figure 5.1.

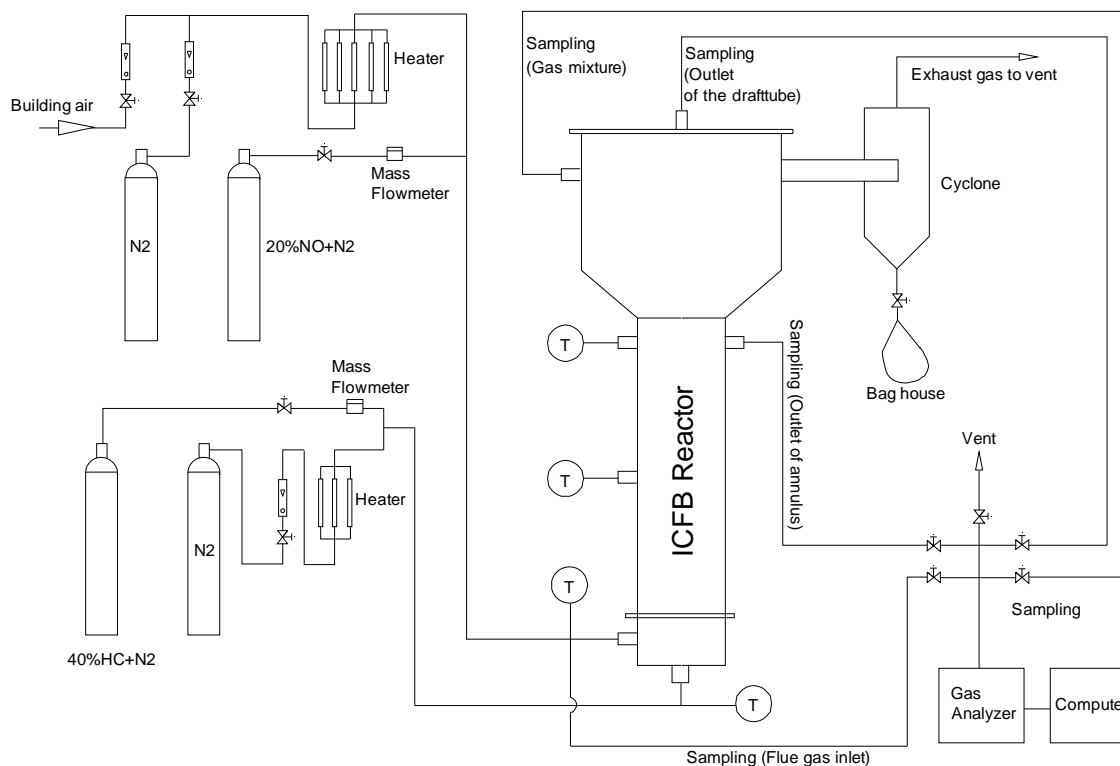


Figure 5.1 Schematic of hot model ICFB reaction system

In the experiment, the ICFB reactor was first preheated by passing the preheated building air through both the annulus and the draft tube. After the desired reaction temperature was reached in the reactor, the gas bypass between the annulus and the draft tube was first measured based on the O_2 mass balance method over the annulus and the draft tube by adjusting the flow rate of either the flue gas or the reductant gas, as illustrated in Chapter 4. After the gas bypass measurement, NO from the gas cylinder was blended with preheated building air and pure N_2 to prepare the simulated model flue gas at desired NO and O_2 concentrations. At the same time, propylene was injected into the preheated N_2 to prepare the reductant gas mixture. The model flue gas was injected into the adsorption zone (annulus)

through the conical distributor plate and NO_x was adsorbed by the catalyst in the annulus. The reductant gas mixture was injected into the reduction zone (draft tube) via a gas nozzle and NO_x adsorbed on the catalyst particles flowing from the annulus into the draft tube was reduced by the hydrocarbon in the reductant gas. The adsorption and reduction performance was evaluated by measuring the gas composition at the inlet and outlet of the annulus, the outlet of the draft tube and the gas mixture at the exit of the reactor. The geometric dimensions of the ICFB reactor are given in Table 5.1.

Table 5.1 Geometric dimensions of the ICFB reactor

Item	Dimension
Draft tube diameter, mm	54.8 (I.D.), 60.3 (O.D.)
Draft tube length, mm	1016.0
Column diameter, mm	108.2 (I.D.), 114.3 (O.D.)
Column height, mm	1092.2
Freeboard height, mm	1016.0
Freeboard diameter, mm	260.4 (I.D.), 273.1 (O.D.)
Annulus distributor opening ratio	1.62%, 52 holes of 1.6mm diameter
Gas nozzle diameter, mm	34.9 (I.D.), 38.1 (O.D.)
Gas nozzle distributor opening ratio	9.19%, 61 holes of 1.6mm diameter
Fluidized bed distributor opening ratio	3.25%, 151 holes of 1.6mm diameter
Effective gap opening for the solids circulation, mm	10.0

Two types of Fe/ZSM-5 catalysts were selected and tested in this experiment, i.e., Fe/ZSM-5(PUC) and Fe/ZSM-5(Albemarle). Both catalysts were prepared following the same procedure of the impregnation in organic solution (IMPO) method, as described in Chapter 3. The properties of the catalysts were given in Table 5.2.

Table 5.2 Properties of catalysts used in the hot model experiments

Catalyst	Average particle size	Bulk density	S _{BET}	U _{mf} (T=350°C)
Fe/ZSM-5 (PUC)	1042 μm	926 kg/m ³	110 m ² /g	0.39 m/s
Fe/ZSM-5 (Albemarle)	155 μm	979 kg/m ³	162 m ² /g	0.01 m/s

The model flue gas used in the experiment was a mixture prepared from a gas cylinder containing 20% NO balanced with N₂ and a liquid N₂ Dewar, with both supplied from Praxair Products Inc. Building air was used as the source of O₂. NO_x concentration in the model flue gas was controlled to be 300~900 ppm with O₂ concentration ranging from 4 to 12%.

The reducing agent used in the experiment was propylene. The gas cylinder containing 40% propylene balanced with N₂ was supplied by Praxair Products Inc. The reducing agent stream consisted of propylene + N₂, with propylene-to-NO_x molar flow ratio varied from 1 to 4. It should be noted that NO and HC were in different gas streams in the ICFB reactor, i.e., the flue gas stream in the adsorption zone and the reductant gas stream in the reduction zone. To investigate the effect of gas velocities and other factors on the performance of the catalyst without changing HC:NO ratio, the ratio of HC:NO was defined as the molar flow rate of propylene to the reduction zone divided by the molar flow rate of NO to the adsorption zone.

5.2 Estimation of NO_x and HC conversions and NO_x adsorption ratio

The overall NO_x conversion (X_{NO_x}) was calculated by equations 5.1 and 5.2 based on the initial concentration of NO_x in the total gas flow of the annulus and the draft tube, and the concentration of NO_x in the gas mixture at the exit of the reactor.

$$C_{NOx,in} = \frac{C_{NOx,0} \times F_{F,0}}{(F_{F,0} + F_{R,0})} \quad (5.1)$$

$$X_{NOx} = \frac{C_{NOx,in} - C_{NOx,out}}{C_{NOx,in}} \times 100\% \quad (5.2)$$

where

$C_{NOx,0}$, initial NO_x concentration in the flue gas feed, ppm

$C_{NOx,in}$, initial NO_x concentration in the total gas feed into the annulus and the draft tube, ppm

$C_{NOx,out}$, NO_x concentration in the gas mixture at the exit of the reactor, ppm

$F_{F,0}$, flue gas flow rate, m^3/s

$F_{R,0}$, reductant gas flow rate, m^3/s

X_{NOx} , overall NO_x conversion, %

The conversion of propylene was calculated based on the measured concentrations of CO and CO_2 in the gas mixture at the exit of the reactor by assuming that all converted propylene goes to CO and CO_2 , as shown in equation 5.3:

$$X_{HC} = \frac{C_{CO,out} (ppm) \times 10^{-4} + (C_{CO_2,out} (\%) - \frac{C_{CO_2,0} (\%) \times F_{F,0}}{F_{F,0} + F_{R,0}})}{3 \times (F_{HC,0} \times 40\%)} \times (F_{F,0} + F_{R,0}) \times 100\% \quad (5.3)$$

where

$C_{CO_2,0}$, initial CO_2 concentration in the flue gas feed, %

$C_{CO,out}$, CO concentration in the gas mixture at the outlet of the reactor, ppm

$C_{CO_2,out}$, CO_2 concentration in the gas mixture at the outlet of the reactor, %

$F_{F,0}$, flue gas flow rate, m^3/s

$F_{R,0}$, reductant gas flow rate, m^3/s

$F_{HC,0}$, flow rate of 40% Propylene + N₂ gas mixture from the cylinder, m³/s

X_{HC} , overall HC conversion, %

Since the building air contained a certain amount of CO₂, the measured initial concentration of CO₂ in the flue gas feed must be converted to the concentration based on the total flow rate of the flue gas and the reductant gas ($F_{F,0} + F_{R,0}$) and then subtracted from the measured CO₂ concentration at the exit of the reactor. The initial concentration of propylene was estimated based on the flow rate of certified 40% propylene + N₂ added to the reductant gas feed. Again, a coefficient of 3 was introduced in equation 5.3 to reflect the fact that one mole of propylene contains 3 moles of carbon.

Because the overall mass balance on carbon was used to calculate HC conversion in eq. (5.3), the carbon balance could not be carried out to check the experiment reliability. Because pure N₂ was used as the carrier gas for the reducing agent while NO concentration was much lower than N₂ in the total gas flow, it is inaccurate to use total nitrogen balance to check the experiment reliability.

To evaluate the adsorption performance of the catalyst in the ICFB reactor, NO_x adsorption ratio in the annulus was calculated and compared with the overall NO_x conversion. Because the gas bypass from both the annulus to the draft tube and the draft tube to the annulus existed, the real NO_x concentration and the gas flow rate inside the adsorption zone must be corrected by the gas bypass data, and the NO_x reduction caused by the hydrocarbon in the bypassing gas from the reduction zone to the adsorption zone should also be deducted from the initial NO_x concentration.

The adsorption ratio of NO_x ($X_{NO_x,ads}$) in the adsorption zone was calculated by

$$X_{NO_x,ads} = \frac{C_{NO_x,ads,real} - C_{NO_x,ads,out}}{C_{NO_x,ads,real}} \times 100\% \quad (5.4)$$

where $C_{NO_x,ads,out}$ was the NO_x concentration at the outlet of the adsorption zone, and the real initial NO_x concentration, $C_{NO_x,ads,in}$, in the adsorption zone was calculated by

$$C_{NO_x,ads,in} = \frac{C_{NO_x,0} \times (F_{F,0} - F_{FR})}{F_{F,0} - F_{FR} + F_{RF}} \times (1 - X_{NO_x,BM}) \quad (5.5)$$

where

$C_{NO_x,0}$, initial NO_x concentration in the flue gas feed, ppm

$F_{F,0}$, flue gas flow rate, m^3/s

F_{FR} , calculated gas bypass from the adsorption zone to the reduction zone, m^3/s

F_{RF} , calculated gas bypass from the reduction zone to the adsorption zone, m^3/s

$X_{NO_x,BM}$, benchmark NO_x conversion caused by the bypassing HC from the reduction zone, %

$C_{NO_x,ads,in}$, real initial NO_x concentration used for the adsorption in the adsorption zone, ppm

The benchmark NO_x conversion used in equation 5.5 was determined individually for each case based on the fixed bed experimental results and the real concentrations of O_2 and HC at the inlet of the adsorption zone with the effect of the gas bypass being considered.

The fluidized bed experiment was also conducted and compared to the results from the ICFB reactor. The draft tube in the ICFB reactor was removed and a new flat gas distributor plate was installed to construct the fluidized bed reactor system. The model flue gas and the reductant gas were mixed in the gas chamber below the distributor before entered the catalyst bed for tests conducted in the fluidized bed. Effects of gas velocities, NO , O_2 and HC concentrations on the NO_x conversion were investigated.

5.3 Performance with Fe/ZSM-5(PUC) catalyst

5.3.1 Selection of adsorption zone in the ICFB reactor

Either the annulus or the draft tube could be used as the adsorption zone, while the other one as the reduction zone. The adsorption and reduction zones were switched between the annulus and the draft tube using Fe/ZSM-5(PUC) catalyst to investigate the effect of the zone switch on NO_x conversion in the ICFB reactor.

The influence of gas velocities and the HC:NO ratio on NO_x conversion using the draft tube as the adsorption zone is shown in Figure 5.2. For a given HC:NO molar ratio of 1 or 2 and a reductant gas velocity (U_A), the increase in the flue gas velocity (U_D) led to the decrease in NO_x conversion. This could be attributed to the fact that the increase of U_D decreased the contact time between the flue gas and catalyst particles in the adsorption zone, leading to a decrease in the amount of NO_x adsorbed. Although NO_x conversions in all runs were generally lower than 15%, the data clearly showed that increasing the HC:NO ratio and the reductant gas velocity (U_A) improved the reactor performance. Such a low NO_x conversion for this kind of configuration confirms that the annulus should be used as the adsorption zone and the draft tube as the reduction zone in order to achieve a high NO_x conversion in the current ICFB reactor design.

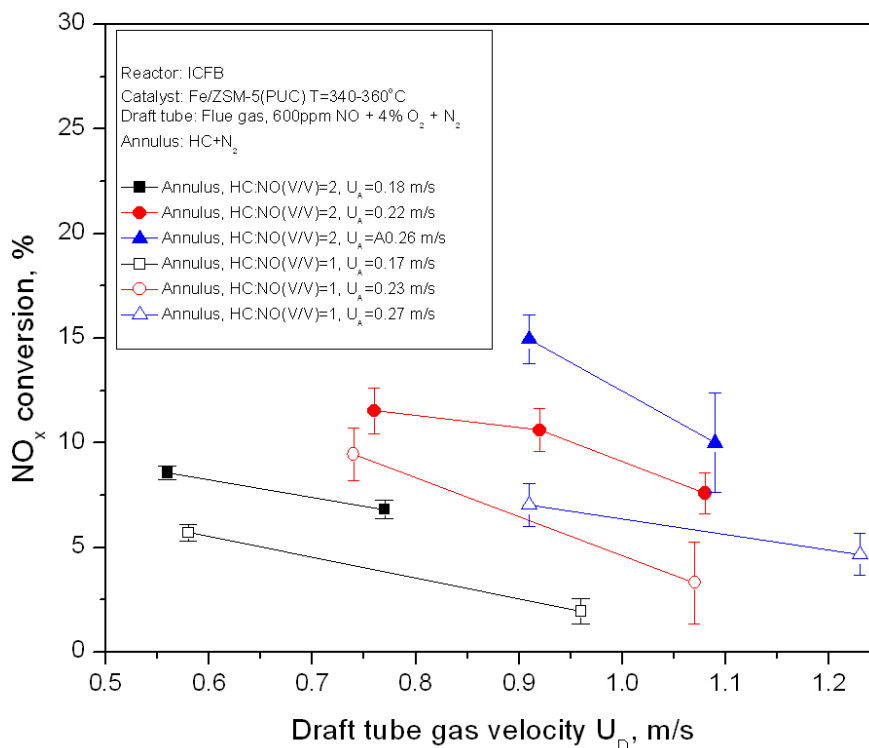


Figure 5.2 Effect of gas velocities and HC:NO ratio on NO_x conversion using the draft tube as the adsorption zone (ICFB, Fe/ZSM-5(PUC))

The experimental results presented below were thus all obtained with the annulus as the adsorption zone.

5.3.2 Effect of catalyst loading in the ICFB reactor

The overall NO_x conversion and adsorption ratio in the annulus are given in Figure 5.3 for the ICFB reactor with Fe/ZSM-5(PUC) with a catalyst loading of 1.1, 2.2 and 3.3 kg, respectively. The model flue gas was 600 ppm NO + 4% O₂ + N₂, with the reductant gas containing propylene + N₂ at HC:NO=2. The experiment was carried out with a fixed reductant gas velocity of $U_D=0.6$ m/s, while the flue gas velocity in the annulus changed from 0.27 to 0.55 m/s. It clearly demonstrated that the increase in the catalyst loading increased both NO_x conversion and NO_x adsorption ratio. Both NO_x conversion and adsorption ratio

decreased slightly with the increase of U_A in all cases, and the NO_x conversion and adsorption ratio appear to be matched each other very closely, indicating that all NO_x adsorbed in the annulus zone was completely converted to N_2 in the draft tube zone no matter how much the catalyst loading was.

Although increasing the catalyst loading will be beneficial to NO_x adsorption as well as NO_x conversion, the maximum catalyst loading for both Fe/ZSM-5(PUC) and Fe/ZSM-5(Albemarle) was set to 3.3 kg in all experiments carried out in this study.

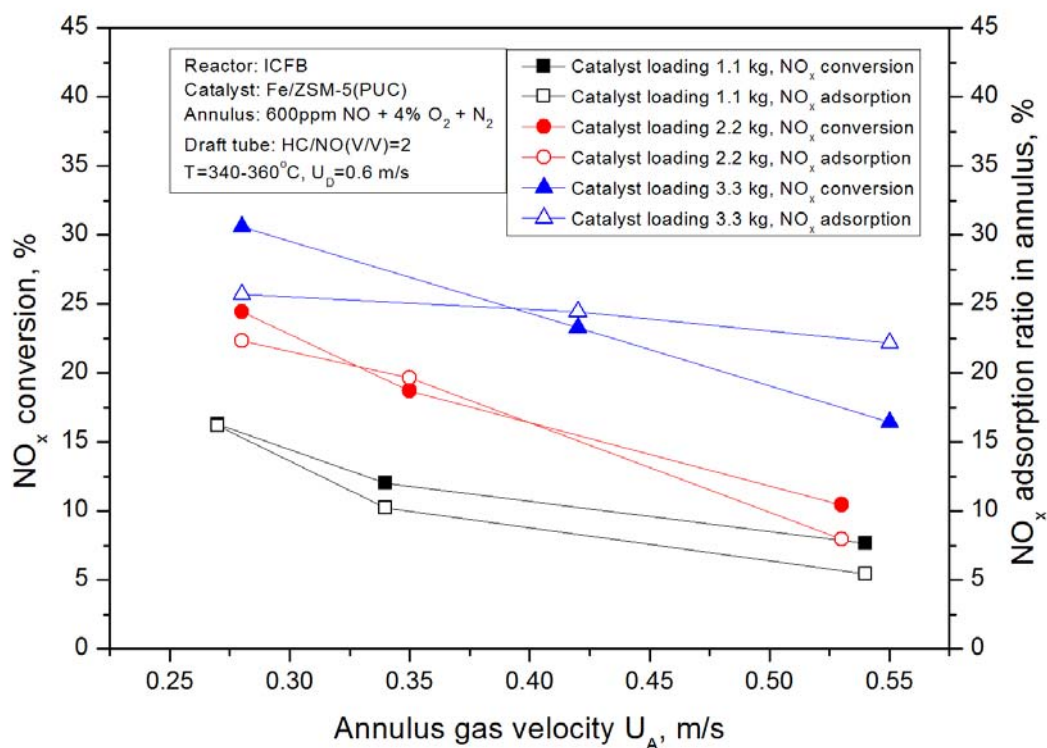


Figure 5.3 Effect of catalyst loading on NO_x conversion and adsorption (ICFB, Fe/ZSM-5(PUC))

5.3.3 Effect of HC:NO molar ratio on NO_x conversion

The influence of HC:NO molar ratio on NO_x conversion is shown in Figure 5.4. For a given HC:NO ratio, NO_x conversion decreased with increasing U_A because the decrease in the contact time between the flue gas and the catalyst in the annulus reduced the adsorption rate. On the contrary, NO_x conversion increased with increasing U_D, likely due to the increased reaction rate in the draft tube and catalyst circulation rate. The NO_x conversion increased when HC:NO ratio increased from 1 to 2, which agrees with the results from the fixed bed experiment. The difference in NO_x conversion between HC:NO=1 and 2 at a given U_A decreased with increasing U_D. For example, at U_A=0.4m/s, the difference in NO_x conversion was 6%, 5% and 2% for U_D=0.6, 0.9 and 1.2 m/s, respectively, which indicates that the benefit of a larger HC:NO ratio for a higher NO_x conversion diminished at high U_D. At low U_D, the reactor performance was limited by the reaction in the draft tube region. Therefore, increasing the HC:NO ratio improved the reactor performance significantly. At a high U_D, the reactor performance was controlled by the adsorption in the annulus zone, insensitive to the change of HC:NO ratio, due to the enhanced mass transfer of hydrocarbons from the reductant gas flow to the catalyst surface. U_A showed less influence on NO_x conversion than U_D because NO_x conversion was controlled mainly by the draft tube gas velocity.

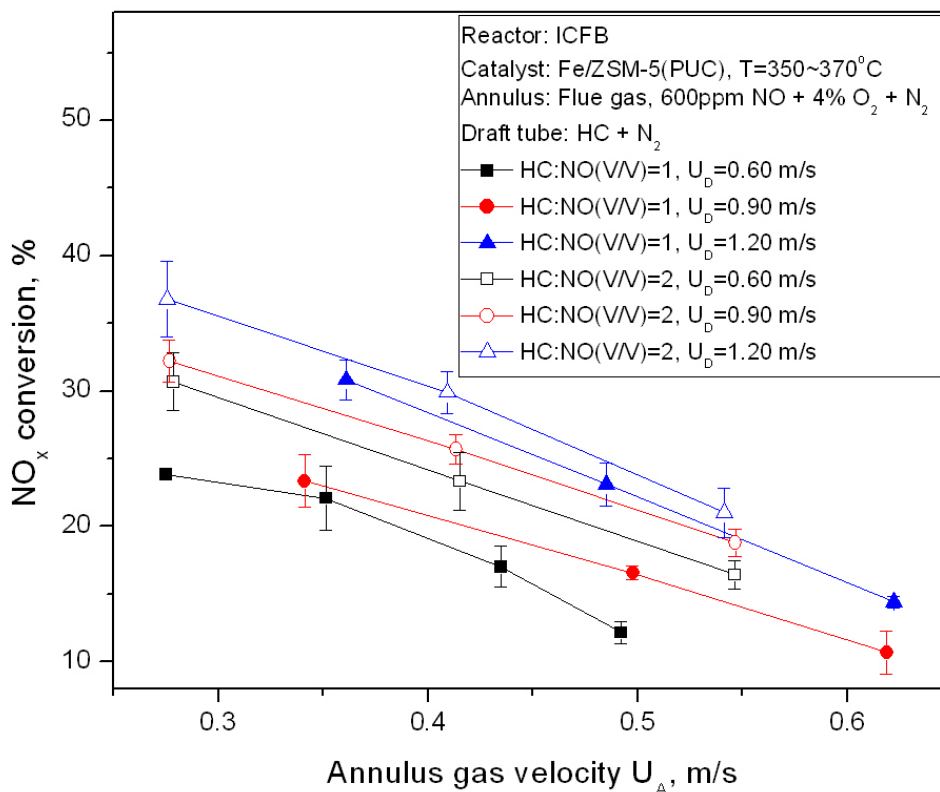


Figure 5.4 Effect of HC:NO ratio on NO_x conversion (ICFB, Fe/ZSM-5(PUC))

5.3.4 Effect of flue gas O₂ content on NO_x conversion

As shown in Figures 5.5, for a given U_D, increasing U_A caused a steady decrease in NO_x conversion for tests with 4% and 8% O₂, and only a slight decrease at 12% O₂. A highest NO_x conversion of 31% was observed at low U_A at 4% O₂. With the increase of O₂ concentration from 4% to 12% in the model flue gas, the maximum NO_x conversion decreased significantly from 31% to ~20%. For a given O₂ concentration and U_A, the increase of U_D from 0.6 to 0.75 m/s showed little influence on NO_x conversion. This result shows that the flue gas O₂ concentration still imposed a significant impact on NO_x conversion in the ICFB reactor when coarse PUC catalyst was used.

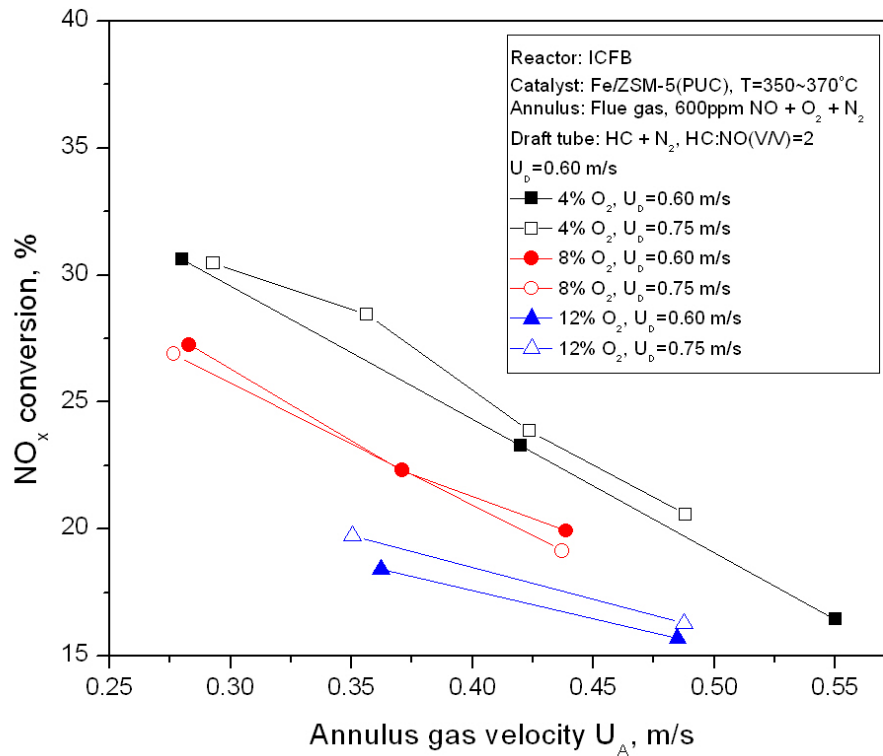


Figure 5.5 Effect of flue gas O₂ concentration on NO_x conversion (ICFB, Fe/ZSM-5(PUC))

5.3.5 Effect of gas velocities on NO_x conversion and adsorption

The influence of gas velocities on the adsorption and conversion of NO_x for the model flue gas with 600 ppm NO + 4% O₂ + N₂ and HC:NO=2 is shown in Figure 5.6. When the draft tube gas velocity was low (U_D=0.6 m/s) which created low solids circulation rate, the increase of U_A had little influence on the NO_x adsorption ratio. This is likely because that the shortened gas residence time in the annulus was compensated by the increased solids circulation rate, as U_A increased. Taking the experimental error into account, one may say that all adsorbed NO_x was reduced when U_A<0.4 m/s for U_D=0.6 m/s and U_A<0.3 m/s for U_D=0.9 m/s. For U_D≥0.9 m/s with a high solids circulation rate, the adsorption ratio of NO_x decreased with the increase of U_A because the solids circulation rate was less sensitive to U_A at a high U_D, and the reduction rate was always lower than the adsorption ratio, which suggests that part of the adsorbed NO_x was not reduced in the reduction zone, probably due

to the shortened gas and catalyst residence time in the draft tube zone at a high U_D . In general, if the reactor was operated at steady state, NO_x adsorbed in the annulus should always be equal to NO_x converted in the draft tube. If NO_x conversion is lower than the adsorption ratio, less NO_x should be adsorbed when the catalyst returns to the adsorption zone. Hence, another possible reason for NO_x conversion lower than the adsorption ratio is that NO_x is weakly adsorbed by Fe/ZSM-5(PUC) catalyst, and the un-reacted NO_x is desorbed before the catalyst particles leave the reduction zone. As a result, NO_x conversion in the draft tube is lower than the NO_x adsorption ratio in the annulus. For each given U_A , with an increase in U_D , both the conversion and the adsorption ratio of NO_x increased, although the influence of U_D on NO_x adsorption ratio was more pronounced at low U_A . To achieve a high NO_x conversion in the ICFB reactor with Fe/ZSM-5(PUC) catalyst, the annulus gas velocity should be kept below 0.3 m/s.

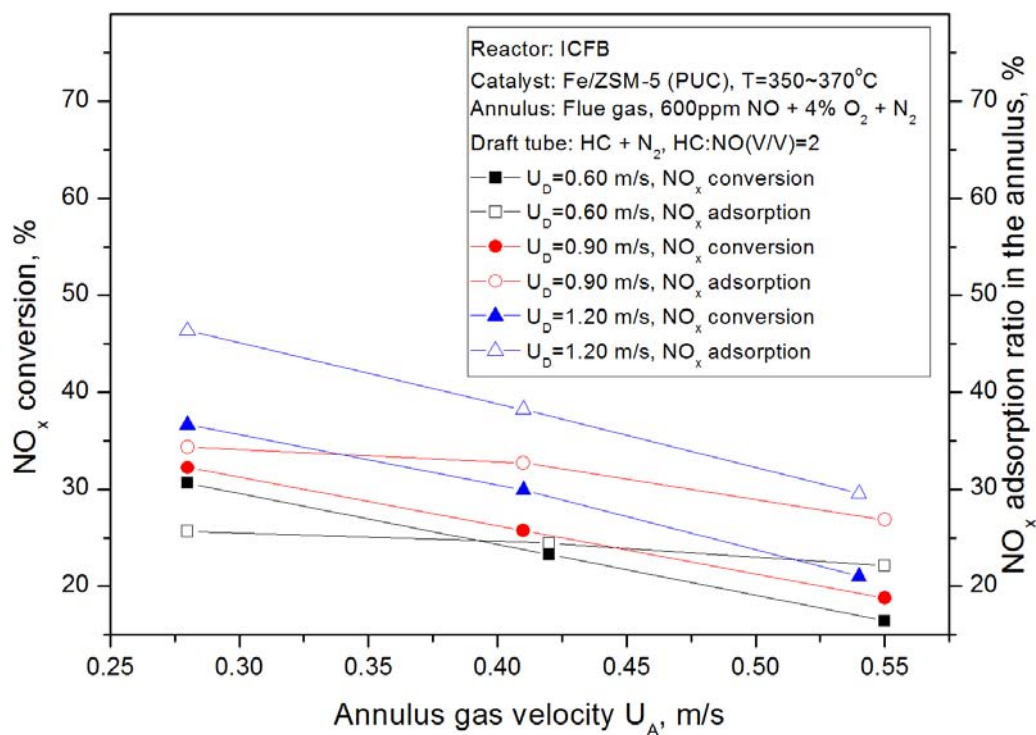


Figure 5.6 Effect of gas velocities on NO_x conversion and adsorption (ICFB, Fe/ZSM-5(PUC))

5.3.6 Performance of fluidized bed reactor with Fe/ZSM-5(PUC)

5.3.6.1 Effect of inlet NO concentration

Figures 5.7 to 5.9 show that the inlet NO concentration in the model flue gas had some influence on NO_x conversion. At O₂ concentrations of 4% (Figure 5.7) and 2.5% (Figure 5.8), NO_x conversion increased monotonically with increasing NO concentration from 300 to 900 ppm at a given fluidizing gas velocity. This may be explained by the fact that the increase in NO_x concentration enhanced the NO_x adsorption capacity of the catalyst and also the reaction rate. For the flue gas with 1% O₂ (Figure 5.9), a 10~15% increase in NO_x conversion was observed when the inlet NO concentration increased from 300 to 600 ppm. The NO_x conversion slightly decreased as the flue gas NO concentration increased from 600 to 900 ppm. As discussed earlier, NO must be oxidized to NO₂ before it is reduced by the HC. At an O₂ concentration of 1% and a NO concentration of 900 ppm, the HC concentration in the gas flow was 1800 ppm at a HC:NO ratio of 2. If all HC was completely converted to CO₂, it could have reduced the flue gas O₂ level from 1% to 0.44%. Therefore, there may not be enough O₂ for the oxidization of NO to NO₂, resulting in a NO_x conversion slightly lower than the case with 600 ppm of NO in the flue gas.

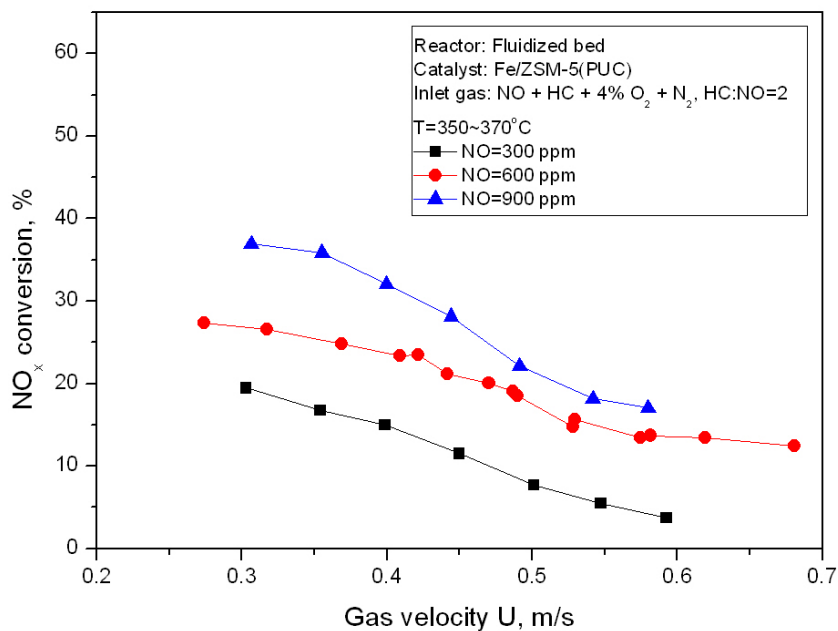


Figure 5.7 Effect of inlet NO concentration on NO_x conversion (Fluidized bed, Fe/ZSM-5(PUC), [O₂]=4%)

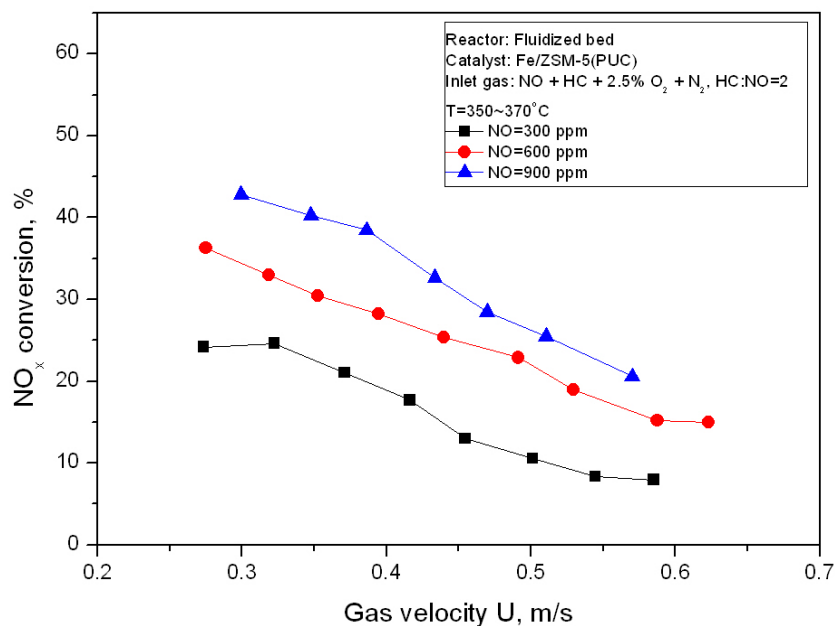


Figure 5.8 Effect of inlet NO concentration on NO_x conversion (Fluidized bed, Fe/ZSM-5(PUC), [O₂]=2.5%)

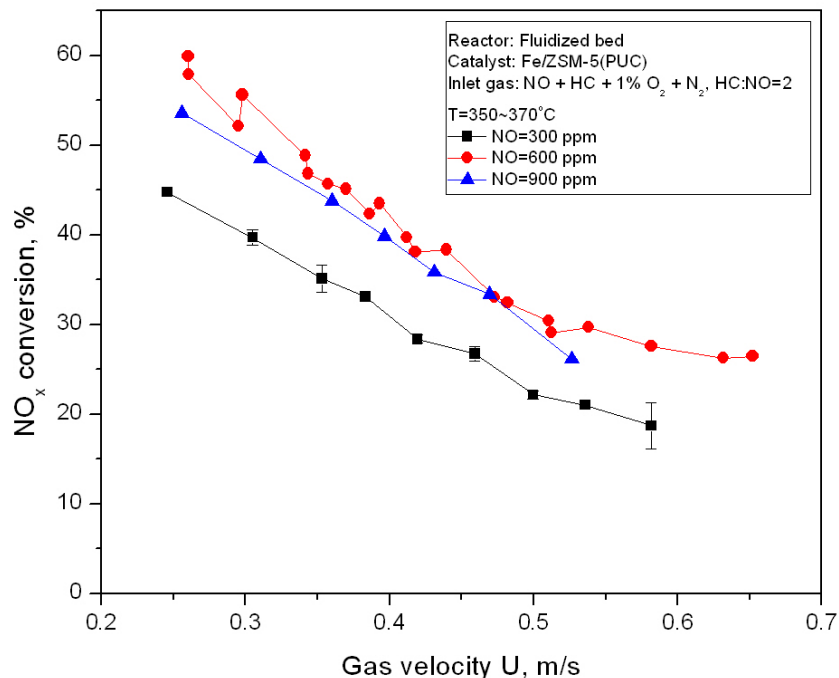


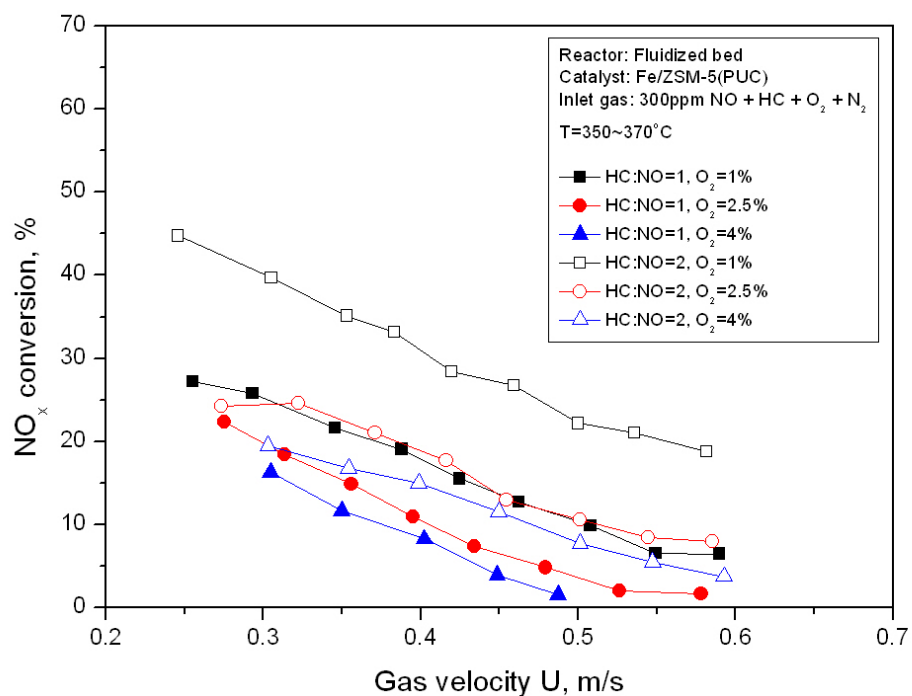
Figure 5.9 Effect of inlet NO concentration on NO_x conversion (Fluidized bed, Fe/ZSM-5(PUC), [O₂] =1%)

5.3.6.2 Effect of HC:NO ratio on NO_x and HC conversions

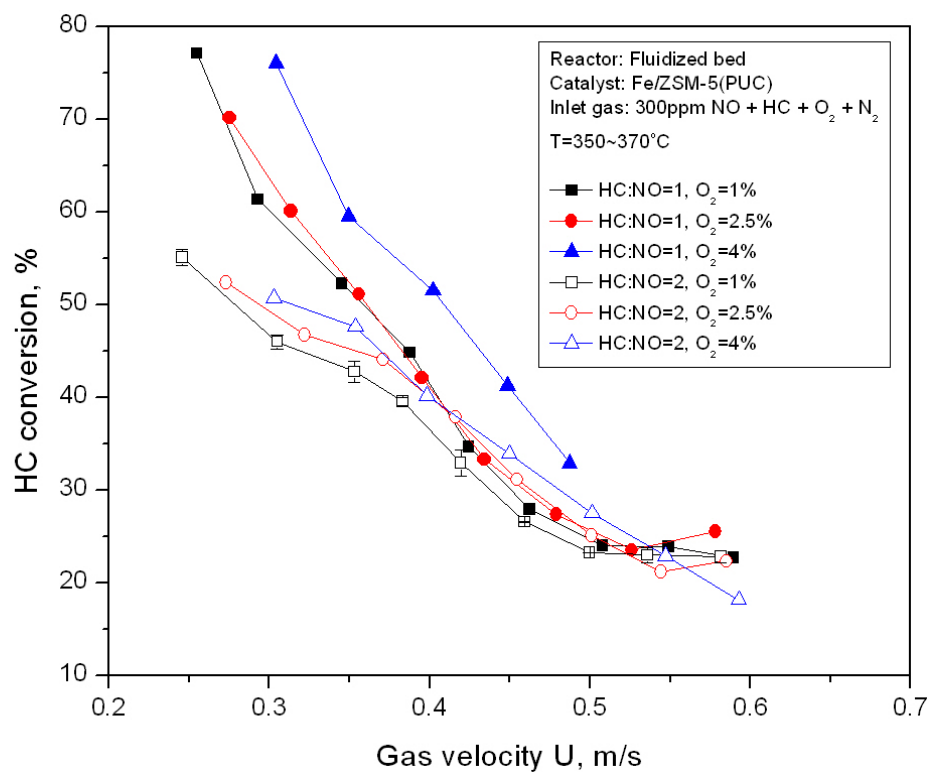
It is anticipated that an increase in HC:NO will enhance the NO_x conversion at given O₂ and NO concentrations in the fluidized bed.

For the flue gas with 300 and 600 ppm NO, as shown in Figure 5.10 and 5.11, at 1% flue gas O₂, the increase of HC:NO ratio from 1 to 2 increased NO_x conversion significantly. At O₂ concentrations of 2.5% and 4%, NO_x conversion also increased by increasing HC:NO ratio, although the effect was not as significant as at 1% O₂. At low gas velocities, HC conversion decreased notably with the increase in HC:NO ratio at all tested O₂ concentrations. When a high gas velocity was used, the effect of HC:NO ratio on HC conversion was insignificant.

For an inlet NO concentration of 900 ppm, as shown in Figure 5.12, the increase of HC:NO led to significant increase in NO_x conversion and a slight decrease in HC conversion at both 2.5% and 4% O₂. For the flue gas with 1% O₂, the effect of HC:NO on NO_x conversion was insignificant at 300 and 600 ppm NO, and the HC conversion dropped to a relatively low level at HC:NO=2. Again, this is likely due to the insufficient supply of O₂. In fact, as observed in the experiment, the outlet O₂ concentration approached zero when the flue gas of 900 ppm NO + 1% O₂ was used with a HC:NO ratio of 2.

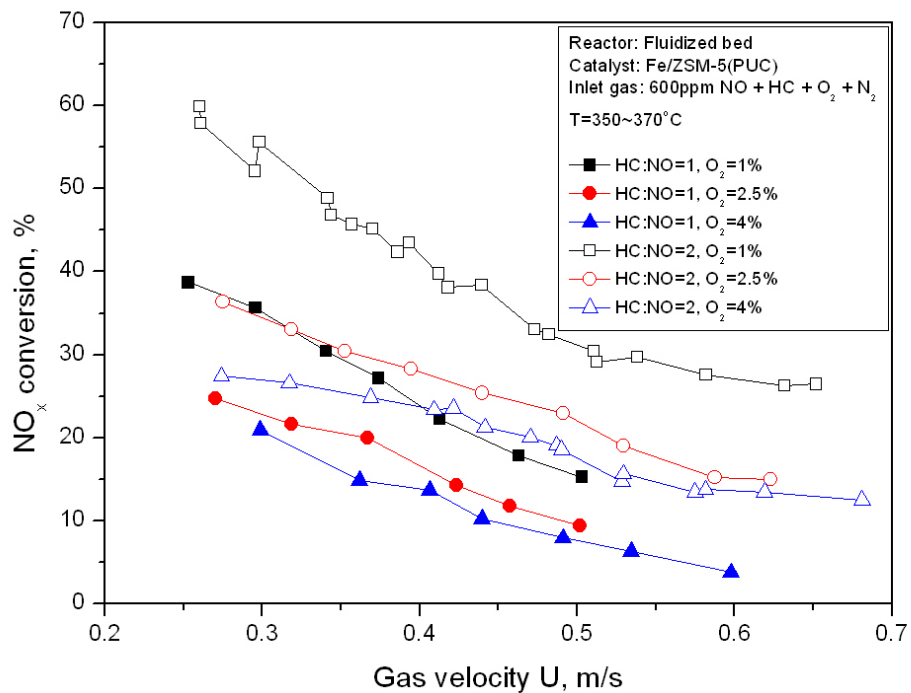


(a) NO_x conversion

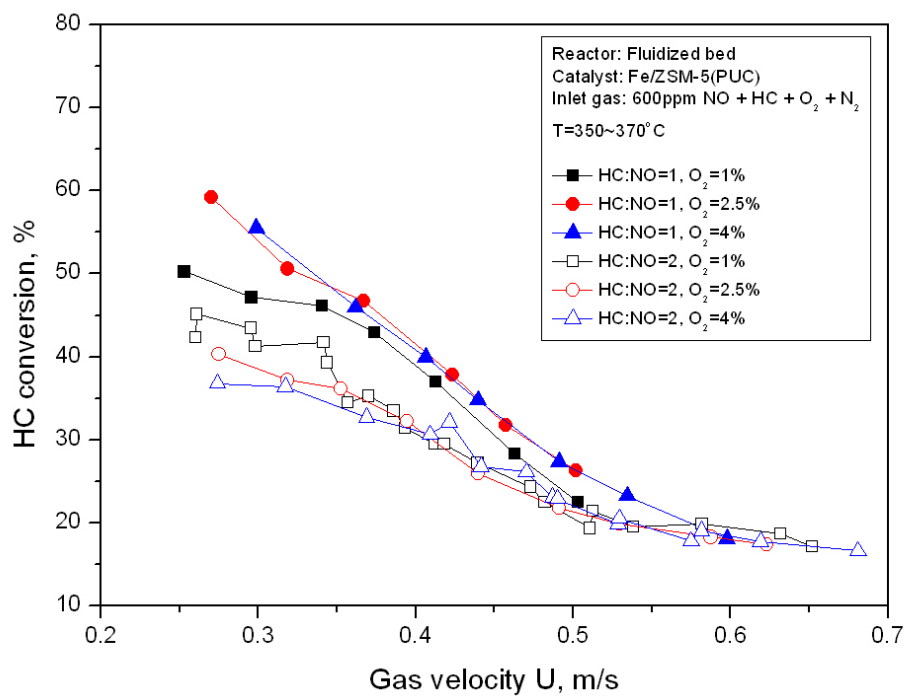


(b) HC conversion

Figure 5.10 Effect of HC:NO on NO_x and HC conversions (Fluidized bed, Fe/ZSM-5(PUC), [NO]=300ppm)

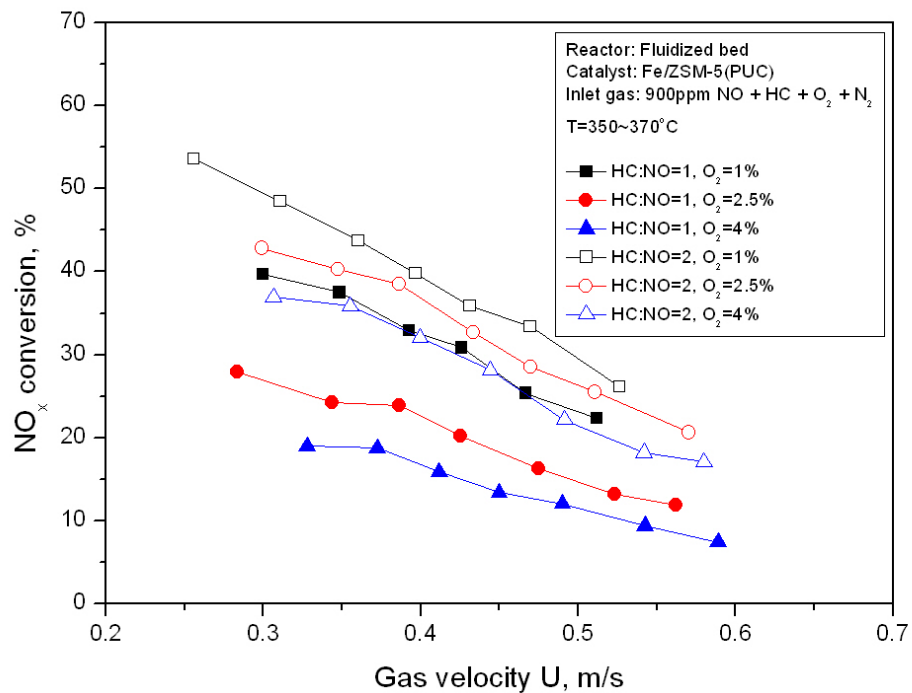


(a) NO_x conversion

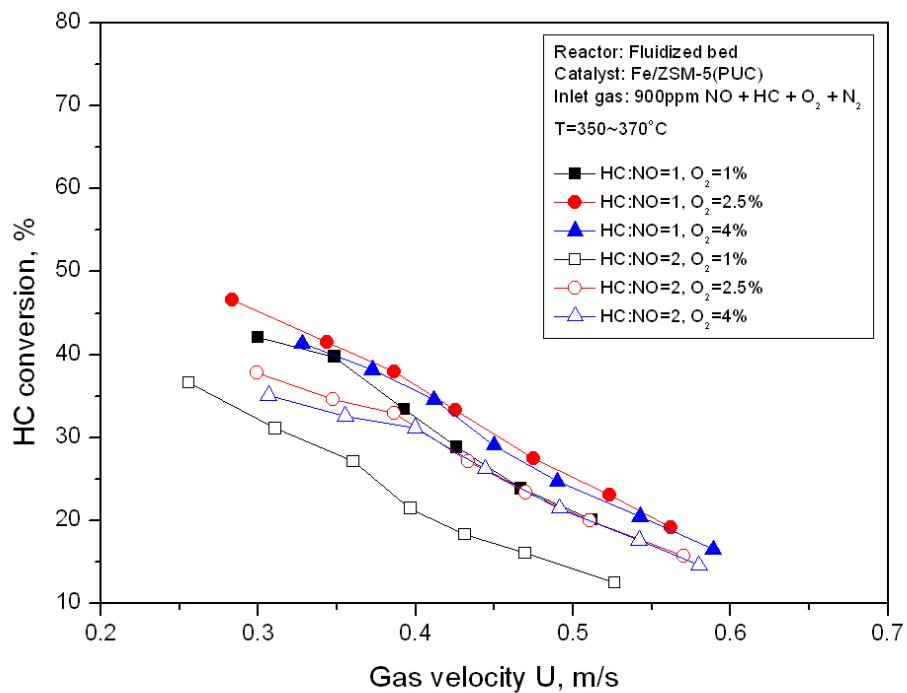


(b) HC conversion

Figure 5.11 Effect of HC:NO on NO_x and HC conversions (Fluidized bed, Fe/ZSM-5(PUC), [NO]=600ppm)



(a) NO_x conversion

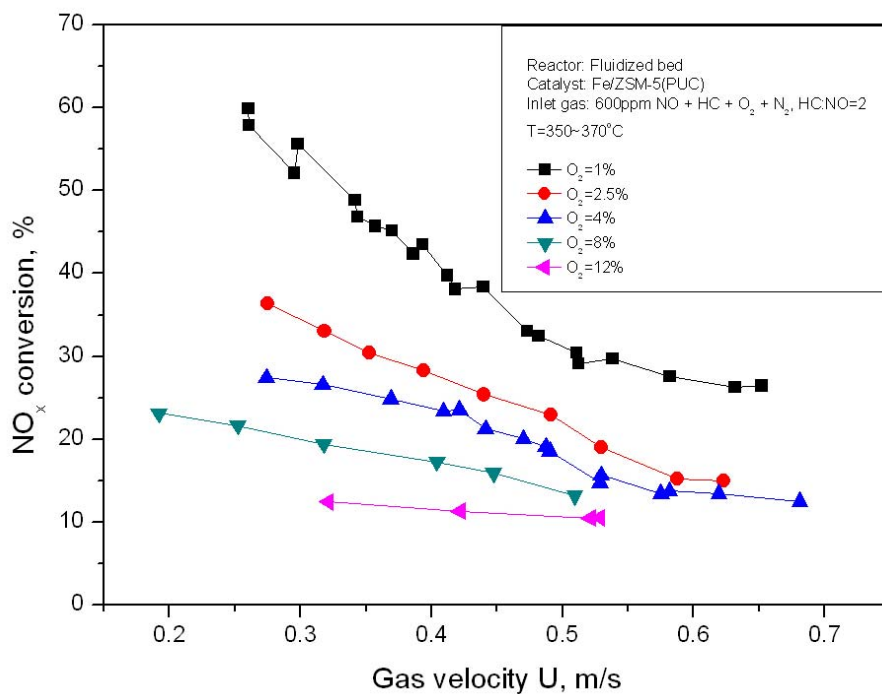


(b) HC conversion

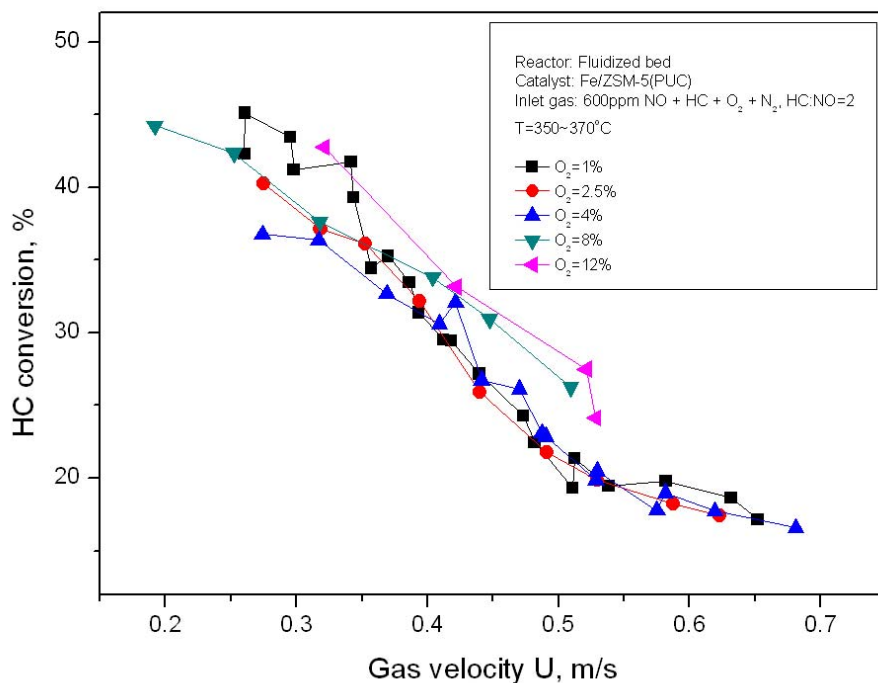
Figure 5.12 Effect of HC:NO on NO_x and HC conversions (Fluidized bed, Fe/ZSM-5(PUC), [NO]=900ppm)

5.3.6.3 Effect of inlet O₂ concentration on NO_x and HC conversions

Fe/ZSM-5(PUC) showed high reactivity on NO_x reduction in the fluidized bed for flue gas with low O₂ concentration, as shown in Figure 5.13. NO_x conversion reached 60% at O₂=1% and U=0.27 m/s. Increase of O₂ concentration led to the decrease of NO_x conversion at a given gas velocity. It is worthwhile to point out that the performance of Fe/ZSM-5(PUC) was negatively influenced by the gas velocity due to the shortened residence time of gas reactants. The catalytic activity was more sensitive to the gas velocity at lower O₂ concentrations than at higher O₂ concentrations. The change in O₂ concentration showed less influence on HC conversion than on NO_x conversion, with the highest HC conversion consistently lower than 50%. However, the increase of the gas velocity decreased HC conversion significantly under current experimental conditions, likely due to the reduced gas residence time, which appears to be consistent with the result from the fixed bed reactor.



(a) NO_x conversion



(b) HC conversion

Figure 5.13 Effect of inlet O₂ concentration on NO_x and HC conversions (Fluidized bed, Fe/ZSM-5(PUC))

5.3.7 Comparison of ICFB reactor and fluidized bed reactor

Figure 5.14 compares the NO_x conversion in the fluidized bed reactor and the ICFB reactor. The results with $U_D=0.60$ and 1.20 m/s for the ICFB reactor were selected as the lower and upper bounds, because the NO_x conversion reached the lowest value at $U_D=0.6$ m/s and the highest at $U_D=1.20$ m/s. Although the ICFB reactor showed higher NO_x conversion (20~25% higher) than the fluidized bed at the same O_2 concentration (4%), the NO_x conversion in the ICFB reactor at high O_2 concentrations was still much lower than the fluidized bed with 1% O_2 only. This suggests that the ICFB reactor with Fe/ZSM-5(PUC) catalyst could improve the HC-SCR performance, but cannot completely eliminate the O_2 effect, as reflected by the significant negative impact of flue gas O_2 level on the overall NO_x conversion in the ICFB reactor.

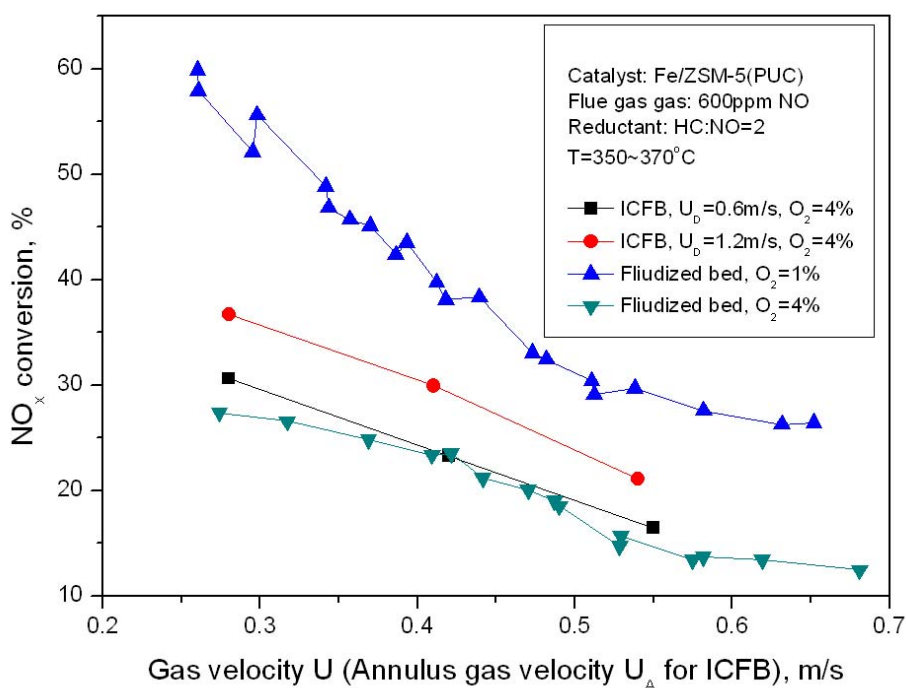


Figure 5.14 Comparison of NO_x conversion between ICFB and fluidized bed reactors (Fe/ZSM-5(PUC))

5.4 Performance of Fe/ZSM-5(Albemarle) catalyst

5.4.1 Effect of HC:NO molar ratio on NO_x and HC conversions

For the flue gas containing 4% O₂ and a draft tube gas velocity (U_D) of 0.6 m/s, the influence of HC:NO ratio on NO_x reduction was shown in Figure 5.15. It is very clear that as the HC:NO molar ratio increased from 1 to 4, NO_x conversion increased notably, especially when HC:NO increased from 2 to 4. At HC:NO=1, the injected HC was completely converted. When HC:NO reached 2, HC was almost completely converted to CO or CO₂ at a low U_A . However, as U_A increased to 0.42 m/s, HC conversion decreased quickly from 100% to 70%. The lowered HC conversion appeared to be directly related to the lowered NO_x conversion. Further increase of HC:NO from 2 to 4 led to even lower HC conversion.

As U_D increased from 0.6 to 0.9 m/s, as shown in Figures 5.15, 5.16 and 5.17, NO_x conversion increased, while HC conversion decreased. The increase in U_D increased the solids circulation rate, thus increasing the NO_x adsorption ratio in the annulus, leading to increased NO_x conversion. On the other hand, high U_D decreased the HC residence time in the draft tube, and thus lowered HC conversion. At $U_D=0.9$ m/s (Figure 5.17), HC conversion was lower than 50% for HC:NO=4, and the influence of HC:NO on NO_x conversion was not as significant as for the case with $U_D=0.60$ and 0.75 m/s.

It is observed that, at a given U_A , high NO_x conversions could be reached by either increasing the HC:NO molar ratio or increasing the gas velocity in the draft tube (U_D). In other words, a high U_D can be used to achieve the same NO_x conversion at a low HC:NO ratio. The same conclusion could be drawn from Figures 5.18 to 5.20 for flue gases with 8% O₂. It is also noticed that NO_x conversion became lower and HC conversion became higher as the flue gas O₂ concentration increased from 4 to 8%.

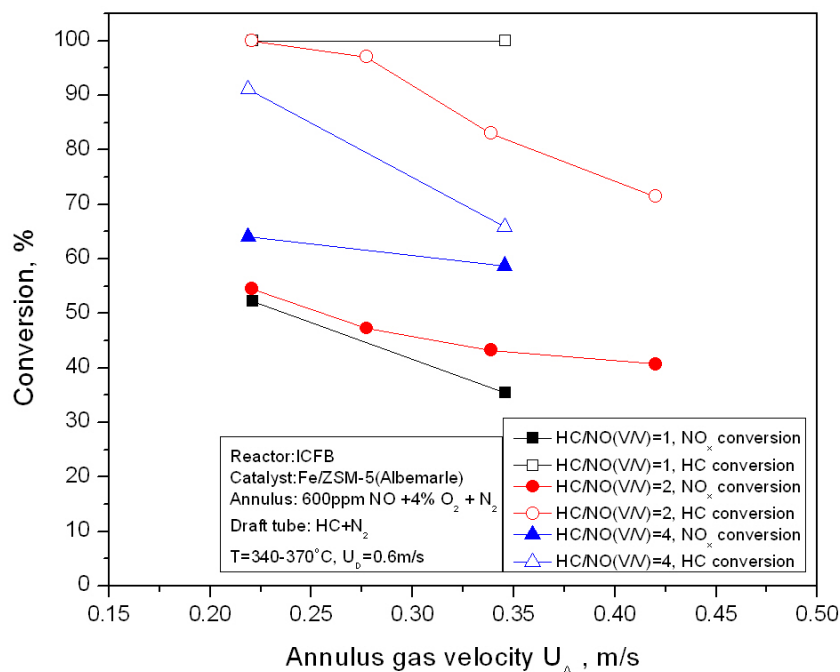


Figure 5.15 Effect of HC:NO ratio on NO_x and HC conversions (ICFB, Fe/ZSM-5(Albemarle), $U_D=0.6$ m/s, $[O_2]=4\%$)

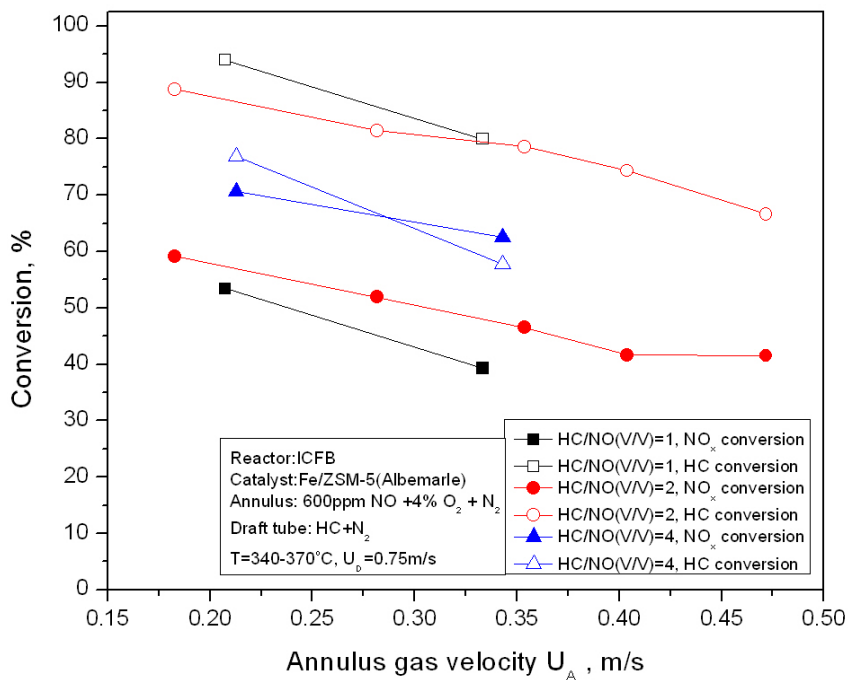


Figure 5.16 Effect of HC:NO ratio on NO_x and HC conversions (ICFB, Fe/ZSM-5(Albemarle), $U_D=0.75$ m/s, $[O_2]=4\%$)

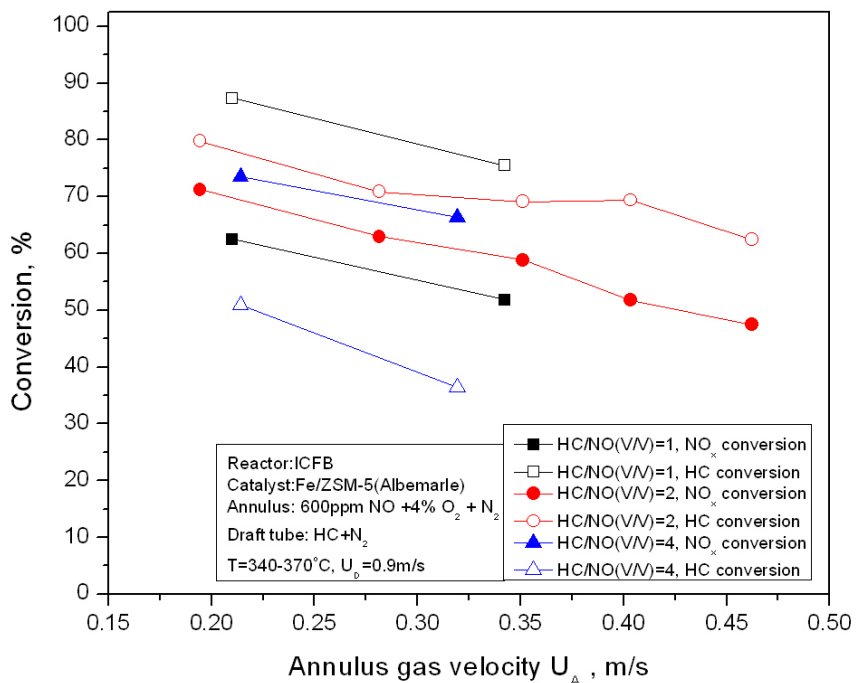


Figure 5.17 Effect of HC:NO ratio on NO_x and HC conversions (ICFB, Fe/ZSM-5(Albemarle), $U_D=0.9$ m/s, $[O_2]=4\%$)

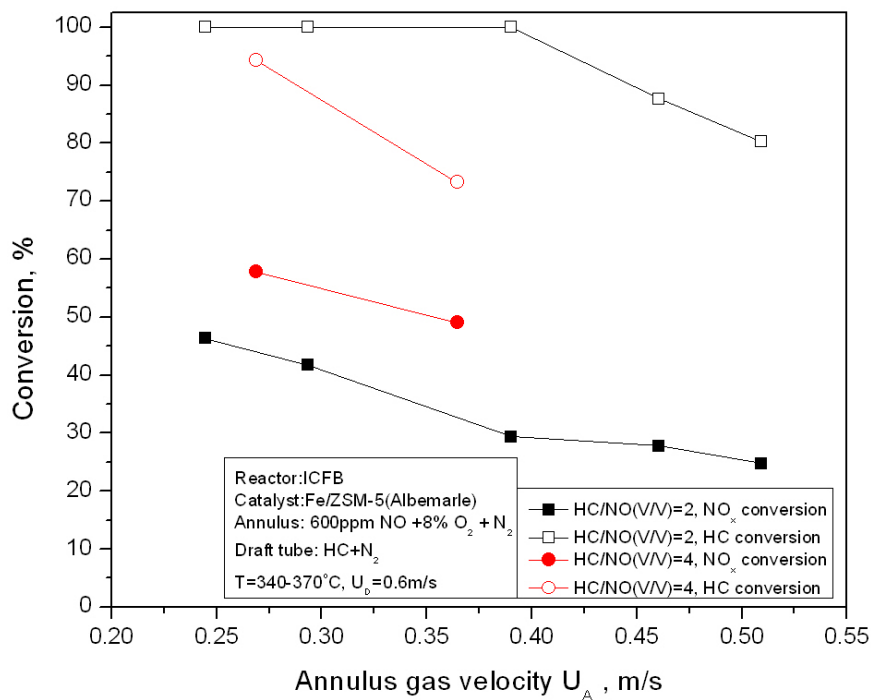


Figure 5.18 Effect of HC:NO ratio on NO_x and HC conversions (ICFB, Fe/ZSM-5(Albemarle), $U_D=0.6$ m/s, $[O_2]=8\%$)

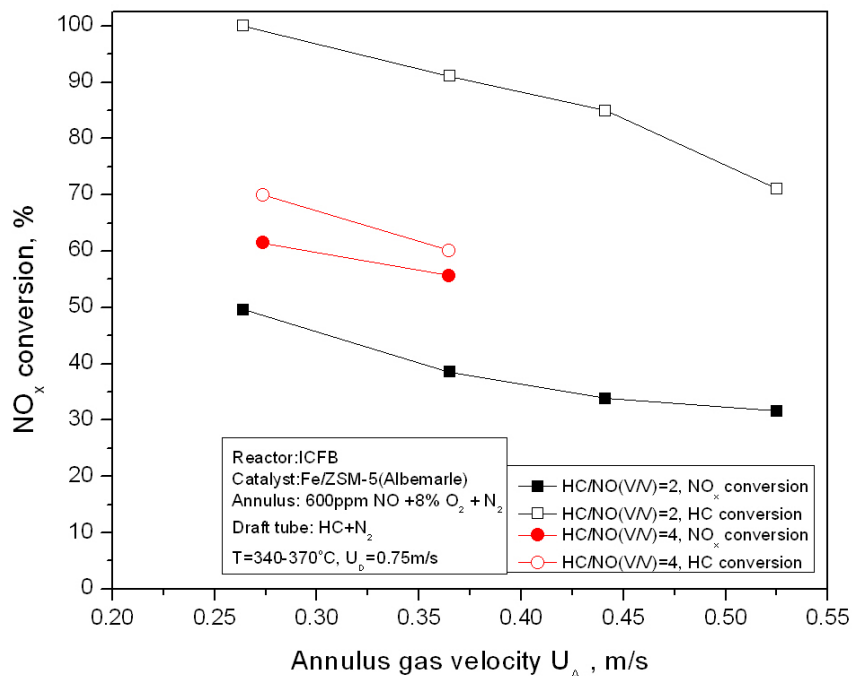


Figure 5.19 Effect of HC:NO ratio on NO_x and HC conversions (ICFB, Fe/ZSM-5(Albemarle), U_D=0.75 m/s, [O₂]=8%)

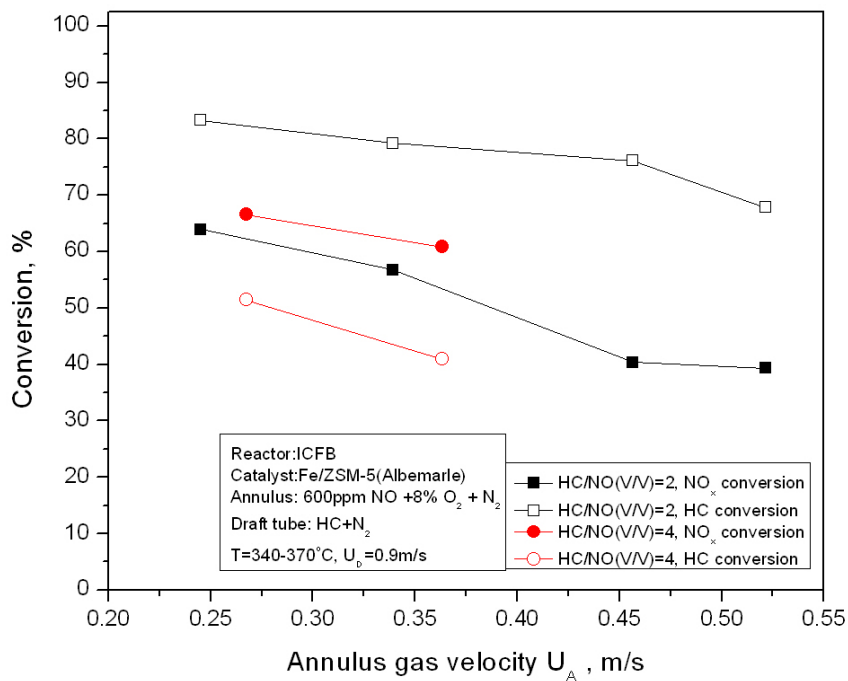


Figure 5.20 Effect of HC:NO ratio on NO_x and HC conversions (ICFB, Fe/ZSM-5(Albemarle), U_D=0.9 m/s, [O₂]=8%)

5.4.2 Effect of flue gas O₂ concentration on NO_x conversion and adsorption

The influence of flue gas O₂ concentration at the reactor inlet on NO_x conversion and adsorption with HC:NO=2 and U_D=0.6 m/s is shown in Figure 5.21. At a given U_A, NO_x adsorption ratio decreased when O₂ concentration increased from 4% to 8%, and the further increase of O₂ concentration from 8% to 12% showed little influence on NO_x adsorption. Correspondingly, NO_x conversion decreased with the increase in O₂ concentration. For a given HC:NO molar ratio, as the O₂ concentration in the flue gas increased, the O₂ concentration in the draft tube increased proportionally due to gas bypassing from the annulus to the draft tube. Therefore, more hydrocarbons were oxidized to CO₂ in the draft tube. As a result, more active sites on the catalyst were occupied by adsorbed CO₂ when the regenerated catalyst circulated back to the annulus region, which led to a decrease in the NO_x adsorption ratio. At a given O₂ concentration, NO_x adsorption ratio was always lower than NO_x conversion, except for 4% and 8% O₂ at U_A<0.25 m/s.

When U_D increased from 0.75 to 0.9 m/s, as shown in Figures 5.22 to 5.23, NO_x conversion was always higher than NO_x adsorption ratio under a given operating condition. The highest NO_x conversion and adsorption ratio were always reached at 4% O₂, and the increase of O₂ from 8% to 12% showed only marginal impact on both NO_x conversion and adsorption. On the other hand, NO_x adsorption ratio is seen to increase with increasing U_D, likely resulting from increased solids circulation rate.

In all cases, the difference of NO_x conversion between various flue gas O₂ contents decreased with increasing U_D, indicating that the increase of O₂ concentration exerted less negative impact on NO_x conversion at a higher U_D. In other words, higher U_D is preferred to maintain a high NO_x conversion by enhancing NO_x adsorption ratio when a flue gas with a high O₂ concentration is to be treated.

The fact that NO_x conversion was generally higher than NO_x adsorption ratio in most cases in Figures 5.21 to 5.23 indicated that the overall performance of the ICFB with Fe/ZSM-5(Albemarle) was limited by the relatively poor adsorption performance of the catalyst. Doping of other NO_x adsorbent, such as barium oxide, to the current Fe/ZSM-5(Albemarle) catalyst can probably further improve the adsorption performance and thus increase the NO_x conversion.

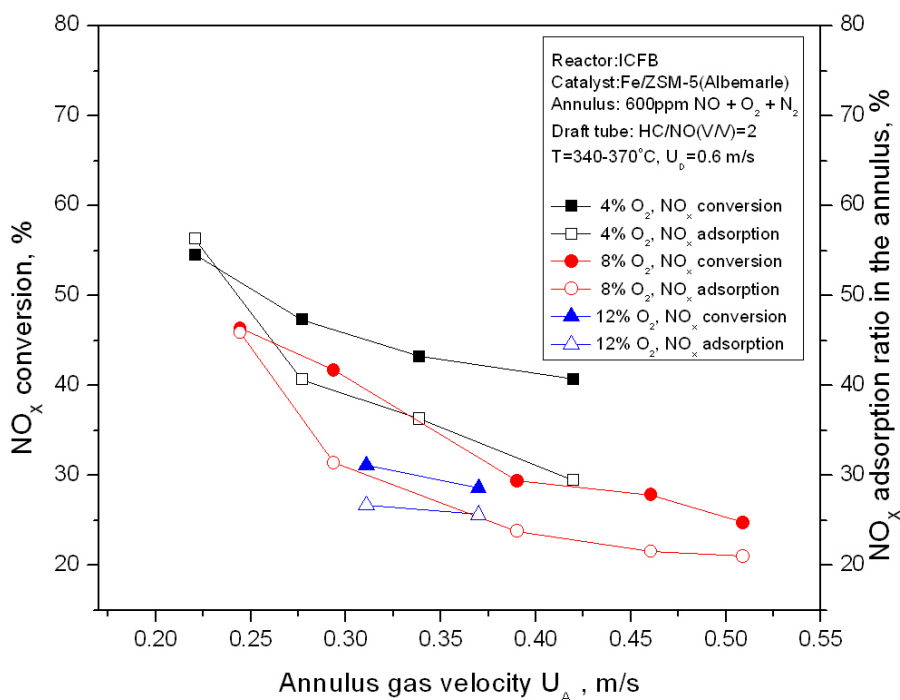


Figure 5.21 Effect of flue gas O₂ concentration on NO_x conversion and adsorption (ICFB, Fe/ZSM-5(Albemarle), U_D=0.6 m/s, HC:NO=2)

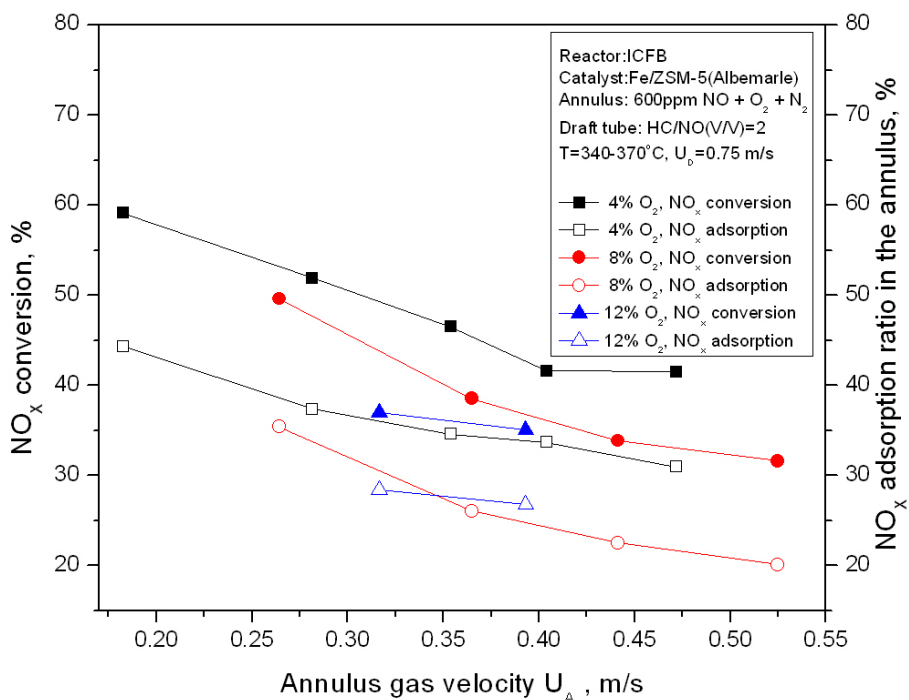


Figure 5.22 Effect of flue gas O₂ concentration on NO_x conversion and adsorption (ICFB, Fe/ZSM-5(Albemarle), U_D=0.75 m/s, HC:NO=2)

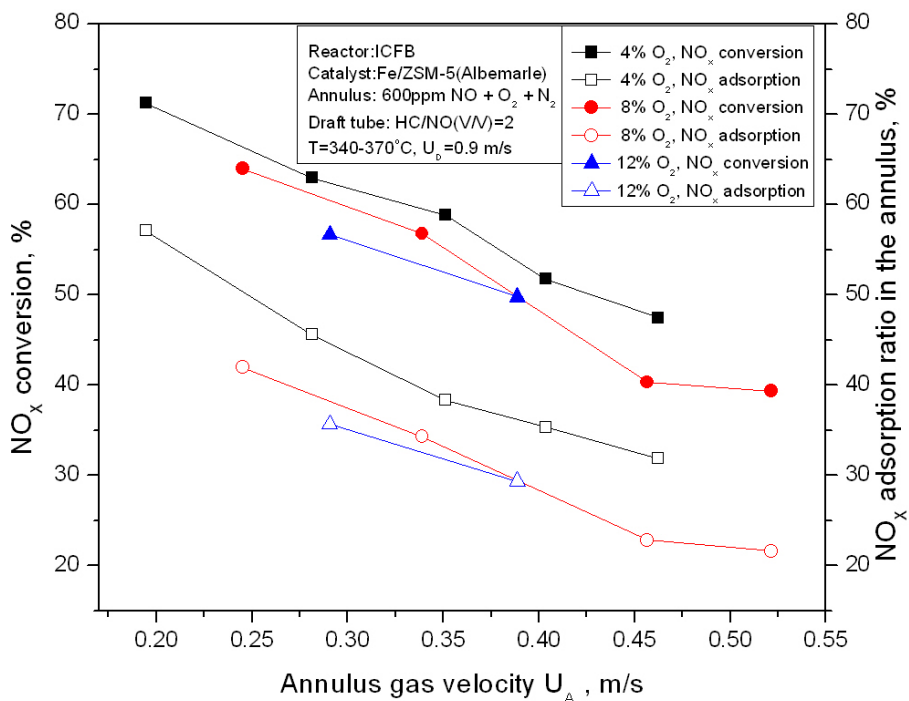


Figure 5.23 Effect of flue gas O₂ concentration on NO_x conversion and adsorption (ICFB, Fe/ZSM-5(Albemarle), U_D=0.9 m/s, HC:NO=2)

5.4.3 Effect of gas velocities on NO_x conversion and adsorption

The influence of gas velocities on NO_x conversion and adsorption is shown in Figure 5.24 with HC:NO=1, and Figure 5.25 with HC:NO=2 at a flue gas inlet O₂ concentration of 4%. It is seen that both U_A and U_D significantly influenced NO_x conversion and adsorption. In Figure 5.24, NO_x conversion increased monotonically with increasing U_D, while NO_x adsorption ratio first decreased as U_D increased from 0.6 to 0.75 m/s, and then increased as U_D further increased from 0.75 to 0.9 m/s. For HC:NO=2 (Figure 5.25), U_D showed more influence on NO_x conversion than on NO_x adsorption, although there is a lack of clear trend on the effect of U_D on NO_x adsorption. For both cases, NO_x conversion and adsorption ratio generally decreased with increasing U_A, and the influence of U_D on NO_x adsorption ratio was more significant at a low U_A than at a high U_A. For U_D=0.6 m/s (Figure 5.24) or U_D=0.45 m/s (Figure 5.25), NO_x conversion was approximately equal to the NO_x adsorption ratio, meaning that the adsorbed NO_x was completely converted by the catalyst in the draft tube. At high values of U_D, NO_x conversion was higher than the NO_x adsorption ratio, and their difference increased as U_D increased from 0.75 to 0.9 m/s in Figure 5.24 or from 0.6 to 1.05 m/s in Figure 5.25. One of possible explanations is that, at low draft tube gas velocities (U_D), when catalyst particles moved up the draft tube and left from the top outlet, they immediately dropped down to the annulus region without ejecting to the upper freeboard region. At a high U_D, particles leaving the draft tube might continue their upward movement, forming a “fountain” region, as in a spouted bed, which delayed the catalyst particles returning to the annulus region. As a result, NO_x escaping from the annulus adsorption region and the draft tube reaction region was reduced in the freeboard region due to the high solids holdup in the “fountain” region, creating the difference between the measured total NO_x conversion and the

adsorption ratio. The increase in gas velocity in the annulus region (U_A) decreased the contact time between the flue gas and the catalyst, leading to a decrease in the NO_x adsorption ratio, which, as a limiting step, reduced the overall NO_x conversion.

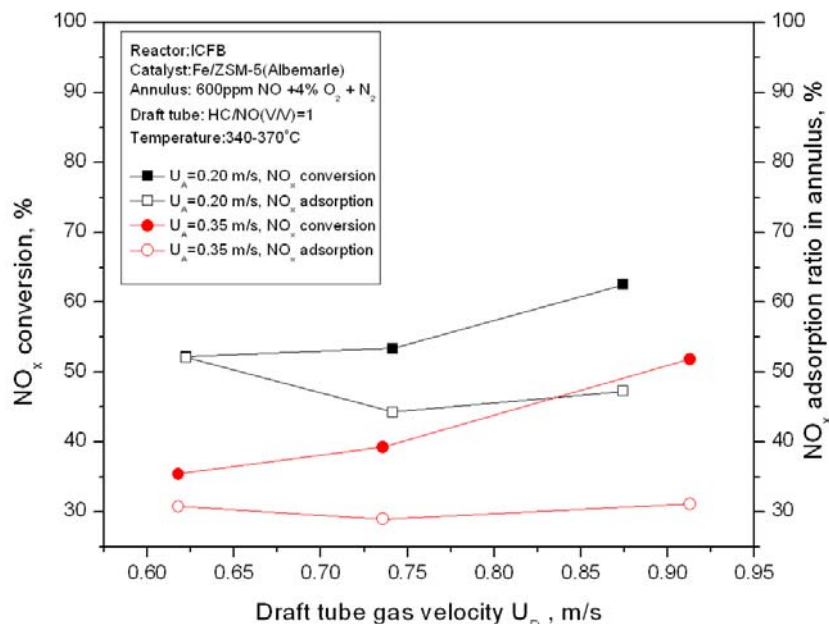


Figure 5.24 Effect of gas velocities on NO_x conversion and adsorption (ICFB, Fe/ZSM-5(Albemarle), $[\text{O}_2]=4\%$, HC:NO=1)

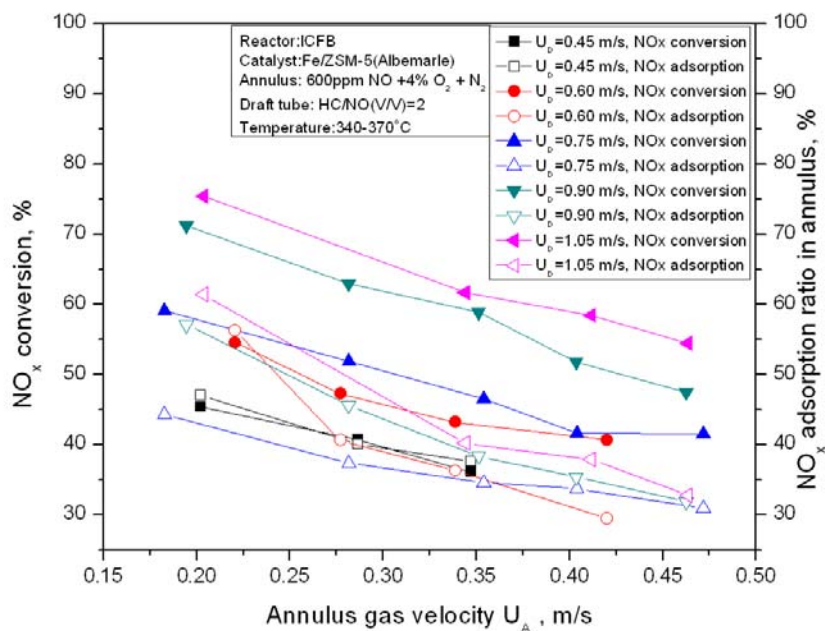


Figure 5.25 Effect of gas velocities on NO_x conversion and adsorption (ICFB, Fe/ZSM-5(Albemarle), $[\text{O}_2]=4\%$, HC:NO=2)

The influence of gas velocities on NO_x conversion and adsorption for 8% and 12% flue gas O_2 concentration is shown in Figures 5.26 and 5.27, respectively, both with $\text{HC:NO}=2$. U_A showed similar influence on NO_x conversion and adsorption ratio as at 4% O_2 . However, NO_x adsorption ratio showed a steady increase with increasing U_D . This further confirms the postulate that the high solids circulation rate at a high draft tube gas velocity, U_D , promotes NO_x adsorption in the annulus region because of lower NO_x concentration on the catalyst surface. Again, for the same reason described earlier, NO_x conversion was always higher than the adsorption ratio, especially at a high U_D . For $\text{O}_2=12\%$, the annulus gas velocity U_A had little influence on both NO_x conversion and adsorption ratio.

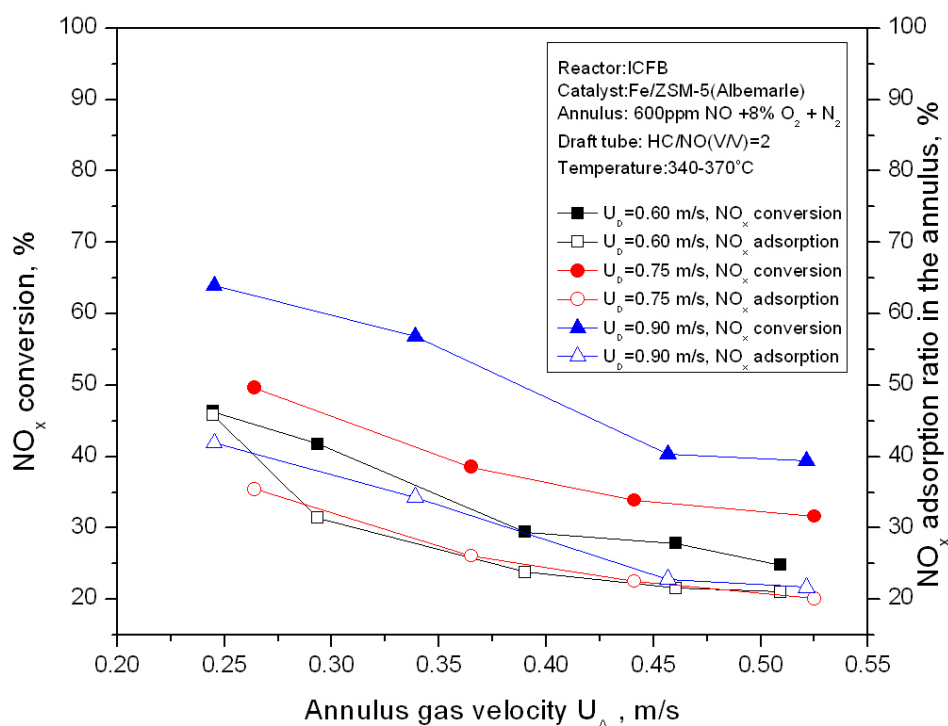


Figure 5.26 Effect of gas velocities on NO_x conversion and adsorption (ICFB, Fe/ZSM-5(Albemarle), $[\text{O}_2]=8\%$, $\text{HC:NO}=2$)

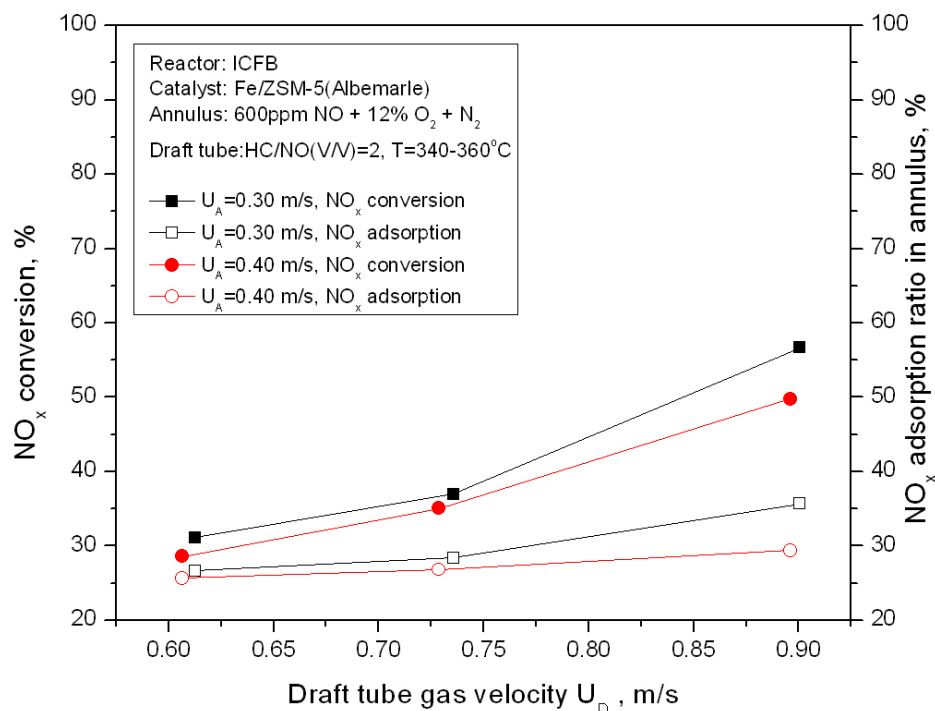


Figure 5.27 Effect of gas velocities on NO_x conversion and adsorption (ICFB, Fe/ZSM-5(Albemarle), [O₂]=12%, HC:NO=2)

5.4.4 Performance of the fluidized bed reactor with Fe/ZSM-5(Albemarle)

5.4.4.1 Effect of HC:NO ratio on NO_x and HC conversions

Figures 5.28 to 5.30 show that the gas velocity in the fluidized bed with Fe/ZSM-5(Albemarle) catalyst had less influence on NO_x conversion than with Fe/ZSM-5(PUC). Increasing HC:NO ratio had a positive impact on NO_x conversion but negative impact on HC conversion in all cases, especially at low gas velocities. For O₂=1% (Figure 5.28), NO_x conversion increased by ~10%, while HC conversion decreased by ~5% as the HC:NO ratio increased from 1 to 2. For O₂=4% (Figure 5.29), when HC:NO increased from 1 to 2, NO_x conversion increased to ~40% from less than 30%, while HC conversion decreased. Further increase of HC:NO from 2 to 4 gave 10% further increase of NO_x conversion and about a 5%

drop in HC conversion. A similar trend was observed when HC:NO increased from 1 to 2 at 8% O₂ (Figure 5.30).

As discussed previously for Fe/ZSM-5(PUC) catalyst, NO_x and HC conversions were significantly influenced by varying the gas velocity in the fluidized bed. Figures 5.28 to 5.30 show that NO_x conversion was enhanced with increasing gas velocity in the fluidized bed with Fe/ZSM-5(Albemarle) particles under most experimental conditions, contrary to the Fe/ZSM-5(PUC) catalyst where NO_x conversion decreased as the gas velocity increased. One possible explanation is that the interphase mass transfer between the bubble phase and the dense phase in the fluidized bed with fine Fe/ZSM-5(Albemarle) catalyst improved significantly due to increased solids holdup in the freeboard region as the gas velocity increased. As a result, NO_x conversion increased. Although HC conversion decreased with increasing gas velocity for Fe/ZSM-5 (Albemarle), the influence of the gas velocity on HC conversion was not as significant as for the Fe/ZSM-5(PUC) catalyst.

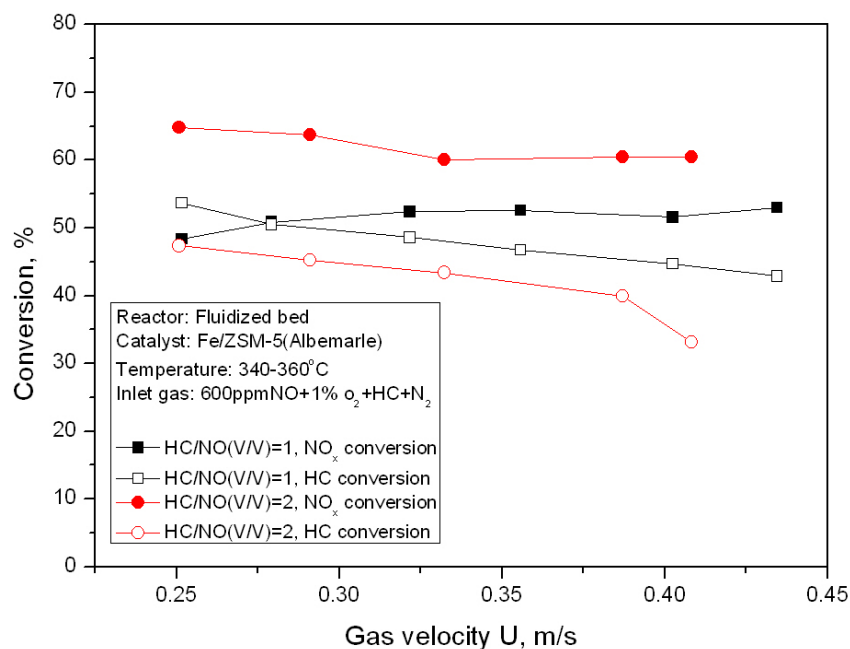


Figure 5.28 Effect of HC:NO ratio on NO_x and HC conversions (Fluidized bed, Fe/ZSM-5(Albemarle), [O₂]=1%)

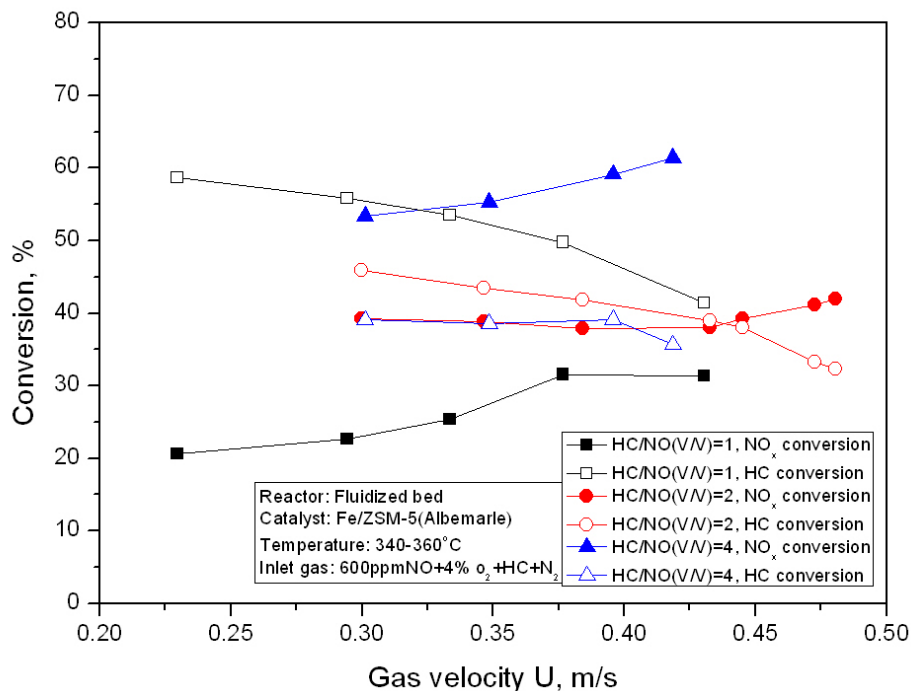


Figure 5.29 Effect of HC:NO ratio on NO_x and HC conversions (Fluidized bed, Fe/ZSM-5(Albemarle), [O₂]=4%)

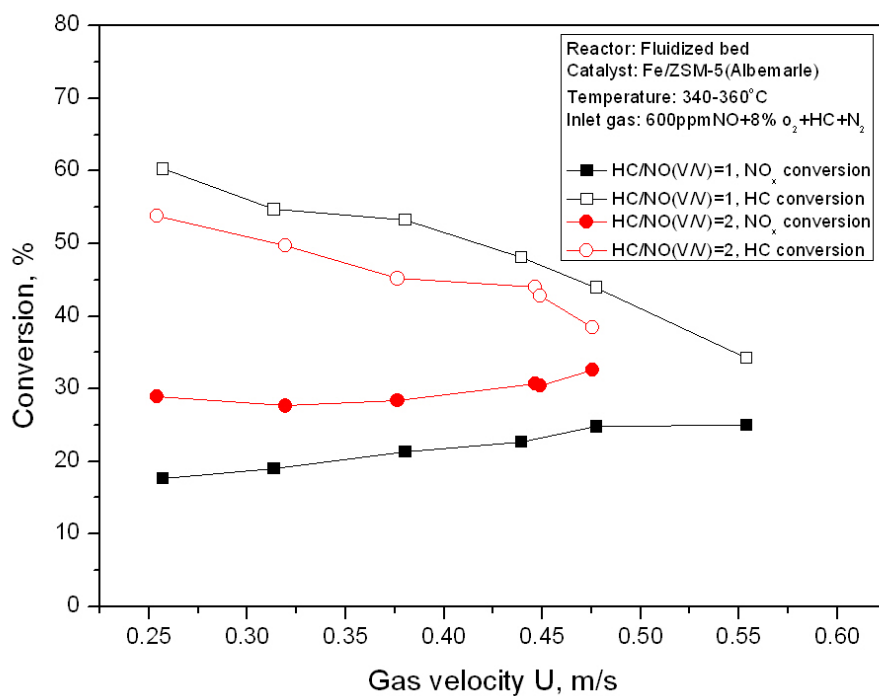


Figure 5.30 Effect of HC:NO ratio on NO_x and HC conversions (Fluidized bed, Fe/ZSM-5(Albemarle), [O₂]=8%)

5.4.4.2 Effect of O₂ concentration on NO_x and HC conversions

Figures 5.31 and 5.32 show that increasing the flue gas O₂ concentration had significant negative impact on NO_x conversion in the fluidized bed using Fe/ZSM-5(Albemarle) catalyst, where the increase of O₂ concentration could greatly reduce NO_x conversion with a slightly increased HC conversion. In Figure 5.31, at 1% O₂ and HC:NO=1, NO_x conversion reached around 51%, which was the same as obtained in the fixed bed experiment, but the HC conversion was much lower than in the fixed bed experiment. However, at O₂=4% and 8% and HC:NO=1, both NO_x and HC conversions in the fluidized bed were much lower than in the fixed bed. This means that the SCR performance of the Fe/ZSM-5(Albemarle) catalyst in the fluidized bed became worse than in the fixed bed when the reactor was operated at high O₂ concentrations with a low reductant-to-NO_x feed ratio. This is likely related to the existence of interphase mass transfer between the bubble and the dense phase in the fluidized bed and the reduced mean gas-solids contact time due to the gas bypass through bubbles. The increase in the gas velocity slightly enhanced NO_x reduction but decreased HC conversion at a given O₂ concentration. This could be explained by the improved interphase mass transfer, on one hand, and shortened contact time, on the other hand, as the gas velocity increased in the fluidized bed.

As HC:NO ratio increased from 1 to 2, as shown in Figure 5.32, the same trend was observed for the influence of O₂ concentration on NO_x and HC conversions as found in Figure 5.31. Although NO_x conversion was improved by 10% compared to HC:NO=1 at the same O₂ concentration, it was still 6-10% lower (for NO_x conversion) and 45~50% lower (for HC conversion) than that in the fixed bed. The increase of the gas velocity had no significant influence on NO_x conversion, but decreased the HC conversion at a given O₂ concentration.

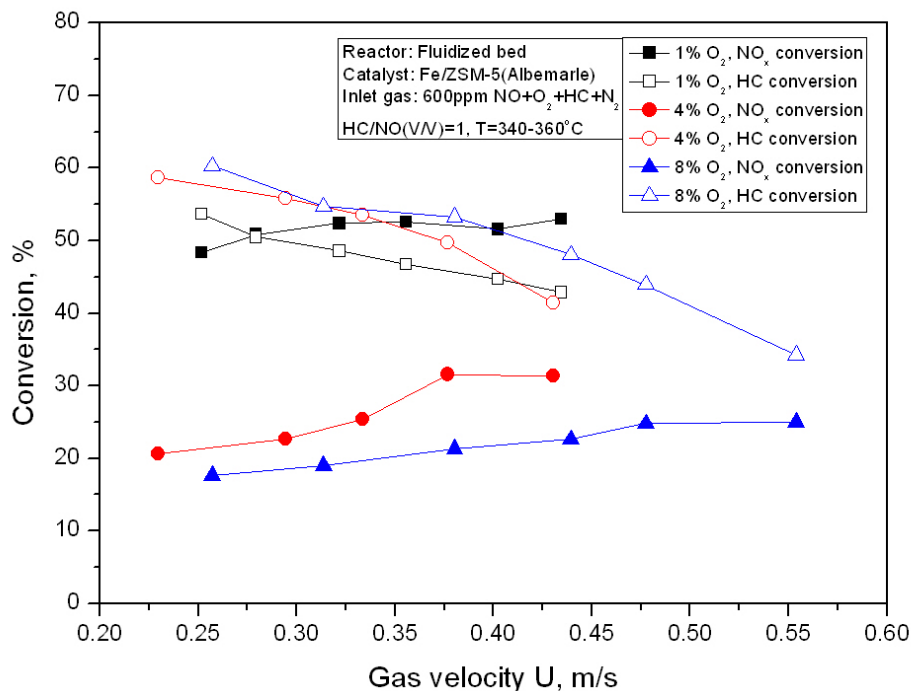


Figure 5.31 Effect of inlet O₂ concentration on NO_x and HC conversions (Fluidized bed, Fe/ZSM-5(Albemarle), HC:NO=1)

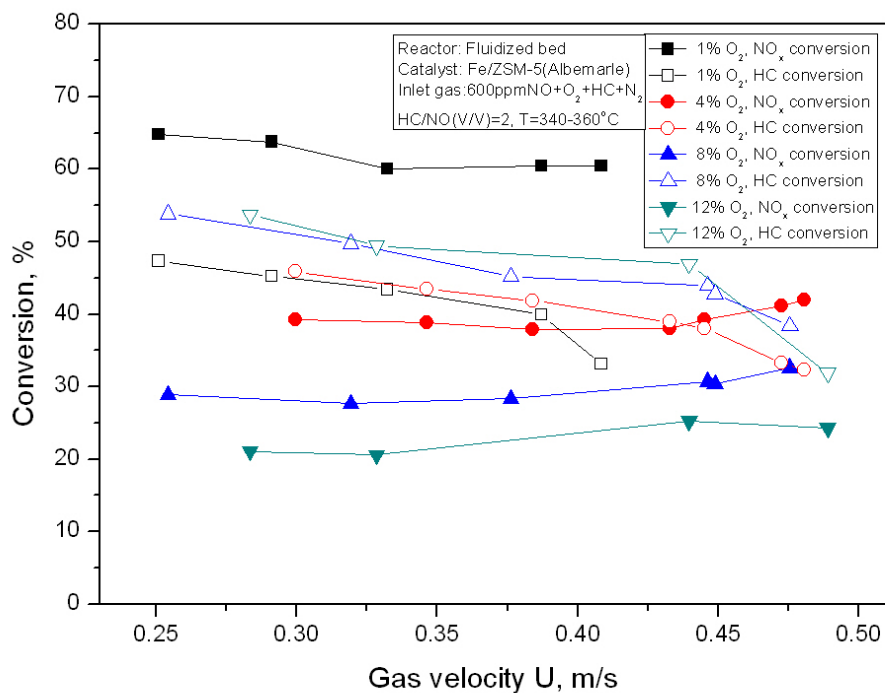


Figure 5.32 Effect of inlet O₂ concentration on NO_x and HC conversions (Fluidized bed, Fe/ZSM-5(Albemarle), HC:NO=2)

5.4.5 Comparison of reactor types

Figure 5.33 compares NO_x conversion in the fluidized bed reactor and the ICFB reactor. The results from the fluidized bed experiment with 1% and 4% O₂ were plotted. For the ICFB reactor, the conditions with U_D=0.45 and 1.05 m/s and O₂=4% were selected because they represented the lowest (U_D=0.45 m/s) and highest (U_D=1.05 m/s) NO_x conversion. NO_x conversions at U_D=0.9 m/s with O₂=8% and 12%, are also plotted.

When the ICFB reactor was operated at U_D=0.45 m/s which had a low solids circulation rate, the ICFB showed similar performance as the fluidized bed reactor with a NO_x conversion of ~40% for the flue gas with 4% O₂, which means that the ICFB reactor had no advantage if operated at a low U_D. When U_D increased to 1.05 m/s, ICFB showed much better performance than the fluidized bed, with the NO_x conversion close to, or even higher than achieved in the fluidized bed with a flue gas of only 1% O₂. At U_D=0.9 m/s, NO_x conversion for 8% and 12% O₂ in the ICFB reactor was 10% higher than that achieved in the fluidized bed for the flue gas with 4% O₂ content when U (or U_A) was lower than 0.4 m/s. This result clearly demonstrates the advantage of the ICFB reactor over the fluidized bed reactor for the treatment of flue gases containing excessive O₂, and proves that the dual-zone ICFB reactor can almost completely eliminate the negative impact imposed by the high flue gas O₂ concentration.

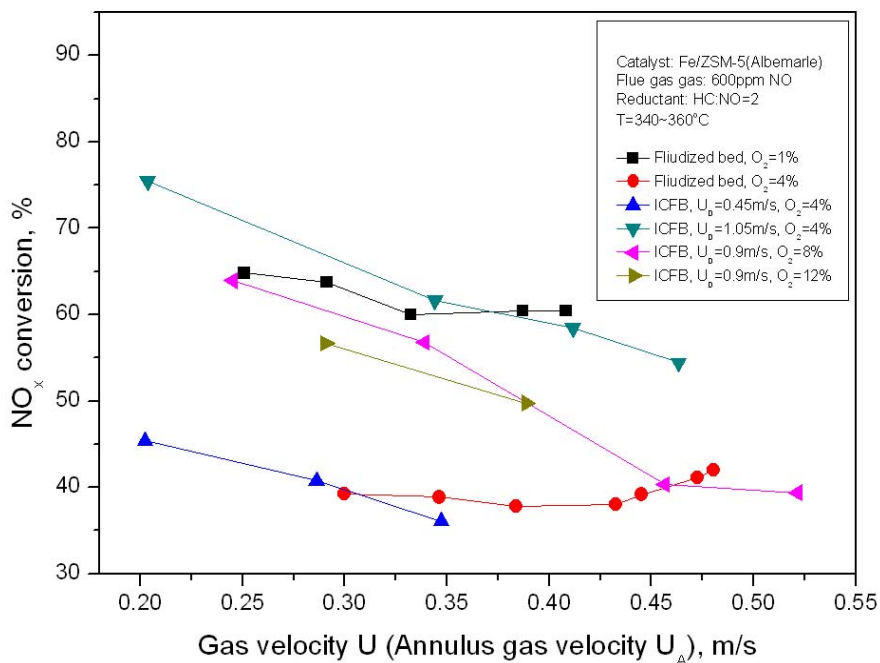


Figure 5.33 Comparison of NO_x conversion between ICFB and fluidized bed reactors (Fe/ZSM-5(Albemarle))

5.5 Summary

Experiments on the catalytic reduction of NO_x with propylene in the presence of excessive O_2 were carried out over Fe/ZSM-5(PUC) and Fe/ZSM-5(Albemarle) catalysts in the fluidized bed and ICFB reactor, respectively.

To pursue a better performance of the ICFB reactor for the reduction of NO_x , the annulus must be used as the adsorption zone and the draft tube as the reduction zone. Increasing the catalyst load will be of benefit to NO_x adsorption ratio as well as NO_x conversion in ICFB reactor.

Increasing the ratio of HC:NO improved the reduction performance of both Fe/ZSM-5(PUC) and Fe/ZSM-5(Albemarle) catalysts in both the fluidized bed and ICFB reactor. For both catalysts, at a given ratio of HC:NO, NO_x conversion decreased with increasing U_A in

the ICFB reactor. On the contrary, NO_x conversion increased with an increase of U_D . Using a higher U_D , the catalyst operated under a lower HC:NO ratio could reach the similar catalytic activity as that using a lower U_D but a higher HC:NO ratio.

NO_x conversion and adsorption ratio decreased with increasing U_A for both catalysts. NO_x conversion increased with increasing U_D because more particles were entrained into the gas mixture of the flue gas and the reductant gas, and formed a “fountain” in the freeboard region at higher U_D . In most cases, the NO_x conversion was lower than adsorption ratio for Fe/ZSM-5(PUC) which means that the catalytic activity was too low and could not match the adsorption performance. In contrast, the NO_x conversion was higher than the adsorption ratio for Fe/ZSM-5(Albemarle) meaning that the adsorption performance should be improved in order to fully utilize the catalytic activity of the catalyst.

Inlet NO concentration of the model flue gas had some impacts on NO_x conversion over Fe/ZSM-5(PUC) in the fluidized bed, because the change of NO_x concentration influences the ability of NO_x to be adsorbed by the catalyst in a fixed period of contact time (or gas velocity).

Lower O_2 concentration could greatly enhance the catalytic activity of both Fe/ZSM-5(PUC) and Fe/ZSM-5(Albemarle) in the fluidized bed, which agrees well with the findings in the fixed bed experiment from this study and other research groups.

The performance of Fe/ZSM-5(PUC) was not as good as in the fixed bed experiment. In contrast, Fe/ZSM-5(Albemarle) showed promising reduction performance and strong inhibiting ability on the negative impact of excessive O_2 in the ICFB reactor. Using Fe/ZSM-5(Albemarle), at the same gas velocity in the annulus of the ICFB reactor and the fluidized bed reactor, and HC:NO=2, the NO_x conversion in the ICFB reactor with the flue gas

containing 4% O₂ was higher than in the fluidized bed with the flue gas containing 1% O₂ if U_D=1.05 m/s was used in the ICFB reactor.

Chapter 6

Conclusions and Recommendations for Future Work

6.1 Conclusions

The objectives of this research were to identify the possible application of the integrated adsorption-reduction process for the selective catalytic reduction of NO_x with hydrocarbons (HC-SCR) over selected catalysts in an internal circulating fluidized bed. The adsorption and reaction performances of the selected catalysts were investigated in a fixed bed reaction system. Hydrodynamic studies were carried out in a cold model ICFB unit. The concept of the integrated adsorption-reduction process of NO_x was implemented by means of a hot model ICFB reactor, and the reactor performance was tested under various operating conditions. The following conclusions can be drawn.

6.1.1 Adsorption and reaction performance of Fe/ZSM-5 catalyst

The adsorption performance of Fe/ZSM-5 catalysts tested in this study is closely related to the particle size and the structure of the catalyst support. The fine Fe/ZSM-5(Albemarle) catalyst exhibited highest NO_x adsorption capacity. The presence of H_2O in the model flue gas flow had almost no effect on the adsorption capacity of Fe/ZSM-5(Albemarle). In contrast, a negative impact was observed when CO_2 was added into the flue gas, and the addition of H_2O into a CO_2 -containing flue gas slightly improved the adsorption performance of the Fe/ZSM-5(Albemarle) catalyst.

The catalytic activity of Fe/ZSM-5 was sensitive to the reaction temperature and space velocity. The catalyst deactivated very quickly at temperatures lower than 325°C

because of the deposit of graphitic carbon on the catalyst surface. Among tested catalysts, Fe/ZSM-5 prepared by IMPO method exhibited stable activity at $T \geq 350^\circ\text{C}$ and $\text{GHSV} = 5000 \text{ h}^{-1}$, and the reaction activity of the catalyst is not directly proportional to the adsorption capacity in the conventional HC-SCR process. A HC:NO molar ratio of 2 is recommended with the consideration of both the economic aspect and the reduction efficiency of NO_x .

O_2 concentration played an important role in the SCR of NO_x with propylene as the reducing agent. Fe/ZSM-5 exhibited acceptable activity when O_2 concentration was controlled at relatively low level ($\leq 1\%$). H_2O could slightly enhance the activity of Fe/ZSM-5(Albemarle) in HC-SCR, while CO_2 showed negligible effect. The catalyst could be permanently deactivated by SO_2 in HC-SCR, and only partial catalytic activity could be recovered via calcination at a high temperature.

6.1.2 Hydrodynamic study of the ICFB reactor

In the cold model experiment, both the flat and cylindrical distributors showed relatively narrow window of operating gas velocities, while the conical distributor exhibited flexible and stable operation in a wide range of velocities for both U_A and U_D . All three types of distributors showed very low gas bypass from the draft tube to the annulus but high gas bypass at the reverse direction. The increase of U_D could enhance R_{AD} while U_A showed less effect on R_{AD} . R_{AD} and R_{DA} were sensitive to the change of the effective gap opening between the draft tube and the annulus gas distributor. The solids circulation rate was determined by the combined effect of U_A and U_D for the conical and cylindrical gas distributors.

In the ICFB hot model experiment, R_{DA} increased with the increase of U_D , and R_{DA} was always higher than R_{AD} for both Fe/ZSM-5(PUC) and Fe/ZSM-5(Albemarle) catalysts.

At given U_A and U_D , the fine Fe/ZSM-5(Albemarle) gained higher R_{DA} but lower R_{AD} than the coarse Fe/ZSM-5(PUC). The gas bypass ratio of Fe/ZSM-5(PUC) from the annulus to draft tube (R_{AD}) reached a maximum value when the draft tube gas velocity (U_D) was 0.9~1.0 m/s in this study.

The difference in the gas bypass characteristics between the cold model and the hot model unit further shows that the reactor configuration could have a significant impact on the performance of the ICFB reactor.

6.1.3 Adsorption and reduction performance of Fe/ZSM-5 in the ICFB reactor

For both Fe/ZSM-5(PUC) and Fe/ZSM-5(Albemarle) catalysts, NO_x conversion and adsorption ratio decreased with the increase of U_A . NO_x conversion increased with the increase of U_D . At a high U_D , the catalyst operated at low HC:NO molar ratio could reach similar catalytic reactivity as that using a lower U_D but a higher HC:NO ratio. Increasing the HC:NO molar ratio improved the reduction performance in both the fluidized bed and the ICFB reactor. To obtain better catalytic activity, lower O_2 concentration is preferred in the fluidized bed.

The performance of Fe/ZSM-5(PUC) in the ICFB reactor was not as good as exhibited in the fixed bed experiment. In contrast, Fe/ZSM-5(Albemarle) showed promising reduction performance and great ability to inhibit the negative impact of excessive O_2 in the ICFB reactor. Using Fe/ZSM-5(Albemarle) catalyst, at the same gas velocity in the annulus of the ICFB reactor and the fluidized bed reactor, the NO_x conversion in the ICFB reactor with the flue gas containing 4% O_2 was higher than that in the fluidized bed with the flue gas containing 1% O_2 if $U_D=1.05$ m/s was used in the ICFB reactor. However, the adsorption

performance should be improved in order to further improve the catalytic activity of Fe/ZSM-5(Albemarle) catalyst.

Overall, this study shows that such an ICFB reactor exhibited the ability to overcome the negative impact of excessive O₂ in the flue gas using Fe/ZSM-5(Albemarle) as the deNO_x catalyst.

6.2 Recommendations for future work

Due to the complexity of HC-SCR process and the variation of the combustion flue gases, further study should be undertaken in the following aspects:

1. Although Fe/ZSM-5(Albemarle) catalyst showed acceptable catalytic activity in HC-SCR, its adsorption capacity is still not satisfactory according to the result from the hot model ICFB experiment. The impregnation of other metals, such as Ba, could improve the adsorption performance of Fe/ZSM-5(Albemarle). In addition, the catalytic activity of Fe/ZSM-5(Albemarle) was severely inhibited by SO₂. Therefore, new catalysts with good tolerance to SO₂ and hydrothermal stability need to be developed.
2. Other hydrocarbons, such as propane and i-butane, should be studied as reducing agents to compare their NO_x reduction performance with propylene.
3. More detailed investigation on the effect of H₂O, SO₂, CO₂ and the Fe loading on the catalyst performance should be conducted in the fixed bed experiment.
4. An in-situ gas chromatograph (GC) is needed for the measurement of the hydrocarbon, CO₂ and N₂O concentrations in order to evaluate the HC conversion more precisely and to monitor the conversion of NO_x to N₂O.

5. To minimize the experimental error, rotameters used in the fixed bed experiment should be replaced by mass flow meters for the better control of gas flow rates.
6. The solids circulation rate should be measured in the cold model unit using the annulus gas distributor with the same configuration as in the hot model unit and Fe/ZSM-5(Albemarle) or similar bed materials. The attrition of the catalyst should be examined as well.
7. Effect of H₂O, SO₂ and CO₂ on the reduction performance of Fe/ZSM-5(Albemarle) catalyst should be investigated in the hot model ICFB reactor.
8. The time-on-stream experiment should be performed using the real flue gases from a natural gas burner or a gasoline or diesel engine to evaluate the performance of the ICFB reactor.
9. As discussed previously, the ICFB reactor performance was limited by the catalyst adsorption capacity, because the overall NO_x conversion increased with decreasing gas velocity in the annulus. To promote the adsorption performance of the catalyst, a configuration with larger annulus cross-sectional area should be considered to decrease the annulus gas velocity (or increase the residence time) while keeping the annulus gas flux at a specific amount. For the same reason, the effect of the catalyst loading in the reactor should be investigated as well.
10. The gas bypass from the annulus to draft tube should be more flexible in order to control the O₂ concentration in the draft tube to a desired level. In light of this, other types of gas distributors and/or the relative position between the draft tube and gas nozzle should be investigated, and small diameter gas nozzles should be used to investigate the gas bypass from the draft tube to annulus, in order to minimize the bypass of the reductant gas to the annulus.

11. Temperature programmed desorption (TPD), in-situ electron paramagnetic resonance (EPR), in-situ Fourier transform infrared spectroscopy (FT-IR) or other methods should be performed to elucidate the nature of NO_x adsorption and reduction over Fe/ZSM-5(Albemarle) catalyst.
12. Based on the result from the cold model experiment and the reaction kinetics from fixed bed tests, a mathematical model of the ICFB reactor needs to be developed for the prediction of gas and solids flow structure in the ICFB reactor and the reactor performance for NO_x reduction.

References

- Abdulhamid, H.; Fridell, E.; Skoglundh, M. (2004). **Influence of the type of reducing agent (H_2 , CO , C_3H_6 and C_3H_8) on the reduction of stored NO_x in a $\text{Pt}/\text{BaO}/\text{Al}_2\text{O}_3$ model catalyst.** Topics Catal., 30/31, 161-168.
- Adams, K.M.; Cavataio, J.V.; Hammerle, R.H. (1996). **Lean NO_x catalysis for diesel passenger cars: Investigating effects of sulfur dioxide and space velocity.** Appl.Catal.B: Environ., 10, 157-181.
- Adelman, B. J.; Beutel, T.; Lei, G.-D.; Sachtler, W. M. H. (1996). **Mechanistic cause of hydrocarbon specificity over $\text{Cu}/\text{ZSM-5}$ and $\text{Co}/\text{ZSM-5}$ catalysts in the selective catalytic reduction of NO_x .** J. Catal., 158, 327-335.
- Adelman, B.J.; Sachtler, W.M.H. (1997). **The effect of zeolitic protons on NO_x reduction over $\text{Pd}/\text{ZSM-5}$ catalysts.** Appl. Catal., B: Environ., 14, 1-11.
- Amiridis, M.D.; Roberts, K.L.; Pereira, C.J. (1997). **The selective catalytic reduction of NO by propylene over Pt supported on dealuminated Y zeolite.** Appl. Catal., B: Environ., 14, 203-209.
- Amiridis, M.D.; Zhang, T.; Farrauto, R.J. (1996). **Selective catalytic reduction of nitric oxide by hydrocarbons.** Appl. Catal. B: Environ., 10, 203-227.
- Ando, S.; Maki, T.; Nakagawa, Y.; Namiki, N.; Emi, H.; Otani, Y. (2002). **Analysis of the drying process of seed particles in a spouted bed with a draft tube.** Advanced Powder Technol., 103(1), 73-91.
- Angelidis, T. N.; Christoforou, S.; Bongiovanni, A.; Kruse, N. (2002). **On the promotion by SO_2 of the SCR process over $\text{Ag}/\text{Al}_2\text{O}_3$: influence of SO_2 concentration with C_3H_6 versus C_3H_8 as reductant.** Appl. Catal., B: Environ., 39(3), 197-204.
- Armor, J.N. (1997). **Catalytic solutions to reduce pollutants.** Catal. Today, 38, 163-167.
- Armor, J.N.; Li, Y. (1995). **The effect of SO_2 on the catalytic performance of Co-ZSM-5 and Co-ferrierite for the selective reduction of NO by CH_4 in the presence of O_2 .** Appl. Catal., B: Environ., 5, L257-L270.
- Baerns, M.; Rottlander, C.; Andorf, R.; Plog, C.; Krutzsch B. (1996). **Selective NO reduction by propane and propene over a $\text{Pt}/\text{ZSM-5}$ catalyst: A transient study of the reaction mechanism.** Appl. Catal., B: Environ., 11, 49-63.
- Battiston, A.A.; Bitter, J.H.; Koningsberger, D.C. (2003). **Reactivity of binuclear Fe complexes in over-exchanged $\text{Fe}/\text{ZSM5}$, studied by in situ XAFS spectroscopy 2. Selective catalytic reduction of NO with isobutane** J. Catal., 218, 163-177.

- Beretta, A.; Orsenigo, C.; Ferlazzo, N.; Tronconi, E.; Forzatti, P.; Berti, F. (1998). **Analysis of the performance of plate-type monolithic catalysts for selective catalytic reduction DeNO_x applications.** *Ind. Eng. Chem. Res.*, 37, 2623-2633.
- Berndt, H.; Schutze, F.H.; Richter, M.; Sowade, T.; Grunert, W. (2003). **Selective catalytic reduction of NO under lean conditions by methane and propane over indium/cerium-promoted zeolites.** *Appl. Catal. B: Environ.*, 40, 51-67.
- Bogner, W.; Krämer, M.; Krutzsch, B.; Pischinger, S.; Voigtländer, D.; Wenninger, G.; Wirbeleit, F.; Brogan, M.S.; Brisley R.J.; Webster, D.E. (1995). **Removal of nitrogen oxides from the exhaust of a lean-tune gasoline engine.** *Appl. Catal. B: Environ.*, 7, 153-171.
- Boix, A.; Miro, E. E.; Lombardo, E. A.; Banares, M. A.; Mariscal, R.; Fierro, J. L. G. (2003). **The nature of cobalt species in Co and Pt-Co/ZSM5 used for the SCR of NO_x with CH₄.** *J. Catal.*, 217(1), 186-194.
- Bosch, H.; Janssen, F. (1988). **Catalytic reduction of nitrogen oxides. A review on the fundamentals and technology.** *Catal. Today*, 2(4), 369-521.
- Brilhac, J.F.; Sultana, A.; Gilot, P.; Martens, J.A. (2002). **Adsorption and pressure swing desorption of NO_x in Na-Y zeolite: Experiments and Modeling.** *Environ. Sci. Tech.*, 36, 1136-1140.
- Burch, R.; Halpin, E.; Sullivan, J.A. (1998). **A comparison of the selective catalytic reduction of NO_x over Al₂O₃ and sulphated Al₂O₃ using CH₃OH and C₃H₈ as reductants.** *Appl. Catal., B: Environ.*, 17, 115-129.
- Burch, R.; Ottery, D. (1996a). **Selective catalytic reduction of NO_x by hydrocarbons on Pt/Al₂O₃ catalysts at low temperatures without the formation of N₂O.** *Appl. Catal., B: Environ.*, 9, L19-L24.
- Burch, R.; Scire, S. (1994). **Selective catalytic reduction of nitric oxide with ethane and methane on some metal exchanged ZSM-5 zeolites.** *Appl. Catal. B: Environ.*, 3, 295-318.
- Burch R.; Watling, T.C. (1996b). **Adsorbate-assisted NO decomposition in NO reduction by C₃H₆ over Pt/Al₂O₃ catalysts under lean-burn conditions.** *Catal. Lett.*, 37, 51-55.
- Bustamante, F.; Cordoba, F.; Yates, M.; Correa, C. (2002). **The promotion of cobalt mordenite by palladium for the lean CH₄-SCR of NO_x in moist streams.** *Appl. Catal., A: General*, 234, 127-136.
- Campa, M.C.; De Rossi, S.; Ferraris, G.; Indovina, V. (1996) **Catalytic activity of Co-ZSM-5 for the abatement of NO_x with methane in the presence of oxygen.** *Appl. Catal., B: Environ.*, 8(3), 315-331.
- Cant, N.W.; Liu, I.O.Y. (2000). **The mechanism of the selective reduction of nitrogen oxides by hydrocarbons on zeolite catalysts.** *Catal. Today*, 63, 133-146.

- Capek, L.; Vradman, L.; Sazama, P.; Herskowitz, M.; Wichterlova, B.; Zukerman, R.; Brosius, R.; Martens, J.A. (2007). **Kinetic experiments and modeling of NO oxidation and SCR of NO_x with decane over Cu- and Fe -MFI catalysts.** Appl. Catal., B: Environ., 70(1-4), 53-57.
- Captain, D. K.; Amiridis, M. D. (1999). **In situ FTIR studies of the selective catalytic reduction of NO by C₃H₆ over Pt/Al₂O₃.** J. Catal., 184(2), 377-389.
- Captain, D. K.; Roberts, K.L.; Amiridis, M. D. (1998). **The selective catalytic reduction of nitric oxide by propylene over Pt/SiO₂.** Catal. Today, 42, 93-100.
- Centi, G.; Generali, P.; dall'Olio, L.; Perathoner, S. (2000). **Removal of N₂O from industrial gaseous streams by selective adsorption over metal-exchanged zeolites.** Ind. Eng. Chem. Res., 39, 131-137
- Chen, H.Y.; Sachtler, W. M. H. (1998a). **Activity and durability of Fe/ZSM-5 catalysts for lean burn NO_x reduction in the presence of water vapor.** Catal. Today, 42(1-2), 73-83.
- Chen, H.Y.; Voskoboinikov, T.; Sachtler, W. M. H. (1998b). **Reduction of NO_x over Fe/ZSM-5 catalysts: Adsorption complexes and their reactivity toward hydrocarbons.** J. Catal., 180(2), 171-183.
- Chen, H.Y.; Voskoboinikov, T.; Sachtler, W. M. H. (1999). **Reduction of NO_x over Fe/ZSM-5 catalysts: Mechanistic causes of activity differences between alkanes.** Catal. Today, 54, 483-494.
- Chen, H.Y.; Wang, X.; Sachtler, W. M. H. (2000a). **Reduction of NO_x over zeolite MFI supported iron catalysts: Nature of active sites.** Phys. Chem. Chem. Phys., 2(13), 3083-3090.
- Chen, H.Y.; Wang, X.; Sachtler, W.M.H. (2000b). **Reduction of NO_x over various Fe/zeolite catalysts.** Appl. Catal. A: General, 194/195, 159-168
- Chin, Y.-H.; Pisanu, A.; Serventi, L.; Alvarez, W. E.; Resasco, D. E. (1999). **NO reduction by CH₄ in the presence of excess O₂ over Pd/sulfated zirconia catalysts.** Catal. Today, 54(4), 419-429.
- Cho, B.K. (1997). **Activity normalization for lean-NO_x catalysts.** Appl. Catal. B: Environ., 12, 147-160.
- Cho, B. K.; Blint, R. J.; Subbiah, A. (2003). **Hydrothermally stable catalyst for improved lean NO_x reduction,** Eur. Pat. Appl., EP 1304165, 12 pp.
- Cho, B.K.; Yie, J.E.; Rahmoeller, K.M. (1995). **Autonomous kinetic oscillations during NO + C₂H₄ + O₂ reaction over Pt-ZSM-5 under highly oxidizing conditions.** J. Catal., 157, 14-24.

- Corma, A.; Fornes V.; Palomares E. (1997). **Selective catalytic reduction of NO_x on Cu-beta zeolites.** Appl. Catal., B: Environ., 11, 233-242.
- Cowan, A.D.; Dumpelmann, R.; Cant, N.W. (1995). **The rate-determining step in the selective reduction of nitric-oxide by methane over a Co-ZSM5 catalyst in the presence of oxygen.** J. Catal., 151, 356-363.
- Decyk, P.; Kim, D.K.; Woo, S.I. (2001). **Poisoning effect of SO₂ on NO reduction by i-butane over Fe/ZSM-5 prepared by sublimation method.** J. Catal., 203 (2), 369-374.
- Delahay, G.; Ensuque, E.; Coq, B.; Figueras, F. (1998). **Selective catalytic reduction of nitric oxide by n-decane on Cu/sulfated-zirconia catalysts in oxygen rich atmosphere: Effect of sulfur and copper contents.** J. Catal., 175, 7-15.
- Delahay, G.; Guzman-Vargas, A.; Coq, B. (2007). **Deactivation of a Fe-ZSM-5 catalyst during the selective catalytic reduction of NO by n-decane: An operando DRIFT study.** Appl. Catal., B: Environ., 70(1-4), 45-52.
- Delahay, G.; Valade, D.; Guzman-Vargas, A.; Coq, B.. (2005). **Selective catalytic reduction of nitric oxide with ammonia on Fe-ZSM-5 catalysts prepared by different methods.** Appl. Catal., B: Environ., 55, 149-155.
- De Lucas, A.; Valverde, J.L.; Dorado, F.; Romero, A.; Asencio, I. (2005). **Influence of the ion exchanged metal (Cu, Co, Ni and Mn) on the selective catalytic reduction of NO_x over mordenite and ZSM-5.** J. Mol. Catal. A: Chem., 225, 47-58.
- de Nevers, N. (2000). **Air pollution control engineering.** 2nd ed. McGraw-Hill Higher Education. 439-470.
- Desai, A. J.; Kovalchuk, V. I.; Lombardo, E. A.; D'Itri, J. L. (1999). **Co/ZSM-5: why this catalyst selectively reduces NO_x with methane.** J. Catal. , 184(2), 396-405.
- Efthimiadis, E.A.; Lappas, A.A.; Iatrides, D.K.; Vasalos, I.A. (2001). **Selective catalytic reduction of NO_x by hydrocarbons/oxygenates. Application for the control of NO_x from the regenerator of a fluid catalytic cracking pilot-plant unit.** Ind. Eng. Chem. Res., 40, 515-521.
- Efthimiadis, E. A.; Lionta, G. D.; Christoforou, S.C.; Vasalos, I.A. (1998). **The effect of CH₄, H₂O and SO₂ on the NO reduction with C₃H₆.** Catal. Today, 40, 15-26.
- Elkaim, D.; Bai, D. (2000). **Selective catalytic reduction of nitrogen oxides.** Canadian Patent Appl., CA 2,249,708, 46 pages.
- Epling, W. S.; Campbell, G. C.; Parks, J. E. (2003). **The effects of CO₂ and H₂O on the NO_x destruction performance of a model NO_x storage/reduction catalyst.** Catal. Lett., 90, 45-56.

- Feng, X.; Hall, W.K. (1996). **On the unusual stability of overexchanged Fe-ZSM-5.** Catal. Lett., 41, 45-46.
- Feng, X.; Hall, W. K. (1997a). **FeZSM-5: A durable SCR catalyst for NO_x removal from combustion streams.** J. Catal., 166, 368-376.
- Feng, X.; Hall, W.K. (1997b). **Limitations on the formation of oxygen-bridged divalent cations in FeZSM-5.** Catal. Lett., 46, 11-16.
- Forzatti, P. (2001). **Present status and perspectives in De-NO_x SCR catalysis.** Appl. Catal., A: General, 222, 221-236.
- Freitas, L.A.P; Freire, J.T. (2001). **Gas-to-particle heat transfer in the draft tube of a spouted bed.** Drying Tech., 19(6), 1065-1082.
- Fridell, E.; Skoglundh, M.; Westerberg, B.; Johansson, S.; Smedler, G. (1999). **NO_x storage in barium-containing catalysts.** J. Catal., 183, 196-209.
- Fritz, A.; Pitchon, V. (1997). **The current state of research on automotive lean NO_x catalysis.** Appl. Catal. B: Environ., 13, 1-25.
- Fusey, I.; Lim, C.J.; Grace, J.R. (1986). **Fast fluidization in a concentric circulating bed. in Circulating Fluidized Bed Technology II** (P. Basu ed.) Pergamon Press, Oxford, pp.409-416.
- Gao, S.; Nakagawa, N.; Kato, K.; Inomata, M.; Tsuchiya, F. (1996). **Simultaneous SO₂/NO_x removal by a powder-particle fluidized bed.** Catal. Today, 29, 165-169.
- Gao, Z.X.; Sun, Q.; Sachtler, W.M.H. (2001). **Adsorption complexes of O₂ on Fe/MFI and their role in the catalytic reduction of NO_x.** Appl. Catal., B: Environ., 33, 9-23.
- Garcia-Cortes, J.M.; Perez-Ramirez, J.; Illan-Gomez, M.J.; Kapteijn, F.; Moulijn, J.A.; Salinas-Martinez de Lecea, C. (2001). **Comparative study of Pt-based catalysts on different supports in the low-temperature de-NO_x-SCR with propene.** Appl. Catal., B: Environ., 30(3,4), 399-408.
- Garcia-Cortes, J. M.; Perez-Ramirez, J.; Illan-Gomez, M. J.; Kapteijn, F.; Moulijn, J. A.; De Lecea, C. S.M. (2000). **Effect of the support in de-NO_x HC-SCR over transition metal catalysts.** React. Kinet. Catal. Lett., 70(2), 199-206.
- Garcia-Cortes, J. M.; Perez-Ramirez, J.; Rouzaud, J.N.; Vaccaro, A.R.; Illan-Gomez, M. J.; De Lecea, C. S.M. (2003). **On the structure sensitivity of denox HC-SCR over Pt-beta catalysts.** J. Catal., 218, 111-122.
- Gerlach, T.; Illgen, U.; Bartoszek, M.; Baerns, M. (1999). **Reduction of nitrogen dioxide by propene over acidic mordenites: influence of acid site concentration, formation of by-products and mechanism.** Appl. Catal., B: Environ., 22, 269-278.

- Gilot P.; Guyon, M.; Stanmore, B.R. (1997). **A review of NO_x reduction on zeolitic catalysts under diesel exhaust conditions.** *Fuel*, 76(6), 507-515.
- Gomez, S. A.; Campero, A.; Martinez-Hernandez, A. ; Fuentes, G. A. (2000). **Changes in Cu²⁺ environment upon wet deactivation of Cu-ZSM-5 deNO_x catalysts.** *Appl. Catal. A: General*, 197, 157-164.
- Goralski, C.T.; Schneider, W.F. (2002). **Analysis of the thermodynamic feasibility of NO_x decomposition catalysis to meet next generation vehicle NO_x emissions standards.** *Appl. Catal., B: Environ.*, 37(4), 263–277.
- Goursot, A.; Coq, B.; Fajula, F. (2003). **Toward a molecular description of heterogeneous catalysis: transition metal ions in zeolites.** *J. Catal.*, 216, 324-332.
- Gutierrez, L.; Boix, A.; Petunchi, J.O. (1998). **Promoting effect of Pt on Co-zeolites upon the SCR of NO_x.** *J. Catal.*, 179(1), 179-191.
- Hall, W.K.; Feng, X.; Dumesic, J.; Watwe, R. (1998). **Problems in preparation of Fe/ZSM-5 catalysts.** *Catal. Lett.*, 52, 13-19.
- Ham, S.W.; Nam, I.S. (2002). **Selective Catalytic Reduction of Nitrogen Oxides by Ammonia.** *Catalysis (The Royal Society of Chemistry)*, Vol.16, 236-271.
- Hamada, H.; Kintaichi, Y.; Inaba, M.; Haneda, M.; Sato, K.; Fujimoto, T.; Kanai, S. (1997). **Catalytic performance of silver ion-exchanged saponite for the selective reduction of nitrogen monoxide in the presence of excess oxygen.** *Appl. Catal., B: Environ.*, 13, 27-33.
- Hammache, S.; Evans, L.R.; Coker, E.N.; Miller, J.E. (2008). **Impact of copper on the performance and sulfur tolerance of barium-based NO_x storage-reduction catalysts.** *Appl. Catal., B: Environ.*, 78(3-4), 315-323.
- Heinisch, R.; Jahn, M.; Langohr, J.; Pohl, M. (2001). **Modeling of a fixed bed reactor and kinetic investigations for the catalytic reduction of nitrogen oxides with methane.** *Chem. Eng. Technol.*, 24(4), 381-386.
- Henderson M.A.; Szanyi J.; Peden C.H.F. (2003). **Conversion of N₂O to N₂ on TiO₂(110).** *Catal. Today*, 85, 251-266.
- Hodjati, S.; Bernhardt, P.; Petit, C.; Pitchon, V.; Kiennemann, A. (1998a). **Removal of NO_x: Part I. Sorption/desorption processes on barium aluminate.** *Appl. Catal., B: Environ.*, 19, 209-219.
- Hodjati, S.; Bernhardt, P.; Petit, C.; Pitchon, V.; Kiennemann, A. (1998b). **Removal of NO_x: Part II. Species formed during the sorption/desorption processes on barium aluminates.** *Appl. Catal., B: Environ.*, 19, 221-232.
- Hums E. (1998). **Is advanced SCR technology at a standstill? A provocation for the academic community and catalyst manufacturers.** *Catal. Today*, 42, 25-35.

- Hayes, N.W.; Joyer, R.W.; Shpiro, E.S. (1996). **Infrared spectroscopy studies of the mechanism of the selective reduction of NO_x over Cu-ZSM-5 catalysts.** *Appl. Catal., B: Environ.*, 8, 343-363.
- Inui, T.; Iwamoto, S.; Kojo, S.; Shimizu, S.; Hirabayashi, T. (1994). **Removal of nitric oxide on metallosilicate catalysts.** *Catal. Today*, 22, 41-57.
- Inui, T.; Iwamoto, S.; Kon, S.; Sakimon, T.; Kagawa, K. (1997). **Evidently advantageous features of metallosilicates as the catalysts for elimination of NO in the exhaust gases containing a large excess of O₂ and H₂O.** *Catal. Today*, 38, 169-174.
- Ishikura, T.; Nagashima, H.; Ide, M. (2003). **Hydrodynamics of a spouted bed with a porous draft tube containing a small amount of finer particles.** *Powder Technol.*, 131, 56-65.
- Iwamoto, M.; Hernandez, A. M.; Zengyo, T. (1997). **Oxidation of NO to NO₂ on a Pt-MFI zeolite and subsequent reduction of NO_x by C₂H₄ on an In-MFI zeolite: a novel de-NO_x strategy in excess oxygen.** *Chem. Comm.*, 37-38.
- Iwamoto, M.; Takeda, H. (1996). **Pulse study on reactivity of ethane adsorbed on Cu-MFI with nitrogen oxides and oxygen.** *Catal. Today*, 27, 71-78.
- Iwamoto, M.; Yahiro, H.; Tanda, K. (1988). **Successful design of catalysts.** Inui, T., ed., Elsevier, Amsterdam, p. 219.
- Iwamoto, M.; Yahiro, H.; Yuu, Y.; Shundo, S.; Mizuno, N. (1990). **Selective reduction of NO by lower hydrocarbons in the presence of O₂ and SO₂ over copper ion-exchanged zeolites.** *Shokubai*, 32(6), 430-433.
- Iwamoto M.; Zengyo, T.; Hernandez, A.M.; Araki, H. (1998). **Intermediate addition of reductant between an oxidation and a reduction catalyst for highly selective reduction of NO in excess oxygen.** *Appl. Catal. B: Environ.*, 17, 259-266.
- James, D.; Fourre, E.; Ishii, M.; Bowker, M. (2003). **Catalytic decomposition / regeneration of Pt/Ba(NO₃)₂ catalysts: NO_x storage and reduction.** *Appl. Catal., B: Environ.*, 45(2), 147-159.
- Javed, M.T.; Irfan, N.; Gibbs, B.M. (2007). **Review: Control of combustion-generated nitrogen oxides by selective non-catalytic reduction.** *J. Environ. Manag.*, 83, 251-289.
- Jen, H.W. (1998). **Study of nitric oxide reduction over silver/alumina catalysts under lean conditions: Effects of reaction conditions and support.** *Catal. Today*, 42, 37-44.
- Jeong, S.M.; Kim, S.D. (2000). **Removal of NO_x and SO₂ by CuO/γ-Al₂O₃ sorbent/catalyst in a fluidized-bed reactor.** *Ind. Eng. Chem. Res.*, 39, 1911-1916.

- Jeong, S.K.; Park, T.S.; Hong, S.C. (2001). **Simultaneous SO_x/NO_x removal in a fluidized bed reactor using natural manganese ore.** J. Chem. Technol. Biotechnol., 76, 1080-1084.
- Joyner, R.; Stockenhuber, M. (1997). **Unusual structure and stability of iron-oxygen nano- clusters in Fe-ZSM-5 catalysts.** Catal. Lett., 45, 15-19.
- Joyner, R.; Stockenhuber, M. (1999). **Preparation, Characterization, and performance of Fe-ZSM-5 catalysts.** J. Phys. Chem. B, 103, 5963-5976.
- Kagawa, K.; Ichikawa Y.; Iwamoto S.; Inui T. (1998). **Broadening of the effective temperature range for NO removal on Co-Pd-modified H-ZSM-5 catalyst by suppression of CH₄ combustion.** Catal. Lett., 52, 145-149.
- Kameoka, S.; Suzuki, T.; Yuzaki, K.; Takeda, T.; Tanaka, S.; Ito, S.; Miyadera, T.; Kunimori, K. (2000). **Selective catalytic reduction of N₂O with methane in the presence of excess oxygen over Fe-BEA zeolite.** Chem. Comm., 745-746.
- Kato, H.; Yokoyama C.; Misono, M. (1997). **Rate-determining step of NO-CH₄-O₂ reaction catalyzed by Pd/H-ZSM-5.** Catal. Lett., 47, 189-191.
- Kato, K.; Takarada, Y.; Sagara, H.; Inomata, M. (1994). **Simultaneous desulfurization and denitration of combustion flue gases with fluidized-bed catalysts.** Jpn. Kokai Tokkyo Koho, JP 06170165, 6 pp.
- Kato, T.; Shinoda, K.; Masuda, K.; Tsujimura, K. (1998). **Activity enhancement of Ag/mordenite catalysts by addition of palladium for the removal of nitrogen oxides from diesel engine exhaust gas.** Appl. Catal., B: Environ., 15, 29-35.
- Kaucky, D.; Vondrova, A.; Dedecek, J.; Wichterlova, B. (2000). **Activity of Co ion sites in ZSM-5, ferrierite, and mordenite in selective catalytic reduction of NO with methane.** J. Catal., 194(2), 318-329.
- Kawai, Y. (1992). **Catalyst for treatment of exhaust gases.** Eur. Pat. Appl. EP 499,286, 16 pp.
- Keiski, R.L.; Raeisaenen, H.; Haerkoenen, M.; Maunula, T.; Niemistoe, P. (1996). **NO_x abatement in lean exhaust gas conditions over metal substrated zeolite catalysts.** Catal. Today, 27, 85-90.
- Kikuchi, E.; Ogura, M. (2000). **Palladium species in Pd/H-ZSM-5 zeolite catalysts for CH₄-SCR.** Res. Chem. Int., 26(1), 55-60.
- Kikuchi, E.; Ogura, M.; Terasaki, I.; Goto Y. (1996). **Selective reduction of nitric oxide with methane on gallium and indium containing H-ZSM-5 catalysts: Formation of active sites by solid-state ion exchange.** J. Catal., 161, 465-470.
- Kim, Y.J.; Lee, J.M.; Kim, S.D. (2000). **Modeling of coal gasification in an internally circulating fluidized bed reactor with draught tube.** Fuel, 79, 69-77.

- Kim, Y.T.; Song, B.H.; Kim, S.D. (1997). **Entrainment of solids in an internally circulating fluidized bed with draft tube.** Chem. Eng. J., 66, 105-110.
- Kogel, M.; Monnig, R.; Schwieger, W.; Tissler, A.; Turek, T. (1999). **Simultaneous catalytic removal of NO and N₂O using Fe-MFI.** J. Catal., 182, 470-478.
- Kogel, M.; Sandoval, V.H.; Schwieger, W.; Tissler, A.; Turek, T. (1998). **Simultaneous catalytic reduction of NO and N₂O using Fe-MFI prepared by solid-state ion exchange.** Catal. Lett., 51, 23-25.
- Laurent F.; Pope, C.J.; Mahzoul, H.; Delfosse, L.; Gilot, P. (2003). **Modeling of NO_x adsorption over NO_x adsorbers.** Chem. Eng. Sci., 58, 1793-1803.
- Lee, C.W.; Chong, P.J.; Lee, Y.C.; Chin, C.S.; Kevan, L. (1997). **Wetness method preparation of catalysts for selective catalytic reduction of NO by propane.** Catal. Lett., 48, 129-133.
- Lee, L. (2000). **Oxygen effect on the selective catalytic reduction of NO_x using hydrocarbon reductants.** Undergraduate thesis, UBC.
- Lee, Y.W.; Choi, D.K.; Park, J.W. (2002). **Characteristics of NO_x adsorption and surface chemistry on impregnated activated carbon.** Sep. Sci. Technol., 37(4), 937-956.
- Li, J.; Hao, J.; Fu, L.; Liu, Z.; Cui, X. (2004). **The activity and characterization of sol-gel Sn/Al₂O₃ catalyst for selective catalytic reduction of NO_x in the presence of oxygen.** Catal. Today, 90 (3-4), 215-221.
- Li, L.; Chen, J.; Zhang, S.; Guan, N.; Richter, M.; Eckelt, R.; Fricke, R. (2004). **Study on metal-MFI/cordierite as promising catalysts for selective catalytic reduction of nitric oxide by propane in excess oxygen.** J. Catal., 228 (1), 12-22.
- Li, Y.; Armor, J.N. (1992a). **Catalytic reduction of nitrogen oxides using methane in the presence of oxygen.** US Patent 5,149,512, 10 pp.
- Li, Y.; Armor, J.N. (1992b). **Catalytic decomposition of nitrous oxide on metal exchanged zeolites.** Appl. Catal., B: Environ., 1, L21-L29.
- Li, Y.; Armor, J.N. (1993a). **Selective catalytic reduction of NO_x with methane over metal exchange zeolites.** Appl. Catal., B: Environ., 2, 239-256.
- Li, Y.; Armor, J.N. (1993b). **Metal exchanged ferrierites as catalysts for the selective reduction of NO_x with methane.** Appl. Catal., B: Environ., 3, L1-L11.
- Li, Y.; Armor, J.N. (1994a). **Selective reduction of NO_x by methane on Co-Ferrierites: I. Reaction and kinetic Studies.** J. Catal., 150, 376-387.

- Li, Y.; Armor, J.N. (1994b). **Selective catalytic reduction of NO with methane on gallium catalysts.** *J. Catal.*, 145, 1-9.
- Li, Y.; Slager, T.L.; Armor, J.N. (1994c). **Selective reduction of NO_x by methane on Co-Ferrierites: II. Catalyst characterization .** *J. Catal.*, 150, 388-399.
- Lick, I. D.; Carrascull, A.; Ponzi, M.; Ponzi, E.N. (2003a). **The catalytic activity of Co/ZrO₂ for NO reduction with propane in O₂ presence.** *Catal. Lett.*, 89(3-4), 179-184.
- Lick, I. D.; Ponzi, E. N. (2003b). **NO reduction with C₃H₈ on Co/Al₂O₃ catalyst. Effect of O₂ concentration.** *React. Kinet. Catal. Lett.*, 79(1), 197-203.
- Lietti, L.; Forzatti, P.; Nova I.; Tronconi, E. (2001). **NO_x storage reduction over Pt---Ba/γ-Al₂O₃ catalyst.** *J. Catal.*, 204, 175-191.
- Lima, E.; Guzmam-Vargas, A.; Mendez-Vivar J.; Pfeiffer, P.; Fraissard, J. (2008). **Fe-ZSM-5 catalyst: Preparation in organic media, Fe-particle morphology and NO_x reduction activity.** *Catal. Lett.*, 120, 244-251.
- Liotta, L. F.; Pantaleo, G.; Macaluso, A.; Di Carlo, G.; Deganello, G. (2003). **CoO_x catalysts supported on alumina and alumina-baria: influence of the support on the cobalt species and their activity in NO reduction by C₃H₆ in lean conditions.** *Appl. Catal., A: General*, 245(1), 167-177.
- Liu, Z.; Woo, S. (2006). **Recent advances in catalytic deNO_x science and technology.** *Catal. Rev.*, 48(1), 43-89.
- Lobree, L.J.; Aylor, A.W.; Reimer, J.A.; Bell, A.T. (1999). **NO reduction by CH₄ in the presence of O₂ over Pd-H-ZSM-5.** *J. Catal.*, 181, 189-204.
- Lobree, L.J.; Aylor, A.W.; Reimer, J.A.; Bell, A.T. (1997). **Role of cyanide species in the reduction of NO by CH₄ over Co-ZSM-5.** *J. Catal.*, 169, 188-193.
- Lombardo, E.A.; Sill, G.A.; Ditri, J.L.; Hall, W.K. (1998). **The possible role of nitromethane in the SCR of NO_x with CH₄ over M-ZSM5 (M=Co, H, Fe, Cu).** *J. Catal.*, 173, 440-449.
- Long, R.Q.; Yang, R.T. (1998). **Pt/MCM-41 catalyst for selective catalytic reduction of nitric oxide with hydrocarbons in the presence of excess oxygen.** *Catal. Lett.*, 52, 91-96.
- Long, R. Q.; Yang, R. T. (1999). **Catalytic performance of Fe-ZSM-5 catalysts for selective catalytic reduction of nitric oxide by ammonia.** *J. Catal.*, 188, 332-339.
- Lucas, A.D.; Valverde, J.L.; Dorado, F.; Romero, A.; Asencio, I. (2004). **Influence of the ion exchanged metal (Cu, Co, Ni and Mn) on the selective catalytic reduction of NO_x over mordenite and ZSM-5.** *J. Mole. Catal. A*, 225(1), 47-58.

- Lukyanov, D.B.; Lombardo, E. A.; Sill, G. A.; Ditri, J. L.; Hall, W.K. (1996). **Selective catalytic reduction (SCR) of NO with methane over CoZSM-5 and HZSM-5 zeolites: On the role of free radicals and competitive oxidation reactions.** *J. Catal.*, 163, 447-456.
- Lukyanov, D.B.; Sill, G.; Ditri, J.L.; Hall, W.K. (1995). **Comparison of catalyzed and homogeneous reactions of hydrocarbons for selective catalytic reduction (SCR) of NO_x.** *J. Catal.*, 153, 265-274.
- Mahzoul, H.; Brillhac, J.F.; Gilot, P. (1999). **Experimental and mechanistic study of NO_x adsorption over NO_x trap catalysts.** *Appl. Catal., B: Environ.*, 20, 47-55.
- Machida, M.; Kurogi, D.; Kijima, T. (2003). **NO_x storage and reduction characteristics of Pd/MnO_x-CeO₂ at low temperature.** *Catal. Today*, 84(3-4), 201-207.
- Machida, M.; Murakami, H.; Kijima, T. (1998). **Temperature-swing sorption/desorption cycles of nitric oxide through intercalation by double layered cuprate.** *Appl. Catal., B: Environ.*, 17, 195-203.
- Machida, M.; Yoshii, A.; Kijima, T. (2000). **Temperature swing adsorption of NO_x over ZrO₂-based oxides.** *Int. J. Inorg. Mater.*, 2, 413-417.
- Machida, M.; Masuda, N.; Kijima, T. (1999). **Sorption-desorption properties of nitric oxide over La_{2-x}Sr_{1+x}Cu₂O_{6-δ} (0 ≤ x ≤ 2).** *J. Mater. Chem.*, 9, 1369-1374.
- Martinez-Hernandez, A.; Fuentes, G.A. (2005). **Redistribution of cobalt species in Co-ZSM5 during operation under wet conditions in the reduction of NO_x by propane.** *Appl. Catal., B: Environ.*, 57 (3), 167-174.
- Masters, S. G.; Chadwick, D. (1999a). **Effect of SO₂ on selective catalytic reduction of NO by CH₃OCH₃ over γ-alumina in excess oxygen.** *Catal. Lett.*, 61(1,2), 65-69.
- Masters, S. G.; Chadwick, D. (1999b). **Selective reduction of nitric oxide by methanol and dimethyl ether over promoted alumina catalysts in excess oxygen.** *Appl. Catal., B: Environ.*, 23(4), 235-246.
- Matsumoto, H.; Tanabe, S. (1995). **Reduction mechanism of nitrogen monoxide with propane over palladium-Y zeolite catalyst.** *J. Phys. Chem.*, 99, 6951-6956.
- Matsumoto, S. (1996). **DeNO_x catalyst for automotive lean-burn engine.** *Catal. Today*, 29, 43-45.
- Matsumoto, S.; Ikeda, Y.; Suzuki, H.; Ogai, M.; Miyoshi, N. (2000). **NO_x storage-reduction catalyst for automotive exhaust with improved tolerance against sulfur poisoning.** *Appl. Catal., B: Environ.*, 25, 115-124.
- Marturano, P.; Kogelbauer A.; Prins, R. (1999). **Different methods for preparation of Fe-ZSM5 as catalyst for the selective catalytic reduction of nitrogen oxides.** *Porous Materials in Environmentally Friendly Processes, Studies in Surf. Sci. Catal.*, 125, 619-625.

- Masuda, K.; Shinoda, K.; Kato T.; Tsujimura, K. (1998). **Activity enhancement of Ag/mordenite catalysts by addition of palladium for the removal of nitrogen oxides from diesel engine exhaust gas.** *Appl. Catal., B: Environ.*, 15, 29-35.
- Meunier, F.C.; Ukrepec, R.; Stapleton, C.; Ross, J.R.H. (2001). **Effect of the silver loading and some other experimental parameters on the selective reduction of NO with C₃H₆ over Al₂O₃ and ZrO₂-based catalysts.** *Appl. Catal., B: Environ.*, 30(1-2), 163-172.
- Meunier, F. C.; Zuzaniuk, V.; Breen, J. P.; Olsson, M.; Ross, J. R. H. (2000). **Mechanistic differences in the selective reduction of NO by propene over cobalt- and silver-promoted alumina catalysts: kinetic and in situ DRIFTS study.** *Catal. Today*, 59, 287-304.
- Mihaylov, M.; Hadjiivanov, K.; Panayotov, D. (2004). **FTIR Mechanistic studies on the selective catalytic reduction of NO_x with methane over Ni-containing zeolites: Comparison between NiY and Ni-ZSM-5.** *Appl. Catal., B: Environ.*, 51(1),33-42.
- Milne, B.J.; Berruti, F.; Behie, L.A.; de Brujin, T.J.W. (1992). **The internally circulating fluidized bed (ICFB): a novel solution to gas bypassing in spouted beds.** *Can. J. Chem. Eng.*, 70, 910-915.
- Mitome, J.; Karakas, G.; Bryan, K.A.; Ozkan, U.S. (1998). **Effect of H₂O and SO₂ on the activity of Pd/TiO₂ catalysts in catalytic reduction of NO with methane in the presence of oxygen.** *Catal. Today*, 42, 3-11.
- Mongkolsiri, N.; Prasertdam, P.; Silveston, P. L.; Hudgins, R. R. (2000). **Transient study of the effect of residual cations in Cu/ZSM-5 for SCR of NO by hydrocarbon.** *Chem. Eng. Sci.*, 55(12), 2249-2256.
- Mosqueda-Jimenez, B.I.; Jentys, A.; Seshan, K.; Lercher, J.A. (2003). **Structure-activity relations for Ni-containing zeolites during NO reduction II. Influence of acid sites.** *J. Catal.*, 218(2), 348-353.
- Muslehiddinoglu J.; Vannice M.A. (2003). **Adsorption of NO on promoted Ag/ α -Al₂O₃ catalysts.** *J. Catal.*, 217, 442-456.
- Muzio, L.J.; Quartucy, G.C. (1997). **Implementing NO_x control: Research to application.** *Progr. Energ. Combust. Sci.*, 23, 233–266.
- Naito, S.; Tanimoto, M. (1993). **The role of oxygen in the reduction of nitric oxide with propene over rhodium/alumina in an oxidizing atmosphere.** *Chem. Lett.*, 11, 1935-1938.
- Nelli, C.H.; Rochelle, G.T. (1996). **Nitrogen dioxide reaction with alkaline solids.** *Ind. Eng. Chem. Res.*, 35, 999-1005.

- Nikolopoulos, A. A.; Stergioula, E. S.; Efthimiadis, E. A.; Vasalos, I. A. (1999). **Selective catalytic reduction of NO by propene in excess oxygen on Pt- and Rh-supported alumina catalysts.** *Catal. Today*, 54(4), 439-450.
- Nishizaka, Y.; Misono, M. (1994). **Essential role of acidity in the catalytic reduction of nitrogen monoxide by methane in the presence of oxygen over palladium-loaded zeolites.** *Chem. Lett.*, 2237-2240.
- Nova, I.; Castoldi, L.; Lietti, L.; Tronconi, E.; Forzatti, P. (2002). **On the dynamic behavior of "NO_x-storage/reduction" Pt-Ba/Al₂O₃ catalyst.** *Catal. Today*, 75, 431-437.
- Obuchi, A.; Ohi, A.; Nakamura, M.; Ogata, A.; Mizuno, K.; Ohuchi, H. (1993). **Performance of platinum-group metal catalysts for the selective reduction of nitrogen oxides by hydrocarbons.** *Appl. Catal., B: Environ.*, 2(1), 71-80.
- Ogura, M.; Kage, S.; Hayashi, M.; Matsukata, M.; Kikuchi, E. (2000). **Remarkable enhancement in durability of Pd/H-ZSM-5 zeolite catalysts for CH₄-SCR.** *Appl. Catal., B: Environ.*, 27(4), L213-L216.
- Ogura, M.; Kage, S.; Shimojo, T.; Oba, J.; Hayashi, M.; Matsukata, M.; Kikuchi, E. (2002). **Co cation effects on activity and stability of isolated Pd(II) cations in zeolite matrices for selective catalytic reduction of nitric oxide with methane.** *J. Catal.*, 211, 75-84.
- Ohman, L. O.; Ganemi, B.; Bjornbom, E.; Rahkamaa, K.; Keiski, R. L.; Paul, J. (2002). **Catalyst preparation through ion-exchange of zeolite Cu-, Ni-, Pd-, Cu/Ni- and Cu/Pd-ZSM-5.** *Mater. Chem. Phys.* 73(2-3), 263-267.
- Ohtsuka, H.; Tabata, T.; Okada, O.; Sabatino, L.M.F.; Bellussi, G. (1997). **A study on selective reduction of NO_x by propane on Co-Beta.** *Catal. Lett.*, 44, 265-270.
- Olsson L.; Persson, H.; Fridell, E.; Skoglundh, M.; Andersson, B. (2001). **A kinetic study of NO oxidation and NO_x storage on Pt/Al₂O₃ and Pt/BaO/Al₂O₃.** *J. Phys. Chem. B*, 105, 6895-6906.
- Pandey, R.N. ; Ratnani, K.; Varma, R. L.; Elkaim, D.; Pandey, R.N (1997). **Selective catalytic reduction of nitrogen oxides.** US Patent 5,612,010.
- Park, P.W.; Ragle, C.S.; Boyer, C.L.; Balmer, M.L.; Engelhard, M.; McCready, D. (2002). **In₂O₃/Al₂O₃ Catalysts for NO_x reduction in lean condition.** *J. Catal.*, 20, 97-105.
- Park, S.K.; Park, Y.K.; Park, S.E.; Kevan, L. (2000). **Comparison of selective catalytic reduction of NO with C₃H₆ and C₃H₈ over Cu(II)-ZSM-5 and Co(II)-ZSM-5.** *Phys. Chem. Chem. Phys.*, 2(23), 5500-5509.
- Parvulescu, V.I.; Grange, P.; Delmon, B. (1998). **Catalytic removal of NO.** *Catal. Today*, 46, 233-316.

- Perez-Ramirez, J.; Garcia-Cortes, J. M.; Kapteijn, F.; Illan-Gomez, M. J.; Ribera, A.; Salinas-Martinez de Lecea, C.; Moulijn, J. A. (2000). **Dual-bed catalytic system for NO_x-N₂O removal: a practical application for lean-burn deNO_x HC-SCR.** Appl. Catal., B: Environ., 25(2, 3), 191-203.
- Perez-Ramirez, J.; Garcia-Cortes, J. M.; Kapteijn, F.; Mul, G.; Moulijn, J. A.; Salinas-Martinez de Lecea, C. (2001). **Characterization and performance of Pt-USY in the selective catalytic reduction of NO_x with hydrocarbons under lean-burn conditions.** Appl. Catal., B: Environ., 29(4), 285-298.
- Pieterse, J. A. Z.; van den Brink, R. W.; Booneveld, S.; de Bruijn, F. A. (2002). **Durability of ZSM5-supported Co-Pd catalysts in the reduction of NO_x with methane.** Appl. Catal., B: Environ., 39(2), 167-179.
- Qi, G.; Yang, R.T. (2005). **Ultra-active Fe/ZSM-5 catalyst for selective catalytic reduction of nitric oxide with ammonia.** Appl. Catal., B: Environ., 60, 13–22.
- Ramachandran, B.; Herman, R. G.; Choi, S.; Stenger, H. G.; Lyman, C. E.; Sale, J. W. (2000). **Testing zeolite SCR catalysts under protocol conditions for NO_x abatement from stationary emission sources.** Catal. Today, 55(3), 281-290.
- Roh, S. A.; Jung, S. H.; Jeong, S. M.; Kim, S. D. (2003). **Selective catalytic reduction by urea in a fluidized-bed reactor.** J. Chem. Tech. Biotech, 78(10), 1104-1109.
- Saaid, I.M.; Mohamed, A. R.; Bhatia, S. (2002). **Comparative study of Cu-ZSM-5 and Fe-ZSM-5 in the SCR of NO_x with i-C₄H₁₀.** React. Kinet. Catal. Lett. 75(2), 359-365.
- Sadykov, V.A.; Lunin, V.V.; Matyshak, V.A.; Paukshtis, E.A.; Rozovskii, A. Y.; Bulgakov, N.N.; Ross J.R.H. (2003). **The reaction mechanism of selective catalytic reduction of nitrogen oxides by hydrocarbons in excess oxygen: Intermediates, their Reactivity, and routes of transformation.** Kinet. Catal., 44, 379-400.
- Sato, K.; Yoshinari, T.; Kintaichi, Y.; Haneda, M.; Hamada, H. (2003). **Rh-post-doped Ag/Al₂O₃ as a highly active catalyst for the selective reduction of NO with decane.** Catal. Comm., 4(7), 315-319.
- Sato, S.; Hirabayashi, H.; Yahiro, H.; Mizuno, N.; Iwamoto, M. (1992). **Iron ion-exchanged zeolite: The most active catalyst at 473K for selective reduction of nitrogen monoxide by ethene in oxidizing atmosphere.** Catal. Lett., 12(1-3), 193-200.
- Satokawa, S.; Yamaseki, K.; Uchida, H. (2001). **Influence of low concentration of SO₂ for selective reduction of NO by C₃H₈ in lean-exhaust conditions on the activity of Ag/Al₂O₃ catalyst.** Appl. Catal., B: Environ., 34(4), 299-306.
- Satsuma A.; Shimizu, K. (2003). **In situ FT/IR study of selective catalytic reduction of NO over alumina-based catalysts.** Prog. Energy Combust. Sci., 29, 71-84.

- Schmitz, P.J.; Baird, R.J. (2002). **NO and NO₂ adsorption on barium oxide: Model study of the trapping stage of NO_x conversion via lean NO_x traps.** *J. Phys. Chem. B*, 106, 4172-4180.
- Schreier, E.; Eckelt, R.; Richter, M.; Fricke, R. (2005). **Investigation on sulphation and regeneration of a commercial monolithic NO_x-storage/reduction catalyst.** *Catal. Comm.*, 6(6), 409-414.
- Schwidder, M.; Santhosh Kumar, M.; Bentrup, U.; Perez-Ramirez, J.; Brueckner, A.; Gruenert, W. (2008). **The role of Bronsted acidity in the SCR of NO over Fe-MFI catalysts.** *Micro. Meso. Mater.*, 111(1-3), 124-133.
- Sedlmair, Ch.; Seshan, K.; Jentys, A.; Lercher, J.A. (2003). **Elementary steps of NO_x and surface reaction on a commercial storage-reduction catalyst.** *J. Catal.*, 214, 308-316.
- Seyedejn-Azad, F.; Zhang, D.K. (2001). **Selective catalytic reduction of nitric oxide over Cu and Co ion-exchanged ZSM-5 zeolite: the effect of SiO₂/Al₂O₃ ratio and cation loading.** *Catal. Today*, 68(1-3), 161-171.
- Shelf, M. (1995). **Selective catalytic reduction of NO_x with N-free reductants.** *Chem. Rev.* 95, 209-225.
- Shelukar, S.; Ho, J.; Zega, J.; Roland, E.; Yeh, N.; Quiram, D.; Nole, A.; Katdare, A.; Reynolds, S. (2000). **Identification and Characterization of Factors Controlling Tables Coating Uniformity in a Wurster Coating Process.** *Powder Technol.*, 110, 29-37.
- Shen, S.C.; Kawi, S. (2003). **Selective catalytic reduction of NO by hydrocarbons in the presence of excess oxygen using Pt/MCM-41 catalysts.** *Appl. Catal., B: Environ.*, 45(1), 63-76.
- Shi, C.; Cheng, M.; Qu, Z.; Yang X.; Bao, X. (2002). **On the selectively catalytic reduction of NO_x with methane over Ag-ZSM-5 catalysts.** *Appl. Catal., B: Environ.*, 36, 173-182.
- Shi, Y.; Pan, H.; Li, Z.; Zhang, Y.; Li, W. (2008). **Low-temperature decomposition of NO_x over Fe-Mn/H-beta catalysts in the presence of oxygen.** *Catal. Comm.*, 9(6), 1356-1359.
- Shibata, J.; Shimizu, K.; Satsuma, A.; Hattori, T. (2002). **Influence of hydrocarbon structure on selective catalytic reduction of NO by hydrocarbons over Cu-Al₂O₃.** *Appl. Catal., B: Environ.*, 37(3), 197-204.
- Shimizu, K.; Kawabata, H.; Maeshima, H.; Satsuma, A.; Hattori, T. (2001a). **Intermediates in the Selective Reduction of NO by Propene over Cu-Al₂O₃ Catalysts: Transient in-Situ FTIR Study.** *J. Phys. Chem. B*, 104(13), 2885-2893.
- Shimizu, K.; Satsuma, A.; Hattori, T. (2001b). **Metal oxide for selective reduction of NO_x by hydrocarbons: Toward molecular basis for catalyst design.** *Catal. Surv. from Japan*, 4(2), 115-123.

- Shimizu, K.; Satsuma, A.; Hattori, T. (2000). **Catalytic performance of Ag–Al₂O₃ catalyst for the selective catalytic reduction of NO by higher hydrocarbons.** Appl. Catal., B: Environ., 25, 239-247.
- Shin, H.K.; Hirabayashi, H.; Yahiro, H.; Watanabe, M.; Iwamoto, M. (1995). **Selective catalytic reduction of NO by ethene in excess oxygen over platinum ion-exchanged MFI zeolites.** Catal. Today, 26, 13-21.
- Shinjoh, H.; Takahashi, N.; Yokota, K.; Sugiura, M. (1998). **Effect of periodic operation over Pt catalysts in simulated oxidizing exhaust gas.** Appl. Catal., B: Environ., 15, 189-201.
- Snip, O.C.; Woods, M.; Korbee, R.; Schouten, J.C.; van den Bleek, C.M. (1996). **Regenerative removal of SO₂ and NO_x for a 150 MWe power plant in a interconnected fluidized bed facility.** Chem. Eng. Sci., 51(10), 2021-2029.
- Sobalik, Z.; Vondrova, A.; Tvaruzkova, Z.; Wichterlova, B. (2002). **Analysis of the structural parameters controlling the temperature window of the process of SCR-NO_x by low paraffins over metal-exchanged zeolites.** Catal. Today, 75, 347-351.
- Stakheev, A.Y.; Lee, C.W.; Park, S.J.; Chong, P.J. (1996). **Selective catalytic reduction of NO with propane over CoZSM-5 containing alkaline earth cations.** Appl. Catal., B: Environ., 9, 65-76.
- Stocker, R.K.; Eng, J.H.; Behie, L.A. (1990). **Hydrodynamics and thermal modelling of a high temperature spouted bed reactor with a draft tube.** Can. J. Chem. Eng., 68, 302-311.
- Subbiah, A.; Cho, B. K.; Blint, R. J.; Gujar, A.; Price, G. L.; Yie, J. E. (2003). **NO_x reduction over metal-ion exchanged novel zeolite under lean conditions: activity and hydrothermal stability.** Appl. Catal., B: Environ., 42(2), 155-178.
- Sullivan, J.A.; Keane, O. (2007). **A combination of NO_x trapping materials and urea-SCR [selective catalytic reduction] catalysts for use in the removal of NO_x from mobile diesel engines.** Appl. Catal., B: Environ., 70(1-4), 205-214.
- Tabata, T.; Kokitsu, M.; Ohtsuka, H.; Okada, O.; Sabatino, L. M. F.; Bellussi, G. (1996). **Study on catalysts of selective reduction of NO_x using hydrocarbons for natural gas engines.** Catal. Today, 27(1-2), 91-98.
- Tabata, T.; Kokitsu, M.; Okada, O. (1994). **Study on patent literature of catalysts for a new NO_x removal process.** Catal. Today, 22, 147-169.
- Tabata, T.; Kokitsu, M.; Okada, O. (1995). **Relationship between methane adsorption and selective catalytic reduction of nitrogen oxide by methane on gallium and indium ion-exchanged ZSM-5.** Appl. Catal., B: Environ., 6, 225-236.

Takahashi, N.; Shinjoh, H.; Iijima, T.; Suzuki, T.; Yamazaki, K.; Yokota, K.; Suzuki, H.; Miyoshi, N.; Matsumoto, S.; Tanizawa, T.; Tanaka, T.; Tateishi, S.; Kasahara, K. (1996). **The new concept 3-way catalyst for automotive lean-burn engine: NO_x storage and reduction catalyst.** *Catal. Today*, 27, 63-69.

Tonetto, G. M.; Damiani, D. E. (2003). **Performance of Pd-Mo/ γ -Al₂O₃ catalysts for the selective reduction of NO by methane.** *J. Mol. Catal. A: Chem.*, 202(1-2), 289-303.

Toubeli, A.; Efthimiadis, E. A.; Vasalos, I. A. (2000). **NO reduction by C₃H₆ in excess oxygen over fresh and sulfated Pt- and Rh-based catalysts.** *Catal. Lett.*, 69(3,4), 157-164.

Traa, Y.; Burger, B.; Weitkamp, J. (1999). **Zeolite-based materials for the selective catalytic reduction of NO_x with hydrocarbons.** *Micro. Meso. Mater.* 30, 3-41.

Uchida, H.; Yamaseki, K.; Takahashi, I. (1995). **Reduction of NO_x from exhaust gases of lean-burn gas engines.** *Envir. Catal.*, 331-334

Ueda, A.; Oshima, T.; Haruta, M. (1997). **Reduction of nitrogen monoxide with propene in the presence of oxygen and moisture over gold supported on metal oxides.** *Appl. Catal., B: Environ.*, 12 (2-3), 81-93.

van de Grift, C.J.G.; Woldhuis, A.F.; Maaskant, O.L. (1996). **The Shell DENOX system for low temperature NO_x removal.** *Catal. Today*, 27, 23-27.

Vernoux, P.; Leinekugel-Le-Cocq, A.-Y.; Gaillard, F. (2003). **Effect of the addition of Na to Pt/Al₂O₃ catalysts for the reduction of NO by C₃H₈ and C₃H₆ under lean-burn conditions.** *J. Catal.*, 219(1), 247-257.

Walker, A.P. (1995). **Mechanistic studies of the selective reduction of NO_x over Cu/ZSM-5 and related systems.** *Catal. Today*, 26, 107-128.

Wang, A.; Liang, D.; Xu, C.; Sun, X.; Zhang, T. (2001a). **Catalytic reduction of NO over in situ synthesized Ir/ZSM-5 monoliths.** *Appl. Catal., B: Environ.*, 32(3), 205-212.

Wang, C.; Wang, X.; Yu, S.; Xu, Y. (2005). **Acetylene: A new reducing agent used in SCR of NO on zeolite catalysts in an oxygen-rich atmosphere.** *React. Kinet. Catal. Lett.*, 86(1), 59-66.

Wang, X.; Chen, H.Y.; Sachtler, W. M. H. (2001b). **Mechanism of the selective reduction of NO_x over Co/MFI: Comparison with Fe/MFI.** *J. Catal.*, 197(2), 281-291.

Wang, X.; Chen, H.Y.; Sachtler W.M.H. (2000). **Catalytic reduction of NO_x by hydrocarbons over Co/ZSM-5 catalysts prepared with different methods.** *Appl. Catal., B: Environ.*, 26, L227-L239.

Wark, K.; Warner, C.F.; Davis, W.T. (1998). **Air pollution: Its origin and control.** 3rd ed. Addison Wesley Longman, Inc., 430-438.

- Wichtelova, B.; Sobalik, Z.; Dedecek, J. (2003). **Redox catalysis over metallo-zeolites: Contribution to environmental catalysis.** Appl. Catal., B: Environ., 41, 97-114.
- Williams, J.L. (2001). **Monolith structures, materials, properties and uses.** Catal. Today, 69, 3-9.
- Witzel, F.; Sill, G.A.; Hall, W.K. (1994). **Reaction studies of the selective reduction of NO by various hydrocarbons.** J. Catal. 149, 229-237.
- Woo, S.I.; Kim, D.K.; Park, Y.K.; Kim, M.R.; Decyk, P. (2003). **Wide temperature window in the catalytic activity of novel Pt/ZSM-5 prepared by a sublimation method for selective catalytic reduction of NO.** Catal. Lett., 85(1-2), 69-72.
- Xin, M.; Hwang, I. C.; Kim, D. H.; Cho, S. I.; Woo, S. I. (1999). **The effect of the preparation conditions of Pt/ZSM-5 upon its activity and selectivity for the reduction of nitric oxide.** Appl. Catal., B: Environ., 21(3), 183-190.
- Xu, G.; Wang, B.; Suzuki, H.; Kato, K. (1999). **Performance with respect to flue gas composition of a combined desulfurization/denitration process using powder-particle fluidized bed.** Chinese J. Chem. Eng., 7(4), 295-306.
- Xu, G.; Luo, G.; Akamatsu, H.; Kato, K. (2000). **An adaptive sorbent for the combined desulfurization/denitration process using a powder-particle fluidized bed.** Ind. Eng. Chem. Res., 39, 2190-2198.
- Yamada, K.; Pophal, C.; Segawa, K. (1998). **Selective catalytic reduction of N₂O by C₃H₆ over Fe-ZSM-5.** Micro. Meso. Mater. 21, 549-555.
- Yan, J.; Kung, M.C.; Sachtler, W.M.H.; Kung, H.H. (1997). **Co/Al₂O₃ lean NO_x reduction catalyst.** J. Catal., 172(1), 178-186.
- Yan, J.Y.; Lei, G.D.; Sachtler, W.M.H.; Kung, H.H. (1996). **Deactivation of Cu/ZSM-5 catalysts for lean NO_x reduction: Characterization of changes of Cu state and zeolite support.** J. Catal., 161(1), 43-54.
- Yan, J.Y.; Kung, H.H.; Sachtler, W.M.H.; Kung, M.C. (1998). **Synergistic effect in lean NO_x reduction by CH₄ over Co/Al₂O₃ and H-zeolite catalysts.** J. Catal., 175, 294-301.
- Yang, W.C. (1998). **Engineering and Application of Recirculating and Jetting Fluidized Beds. Fluidization, Solids Handling, and Processing: Industrial Applications,** P236-330. Noyes Publications, Westwood, New Jersey.
- Yang, W.C.; Keairns, D.L. (1978a). **Design and operating parameters for a fluidized bed agglomerating combustor/gasifier.** Fluidization, Cambridge: Cambridge University Press, 208-214.
- Yang, W.C.; Keairns, D.L. (1978b). **Design of recirculating fluidized beds for commercial applications.** AIChE Symposium Series, 176(74), 218-228

- Yang, W.C.; Keairns, D.L. (1983). **Studies on the solid circulation rate and gas bypassing in spouted fluid-bed with a draft tube.** *Can. J. Chem. Eng.*, 61, 349-355
- Yentekakis, I.V.; Tellou, V.; Botzolaki, G.; Rapakousios, I.A. (2005). **A comparative study of the C₃H₆-NO-O₂, C₃H₆-O₂ and NO-O₂ reactions in excess oxygen over Na-modified Pt/Al₂O₃ catalysts.** *Appl. Catal., B: Environ.*, 56 (3), 229–239.
- Yogo K.; Kikuchi, E. (1994). **Reaction mechanism of selective reduction of nitric oxide by methane on Ga- and In-ZSM-5 catalysts.** *Study Surf. Sci. Catal.*, 84, 1547-1554.
- Yokoyama, C.; Misono, M. (1994a). **Selective reduction of nitrogen monoxide by propene over cerium-doped zeolites.** *Catal. Today*, 22, 59-72.
- Yokoyama, C.; Misono, M. (1994b). **Catalytic reduction of nitrogen oxides by propene in the presence of oxygen over cerium ion-exchanged zeolite. II. Mechanistic study of roles of oxygen and doped metals.** *J. Catal.*, 150, 9-17.
- Zelenka, P.; Cartellieri, W.; Herzog, P. (1996). **Worldwide diesel emission standards: current experiences and future needs.** *Appl. Catal. B: Environ.*, 10(1996), 3-28.
- Zhou, X.; Zhang, T.; Xu, Z.; Lin, L. (1996). **Selective catalytic reduction of nitrogen monoxide with methane over impregnated In/HZSM-5 in the presence of excess oxygen.** *Catal. Lett.*, 40, 35-38
- Zuzaniuk, V.; Meunier, F.C.; Ross, J. R.H. (2001). **Differences in the reactivity of organo-nitro and nitrito compounds over Al₂O₃-based catalysts active for the selective reduction of NO_x.** *J. Catal.*, 202, 340-353.

Appendix A

Summary of Previous Work

Table A.1 HC-SCR catalysts supported by zeolites

Catalyst	Active site	Support	Authors
Cu/ZSM-5	Cu ²⁺	Na/ZSM-5	Iwamoto et al. (1990)
			Zelenka et al. (1996)
			Saaid et al. (2002)
			Ohman et al. (2002)
			Garcia-Cortes et al. (2000)
Park et al. (2000)			
Cu/Beta	Cu ²⁺	Beta-Zeolite	Corma et al. (1997)
Fe/ZSM-5	Fe ²⁺	Na/ZSM-5	Hall et al. (1998)
		Na/ZSM-5	Garcia-Cortes et al. (2000)
		Na/ZSM-5	Chen et al. (2000b)
		Na/ZSM-5	Joyner et al. (1999)
		H/ZSM-5	Lee et al. (1997)
		H/ZSM-5	Joyner et al. (1999)
		Na/ZSM-5	Lombardo et al. (1998)
Na/ZSM-5	Gao et al. (2001)		
Fe/Beta	Fe ²⁺	NH ₄ /Beta-Zeolite	Chen et al. (2000b)
Fe/FER		Ferrierite	
Fe/MOR		Mordenite	
Fe/Y		Y-Zeolite	
Pt-Fe/ZSM-5	Fe ²⁺ , Pt ²⁺	H/ZSM-5	Kogel et al. (1998)
Co/ZSM-5	Co ²⁺	H/ZSM-5	Wang et al. (2000)
			Park et al. (2000)
			Kaucky et al. (2000)
Co/Beta	Co ²⁺	Beta zeolite	Ohtsuka et al (1997)
Co/FER	Co ²⁺	Ferrierite	Li et al. (1994a)
Pt/ZSM-5	Pt ²⁺	Na/ZSM-5	Xin et al (1999)
			Cho et al. (1995)
Pt/Y	Pt ²⁺	Y-Zeolite	Amiridis et al (1997)
Pt/Beta	Pt ²⁺	Beta-Zeolite	Garcia-Cortes et al.(2003)
Pd/ZSM-5	Pd ²⁺	H/ZSM-5	Kikuchi et al. (2000)
Co-Pd/ZSM-5	Co ²⁺ , Pd ²⁺	H/ZSM-5	Ogura et al. (2002)
			Bustamante et al. (2002)

Catalyst	Active site	Support	Authors
Ga/ZSM-5	Ga ³⁺	H/ZSM-5	Kikuchi et al. (1996)
In/ZSM-5	In ³⁺		
Ce-In/ZSM-5	Ce ³⁺ , In ³⁺	H/ZSM-5	Berndt et al. (2003)
Ag/ZSM-5	Ag ⁺	H/ZSM-5	Shi et al. (2002)
Cu/SUZ-4	Cu ²⁺	K/SUZ-4	Cho et al. (2003)
Ni/ZSM-5	Ni ²⁺	Na/ZSM-5	Mosqueda-Jimenez et al.(2003)
Ni/MCM-22	Ni ²⁺	Na/MCM-22	
Ni/MOR	Ni ²⁺	Na/Mordenite	
Ni/Y	Ni ²⁺	Na/Y	Mihaylov et al. (2004)

Table A.2 HC-SCR catalysts supported by non-zeolites (Metal oxides)

Catalyst	Active site	Support	Authors
Cu/Al ₂ O ₃	Cu ²⁺	γ-Al ₂ O ₃	Garcia-Cortes et al. (2000)
Pt/Al ₂ O ₃	Pt ²⁺	γ-Al ₂ O ₃	Burch et al. (1998)
Co/Al ₂ O ₃	Co ²⁺	γ-Al ₂ O ₃	Garcia-Cortes et al. (2000)
Ag/Al ₂ O ₃	Ag ⁺	γ-Al ₂ O ₃	Jen (1998)
		Boehmite	Shimizu et al. (2000)
			Satokawa et al. (2001)
Rh-Ag/Al ₂ O ₃	Rh ³⁺ , Ag ⁺	γ-Al ₂ O ₃	Sato et al (2003)
Co/ZrO ₂	Co ²⁺	ZrO ₂	Lick et al. (2003a)
Pt/SiO ₂	Pt ²⁺	SiO ₂	Captain et al. (1998)
Co/Al ₂ O ₃	Co ²⁺	γ-Al ₂ O ₃	Liotta et al. (2003)
Pd/Al ₂ O ₃	Pd ²⁺	γ-Al ₂ O ₃	Tonetto et al. (2003)
Pd-Mo/Al ₂ O ₃	Pd ²⁺ , Mo ³⁺	γ-Al ₂ O ₃	
Au/Al ₂ O ₃	Au ³⁺	γ-Al ₂ O ₃	Ueda et al. (1997)

Table A.3 Specifications of some typical HC-SCR catalysts

Catalyst	Metal Source	Metal Loading (wt%)	Loading Method	Specifications	Authors
Co/ZSM-5	CoCl ₂	2.3	WIE	Si/Al=14.0, Co/Al=0.44	Wang et al. (2000)
		5.0	WIE+IMP	Si/Al=14.0, Co/Al=1.01	
		5.0	SSI	Si/Al=14.0, Co/Al=0.98	
		5.6	SUB	Si/Al=14.0, Co/Al=1.13	
Fe/ZSM-5	FeCl ₃	-	SUB	Si/Al=23 Fe/Al=1	Chen et al. (1998b)
	FeSO ₄ ·7H ₂ O		IMP	Si/Al=14.2, Na/Al=0.49, Fe/Al=0.29	Chen et al. (1998a)
	FeC ₂ O ₄ ·2H ₂ O		IMP	Si/Al=14.2, Na/Al=0.42, Fe/Al=0.52	
	FeSO ₄	2.9	WIE		Kameoka et al. (2001)
Rh/Al ₂ O ₃	RhCl ₃ ·3H ₂ O	1.86	IMP	S _{BET} =182m ² /g	Efthimiadis et al. (2001)
Cu/Beta	Cu(CH ₃ COO) ₂ ·H ₂ O	9.2(CuO)	WIE	Si/Al=11.9, Cu/Al=0.97	Corma et al. (1997)
Pt/Y	Pt(NH ₃) ₄ (OH) ₂	1.2	IMP		Amiridis et al. (1997)
Co-Pd/ZSM-5	Pt(NH ₃) ₄ Cl ₂ Co(CH ₃ COO) ₂	Pd:0.4 Co:3.3	WIE+IMP	Si/Al=35.0, Pd/Al=0.03, Co/Al=0.45	Ogura et al. (2002)
Ga/ZSM-5	Ga(NO ₃) ₃	1.20	WIE		Tabata et al. (1995)
In/ZSM-5	In(NO ₃) ₃	1.40	WIE		
Ce-In/ZSM-5	In(NO ₃) ₃ , Ce(OH) ₃ , Ce(NO ₃) ₃	Ce:8 In:13	WIE+ SSIE	S _{BET} =260m ² /g	Berndt et al. (2003)
Ag/Al ₂ O ₃	AgNO ₃	2	IMP	S _{BET} =226m ² /g	Jen (1998)
Ag/Al ₂ O ₃	AgNO ₃	2	IMP	S _{BET} =189m ² /g	Satokawa et al. (2001)
Rh-Ag/Al ₂ O ₃	RhCl ₃ ·3H ₂ O AgNO ₃	Rh:0.05 Ag:4	IMP	S _{BET} =161m ² /g	Sato et al. (2003)
Pd/ZSM-5	Pd(NH ₃) ₄ Cl ₂	4	WIE		Kikuchi et al. (2000)
Cu/SUZ-4	Cu(CH ₃ COO) ₂	1.9-5.5	WIE		Subbiah et al. (2003)
Ni/ZSM-5	Ni(NO ₃) ₂ ·6H ₂ O	2.0	WIE	Si/Al=16.4, Ni/Al=0.4, Na/Al=0.3	Mosqueda-Jimenez et al. (2003)

Table A.4 HC-SCR with methane as reducing agent

Catalyst	Flue Gas Composition				CH ₄ (ppm)	CH ₄ /NO	GHSV (h ⁻¹)	T (°C)	NO Conversion to N ₂ (%)	CH ₄ Conversion (%)	Authors
	NO (ppm)	O ₂ (%)	H ₂ O (%)	SO ₂ (ppm)							
Fe/Beta	950(N ₂ O)	10			500	0.5	60,000	350	100	44	Kameoka et al. (2000)
Fe/ZSM-5	950(N ₂ O)	10			500	0.5	60,000	400	100	52	
Pd-Co/ZSM-5	100	10	10		2000	20	100ml/min (0.1g Cat.)	500	60		Ogura et al. (2002)
Ga-ZSM-5	1000	10	0		1000	1	15,000	500	75	40	Tabata et al. (1995)
			9					600	5	10	
In/ZSM-5	1000	10	0		1000	1	15,000	400	60	43	
			9					500	10	7	
Pd-Co/Mordenite	1300	0	0		2000	1.5	30,000	500	100	12	Bustamante et al. (2002)
			0						96	9	
			5	8					40	72	
	1000	6	8	2700	2.7	30,000	550	60	90		
Ce-In/ZSM-5	1000	10	0		2000	2	24,000	550	100	-	Berndt et al. (2003)
			5					600	88	-	
Co/ZSM-5	2000	10			8000	4	75ml/min (0.25g Cat.)	450	78	41	Witzel et al. (1994)
Ni/ZSM-5			510	78				24			
Mn/ZSM-5			550	65				52			
Ga/ZSM-5			550	30				8			
H/ZSM-5			550	60				20			
Pd/Al ₂ O ₃	735.4				183.9	0.25	40,000feed mol/hmol pd	500	86	100	Tonetto et al. (2003)
Pd-Mo/Al ₂ O ₃								450	100	100	

Catalyst	Flue Gas Composition				CH ₄ (ppm)	CH ₄ /NO	GHSV (h ⁻¹)	T (°C)	NO Conversion to N ₂ (%)	CH ₄ Conversion (%)	Authors
	NO (ppm)	O ₂ (%)	H ₂ O (%)	SO ₂ (ppm)							
Pt-Co/ZSM-5	1000	2			3000	3	30,000	500	91		Gutierrez et al. (1998)
Cu/ZSM-5	2000	2			2000	1	100ml/min (1.0g Cat.)	350	10	70	Seyedeyn-Azad et al. (2001)
Co/ZSM-5			450	50				81			
Ag/Al ₂ O ₃	1000	10	2		6000	6	0.9 gs/ml	550	42		Shimizu et al (2000)
Fe/MFI	1000+100 0 (N ₂ O)	4			1000	1	30,000	450	5 (N ₂ O:100)	90	Kogel et al. (1999)
Ni/Y	1300 (NO _x)	1.5			1000	0.77	30,000	500	3	-	Mihaylov et al. (2004)
Ni/ZSM-5	1300 (NO _x)	1.5			1000	0.77	30,000	500	28	-	
Pd/ZSM-5	100(NO ₂)	0	10		2000	20	100ml/min (0.1g Cat.)	450	98	-	Kikuchi et al. (2000)
		10		22							
Pd/TiO ₂	1780	0.2		0	2.13%	12	62ml/min (37.5mg Cat.)	500	98		Mitome et al. (1998)
				178					10		

Table A.5 HC-SCR with propane as reducing agent

Catalyst	Flue Gas Composition				C ₃ H ₈ (ppm)	C ₃ H ₈ /NO	GHSV (h ⁻¹)	T (°C)	NO Conversion to N ₂ (%)	C ₃ H ₈ Conversion (%)	Authors
	NO (ppm)	O ₂ (%)	H ₂ O (%)	SO ₂ (ppm)							
Cu/ZSM-5	1500	3			4500	3	20,000	400	96	-	Park et al. (2000)
Co/ZSM-5	1500	3			4500	3	20,000	550	75	-	
Co/Beta	500	10	9		1000	2	15,000	450	87	99.7	Ohtsuka et al. (1997)
Cu/Beta	750	2.4			470	0.63		350	80	-	
γ-Al ₂ O ₃	500	5			1000	2	200ml/min	550	80	12 (CO), 62(CO ₂)	Burch et al. (1998)
Sulphated-Al ₂ O ₃	500	5			1000	2	200ml/min	550	10		
Co/ZrO ₂	1500	0.8	0		2000	1.3	15,000	500	60	43	Lick et al. (2003a)
		2.5	0					500	42	65	
		2.5	0				30,000	500	28	42	
			8					550	15	70	
Ce-In/ZSM-5	1000	10	0		2000	2	24,000	550	67	-	Berndt et al. (2003)
			5					600	70	-	
Co/ZSM-5	2000	10			2700	1.35	75ml/min(0.25g Cat.)	400	62	34	Witzel et al. (1994)
Co/Al ₂ O ₃	1500	0			2000	1.3	8600	692	77		Lick et al. (2003b)
		0.61						527	3		
		0.8						527	20	5	
		2						527	34	6	
		8						527	53	38	
Cu/Al ₂ O ₃	1000	6.7			6000	6	18,000	400	13	8	Shibata t al.(2002)

Catalyst	Flue Gas Composition				C ₃ H ₈ (ppm)	C ₃ H ₈ /NO	GHSV (h ⁻¹)	T (°C)	NO Conversion to N ₂ (%)	C ₃ H ₈ Conversion (%)	Authors
	NO (ppm)	O ₂ (%)	H ₂ O (%)	SO ₂ (ppm)							
Ag/Al ₂ O ₃	1000	10		0	1000	1	500ml/min (0.66g Cat.)	480	21(N ₂ Yield), 22(NO ₂ Yield)	100	Angelidis et al. (2002) After 6h in steam
				50					6(N ₂ Yield), 5(NO ₂ Yield)	58	
Co/Beta	150	10	9	0.3	500	3.3	15,000	400	~70		Tabata et al. (1996) During 4000h on stream
Cu/Beta	750	2.4			470	0.63		350	72		Corma et al. (1997)
Cu/ZSM-5								350	68		
Fe/Beta	2000	3	10		2700	2.7	280ml/min (0.2g Cat.)	325	67(Yield)	58 (CO yield), 24 (CO ₂ yield)	Chen et al. (2000b)
			0					325	69(Yield)	62(CO yield), 26(CO ₂ yield)	
Fe/ZSM-5			10				280ml/min (0.2g Cat.)	325	44(Yield)	34 (CO yield), 16(CO ₂ yield)	
			0					325	59(Yield)	37(CO yield), 20(CO ₂ yield)	
Ag/Al ₂ O ₃	1000	10	2		6000	6	0.12 gs/ml	450	100		Shimizu et al (2000)
Ag/Al ₂ O ₃	91	9.1	9.1	0	303	3.33	132,000	527	70	58.2	Satokawa et al (2001)
				4				450	0	-	
				4				500	~0	-	
				4				550	55	-	
Fe/MFI	1000+1000 (N ₂ O)	4			1000	1	7,500	275	70 100(N ₂ O, >450°C)	87	Koget et al., 1999
Co/ZSM-5	1250	4	0		3250	2.6	150,000	500	61	53	Martinez- Hernandez and Fuentes (2005)
			20						30	10	

Table A.6 HC-SCR with propylene as reducing agent

Catalyst	Flue Gas Composition				C ₃ H ₆ (ppm)	C ₃ H ₆ /NO	GHSV (h ⁻¹)	T (°C)	NO Conversion to N ₂ (%)	C ₃ H ₆ Conversion (%)	Authors
	NO (ppm)	O ₂ (%)	H ₂ O (%)	SO ₂ (ppm)							
Cu/ZSM-5	1500	3			4500	3	20,000	500	98	100	Park et al. (2000)
Co/ZSM-5	1500	3			4500	3	20,000	460	31	61(450°C)	Park et al. (2000)
Fe/ZSM-5	950 (N ₂ O)	10			500	0.5	60,000	370	100	-	Kameoka et al. (2001)
Rh/Al ₂ O ₃	80	4		235	500	6.25		300	70	90	Efthimiadis et al. (2001)
Pt/Y	1850	1	10	20	300+100 (C ₃ H ₈)	0.22		300	24	-	Amiridis et al. (1997)
Ag/Al ₂ O ₃	1000	10	0	0	950+520 (C ₃ H ₈)	1.47	500ml/ min (0.2g Cat.)	500	62	82	Jen (1998)
			9	18				550	28	57	
Cu/ZSM-5	1000	5			1000	1	30,000	405	53	95	Inui et al. (1997)
Co/ZSM-5								530	37	90	
Pt/Beta	1000	5			1500	1.5	15,000	218	91(N ₂ Selectivity: 32%)	1	Garcia-Cortes et al. (2003)
Ag/Al ₂ O ₃	1000	10		0	500+500 (C ₃ H ₈)	1	500ml/ min(0.6 6g Cat.)	480	24(N ₂ Yield), 42 (NO ₂ Yield)	100, 59(C ₃ H ₈)	Angelidis et al. (2002)
				25					50 (N ₂ Yield)	100, 80(C ₃ H ₈)	
				50					38(N ₂ Yield)	50, 20(C ₃ H ₈)	
				100					35(N ₂ Yield)	23, 0(C ₃ H ₈)	
				0	21(N ₂ Yield), 30 (NO ₂ Yield)				100	During 6h on stream	
				50	47(N ₂ Yield), 3 (NO ₂ Yield)				58		

Catalyst	Flue Gas Composition				C ₃ H ₆ (ppm)	C ₃ H ₆ /NO	GHSV (h ⁻¹)	T (°C)	NO Conversion to N ₂ (%)	C ₃ H ₆ Conversion (%)	Authors	
	NO (ppm)	O ₂ (%)	H ₂ O (%)	SO ₂ (ppm)								
Cu/ZSM-5	2000	2			2000	1	100ml/ min(1.0 g Cat.)	350	85	100	Seyedeyn-Azad et al. (2001)	
Co/ZSM-5			450	50				100				
Pt/Al ₂ O ₃	1000	5		0	1000	1		300	45	15	Toubeli et al. (2000)	
Sulfated Pt/Al ₂ O ₃				0					250	48		93
				300					250	42		78
Pt/SiO ₂	1000	5	0		1000	1		267	35	0	Captain et al. (1998)	
			0.5							70		11
			1							13		33
Pt/Al ₂ O ₃	2000	5	0	0	2000	1	1000ml/ min (4g Cat.)	285	62	100	Efthimiadis et al. (1998)	
			5	0						55		100
Pt/Al ₂ O ₃	2000	5	0	0	2000	1		267	53			
			0	200						47		
Co/Al ₂ O ₃	950	5	1.5	30	1000	1.05	350ml/ min (1.25g Cat.)	450	63 (0h) 62 (after 6.5h)	78 (0h) 67 (after 6.5h)	Yan et al. (1997)	
			10	0	1000	1.05	500ml/ min (0.5g Cat.)		450	45		80
			1.7	0	1000	1.05	100ml/ min (0.5g Cat.)	450	76	54 (to CO ₂) 24 (to CO)		

Catalyst	Flue Gas Composition				C ₃ H ₆ (ppm)	C ₃ H ₆ /NO	GHSV (h ⁻¹)	T (°C)	NO Conversion to N ₂ (%)	C ₃ H ₆ Conversion (%)	Authors
	NO (ppm)	O ₂ (%)	H ₂ O (%)	SO ₂ (ppm)							
Ag/Al ₂ O ₃	1000	5			1000	1	25,000	450	100	100	Meunier et al. (2001)
Fe/MFI	1000 + 1000(N ₂ O)	4			1000	1	30,000	350	30 100 (N ₂ O, >450°C)	95	Kogel et al., 1999
Au/ Al ₂ O ₃	940	4.7	1.8		940	0.5	100ml/ min (0.3g Cat.)	450	70	-	Ueda et al. (1997)
Pt/ Al ₂ O ₃	1000	5			1000	1	70mg Cat. (Contac t time: 4s)	325	75	100	Yentekakis et al. (2005)
Cu/MOR	1000	5			1000	1	15,000	375	65.1	-	De Lucas et al. (2005)
Cu/ZSM-5	1000	5			1000	1	15,000	375	78.9	-	
Co/MOR	1000	5			1000	1	15,000	375	81.4	-	
Co/ZSM-5	1000	5			1000	1	15,000	375	66.8	-	
Ni/MOR	1000	5			1000	1	15,000	450	79.8	-	
Ni/ZSM-5	1000	5			1000	1	15,000	425	76.6	-	
Mn/MOR	1000	5			1000	1	15,000	400	73.6	-	
Mn/ZSM-5	1000	5			1000	1	15,000	425	65.2	-	

Table A.7 HC-SCR with iso-C₄H₁₀ (iso-butane) as reducing agent

Catalyst	Flue Gas Composition				iso-C ₄ H ₁₀ (ppm)	iso-C ₄ H ₁₀ /NO	GHSV (h ⁻¹)	T (°C)	NO Conversion to N ₂ (%)	iso-C ₄ H ₁₀ Conversion (%)	Authors	
	NO (ppm)	O ₂ (%)	H ₂ O (%)	SO ₂ (ppm)								
Co/ZSM-5 (WIE)	2000	3	0	0	2000	1	42,000	450	88 (N ₂ yield)	21(CO yield) 46(CO ₂ yield)	Wang et al (2000)	
			10					98(N ₂ yield)	31(CO yield) 43(CO ₂ yield)			
Co/ZSM-5 (IMP)	2000	3	0	0	2000	1	42,000	450	80(N ₂ yield)	3(CO yield) 89(CO ₂ yield)		
			10					72(N ₂ yield)	4(CO yield) 73(CO ₂ yield)			
Co/ZSM-5 (SUB)	2000	3	0	0	2000	1	42,000	400	99(N ₂ yield)	4(CO yield) 87(CO ₂ yield)		
			10					92(N ₂ yield)	4(CO yield) 85(CO ₂ yield)			
Co/ZSM-5 (SSI)	2000	3	0	0	2000	1	42,000	400	56(N ₂ yield)	-(CO yield) 59(CO ₂ yield)		
			10					64(N ₂ yield)	2(CO yield) 51(CO ₂ yield)			
Fe/ZSM-5 (WIE)	2000	3	20	0	2000	1	42,000	450	60	70		Hall et al (1998)
Fe/ZSM-5 (SUB)	2000	3	10	0	2000	1	42,000	350	76.6	55 (to CO) 28(To CO ₂)		Chen et al (1998a)
Fe/ZSM-5 (WIE)	2000	3	0	0	2000	1	42,000	350	55	44		

Catalyst	Flue Gas Composition				iso-C ₄ H ₁₀ (ppm)	iso-C ₄ H ₁₀ /NO	GHSV (h ⁻¹)	T (°C)	NO Conversion to N ₂ (%)	iso-C ₄ H ₁₀ Conversion (%)	Authors	
	NO (ppm)	O ₂ (%)	H ₂ O (%)	SO ₂ (ppm)								
Cu/ZSM-5 (WIE)	1000	3	0	0	1500	1.5	100ml/min (0.18g Cat.)	350	100		Saaid et al (2002)	
Cu/ZSM-5 (IMP)								350	100			
Fe/ZSM-5 (WIE)								400	42			
Fe/ZSM-5 (IMP)								350	42			
Fe/ZSM-5 (SUB)								400	60			
Fe/ZSM-5 (SSI)								400	38			
Fe/MFI	2000	3	0	0	2000	1	280ml/min (0.2g Cat.)	350	76	45 (CO yield), 51 (CO ₂ yield)	Chen et al. (2000b)	
			10						77	53 (CO yield), 34 (CO ₂ yield)		
Fe/BEA			0					10	375	67		37 (CO yield), 80 (CO ₂ yield)
										62		41 (CO yield), 57 (CO ₂ yield)
Fe/FER			0					10	350	18		0 (CO yield), 12 (CO ₂ yield)
										15		3 (CO yield), 4 (CO ₂ yield)
Fe/MOR			0					10	400	12		0 (CO yield), 14 (CO ₂ yield)
										9		0 (CO yield), 5 (CO ₂ yield)
Fe/Y			0					10	450	24		6 (CO yield)
										10		4 (CO yield)

Catalyst	Flue Gas Composition				iso-C ₄ H ₁₀ (ppm)	iso-C ₄ H ₁₀ /NO	GHSV (h ⁻¹)	T (°C)	NO Conversion to N ₂ (%)	iso-C ₄ H ₁₀ Conversion (%)	Authors
	NO (ppm)	O ₂ (%)	H ₂ O (%)	SO ₂ (ppm)							
Co/ZSM-5	2000	10	0	0	2000	1	75ml/min (0.25g Cat.)	400	82	100	Witzel et al (1994)
Ni/ZSM-5								400	90	70	
Mn/ZSM-5								400	87	87	
Ga/ZSM-5								400	87	50	
La/ZSM-5								500	62	100	
Cu/ZSM-5								350	95	98	
Fe/ZSM-5	2000	3		0	2000	1	42,000	350	59.1	40 (to CO) 31.9 (to CO ₂)	Decyk et al. (2001)
	2000	3		150(*)	2000	1	42,000	350	36	21.5 (to CO) 13.3 (to CO ₂)	
	2000	3		0 (after *)	2000	1	42,000	350	43.8	27 (to CO) 20.6 (to CO ₂)	
	2000	3		300 (#)	2000	1	42,000	350	24.7	15 (to CO) 9.1 (to CO ₂)	
	2000	3		0 (after #)	2000	1	42,000	350	36.5	20.6 (to CO) 17 (to CO ₂)	

Table A.8 HC-SCR with other hydrocarbons as reducing agent

Catalyst	Flue Gas Composition				HC (ppm)	HC/NO	GHSV (h ⁻¹)	T (°C)	NO Conversion to N ₂ (%)	HC Conversion (%)	Authors
	NO (ppm)	O ₂ (%)	H ₂ O (%)	SO ₂ (ppm)							
Fe/ZSM-5	1000	9			n-C ₁₀ H ₂₂ , 300	0.3	70,000	420	73		Delahay et al. (1998)
3.9%Cu-3.5%Sn/ZrO ₂								380	43		
Ag/Al ₂ O ₃	1000	10	10	0	n-C ₁₀ H ₂₂ , 333	0.333	0.05gs/ml	300	28	52	Sato et al. (2003)
Ag-Rh/Al ₂ O ₃				0				300	46	60	
Rh-Ag/Al ₂ O ₃				0				300	54	53	
				1				350	74		
				20				350	18		
Cu/ZSM-5				0				350	42		
				1				350	30		
				20				350	28		
Cu/Al ₂ O ₃	1000	6.7		C ₂ H ₆ , 6000(C)	6	18,000	500	3	16	Shibata t al. (2002)	
				C ₆ H ₁₄ , 6000(C)			375	25	58		
				C ₈ H ₁₈ , 6000(C)			350	32	55		
Ag/Al ₂ O ₃	1000	10	2	n-butane, 6000(C)	6	0.12 gs/ml	450	100		Shimizu et al. (2000)	
				C ₂ H ₆ , 6000(C)			550	73			
				n-C ₆ H ₁₄ , 6000 (C)			325	80			
				n-C ₈ H ₁₈ , 6000(C)			350	100			
Ag/Al ₂ O ₃	1000	10	2	n-C ₈ H ₁₈ , 6000 (C)	6	0.12 gs/ml	327-377	100			
Co/Al ₂ O ₃							450	70			
Ni/Al ₂ O ₃							450	62			
Ga/Al ₂ O ₃							450	58			
Sn/Al ₂ O ₃							450	68			
Al ₂ O ₃							450	60			

Catalyst	Flue Gas Composition				HC (ppm)	HC/NO	GHSV (h ⁻¹)	T (°C)	NO Conversion to N ₂ (%)	HC Conversion (%)	Authors
	NO (ppm)	O ₂ (%)	H ₂ O (%)	SO ₂ (ppm)							
Co/ZSM-5	1000	10			n-C ₈ H ₁₈ , 1000	1	30,000	510	58		Inui et al. (1997)
Pt/Al ₂ O ₃	500	5			n-C ₈ H ₁₈ , 1000	2		210	60	100	Burch et al. (1998)
1.3%Fe/SUZ-4	230	7	0	0	C ₂ H ₄ , 1200	5.2		500	5(NO _x), 72(NO)	55	Subbiah et al. (2003)
5.9%Ag/SUZ-4			0	0				550	8(NO _x), 80(NO)	40	
0.1%Co/SUZ-4			0	0				550	20(NO _x), 76(NO)	72	
2.3%Cu/SUZ-4	230	7	0	0	C ₂ H ₄ , 1200	5.2		450	68(NO _x), 65(NO)	100	
			2.5	0				475	42(NO _x), 40(NO)		
			0	15				450	46(NO _x), 42(NO)		
			2.5	15				500	43(NO _x), 42(NO)		
Aged 2.3%Cu/SUZ-4	230	7	0	0	C ₂ H ₄ , 1200	5.2		525	55(NO _x), 85(NO)	90	
			2.5	0				525	44(NO _x), 91(NO)	83	
			2.5	15				550	40(NO _x), 68(NO)	88	
2.3%Cu/ZSM-5	230	7	0	0	C ₂ H ₄ , 1200	5.2		350	63(NO)		
Aged 2.3%Cu/ZSM-5								450	24(NO)		
Fe/ZSM-5 (CVD)	1000	9	0	0	n-C ₁₀ H ₂₂ , 300	0.3	35,000	400	53	100	Lima et al (2008)
Fe/ZSM-5 (IMPO)									53	100	
Fe/ZSM-5 (IMPA)									40	100	

Table A.9 HC-SCR with oxygenated hydrocarbons as reducing agent

Catalyst	Flue Gas Composition				O.H. (ppm)	O.H./ NO	GHSV (h ⁻¹)	T (°C)	NO Conversion (%)	O.H. Conversion (%)	Authors
	NO (ppm)	O ₂ (%)	H ₂ O (%)	SO ₂ (ppm)							
γ -Al ₂ O ₃	80	4		235	CH ₃ OH, 1500	18.75		400	80	60	Efthimiadis et al. (2001)
γ -Al ₂ O ₃	500	5			CH ₃ OH, 3000	6	12,000	350	100	16(CO ₂), 40(CO), 25(DME)	Burch et al. (1998)
Sulphated-Al ₂ O ₃	500	5			CH ₃ OH, 3000	6	12,000	350-400	90		
γ -Al ₂ O ₃	1700	3			CH ₃ OH, 3400	2	25,500	485	68	82	Masters et al. (1999b)
5%MoO ₃ - Al ₂ O ₃								420	72	25	
6%V ₂ O ₅ - Al ₂ O ₃								475	27	48	
Pd/Mordenite	91	9.1	9.1		Ethanol, 500	5.5	44,000	350	25	100	Uchida et al. (1995)
					Acetaldehyde, 500	5.5		350	30	100	
					Acetic acid, 500	5.5		350	56		
					Acetic acid, 1000	11		350	78		
					Acetic acid, 2000	22		350	94		
	377				Acetic acid, 1663	4.4	31,932	320	52.2	96.1	Lee (2000)
								28.4	99.3		
								20.4	96.1		
V ₂ O ₅ - γ -Al ₂ O ₃	500				Acetic Acid, 500	1	5000	300	100		Elkaim et al., 2000
					Acetic Acid, 2250	4.5			81		
					Acetic Acid, 2250	4.5			60		
					Acetic Acid, 2250	4.5			38		
					Acetic Acid, 500	1			99.4		
					Acetic Acid, 500	1			99.7		
					Acetic Acid, 500	1			97		

Table A.10 NSR with reducing agent

Catalyst	Exhaust Gas Composition		GHSV (h ⁻¹)	T (°C)	Sorption Efficiency (%)	Reduction Efficiency (%)	Overall NO Conversion (%)	Authors
	Sorption Cycle	Reduction Cycle						
Pt-Ba/Al ₂ O ₃	250ppm NO, 150ppm CO, 8%O ₂ , N ₂	0ppm NO, 150ppm CO, 0%O ₂ , 1500ppm H ₂ , N ₂	25,000	175	80.2	90.4	72.6	Epling et al. (2003)
				200	91.0	94.2	85.7	
				225	95.6	96.1	91.9	
				250	85.1	96.0	81.7	
				278	88.9	96.1	85.4	
				303	91.6	95.3	87.2	
				330	92.9	92.7	86.1	
	250ppm NO, 150ppm CO, 8%O ₂ , 8%H ₂ O, 8%CO ₂ , N ₂	0ppm NO, 150ppm CO, 0%O ₂ , 8%H ₂ O, 8%CO ₂ , 1500ppm H ₂ , N ₂	25,000	175	54.5	85.3	46.5	
				200	69.6	90.4	62.9	
				225	77.9	93.6	72.9	
				250	63.0	93.1	58.6	
				278	66.3	92.4	61.2	
				303	66.2	90.4	59.9	
				330	65.3	87.3	57.0	
Pt/Al ₂ O ₃	1200ppm NO, 800ppm C ₃ H ₆ , 4%O ₂ , He	1200ppm NO, 800ppm C ₃ H ₆ , 0.3%O ₂ , He	95,000	300-500			25-36%	Shinjoh et al. (1998)
							44-55%	
Pt-Ba/Al ₂ O ₃	1200ppm NO, 800ppm C ₃ H ₆ , 4%O ₂ , He	800ppm C ₃ H ₆ , 0.3%O ₂ , He						
Pt-Ba/Al ₂ O ₃	1000 ppm NO, 3%O ₂ , He	2000ppm H ₂ , He	60s storage period: NO adsorbed: 0.74x10 ⁻⁴ , NO desorbed:0.91x10 ⁻⁴ mol/g Cat, 350°C 120s storage period: NO adsorbed: 1.5x10 ⁻⁴ , NO desorbed:1.88x10 ⁻⁴ mol/g Cat, 350°C				Lietti et al. (2001)	
Pt-Rh/Al ₂ O ₃	300-1100ppm NO,	300-1100ppm NO,	No NO _x storage could be observed, N ₂ O was formed				Fridell et al. (1999)	
BaO-Al ₂ O ₃	NO,	NO,	No NO _x storage could be observed, no reaction took place					
Pt-Rh/BaO-Al ₂ O ₃	900 ppm C ₃ H ₆ , 8% O ₂ , 400°C	900ppm C ₃ H ₆ , 400°C	NO _x storage could be observed, N ₂ O was formed					

Appendix B

Calibration

B.1 Gas flow meters

Calibration curves for gas flow meters used in the fixed bed reaction system are shown in Figures G.1 to G.5.

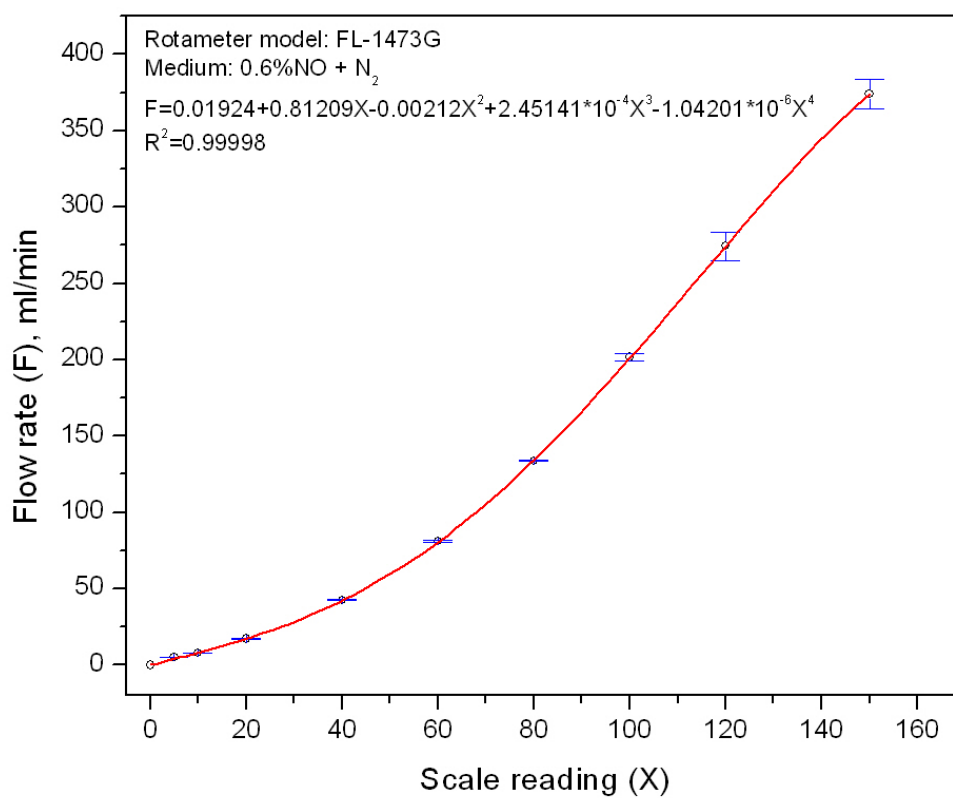


Figure B.1 Calibration curve of FL-1473G rotameter (0.6% NO + N₂)

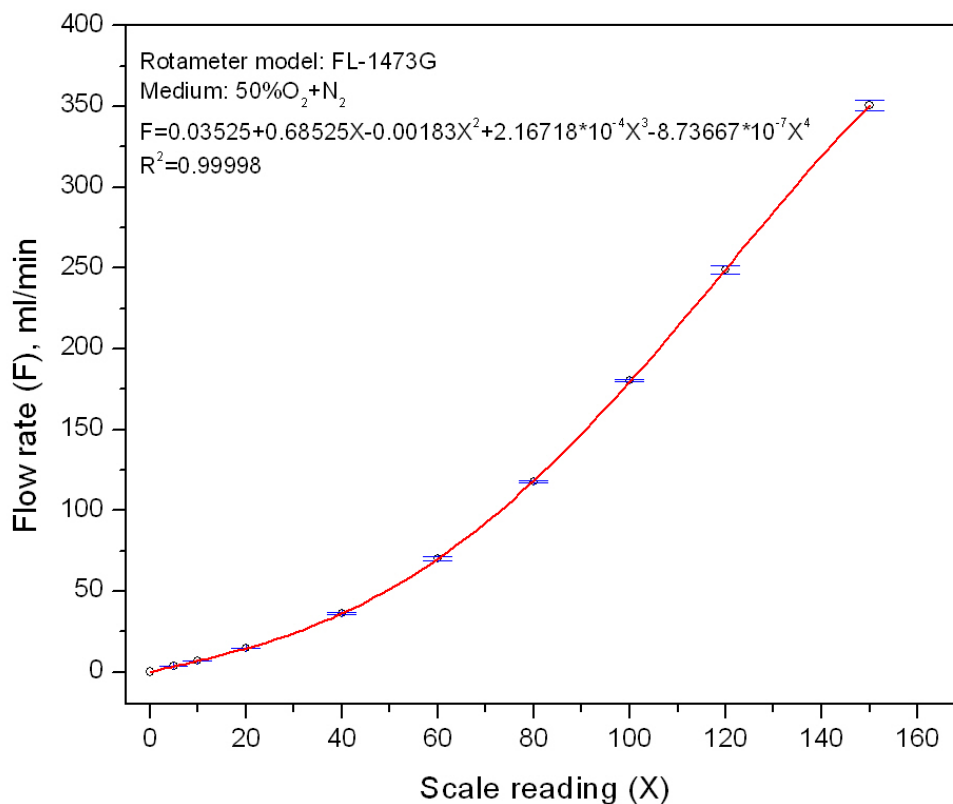


Figure B.2 Calibration curve of FL-1473G rotameter (50% O₂ + N₂)

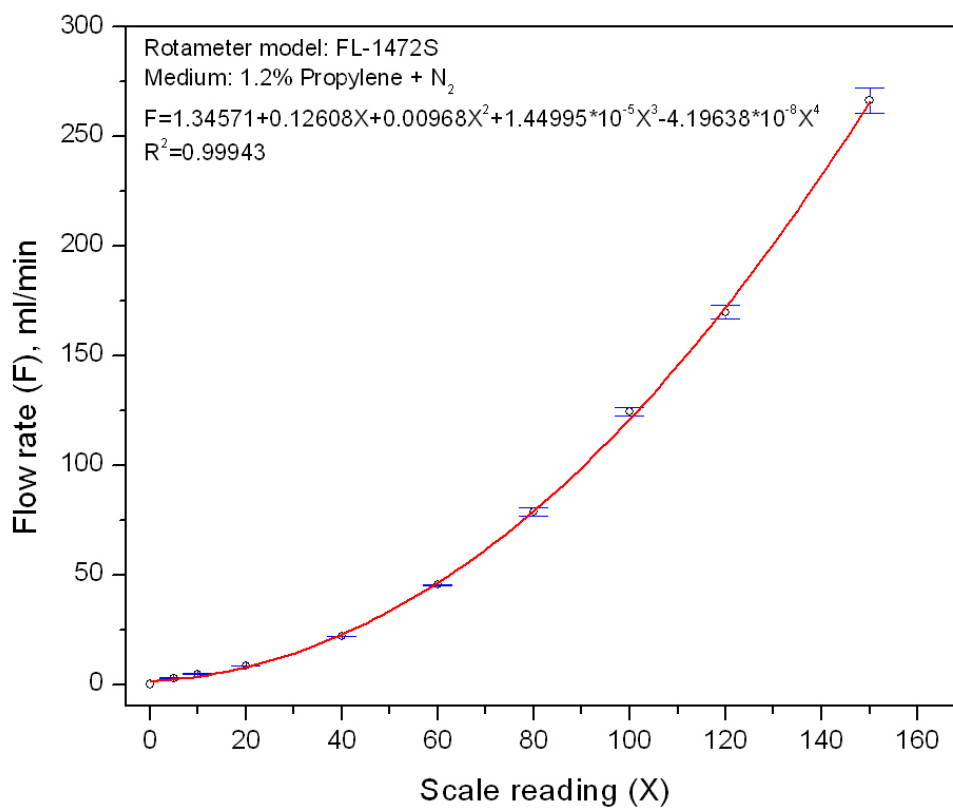


Figure B.3 Calibration curve of FL-1472S rotameter (1.2% Propylene + N₂)

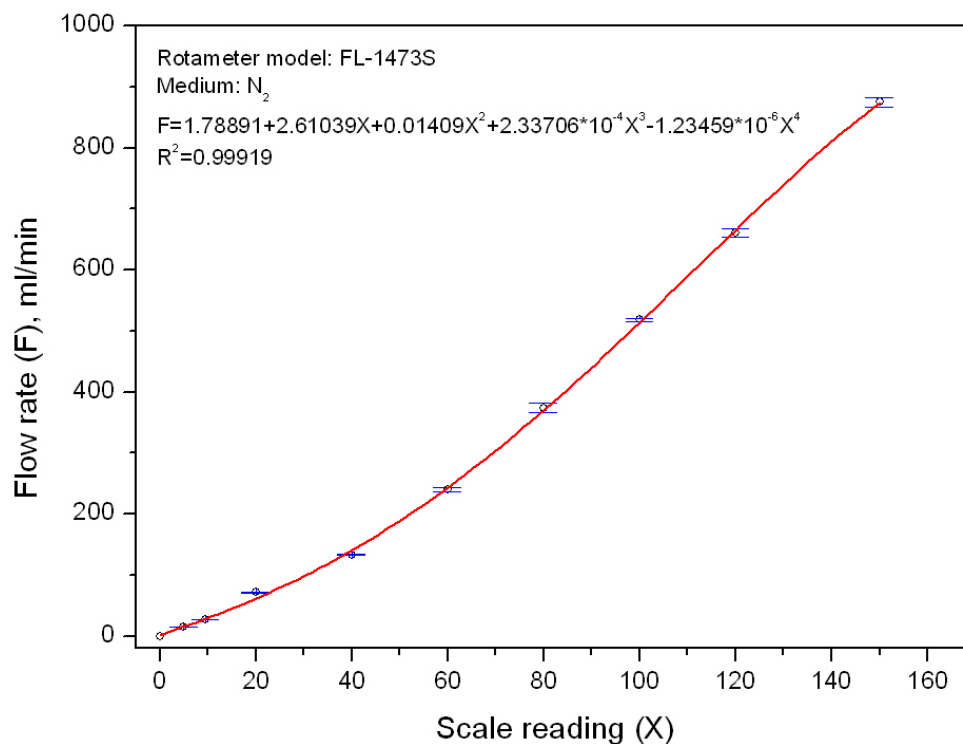


Figure B.4 Calibration curve of FL-1473S rotameter (N₂)

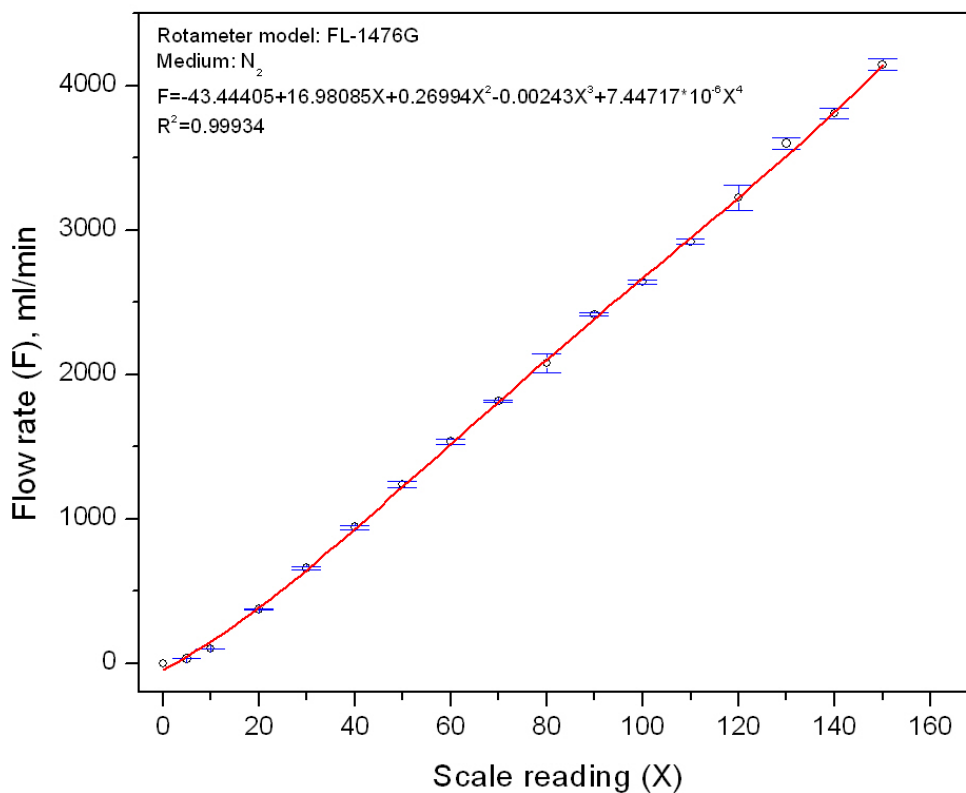


Figure B.5 Calibration curve of FL-1476G rotameter (N₂)

B.2 Peristaltic water pump

In the fixed bed reaction system, liquid water was pumped into the system by a LKB Microperpex peristaltic pump. The pump was calibrated with the relationship between the pump reading and the water flow rate shown in Figure B.6.

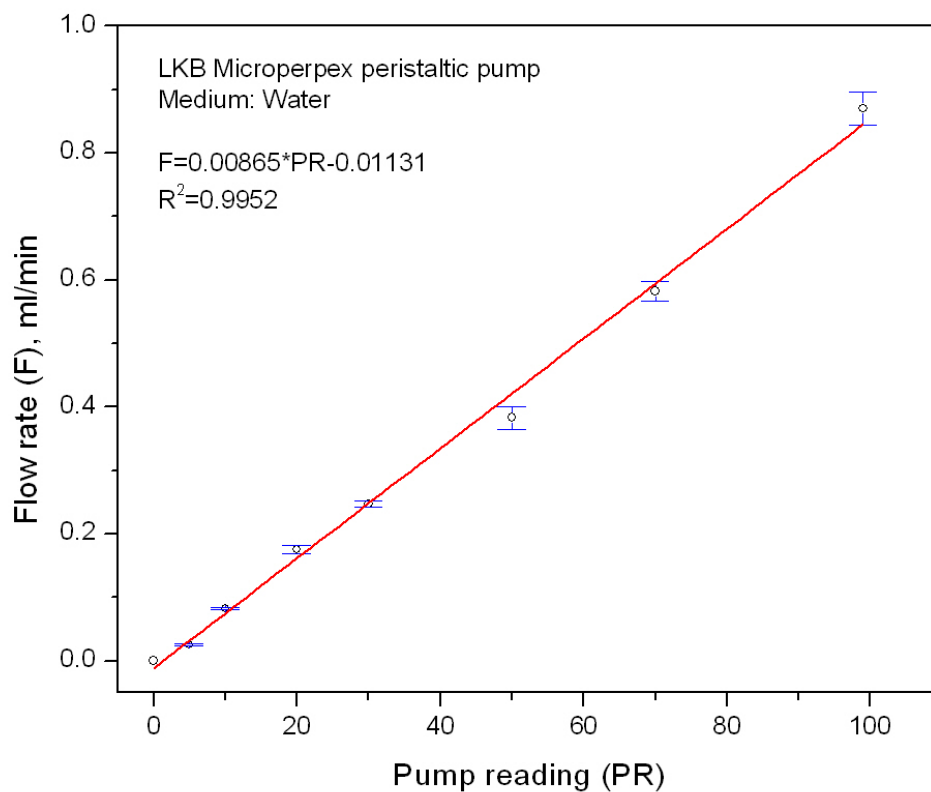


Figure B.6 Calibration curve of peristaltic water pump

B.3 Pressure transducers

Pressure transducers used in the cold model and hot model ICFB systems were calibrated using a U-tube manometer. Relationships between the measured voltage and pressure are shown in Figures B.7 to B.11.

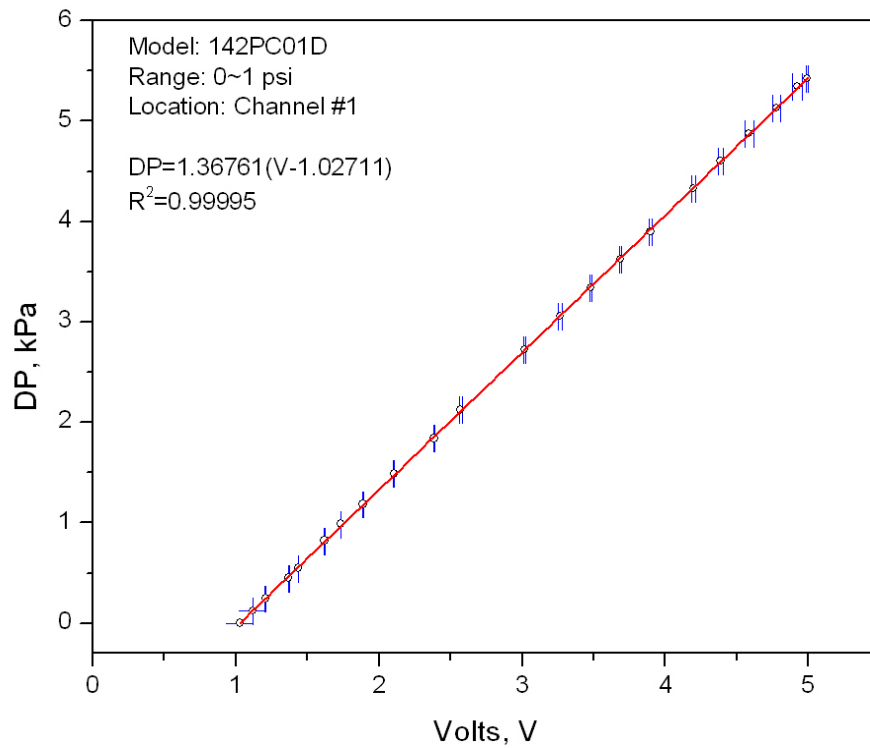


Figure B.7 Calibration curve of pressure transducer (Channel #1)

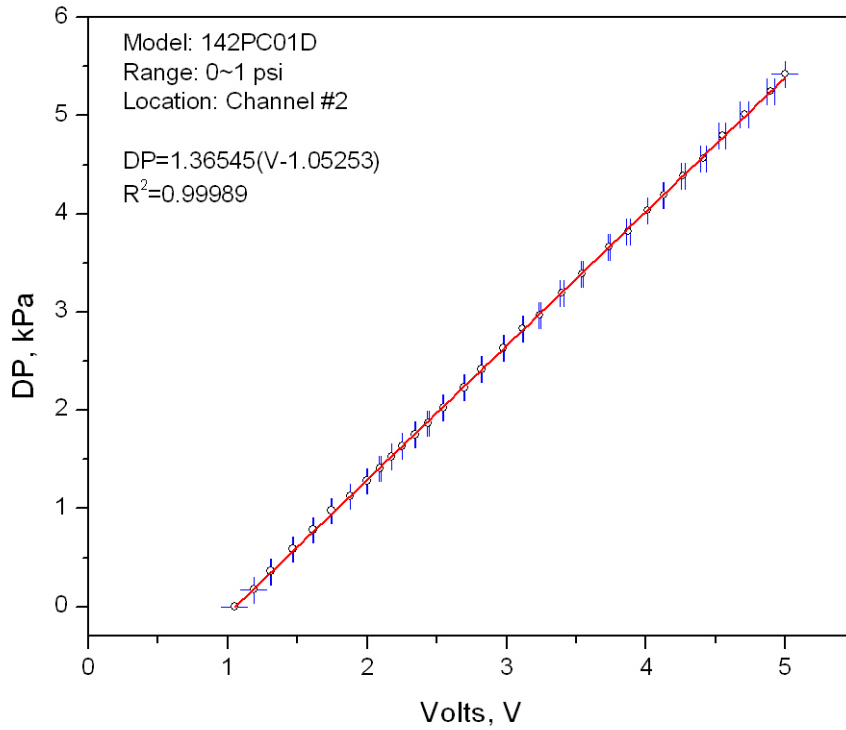


Figure B.8 Calibration curve of pressure transducer (Channel #2)

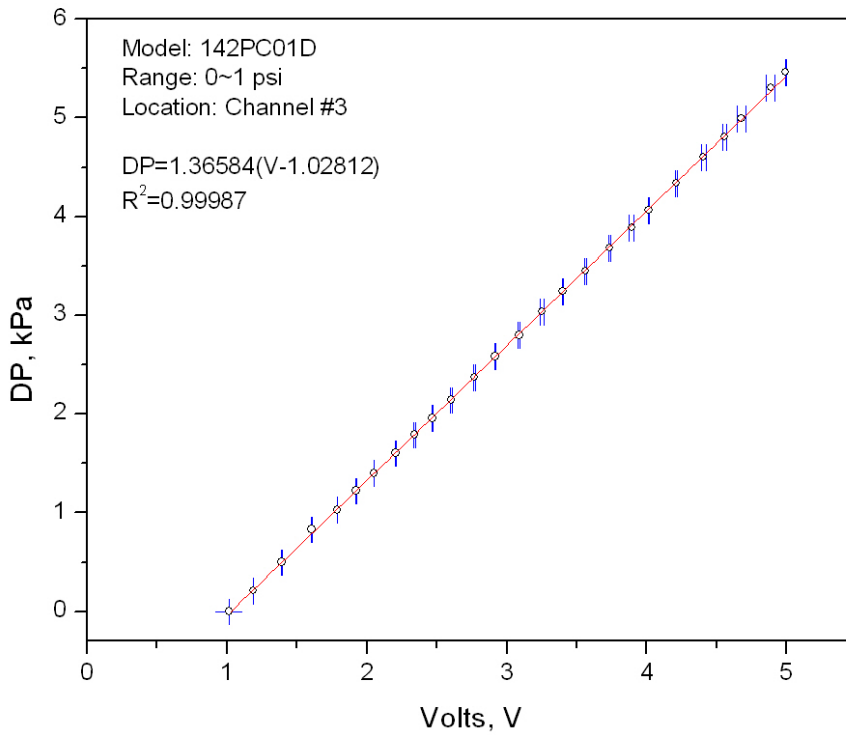


Figure B.9 Calibration curve of pressure transducer (Channel #3)

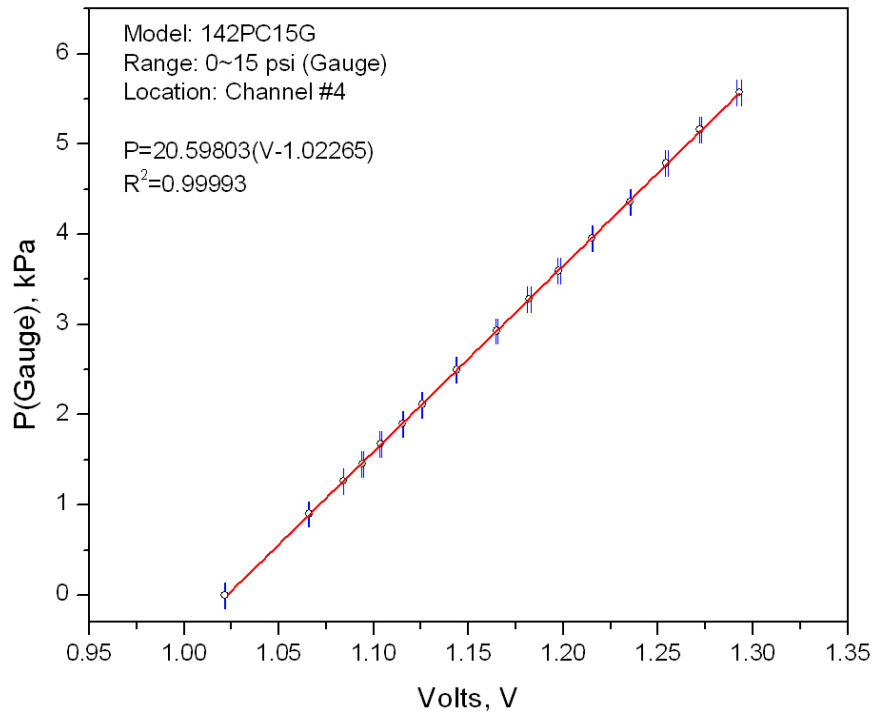


Figure B.10 Calibration curve of pressure transducer (Channel #4)

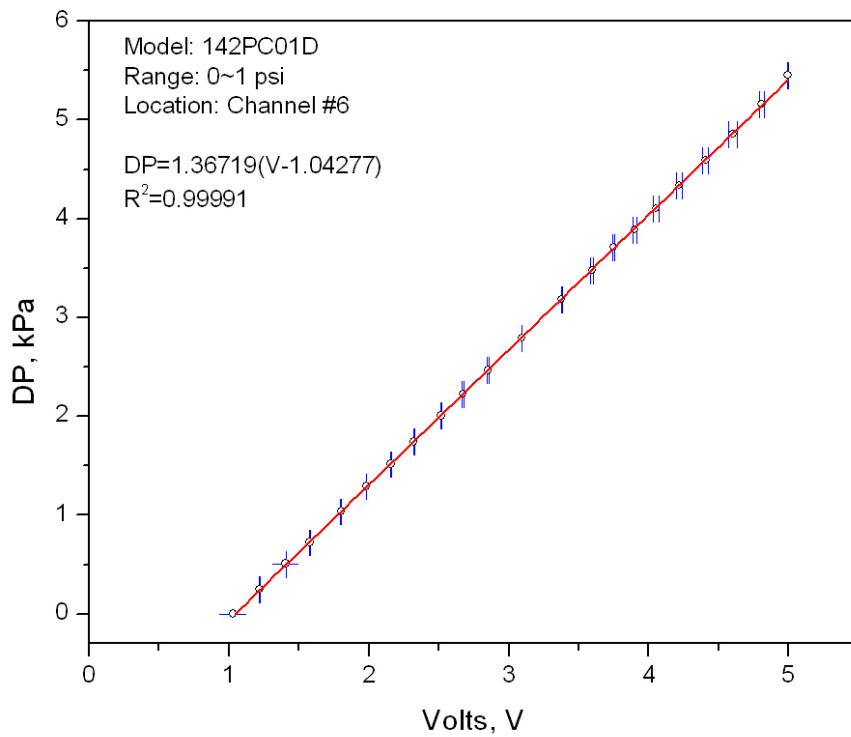


Figure B.11 Calibration curve of pressure transducer (Channel #6)

Appendix C

BET Surface Area

Table C.1 BET surface areas for catalysts used in this work

Sample	Sample weight (g)	Measured surface area (m ²)	S _{BET} (m ² /g)	Average S _{BET} (m ² /g)
Na/ZSM-5(PUC)	0.19	21.98	115.68	118
	0.20	23.96	119.80	
	0.20	23.45	117.25	
Fresh Fe/ZSM-5 (PUC)	0.18	20.03	111.28	110
	0.17	18.62	109.53	
Regenerated Fe/ZSM-5 (PUC)	0.19	20.85	109.74	109
	0.19	20.60	108.42	
Spent Fe/ZSM-5 (PUC)	0.21	14.63	69.67	67
	0.23	14.01	65.26	
Na/ZSM-5 (Crushed PUC)	0.11	21.12	192	192
Fresh Fe/ZSM-5 (Crushed PUC)	0.10	18.42	184.2	184
H/ZSM-5 (Albemarle)	0.11	18.77	170.64	171
Fresh Fe/ZSM-5 (Albemarle)	0.11	17.79	161.73	162
Fe/ZSM-5 (Albemarle) aged by 30ppm SO ₂ (Calcined after placed overnight)	0.11	11.36	103.27	103
Fe/ZSM-5 (Albemarle) aged by 200ppm SO ₂ (Calcined immediately)	0.11	14.19	129	129

Appendix D

Particle Size Distribution

The particle size distribution for the four catalysts used in this study was measured by a Mastersizer 2000 particle size analyzer using the wet dispersion method. Three runs were carried out for each catalyst, with the results shown in Figures D.1 to D.4.

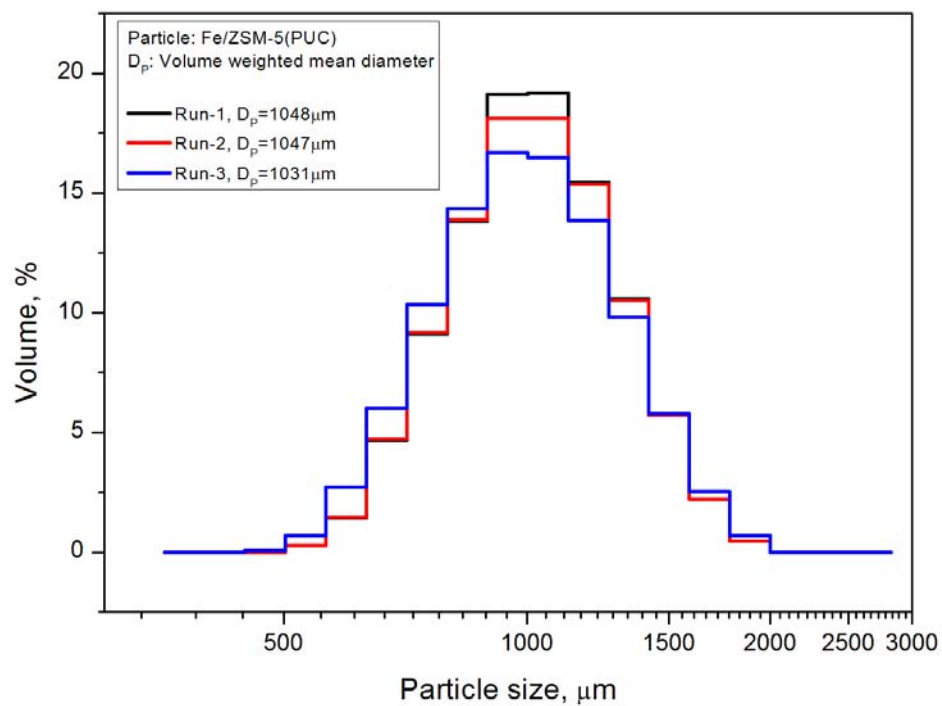


Figure D.1 Particle size distribution (Fe/ZSM-5(PUC))

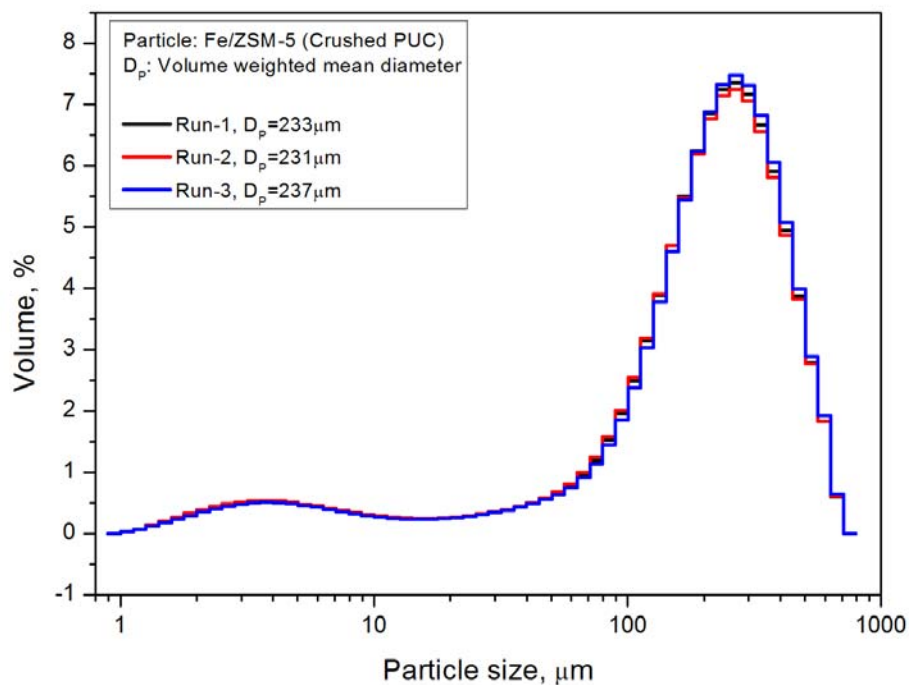


Figure D.2 Particle size distribution (Fe/ZSM-5(crushed PUC))

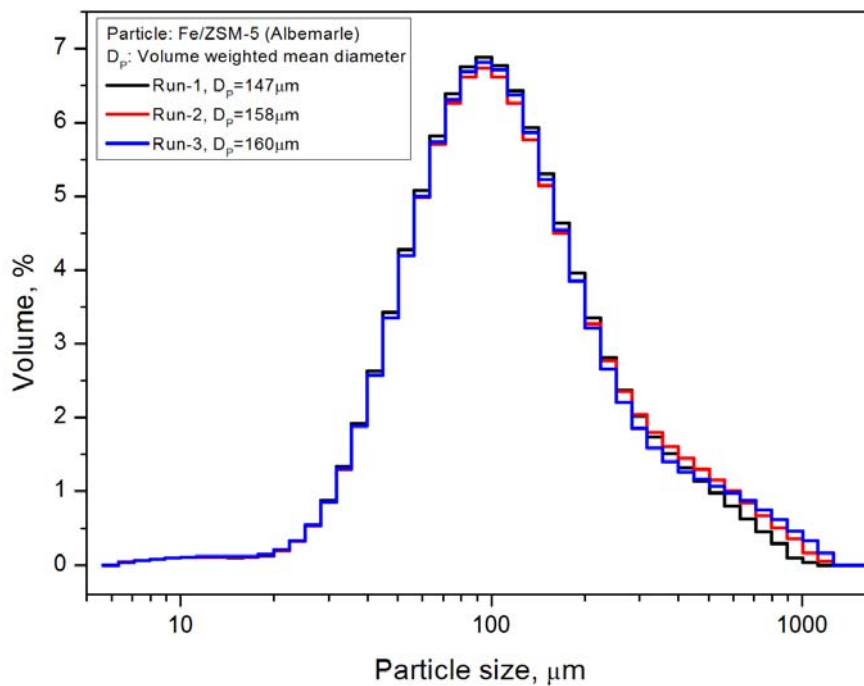


Figure D.3 Particle size distribution (Fe/ZSM-5(Albemarle))

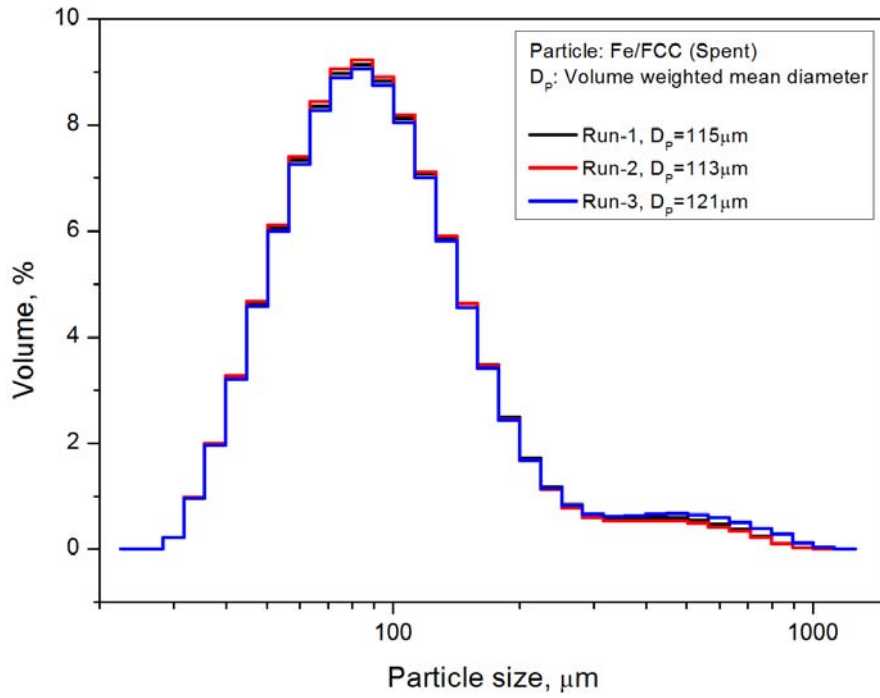


Figure D.4 Particle size distribution (Fe/FCC(Spent))

Appendix E

Adsorption and Reaction Kinetics of Fe/ZSM-5 (Crushed PUC) Catalyst

To investigate the effect of the particle size on the adsorption and reaction performances of the Fe/ZSM-5 (PUC) catalyst prepared via IMPO method, the parent Na/ZSM-5 (PUC) particles were crushed and sieved to obtain fine particles for the preparation of the Fe/ZSM-5(crushed PUC) catalyst by the IMPO method. The adsorption and reaction performances were investigated and compared with the coarse Fe/ZSM-5(PUC) catalyst thereafter.

E.1 Adsorption performance of Fe/ZSM-5(crushed PUC)

The typical adsorption curves for Fe/ZSM-5(crushed PUC) catalyst using the model flue gas containing 4% O₂ and GHSV=5000 h⁻¹ at 325°C, 350°C and 375°C are shown in Figures E.1 to E.3 respectively.

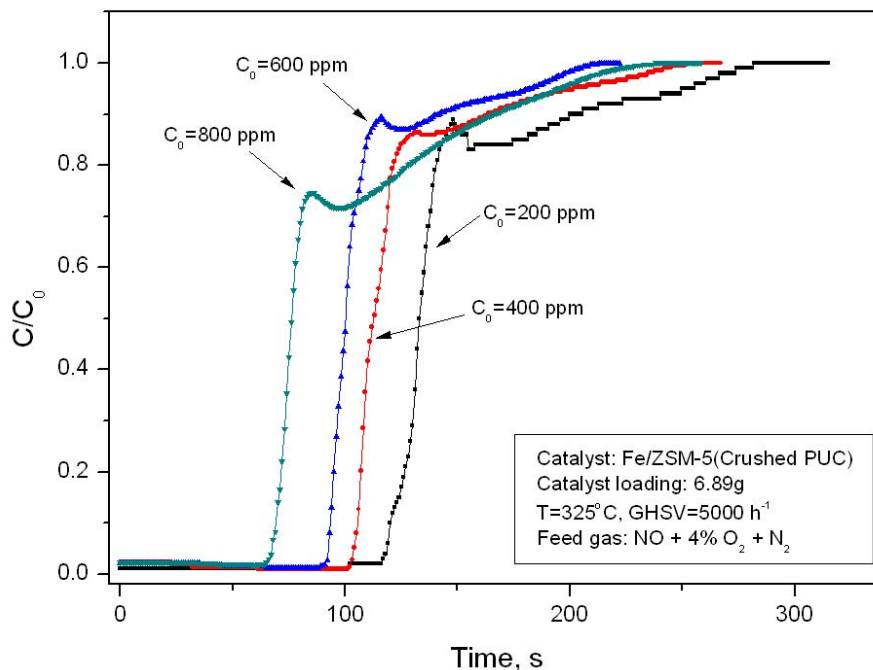


Figure E.1 Adsorption curves based on NO_x concentrations at the reactor outlet (Catalyst: Fe/ZSM-5(crushed PUC), $T=325^\circ\text{C}$)

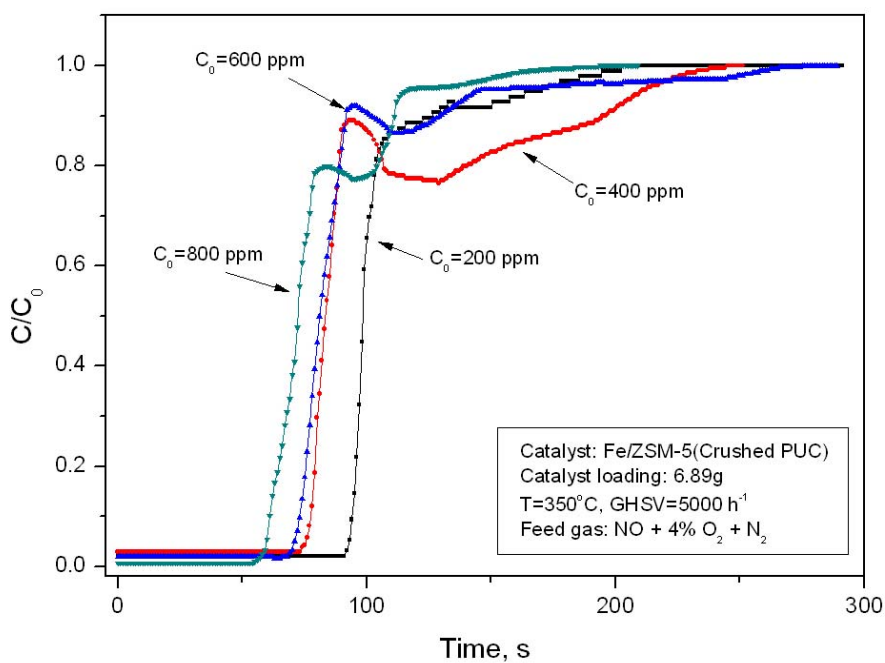


Figure E.2 Adsorption curves based on NO_x concentrations at the reactor outlet (Catalyst: Fe/ZSM-5(crushed PUC), $T=350^\circ\text{C}$)

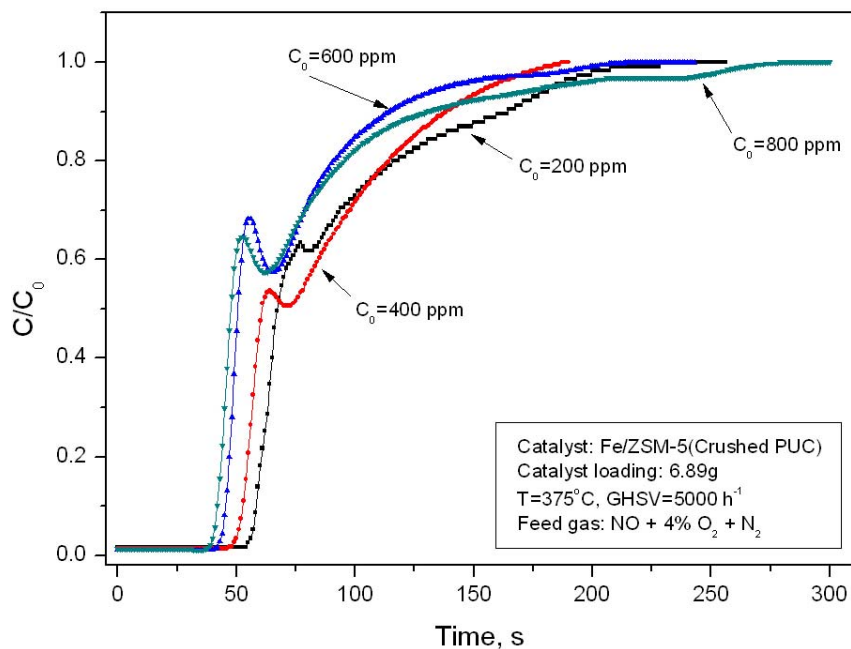


Figure E.3 Adsorption curves based on NO_x concentrations at the reactor outlet (Catalyst: Fe/ZSM-5(crushed PUC), $T=375^\circ\text{C}$)

It can be seen from Figure E.1 that the adsorption curve had an irregular shape, which was different from the one for the coarse Fe/ZSM-5(PUC) catalyst (see Figure 3.2) where the outlet NO_x concentration reached the equilibrium concentration very quickly after the breakthrough of the catalyst bed. At a given temperature, the breakthrough point was reached more quickly at higher inlet NO_x . As the temperature increased, the breakthrough time decreased because more NO_x was adsorbed at low temperatures (Figures E.2 and E.3). Although the breakthrough time did not increase much (60-115s ($T=325^\circ\text{C}$), 55-90s ($T=350^\circ\text{C}$) and 38-55s ($T=375^\circ\text{C}$)) when compared with Fe/ZSM-5(PUC), the equilibrium NO_x concentration was not reached until 100-200 seconds later after the breakthrough of the catalyst bed.

The equilibrium adsorption capacity (q_e) of the catalyst was calculated using equations 3.1 and 3.2. The relationship between q_e and equilibrium NO_x concentration (C_0)

was well fitted by the Freundlich equation (equation 3.3), as shown in Figure E.4. The obtained Freundlich coefficients α and β as a function of the adsorption temperature were also fitted by 2nd order polynomial functions with the results given in Figure E.5.

It is clearly demonstrated in Figure E.4 that the adsorption capacity of the fine Fe/ZSM-5(crushed PUC) catalyst was much higher than the coarse Fe/ZSM-5(PUC). For example, at $T=350^{\circ}\text{C}$ and $C_0=0.4\text{ g/m}^3$, q_e for the fine Fe/ZSM-5(crushed PUC) is 0.058 mg/g cat. , which is 3.6 times of the coarse Fe/ZSM-5(PUC) (0.016 mg/g cat.). Note that the only remarkable difference in the adsorption experiment of the two catalysts was the particle size, with the average particle size of coarse Fe/ZSM-5(PUC) as $1042\mu\text{m}$, 4.5 times of the fine Fe/ZSM-5(crushed PUC) ($234\mu\text{m}$). It can thus be concluded that the adsorption performance of Fe/ZSM-5 catalyst prepared from Na/ZSM-5 (PUC) is closely related to the particle size, and a fine catalyst is preferred in order to achieve a high adsorption capacity.

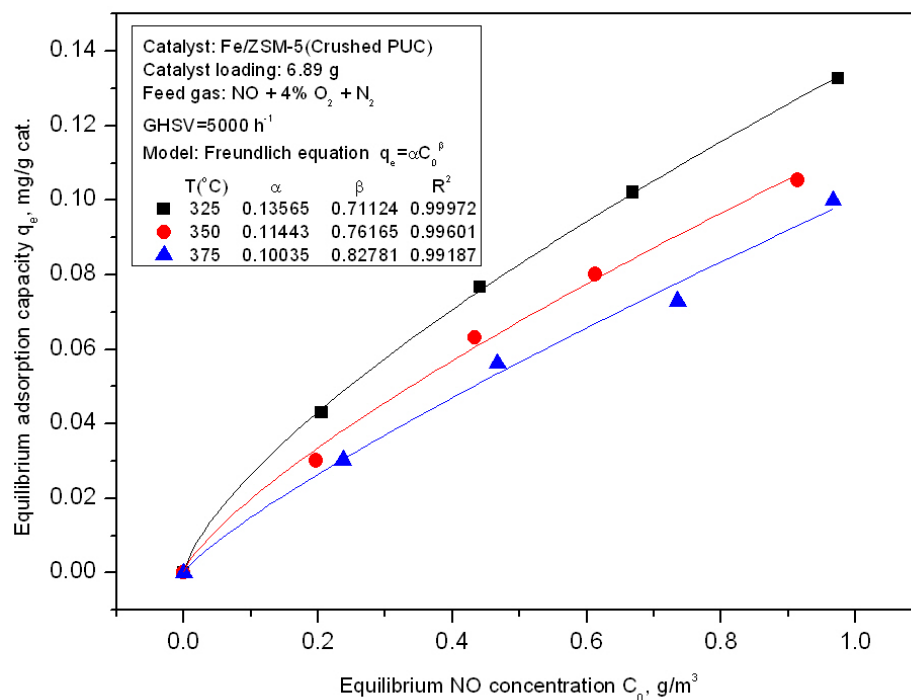


Figure E.4 Fitting of adsorption isotherms of NO_x by Freundlich equation (Catalyst: Fe/ZSM-5(crushed PUC))

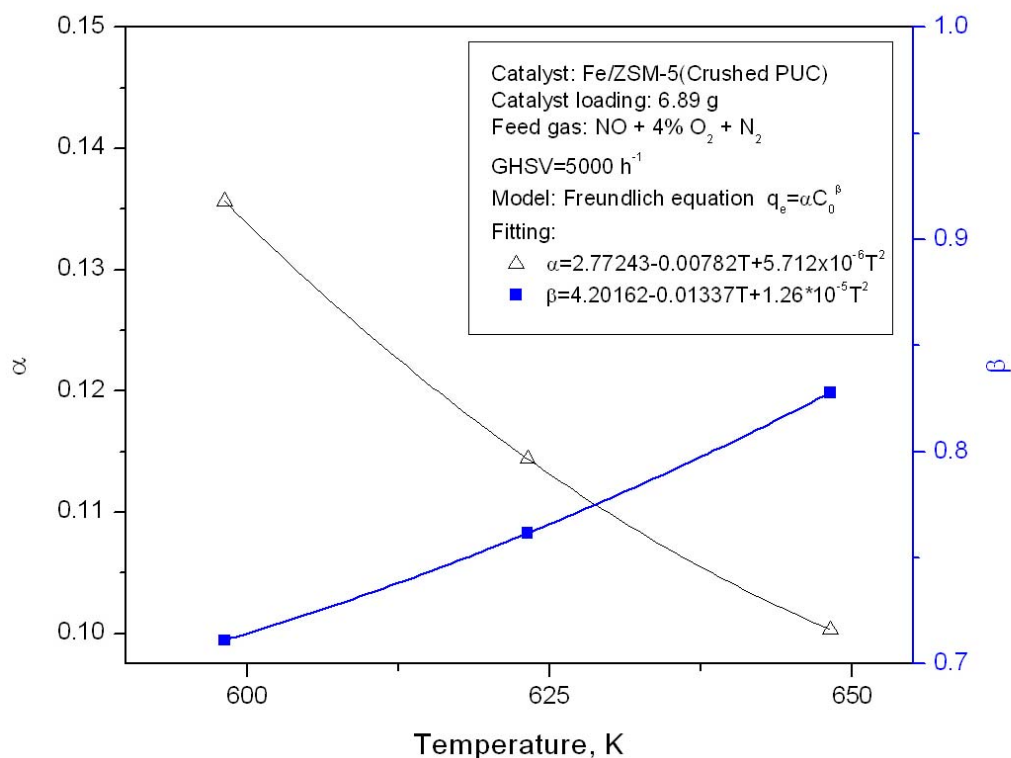


Figure E.5 Relationship between α/β and adsorption temperature (Catalyst: Fe/ZSM-5 (crushed PUC))

E.2 Reaction performance of Fe/ZSM-5(crushed PUC)

The time-on-stream experiment was conducted to evaluate the reaction performance of the selective catalytic reduction of NO_x over the fine Fe/ZSM-5(crushed PUC) catalyst at various temperatures, with the results shown in Figure E.6. The feed gas contained 600ppm NO, 1200ppm HC and 1% O_2 , balanced with N_2 , and the $\text{GHSV}=5000 \text{ h}^{-1}$.

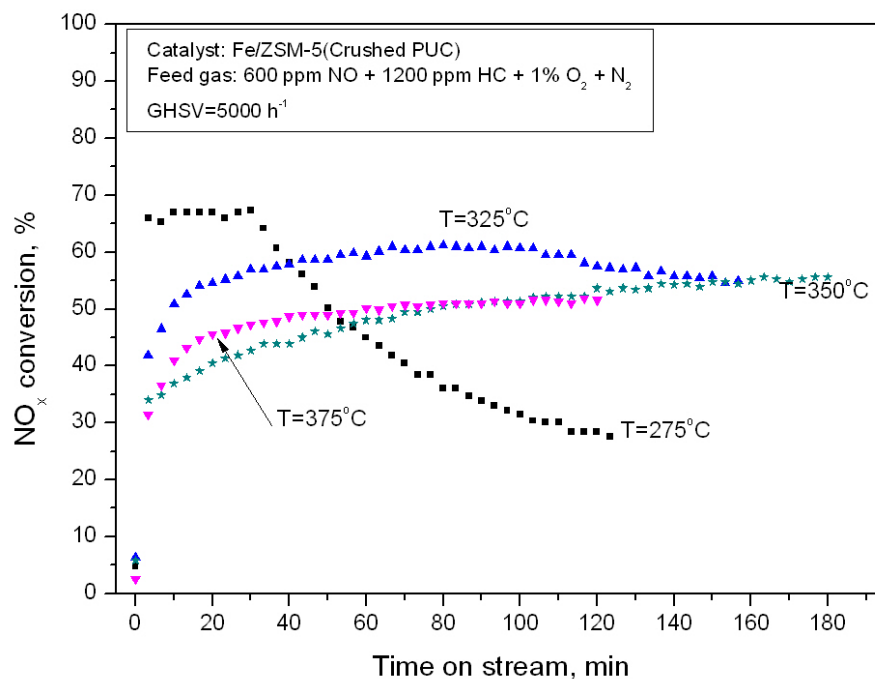


Figure E.6 Effect of reaction temperature on catalytic activity (Catalyst: Fe/ZSM-5(crushed PUC))

At $T=275^{\circ}\text{C}$, a peak NO_x conversion of 67.9% was obtained, but the catalytic activity was unstable with time. With the temperature increased to 325°C , the NO_x conversion became stable over a longer period of time with a peak NO_x conversion of 61.6% when compared with $T=275^{\circ}\text{C}$. The stable yet even lower catalytic activity (55.6% for $T=350^{\circ}\text{C}$ and 51.9% for $T=375^{\circ}\text{C}$) was obtained when $T \geq 350^{\circ}\text{C}$. The influence of reaction temperature on the catalytic activity of both the fine Fe/ZSM-5(crushed PUC) and the coarse Fe/ZSM-5(PUC) is similar with the peak NO_x conversion decreased with the increase in temperature and the catalytic activity remained stable with time at $T \geq 350^{\circ}\text{C}$.

The effect of O_2 concentration was also investigated using model flue gas containing 1% and 4% O_2 at $T=350^{\circ}\text{C}$ and $\text{GHSV}=5000 \text{ h}^{-1}$, with the result shown in Figure E.7. With the inlet O_2 concentration increased from 1% to 4%, the NO_x conversion dropped from

55.6% to 42.5%, reflecting the negative impact of higher O₂ concentration on the performance of HC-SCR reactions.

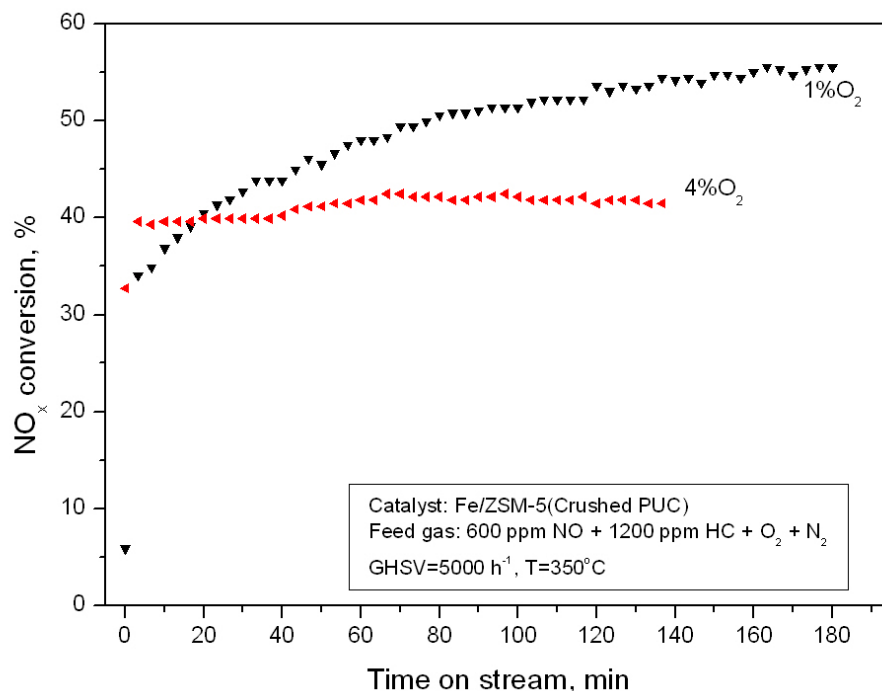


Figure E.7 Effect of inlet O₂ concentration on catalytic activity (Catalyst: Fe/ZSM-5(crushed PUC))

Although the fine Fe/ZSM-5(crushed PUC) exhibited higher NO_x adsorption capacity, for unknown reason, however, its catalytic activity was observed to be lower than the coarse Fe/ZSM-5(PUC) at the same operating conditions. The activity of the catalyst in the HC-SCR process is thus not always directly correlated with the adsorption capability of the catalyst.

Appendix F

HC-SCR Performance of FCC and Fe/FCC Catalyst

A spent Fluid Catalytic Cracking (FCC) catalyst was tested for its possible use as the HC-SCR catalyst. The spent FCC was first calcined in air at 500°C for 4 hours, and then impregnated with Fe using the IMPO method. The SCR test results for both spent FCC and Fe/FCC are shown in Figure F.1. Unfortunately, both spent FCC and Fe/FCC showed very poor catalytic activity. In the temperature range of 300 to 375°C, only 5-10% of the NO_x conversion was achieved.

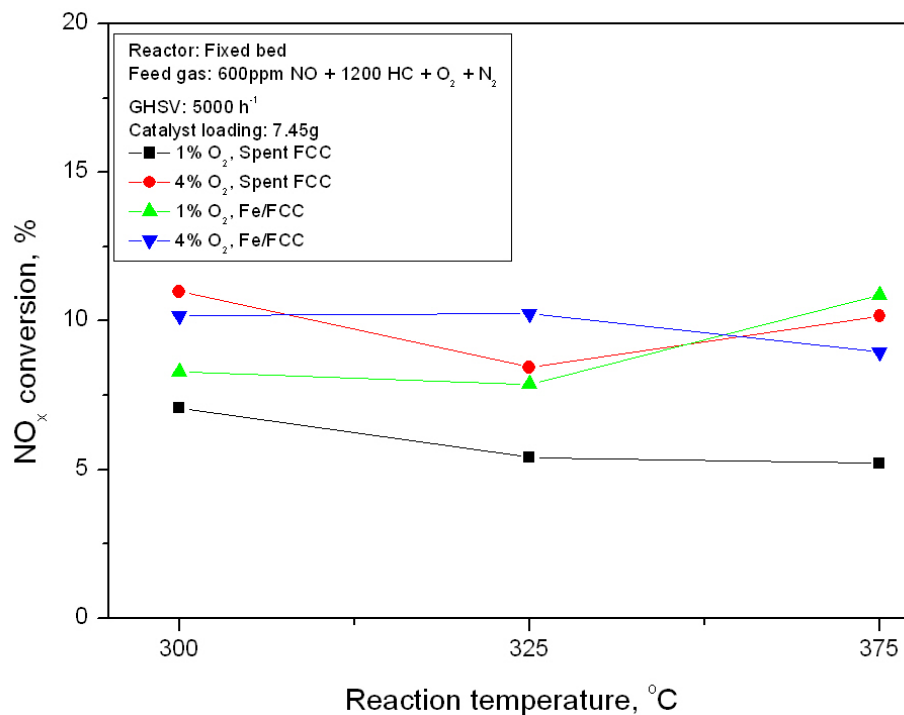


Figure F.1 HC-SCR performance of spent FCC and Fe/FCC

Appendix G

Some Results from the Fixed Bed Experiment

G.1 Adsorption curves for Fe/ZSM-5(PUC) and Fe/ZSM-5(Albemarle)

Adsorption curves for the coarse Fe/ZSM-5(PUC) and fine Fe/ZSM-5(Albemarle) catalyst are shown in Figures G.1 to G.5 and G.6 to G.9, respectively, with the model flue gas containing NO + O₂ + N₂ at various temperatures. Figure G.10 shows adsorption curves for Fe/ZSM-5(Albemarle) catalyst with the model flue gas containing NO + 4% O₂ + 10% H₂O + N₂. The effect of the addition of 10% CO₂ into the model flue gas of NO + 4% O₂ + N₂ is shown in Figure G.11. The combined effect of 10% H₂O and 10% CO₂ on the adsorption performance of Fe/ZSM-5(Albemarle) is shown in Figure G.12.

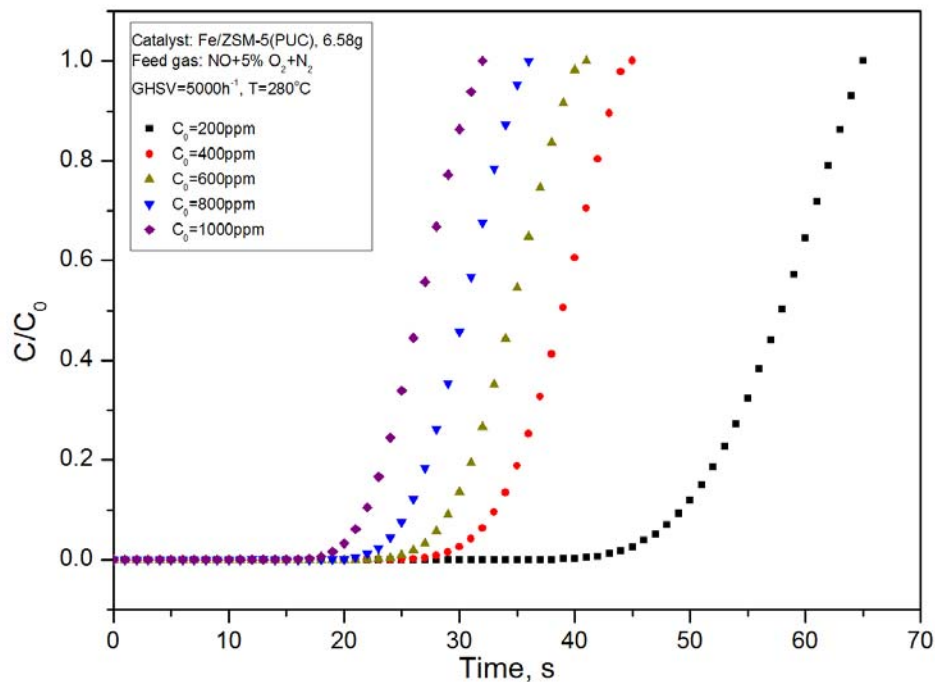


Figure G.1 Adsorption curves based on NO_x concentrations at the reactor outlet (Catalyst: Fe/ZSM-5(PUC), T=280°C)

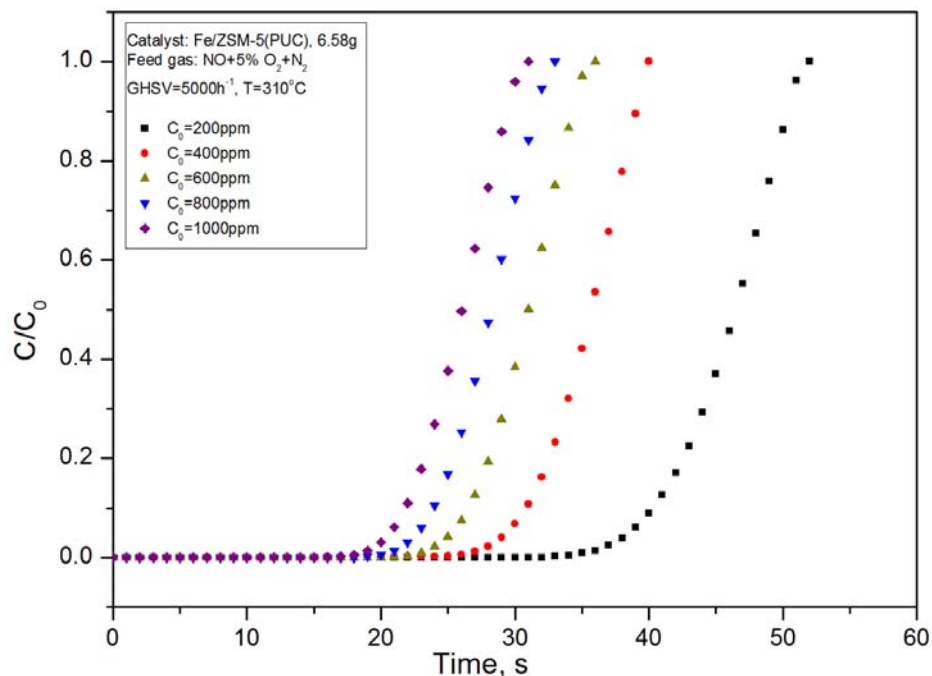


Figure G.2 Adsorption curves based on NO_x concentrations at the reactor outlet (Catalyst: Fe/ZSM-5(PUC), T=310°C)

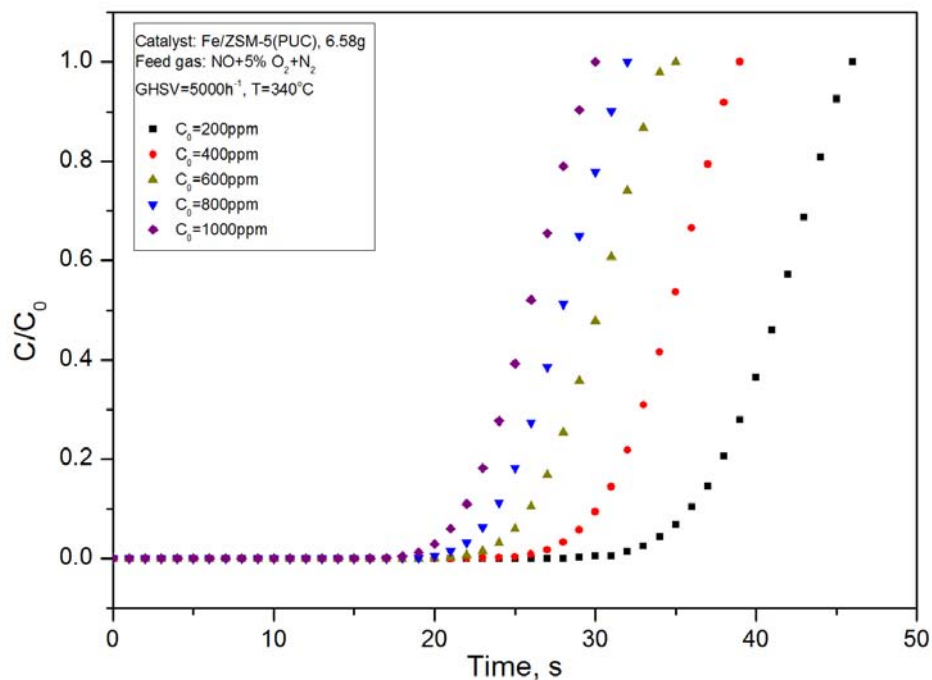


Figure G.3 Adsorption curves based on NO_x concentrations at the reactor outlet (Catalyst: Fe/ZSM-5(PUC), T=340°C)

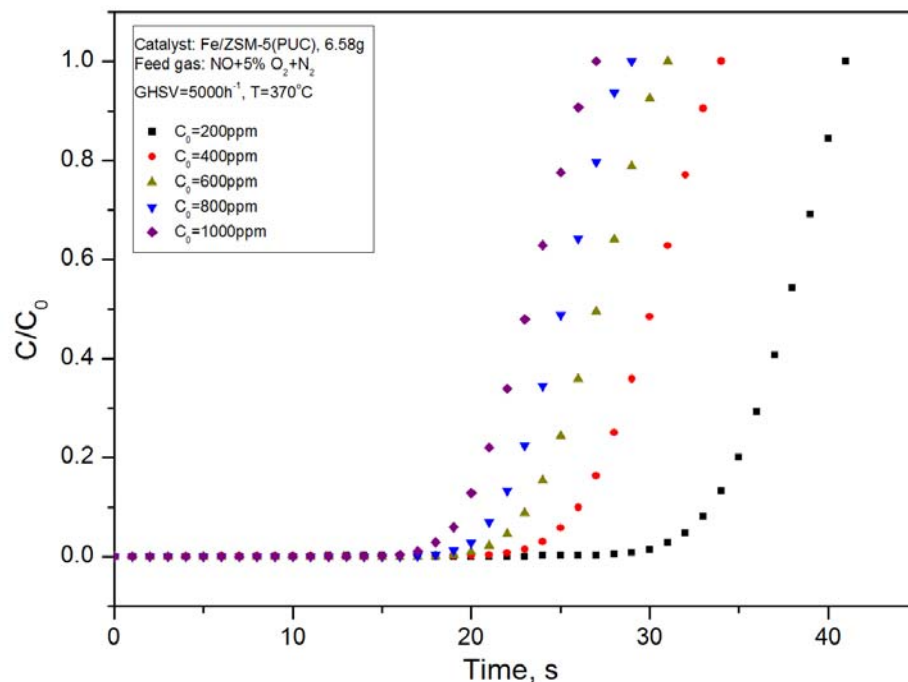


Figure G.4 Adsorption curves based on NO_x concentrations at the reactor outlet (Catalyst: Fe/ZSM-5(PUC), T=370°C)

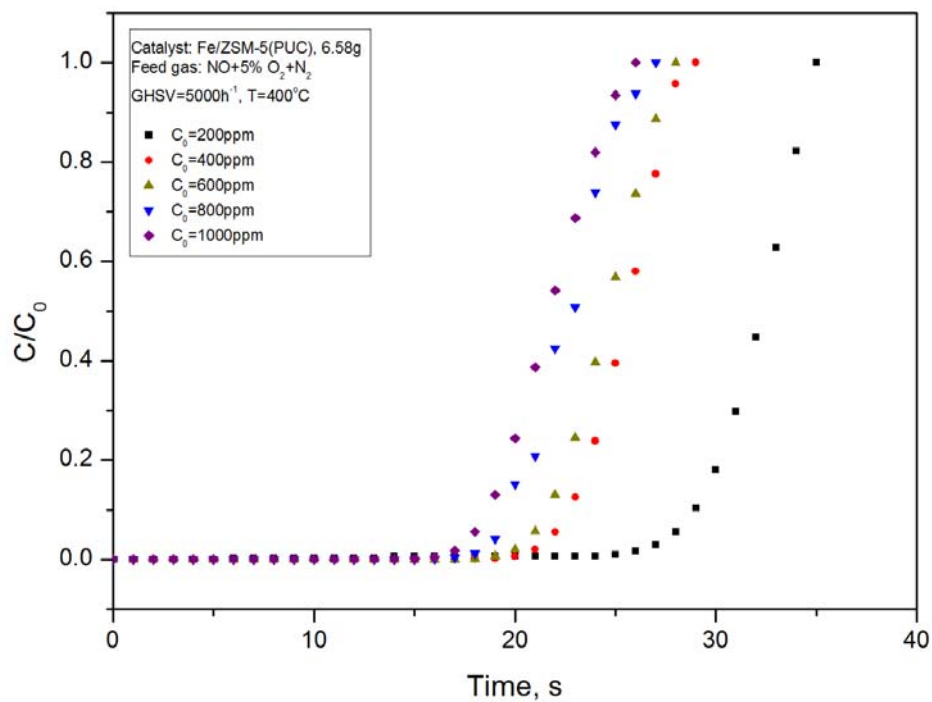


Figure G.5 Adsorption curves based on NO_x concentrations at the reactor outlet (Catalyst: Fe/ZSM-5(PUC), T=400°C)

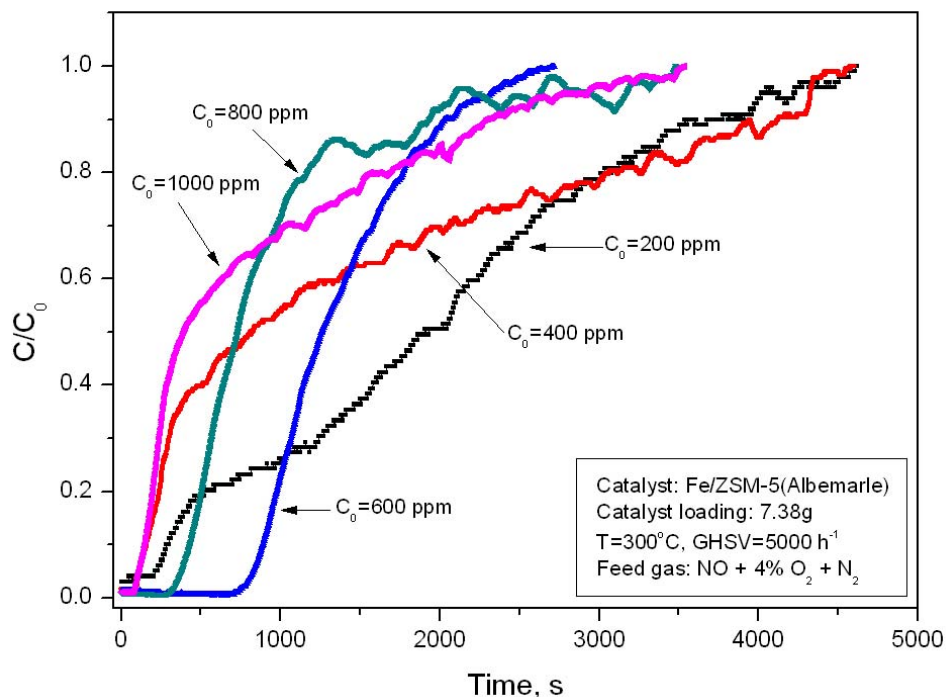


Figure G.6 Adsorption curves based on NO_x concentrations at the reactor outlet (Catalyst: Fe/ZSM-5(Albemarle), $T=300^\circ\text{C}$)

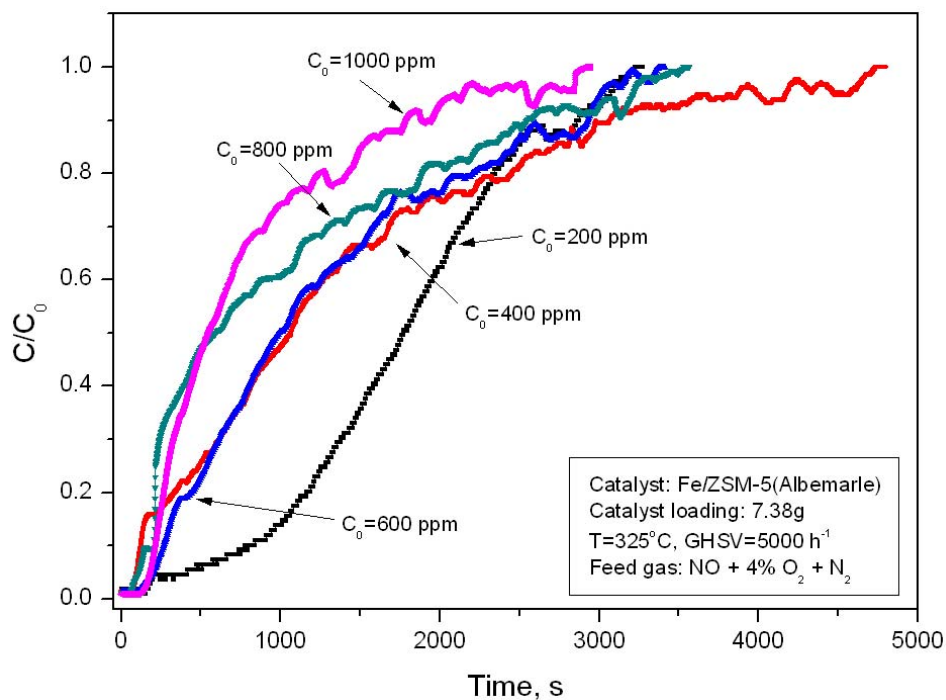


Figure G.7 Adsorption curves based on NO_x concentrations at the reactor outlet (Catalyst: Fe/ZSM-5(Albemarle), $T=325^\circ\text{C}$)

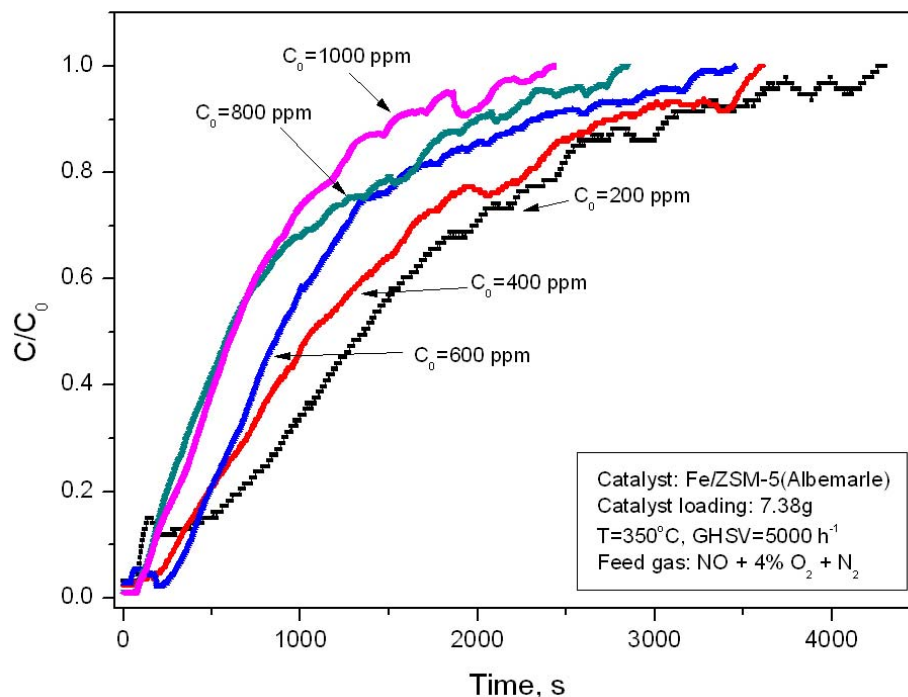


Figure G.8 Adsorption curves based on NO_x concentrations at the reactor outlet (Catalyst: Fe/ZSM-5(Albemarle), $T=350^\circ\text{C}$)

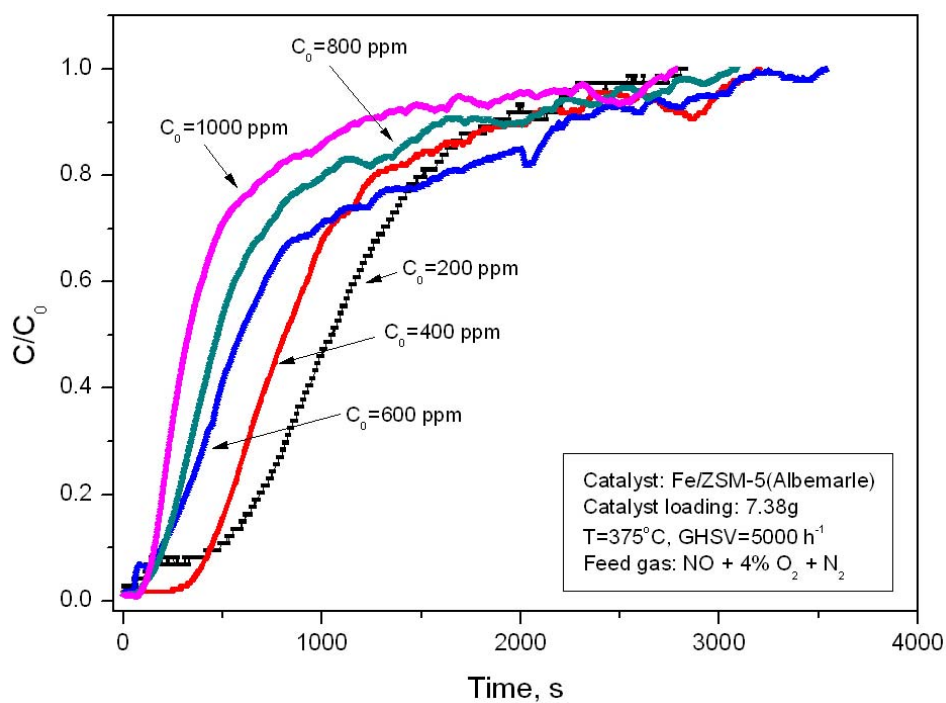


Figure G.9 Adsorption curves based on NO_x concentrations at the reactor outlet (Catalyst: Fe/ZSM-5(Albemarle), $T=375^\circ\text{C}$)

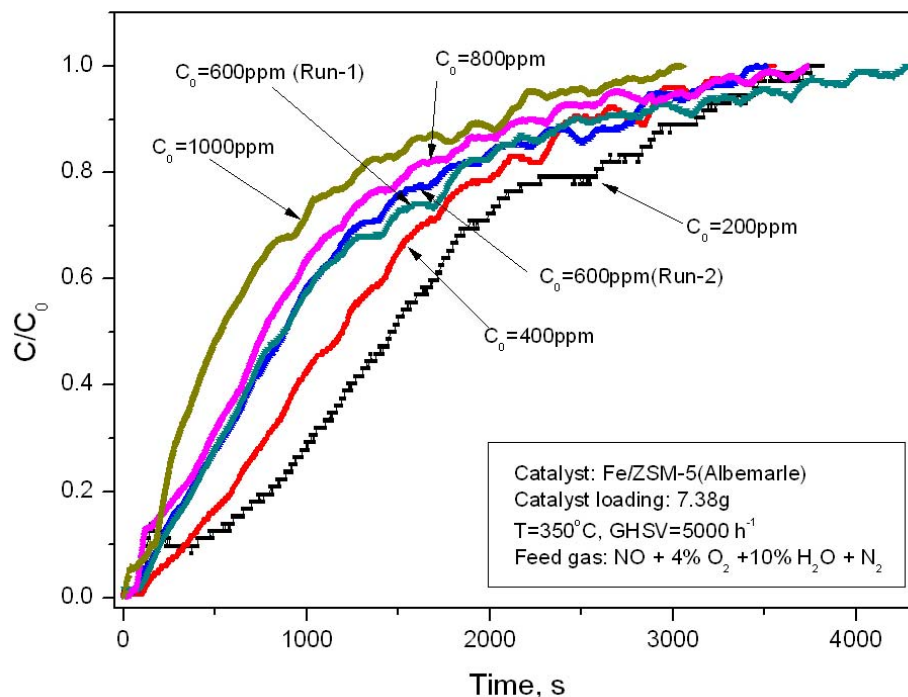


Figure G.10 Adsorption curves based on NO_x concentrations at the reactor outlet (Catalyst: Fe/ZSM-5(Albemarle), $T=350^\circ\text{C}$, 10% H_2O added)

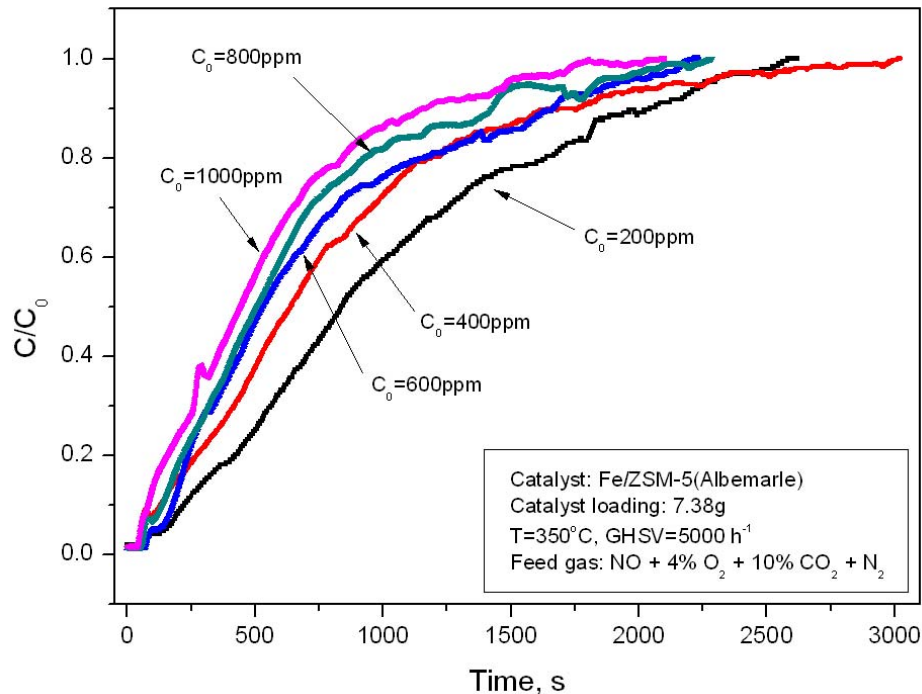


Figure G.11 Adsorption curves based on NO_x concentrations at the reactor outlet (Catalyst: Fe/ZSM-5(Albemarle), $T=350^\circ\text{C}$, 10% CO_2 added)

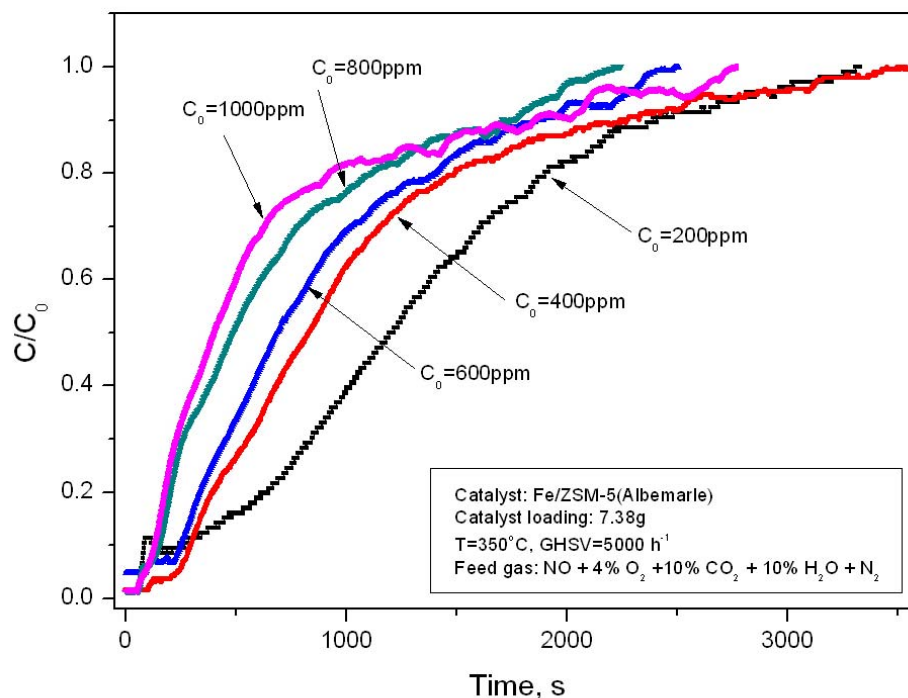


Figure G.12 Adsorption curves based on NO_x concentrations at the reactor outlet (Catalyst: Fe/ZSM-5(Albemarle), $T=350^\circ\text{C}$, 10% H_2O + 10% CO_2 added)

G.2 Profiles of NO_x and HC conversions and outlet CO concentration from time-on-stream test

Profiles of NO_x and HC conversions and the outlet CO concentration in the time-on-stream test over Fe/ZSM-5(PUC) and Fe/ZSM-5(Albemarle) catalysts at various temperatures are shown in Figures G.13 to G.16 and G.17 to G.19, respectively.

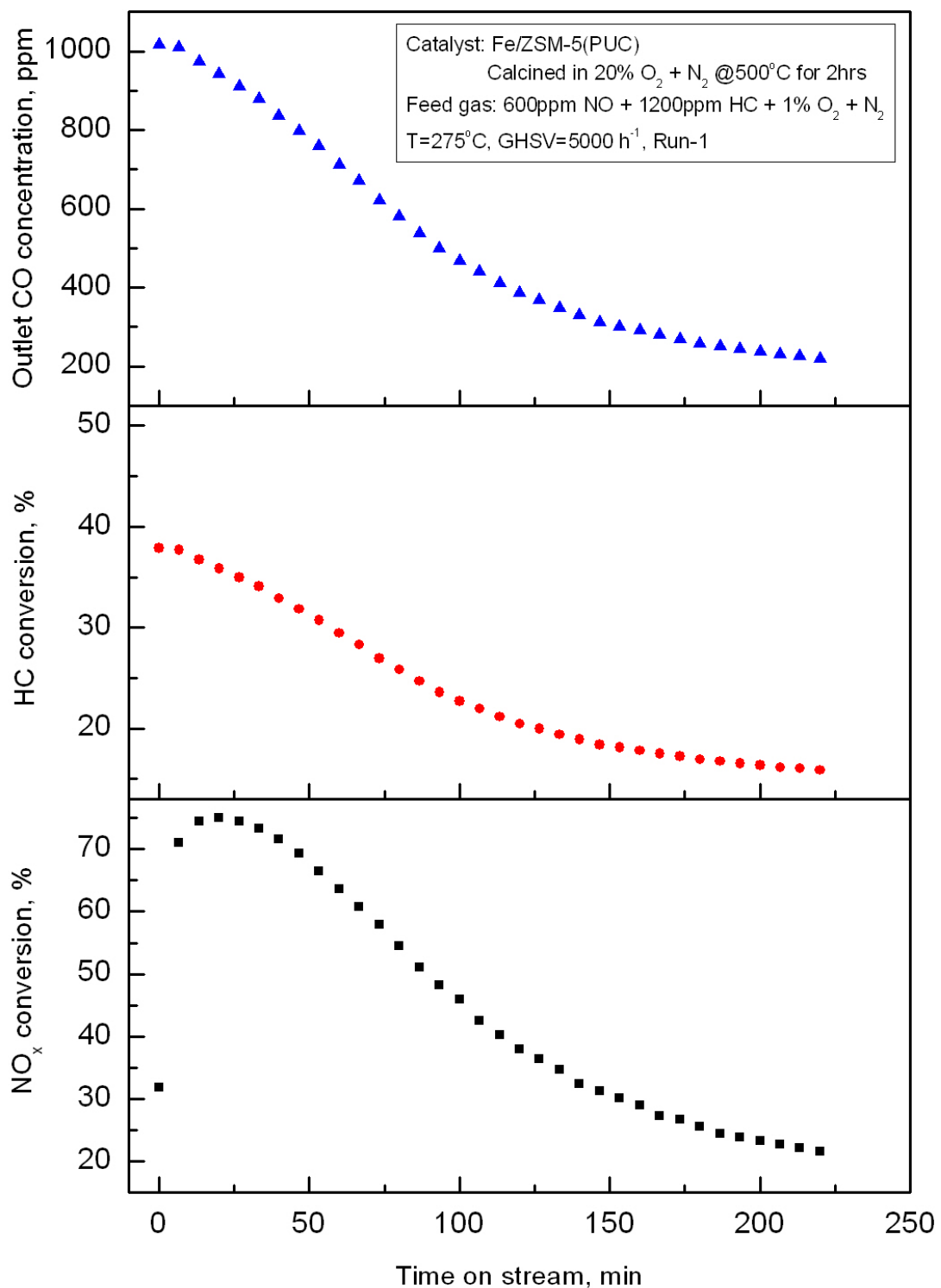


Figure G.13 Profiles of NO_x and HC conversions and outlet CO concentration in time-on-stream test (Catalyst: Fe/ZSM-5(PUC), T=275°C, [O₂]=1%)

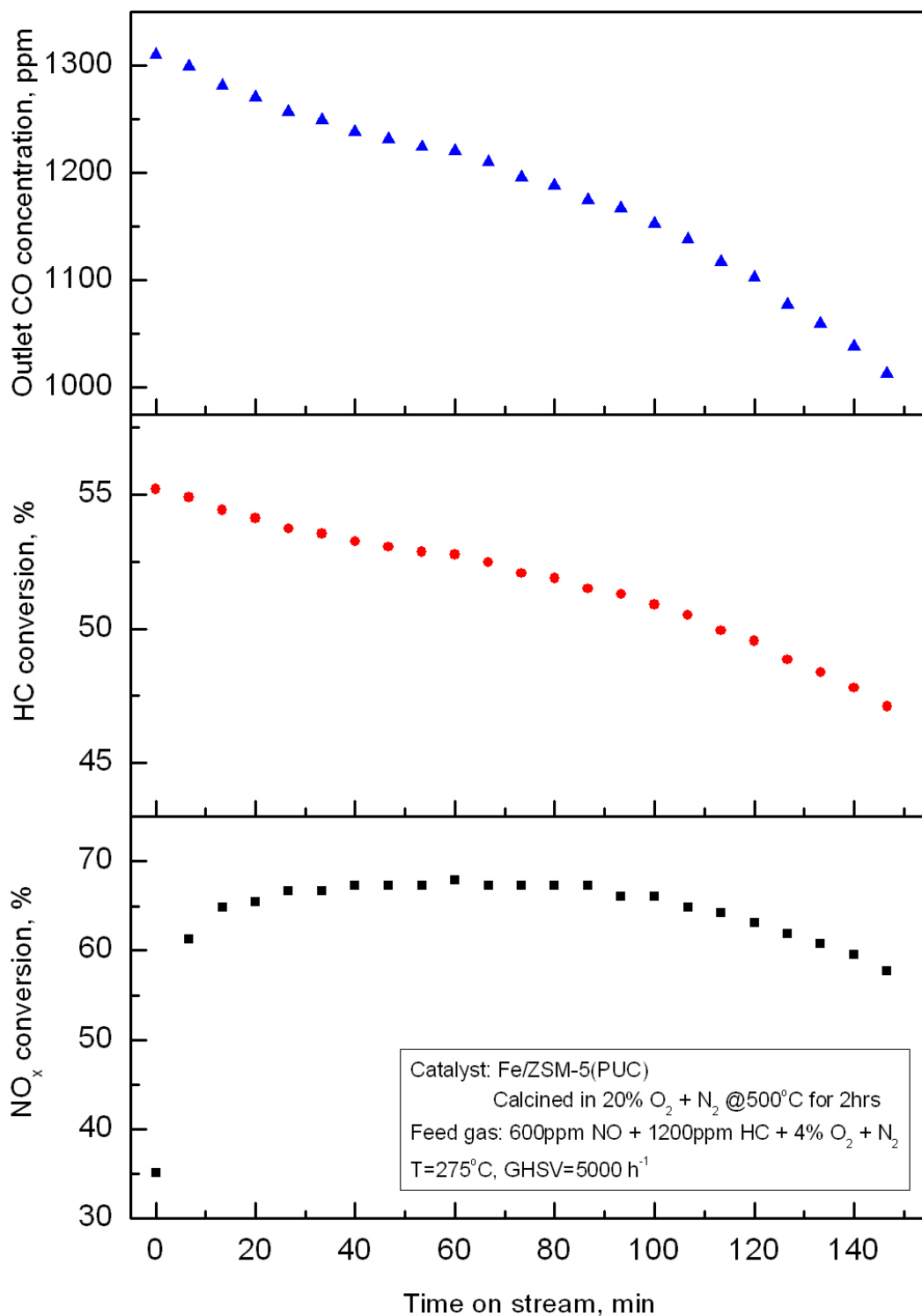


Figure G.14 Profiles of NO_x and HC conversions and outlet CO concentration in time-on-stream test (Catalyst: Fe/ZSM-5(PUC), T=275°C, [O₂]=4%)

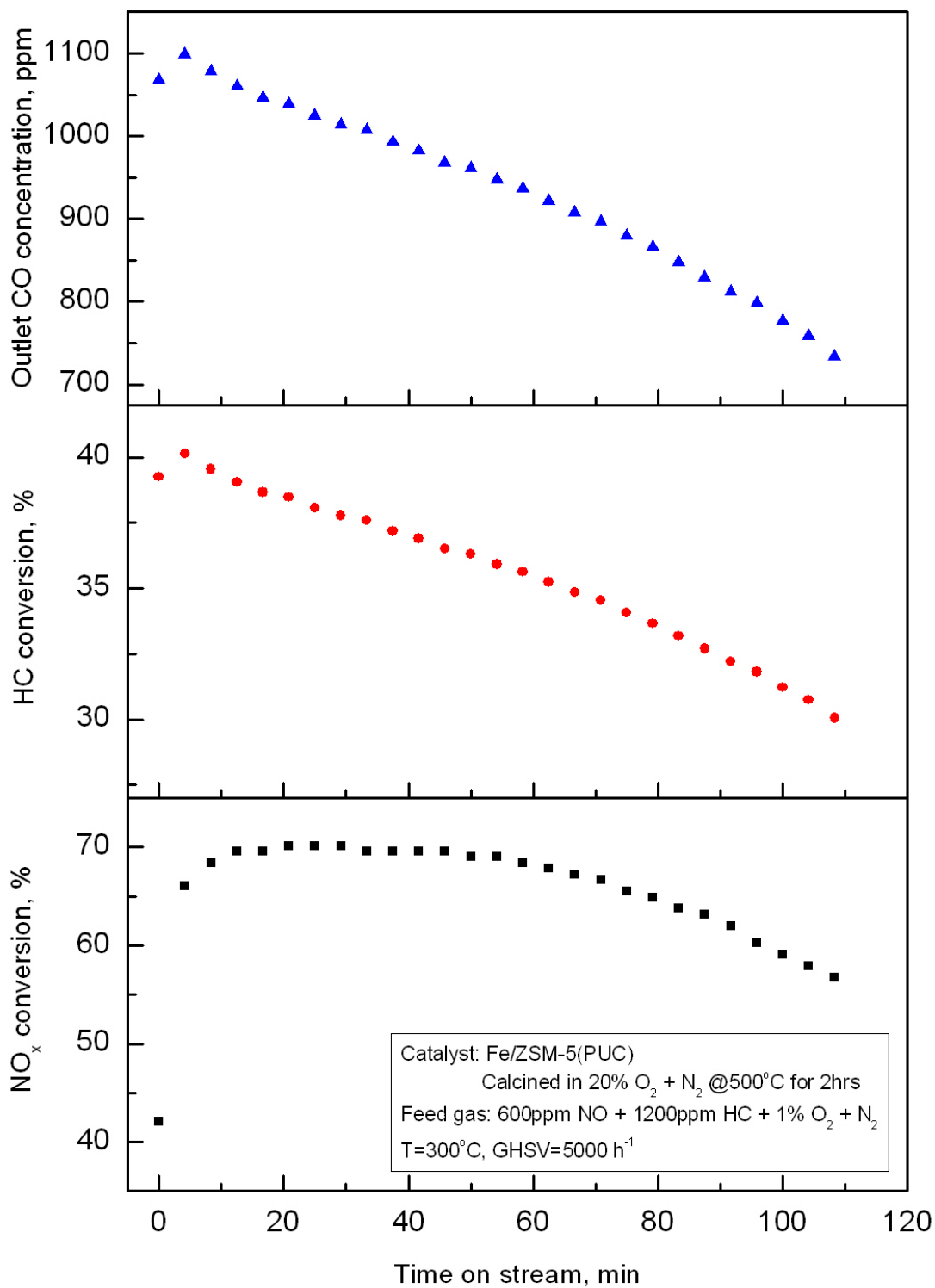


Figure G.15 Profiles of NO_x and HC conversions and outlet CO concentration in time-on-stream test (Catalyst: Fe/ZSM-5(PUC), T=300°C, [O₂]=1%)

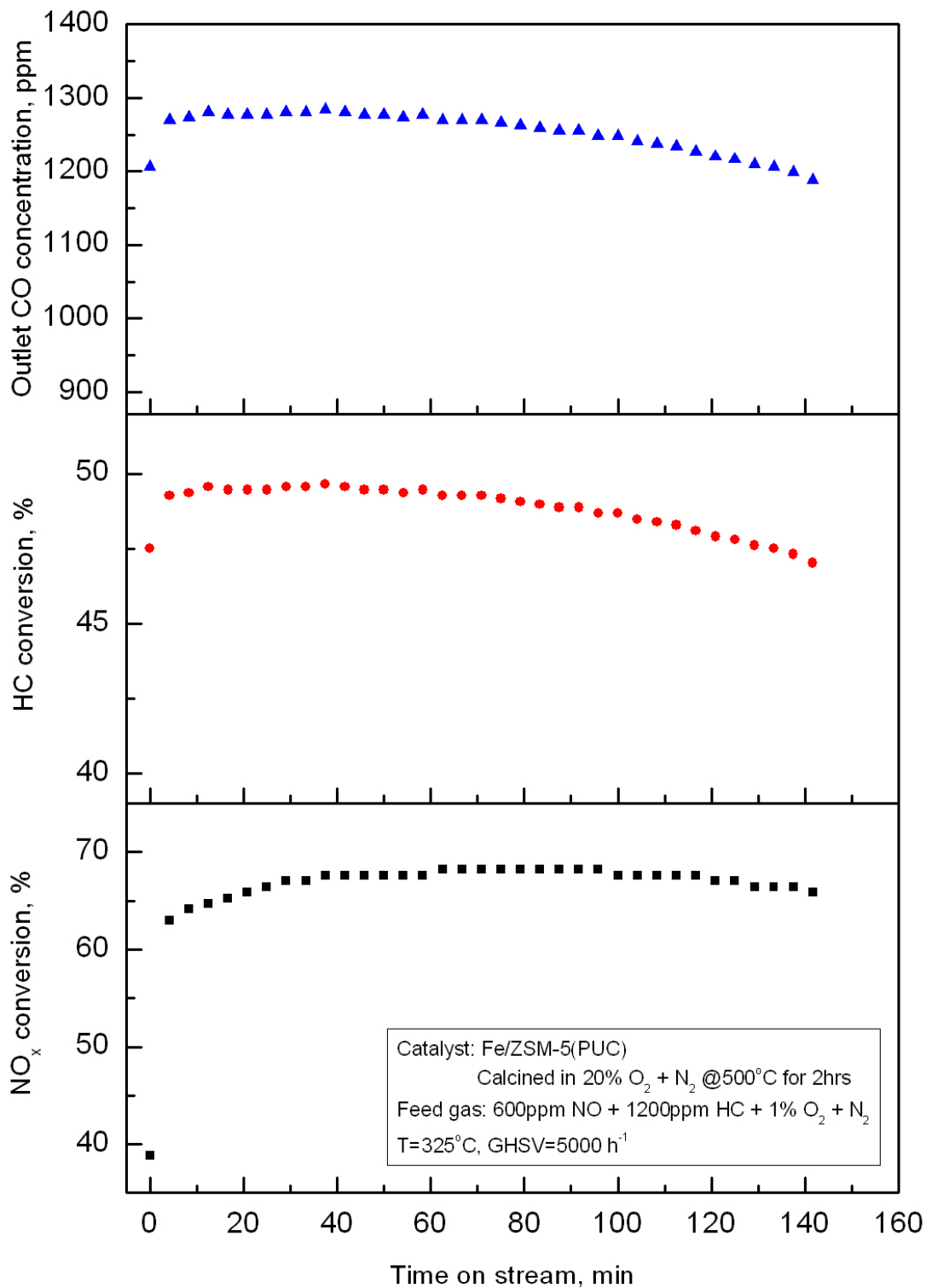


Figure G.16 Profiles of NO_x and HC conversions and outlet CO concentration in time-on-stream test (Catalyst: Fe/ZSM-5(PUC), T=325°C, [O₂]=1%)

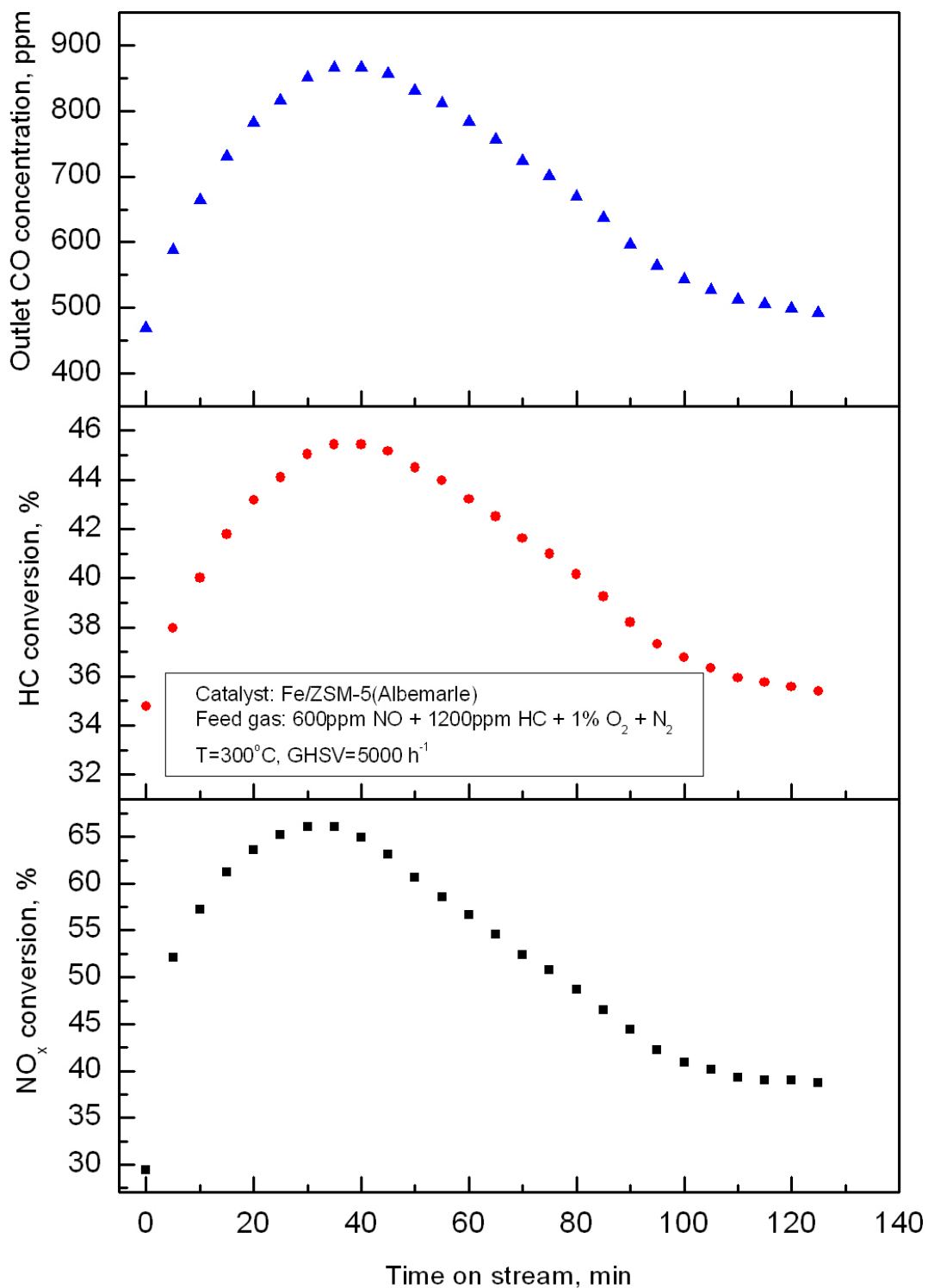


Figure G.17 Profiles of NO_x and HC conversions and outlet CO concentration in time-on-stream test (Catalyst: Fe/ZSM-5(Albemarle), T=300°C, [O₂]=1%)

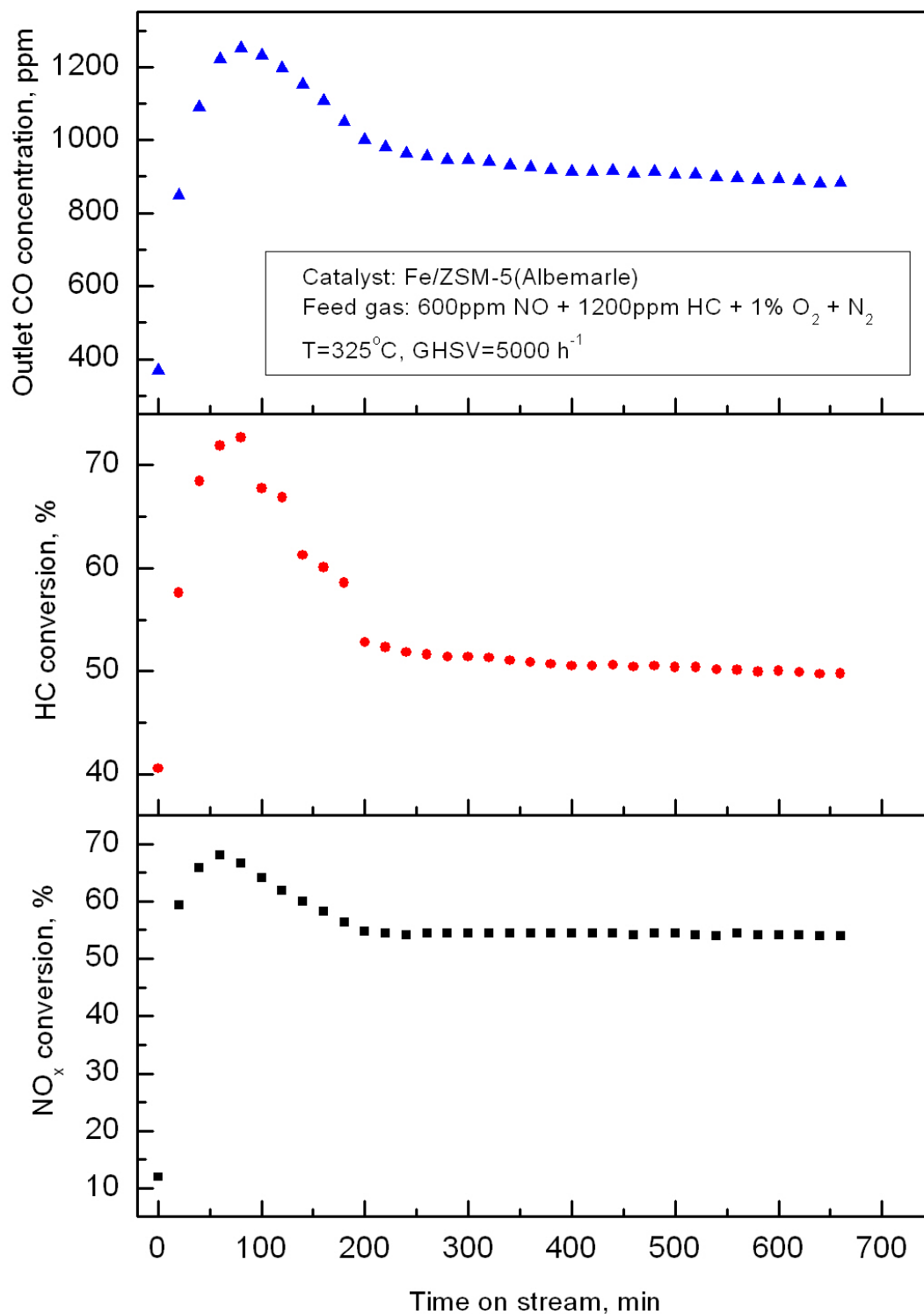


Figure G.18 Profiles of NO_x and HC conversions and outlet CO concentration in time-on-stream test (Catalyst: Fe/ZSM-5(Albemarle), T=325°C, [O₂]=1%)

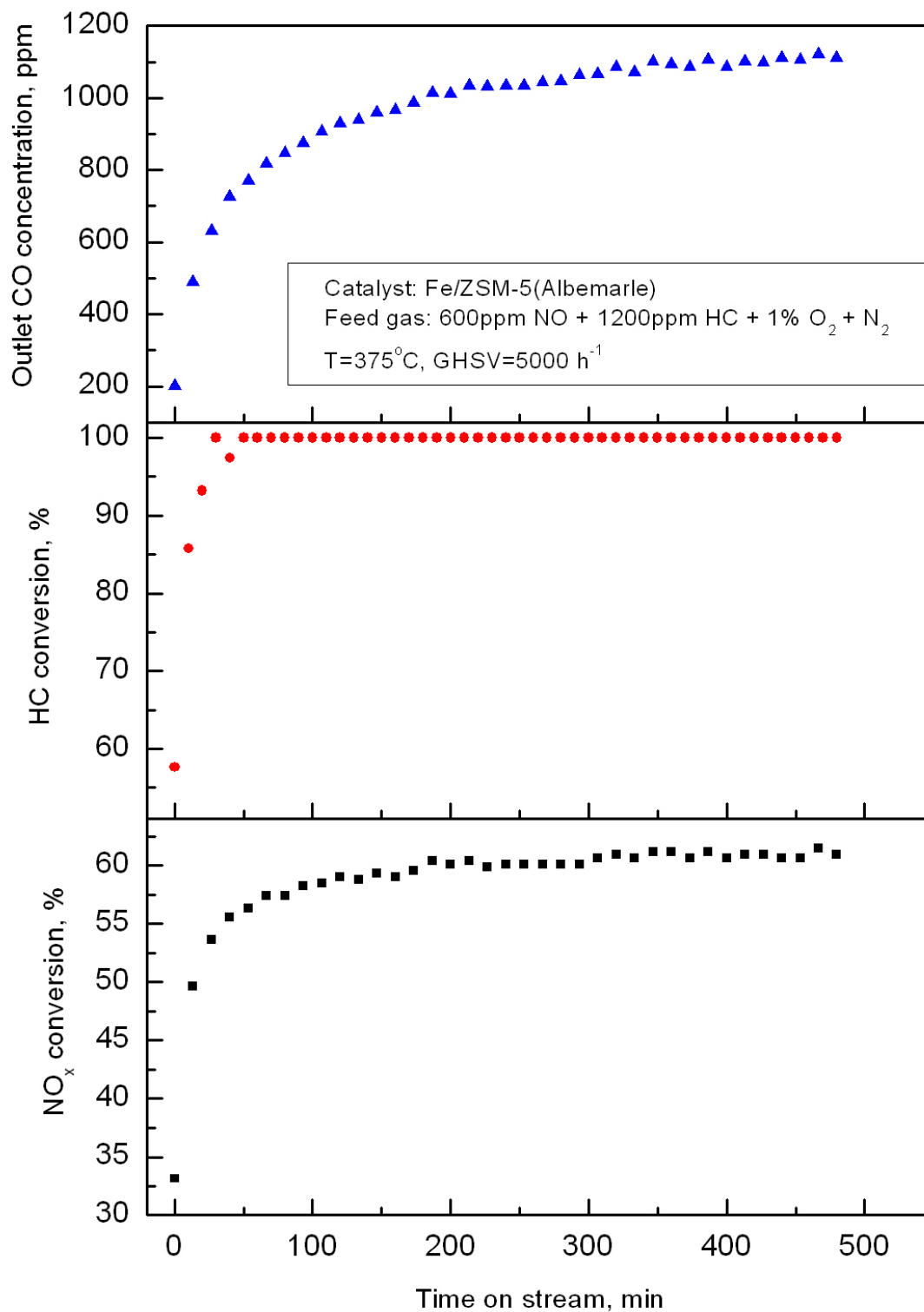


Figure G.19 Profiles of NO_x and HC conversions and outlet CO concentration in time-on-stream test (Catalyst: Fe/ZSM-5(Albemarle), T=375°C, [O₂]=1%)

G.3 XPS analysis for Fe/ZSM-5(PUC)

XPS survey scan spectra for the fresh, spent and regenerated Fe/ZSM-5(PUC) catalysts are shown in Figures G.20 to G.22, respectively. Comparisons of XPS narrow scan spectra of Al 2p, Si 2p, O 1s and Fe 2p 3/2 for the fresh, spent and regenerated Fe/ZSM-5(PUC) catalysts are shown in Figures G.23 to G.26, respectively.

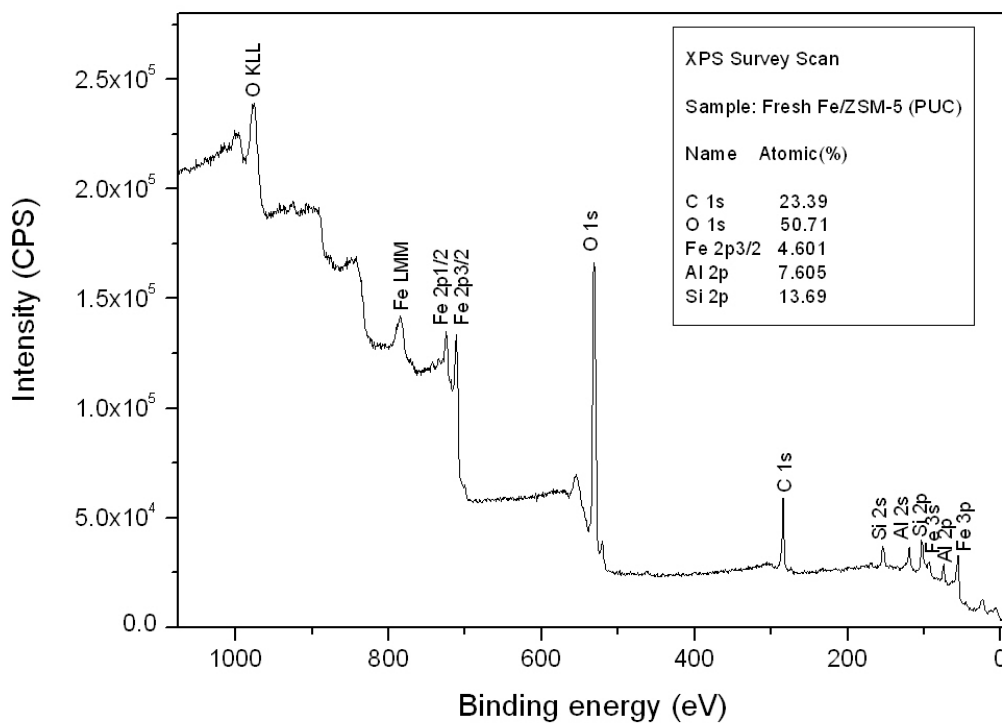


Figure G.20 XPS survey scan for fresh Fe/ZSM-5(PUC)

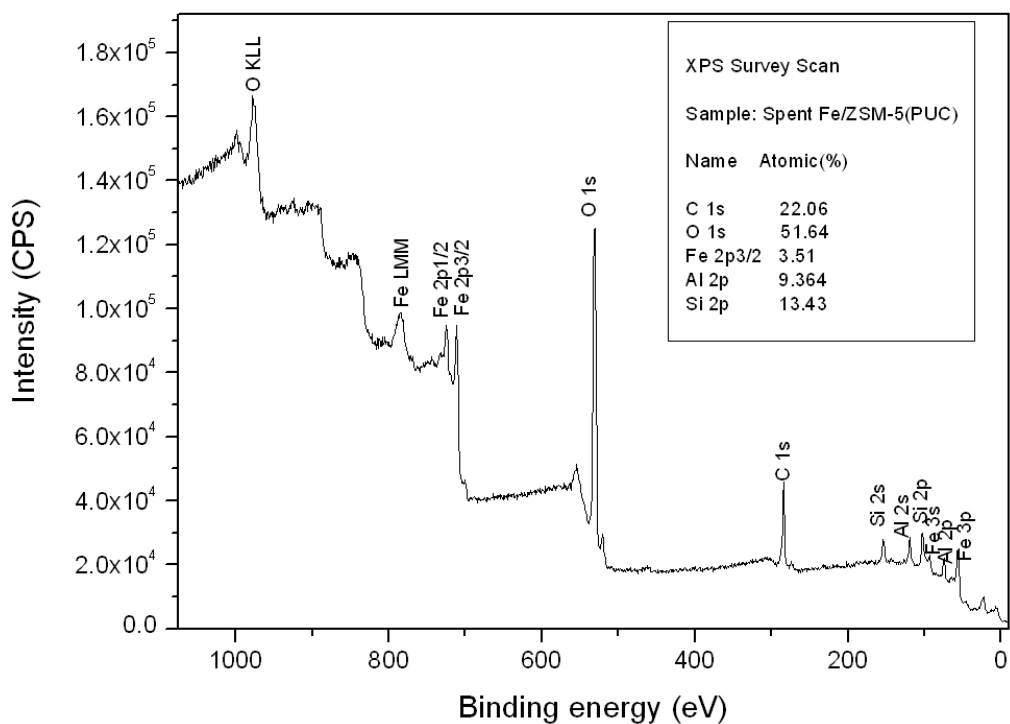


Figure G.21 XPS survey scan for spent Fe/ZSM-5(PUC)

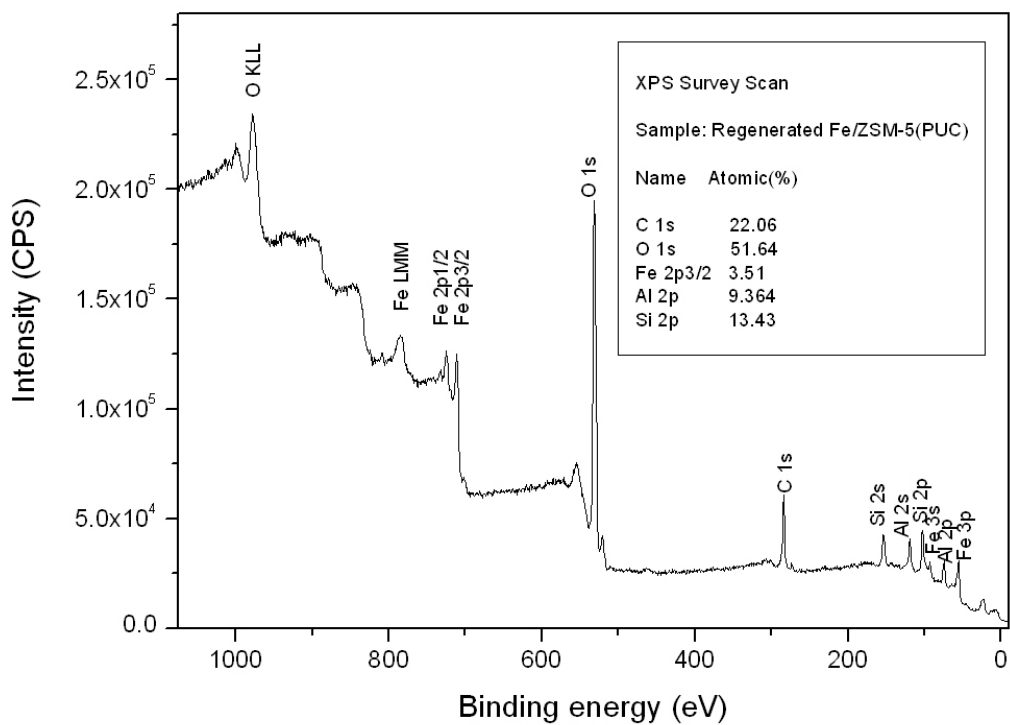


Figure G.22 XPS survey scan for regenerated Fe/ZSM-5(PUC)

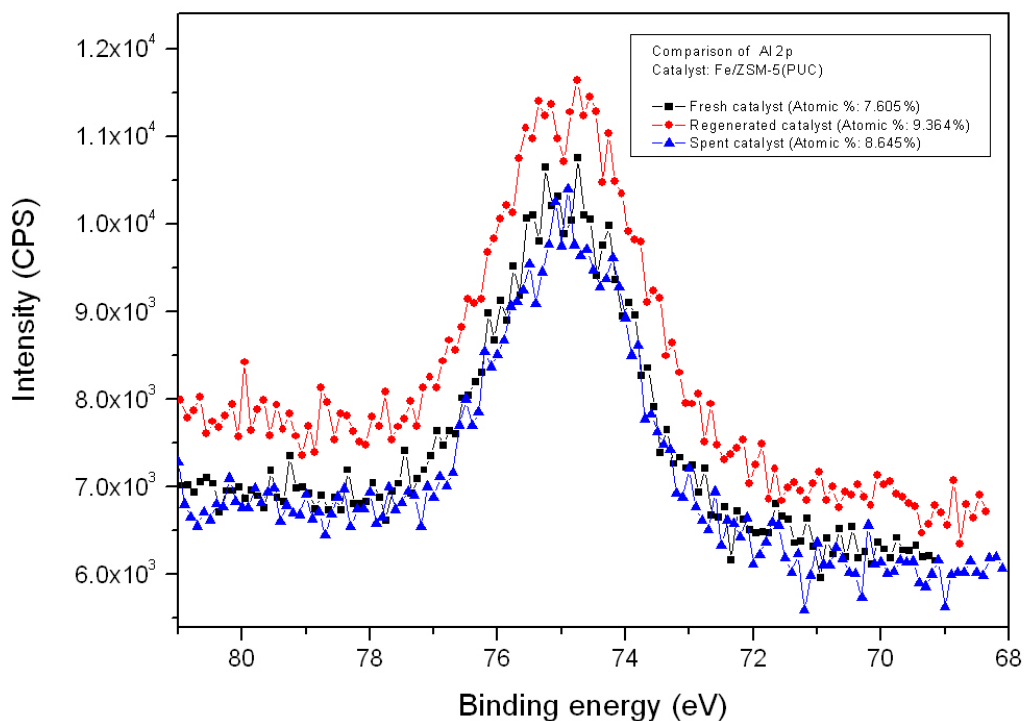


Figure G.23 Comparison of XPS narrow scan of Al 2p

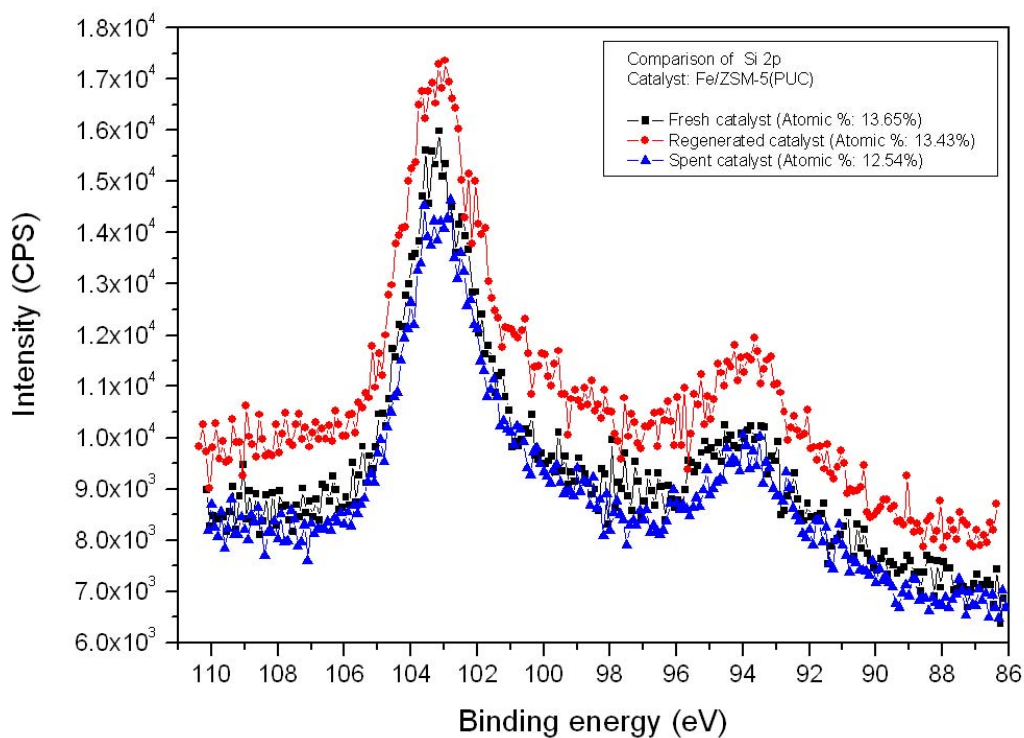


Figure G.24 Comparison of XPS narrow scan of Si 2p

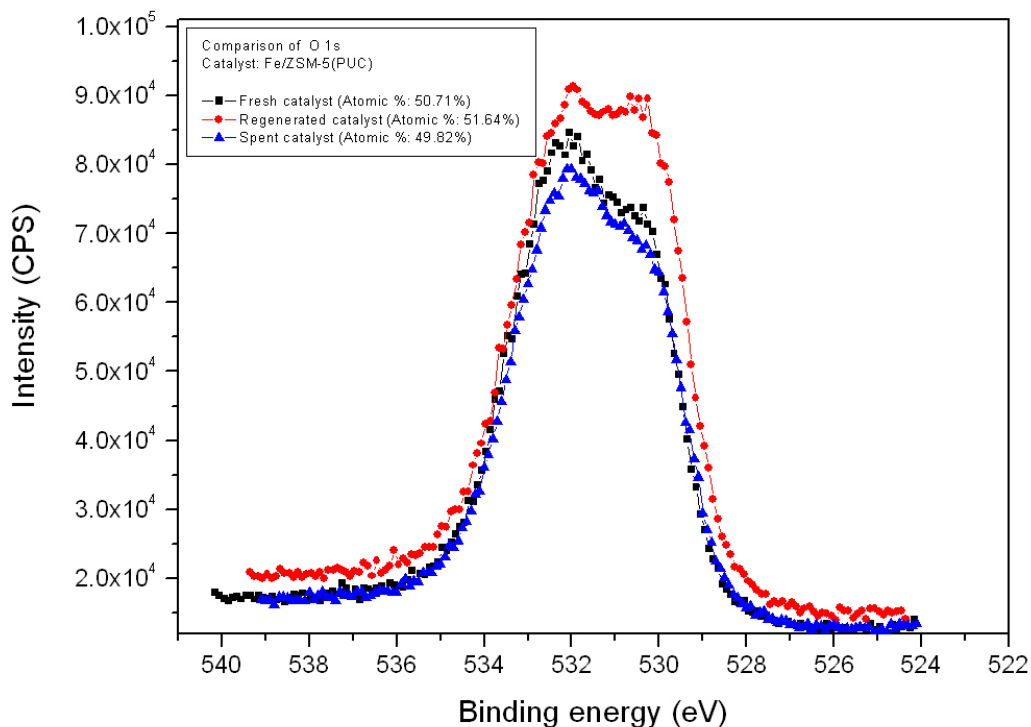


Figure G.25 Comparison of XPS narrow scan of O 1s

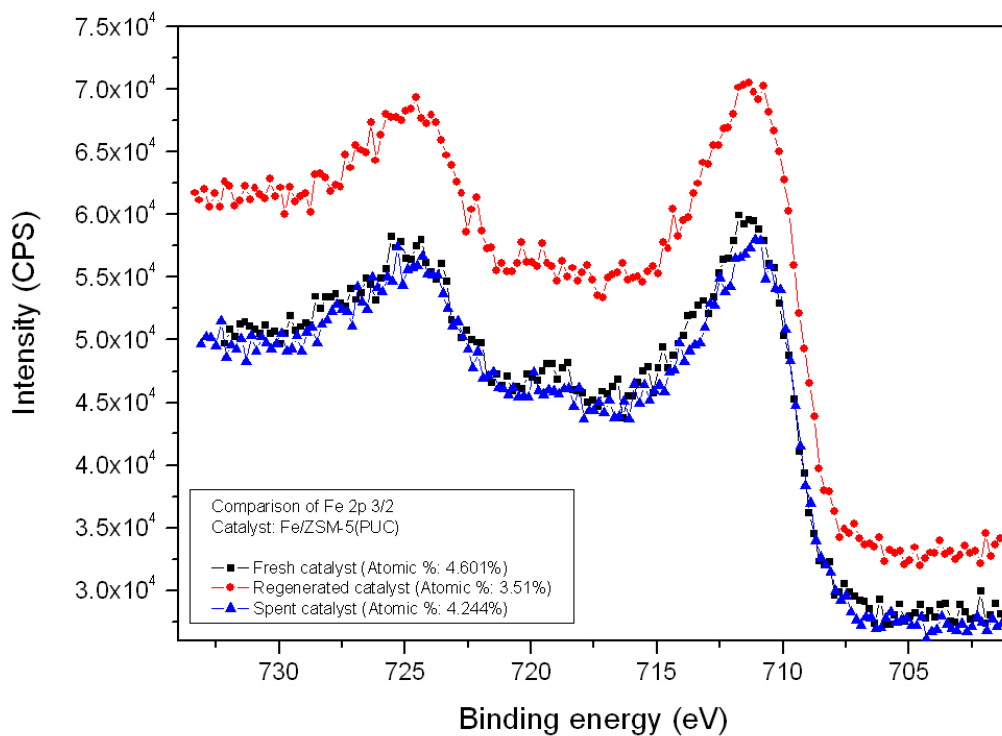


Figure G.26 Comparison of XPS narrow scan of Fe 2p 3/2

Appendix H

Effects of Gas Velocities on Gas Bypass in Hot Model ICFB Reactor

H.1 Fe/ZSM-5(PUC)

Gas bypass ratios from the annulus to draft tube (R_{AD}) and the draft tube to annulus (R_{DA}) using the coarse Fe/ZSM-5(PUC) catalyst in the hot model ICFB reactor at a given annulus gas velocity (U_A) are shown in Figures H.1 to H.7.

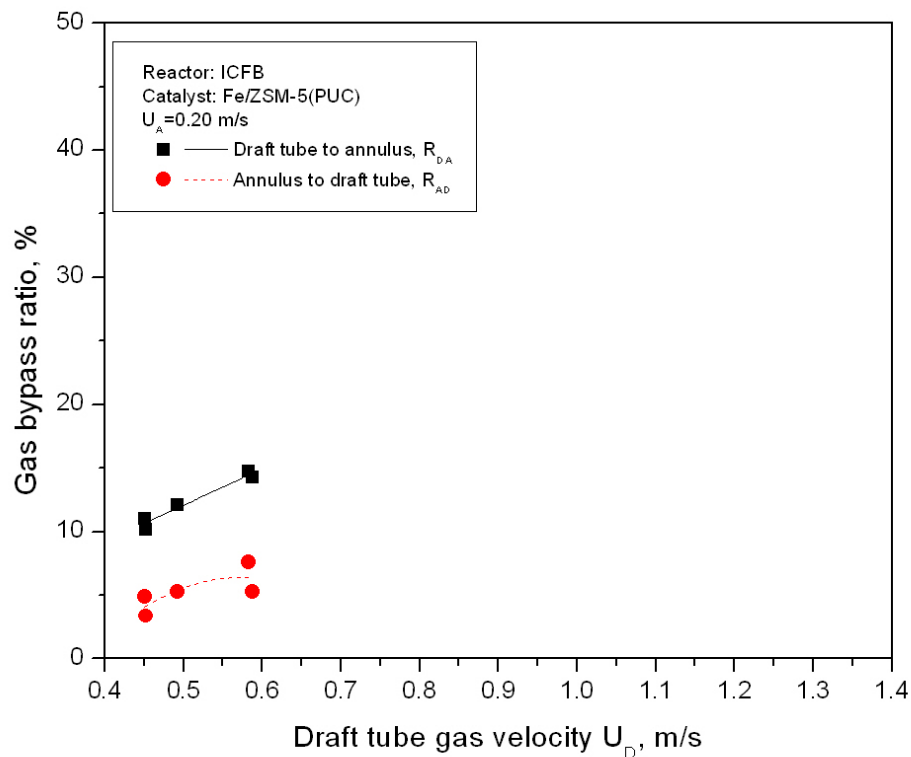


Figure H.1 Effect of U_D on gas bypass (Fe/ZSM-5(PUC), $U_A=0.20$ m/s, $T=350\pm 10^\circ\text{C}$)

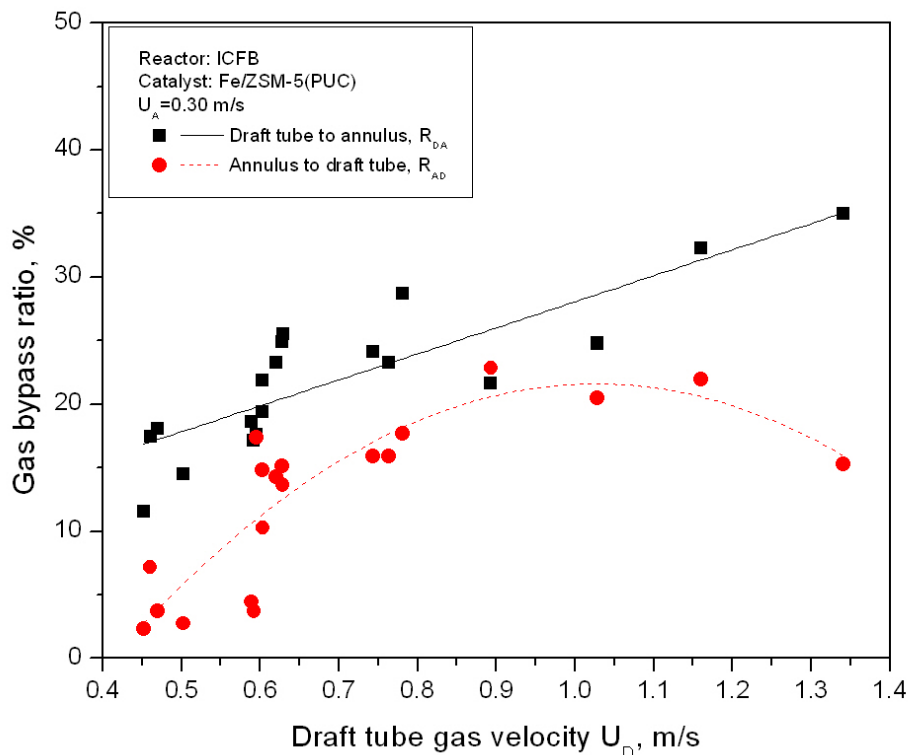


Figure H.2 Effect of U_D on gas bypass (Fe/ZSM-5(PUC), $U_A=0.30$ m/s, $T=350\pm 10^\circ\text{C}$)

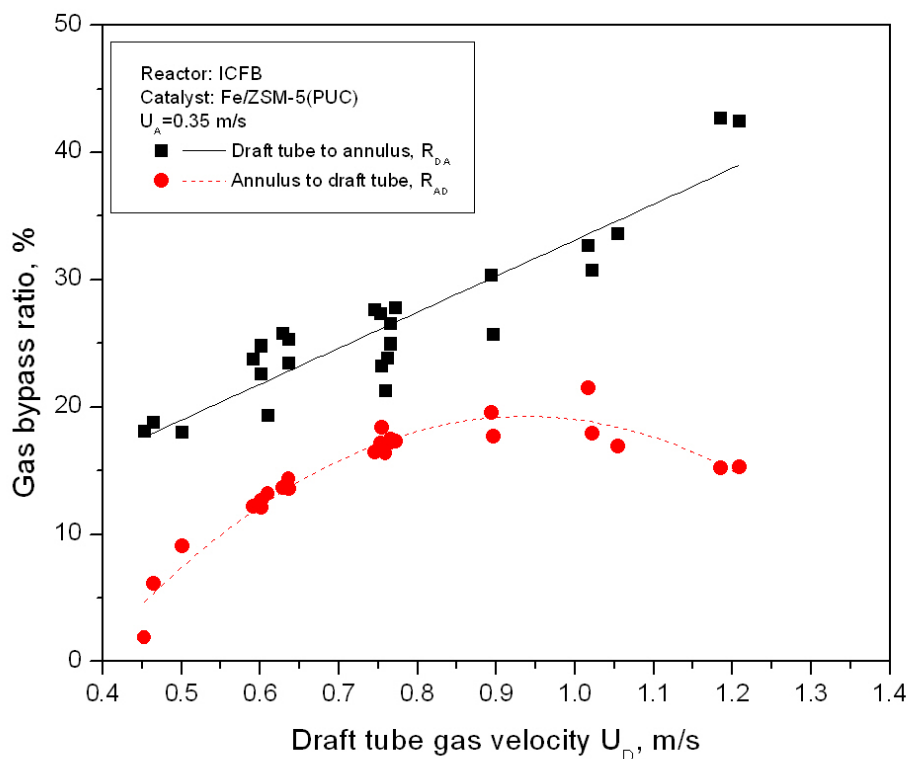


Figure H.3 Effect of U_D on gas bypass (Fe/ZSM-5(PUC), $U_A=0.35$ m/s, $T=350\pm 10^\circ\text{C}$)

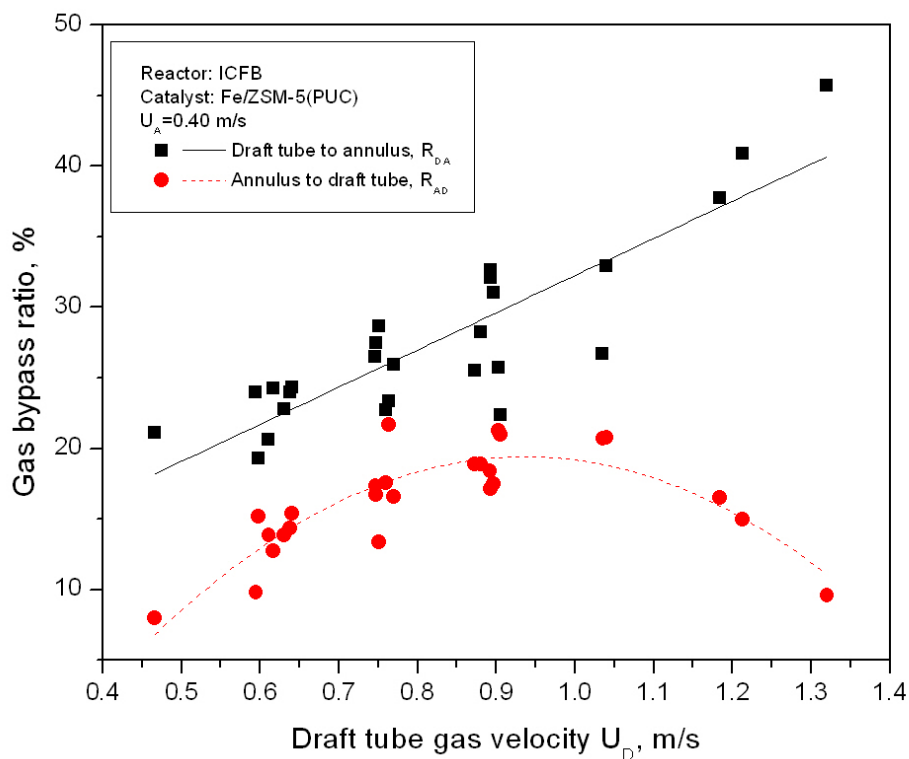


Figure H.4 Effect of U_D on gas bypass (Fe/ZSM-5(PUC), $U_A=0.40$ m/s, $T=350\pm 10^\circ\text{C}$)

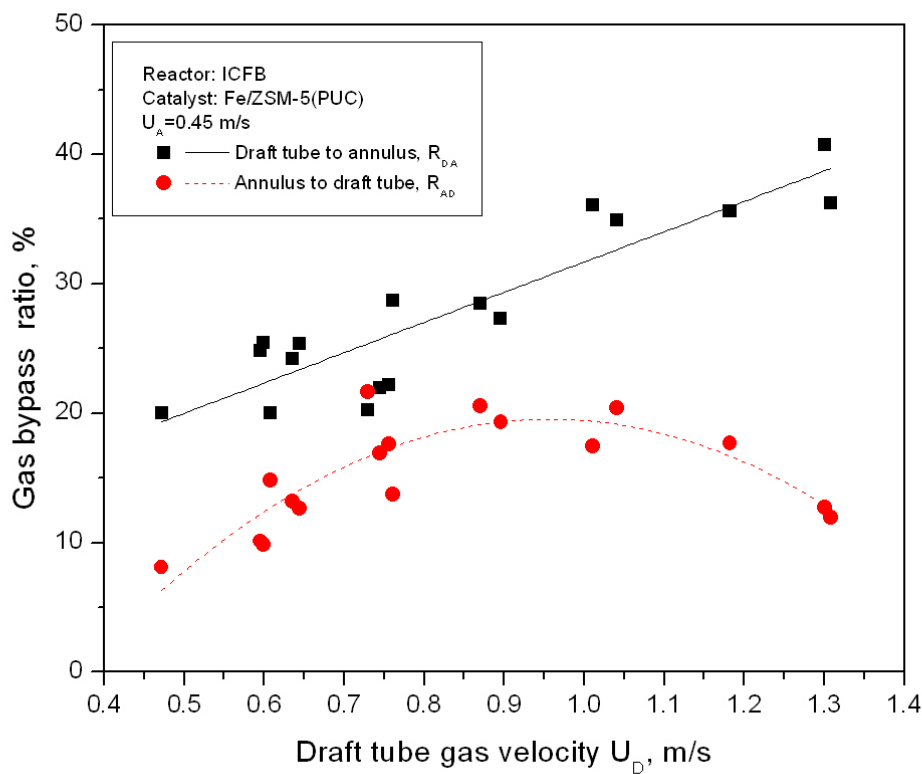


Figure H.5 Effect of U_D on gas bypass (Fe/ZSM-5(PUC), $U_A=0.45$ m/s, $T=350\pm 10^\circ\text{C}$)

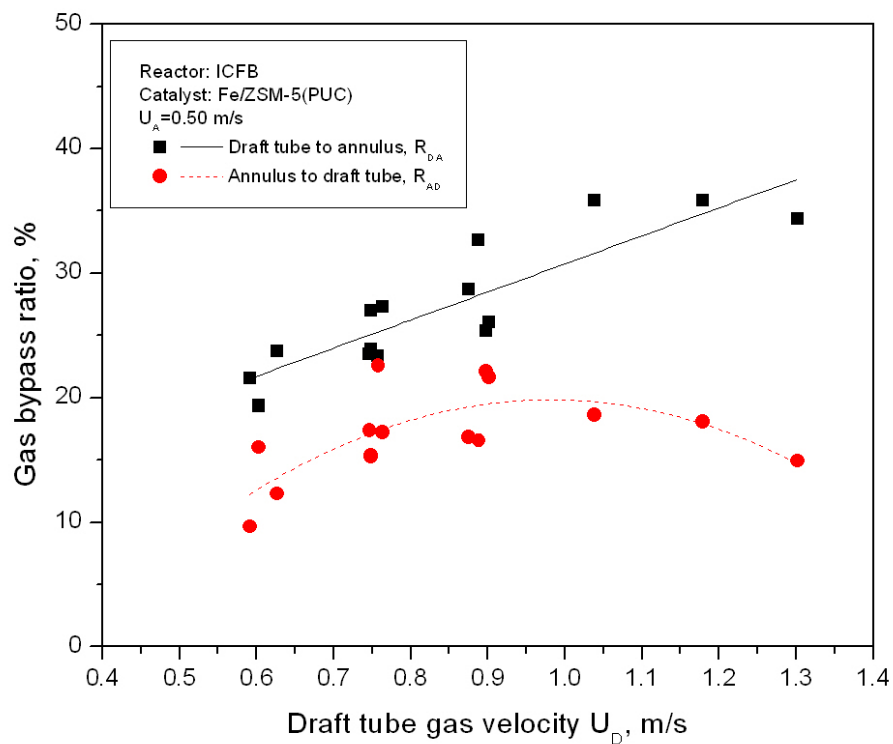


Figure H.6 Effect of U_D on gas bypass (Fe/ZSM-5(PUC), $U_A=0.50$ m/s, $T=350\pm 10^\circ\text{C}$)

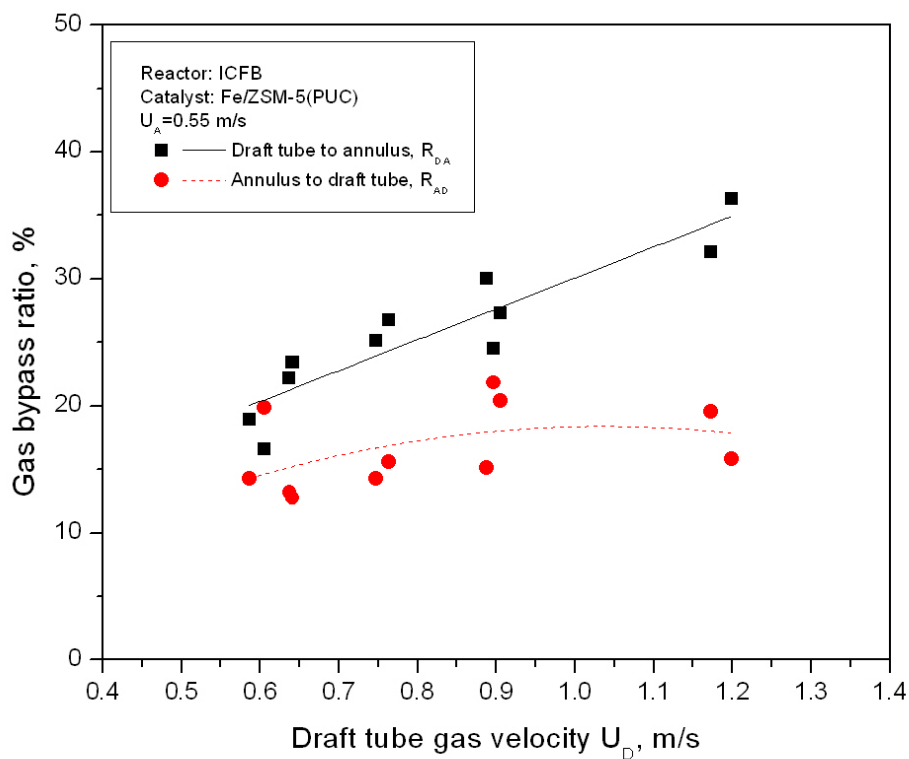


Figure H.7 Effect of U_D on gas bypass (Fe/ZSM-5(PUC), $U_A=0.55$ m/s, $T=350\pm 10^\circ\text{C}$)

H.2 Fe/ZSM-5(Albemarle)

The gas bypass ratio (R_{DA} or R_{AD}) as a function of the annulus gas velocity (U_A) for the fine Fe/ZSM-5(Albemarle) catalyst in the hot model ICFB reactor is shown in Figures H.8 and H.9, respectively. At a given U_A , the influence of the draft tube gas velocity (U_D) on gas bypass ratio is shown in Figures H.10 to H.15. At a given U_D , the influence of the annulus gas velocity (U_A) on gas bypass ratio is shown in Figures H.16 to H.19.

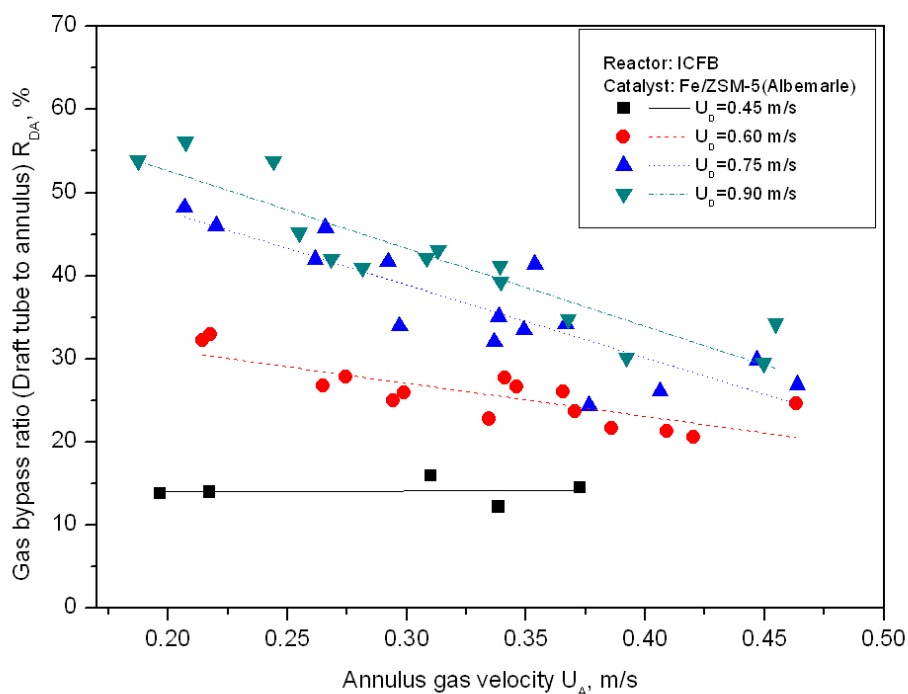


Figure H.8 Effect of gas velocities on R_{DA} (Fe/ZSM-5(Albemarle), $T=355\pm 15^\circ\text{C}$)

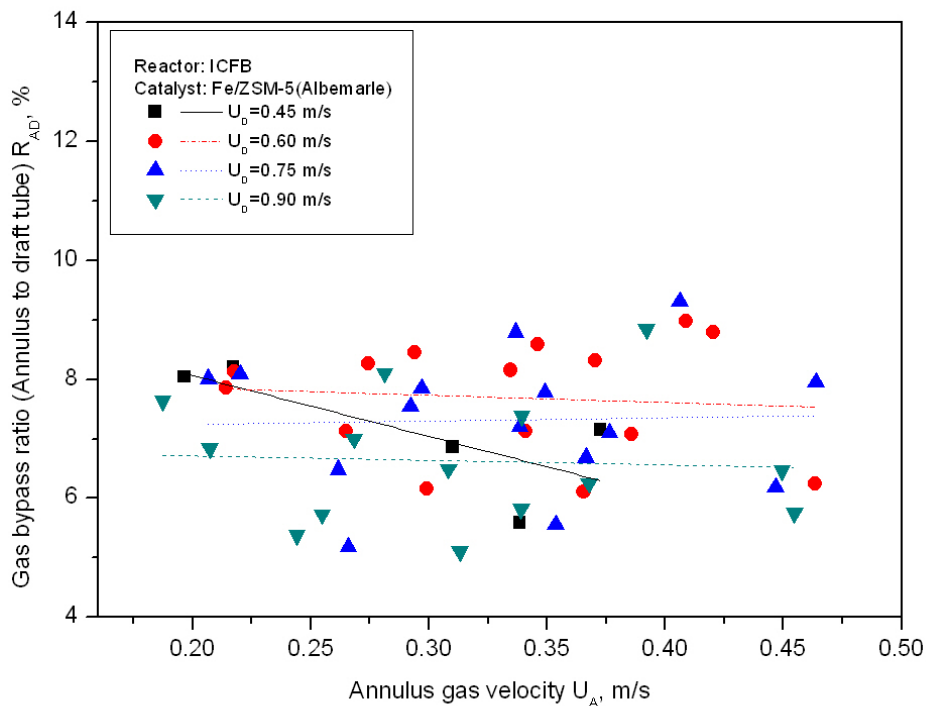


Figure H.9 Effect of gas velocities on R_{AD} (Fe/ZSM-5(Albemarle), $T=355\pm 15^\circ\text{C}$)

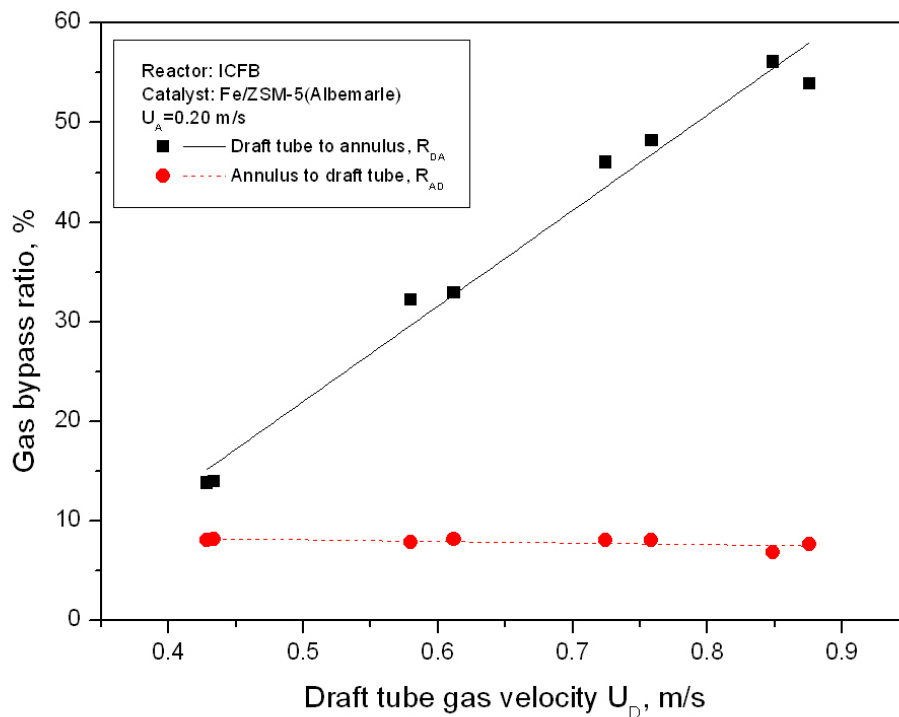


Figure H.10 Effect of U_D on gas bypass (Fe/ZSM-5(Albemarle), $U_A=0.20$ m/s, $T=355\pm 15^\circ\text{C}$)

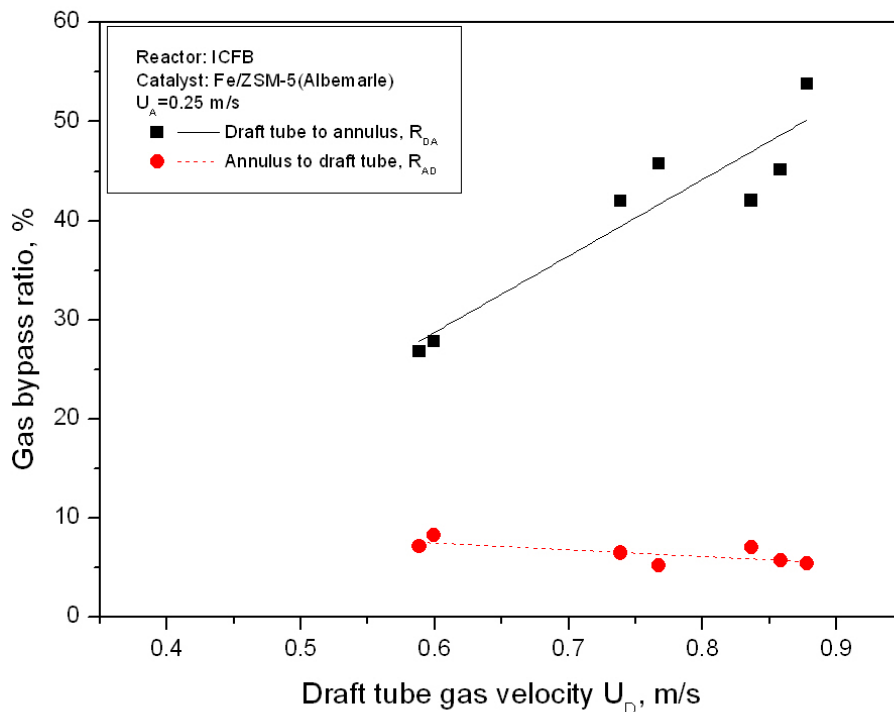


Figure H.11 Effect of U_D on gas bypass (Fe/ZSM-5(Albemarle), $U_A=0.25$ m/s, $T=355\pm 15^\circ\text{C}$)

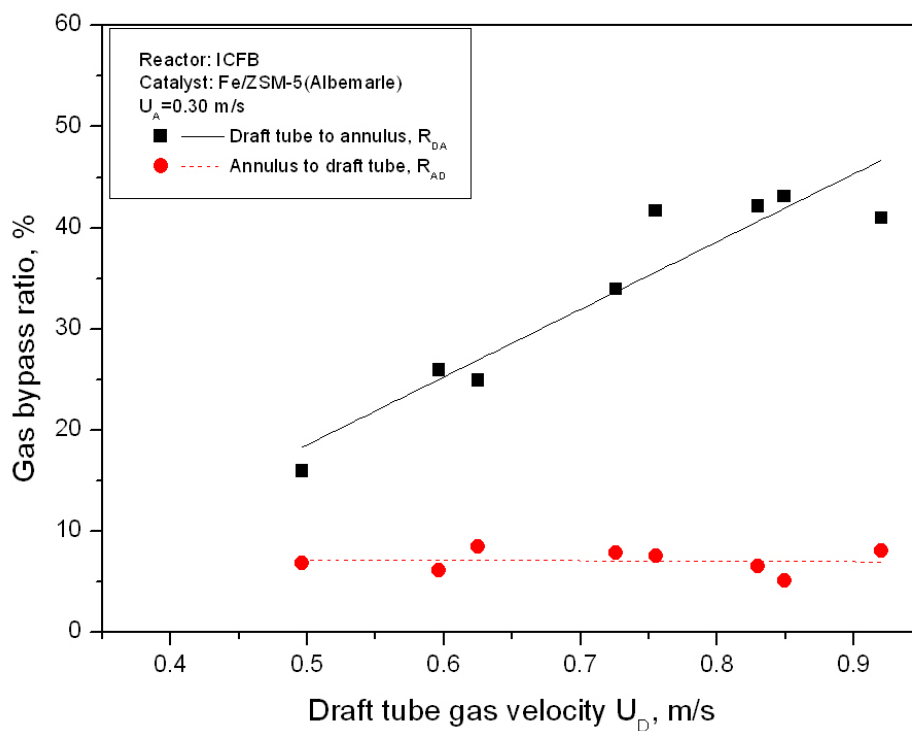


Figure H.12 Effect of U_D on gas bypass (Fe/ZSM-5(Albemarle), $U_A=0.30$ m/s, $T=355\pm 15^\circ\text{C}$)

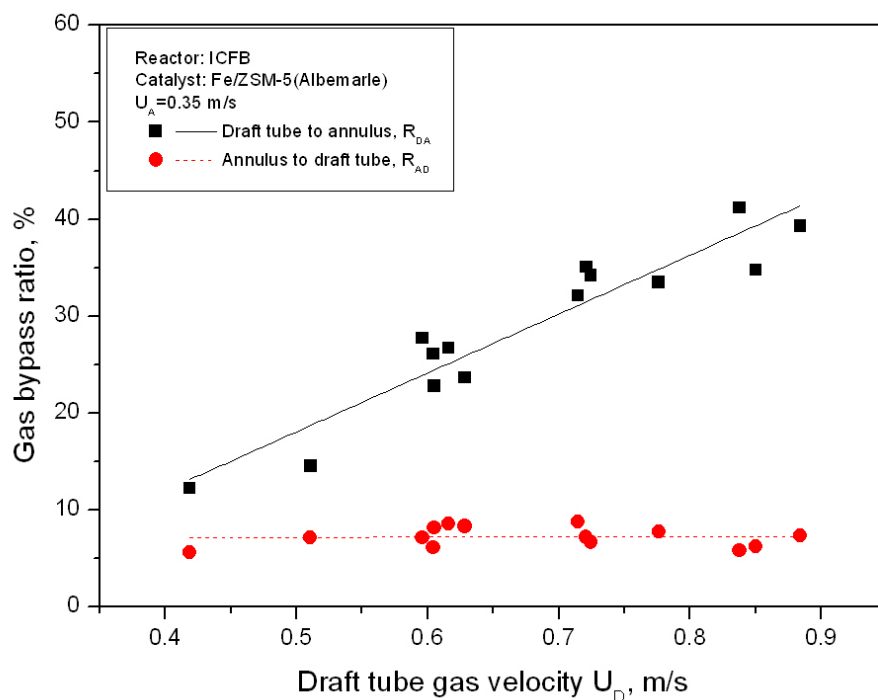


Figure H.13 Effect of U_D on gas bypass (Fe/ZSM-5(Albemarle), $U_A=0.35$ m/s, $T=355\pm 15^\circ\text{C}$)

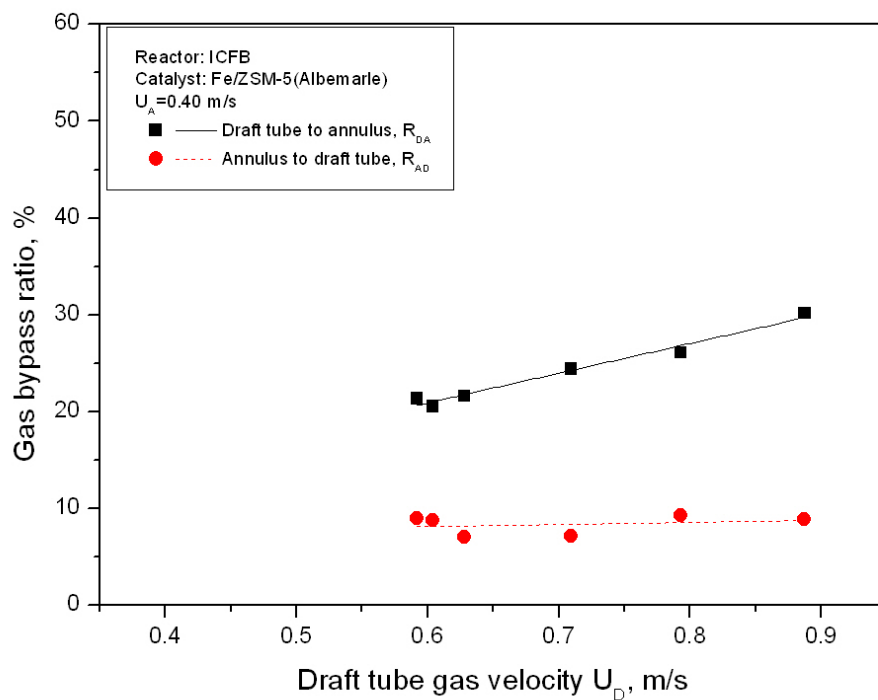


Figure H.14 Effect of U_D on gas bypass (Fe/ZSM-5(Albemarle), $U_A=0.40$ m/s, $T=355\pm 15^\circ\text{C}$)

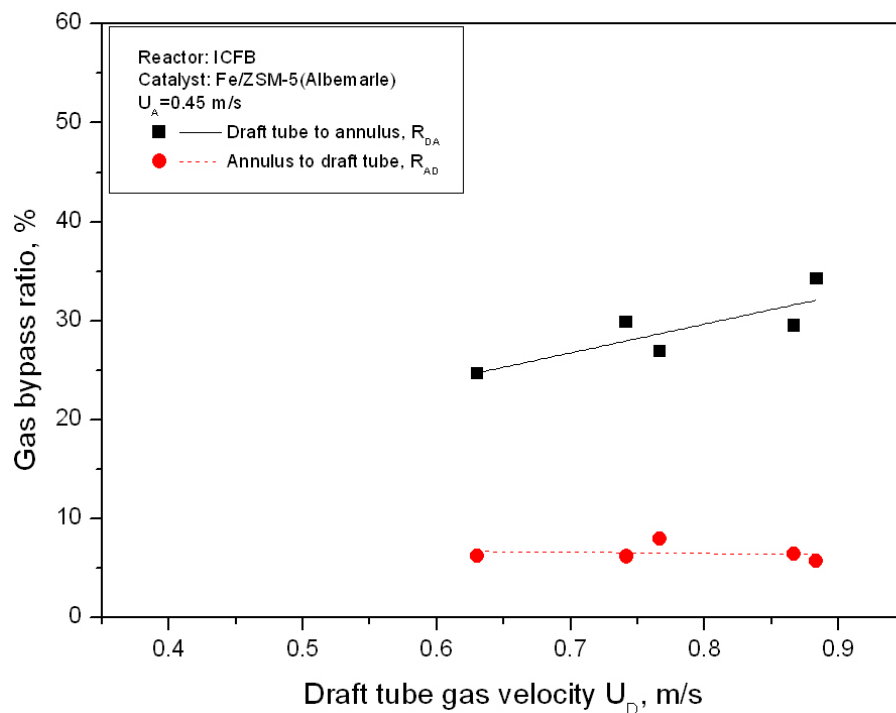


Figure H.15 Effect of U_D on gas bypass (Fe/ZSM-5(Albemarle), $U_A=0.45$ m/s, $T=355\pm 15^\circ\text{C}$)

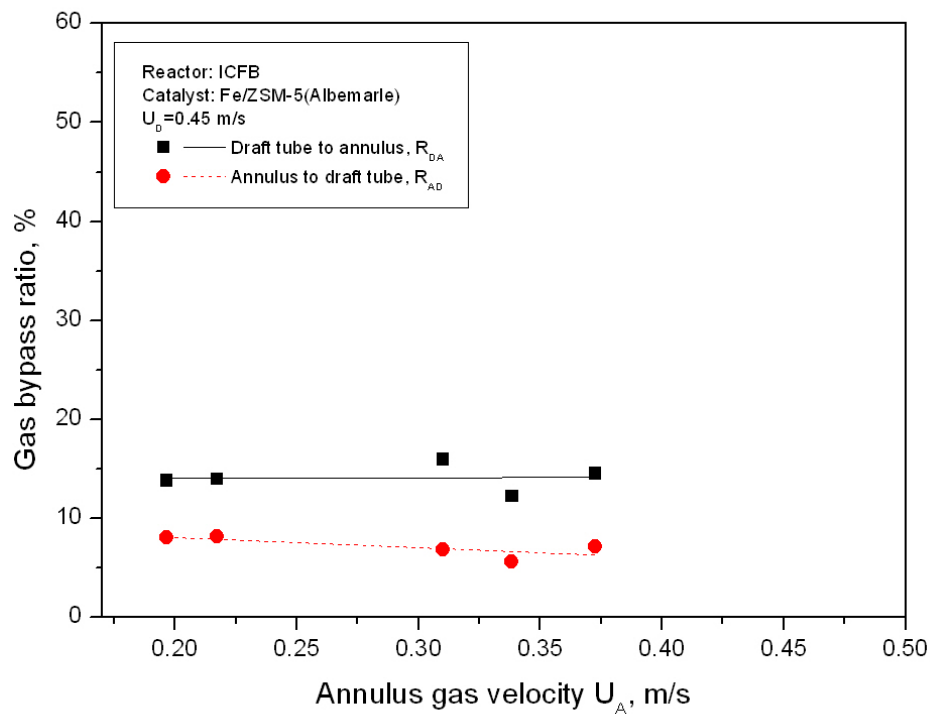


Figure H.16 Effect of U_A on gas bypass (Fe/ZSM-5(Albemarle), $U_D=0.45$ m/s, $T=355\pm 15^\circ\text{C}$)

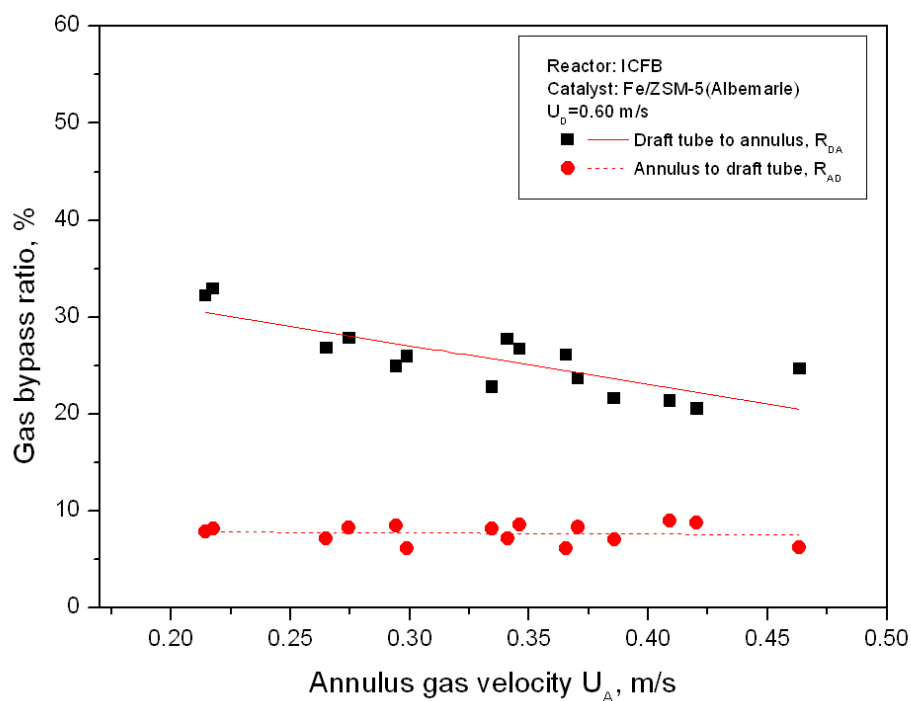


Figure H.17 Effect of U_A on gas bypass (Fe/ZSM-5(Albemarle), $U_D=0.60$ m/s, $T=355\pm 15^\circ\text{C}$)

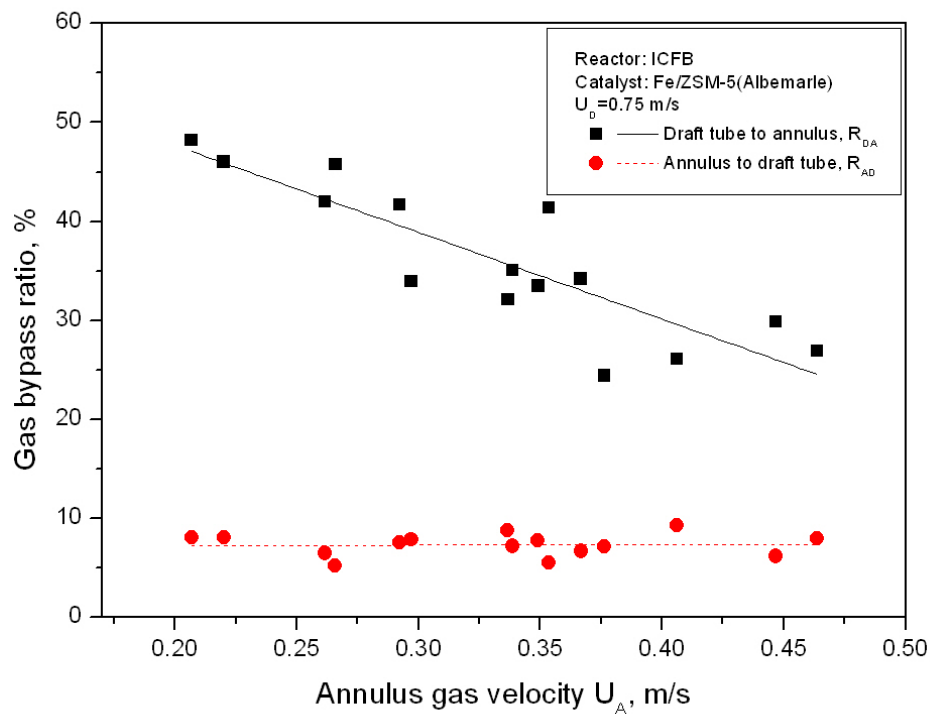


Figure H.18 Effect of U_A on gas bypass (Fe/ZSM-5(Albemarle), $U_D=0.75$ m/s, $T=355\pm 15^\circ\text{C}$)

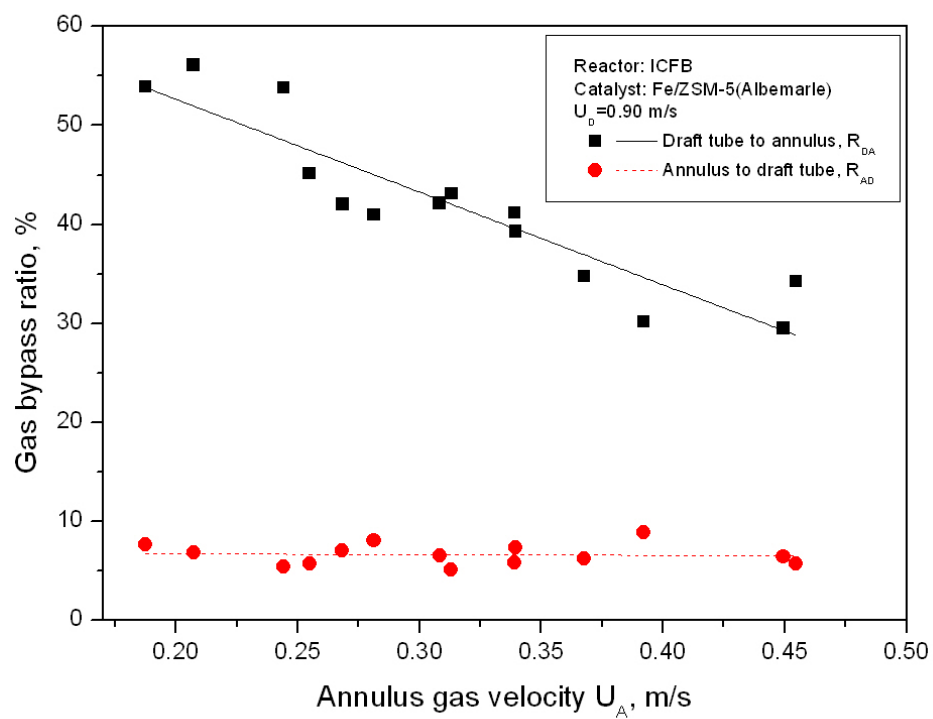


Figure H.19 Effect of U_A on gas bypass (Fe/ZSM-5(Albemarle), $U_D=0.90$ m/s, $T=355\pm 15^\circ\text{C}$)